Quantitative Analysis of Non-viral Gene Therapy in Primary Liver Culture Systems

by

Nathan C. Tedford

Bachelor of Science, Biomedical Engineering
Johns Hopkins University, 2001

Submitted to the Biological Engineering Department
in partial fulfillment of the requirements for the degree of

Doctor of Philosophy in Biological Engineering

at the

Massachusetts Institute of Technology

February, 2007

Signature of Author: _____
Nathan C. Tedford
Biological Engineering Department

Certified by: _____
Linda G. Griffith
Professor of Biological Engineering and Mechanical Engineering
Thesis Advisor

Certified by: _____
Douglas A. Lauffenburger
Professor of Biological Engineering, Biology, and Chemical Engineering
Thesis Advisor

Accepted by: _____
Douglas A. Lauffenburger
Professor of Biological Engineering, Biology, and Chemical Engineering
Director, Biological Engineering Department

This doctoral thesis has been examined by a committee of the Biological Engineering Department as follows:

Chairperson, Graduate Thesis Committee _____

Scott R. Manalis
Professor of Biological Engineering and Media Arts and Sciences

Thesis Supervisor, Committee Member _____

Linda G. Griffith
Professor of Biological Engineering and Mechanical Engineering

Thesis Supervisor, Committee Member _____

Douglas A. Lauffenburger
Professor of Biological Engineering, Biology, and Chemical Engineering

Thesis Committee Member _____

Jongyoon Han
Professor of Biological Engineering and Electrical Engineering and Computer Science

Thesis Committee Member _____

Alexander M. Klibanov
Professor of Biological Engineering and Chemistry

Quantitative Analysis of Non-viral Gene Therapy in Primary Liver Culture Systems

by

Nathan C. Tedford

Submitted to the Biological Engineering Department in partial fulfillment of the requirements for the degree of Doctor of Philosophy in Biological Engineering

Abstract

Gene therapy has the potential to cure thousands of diseases caused by genetic abnormalities, provide novel combination therapies for cancers and viral infections, and offer a new and effective platform for next generation vaccines. However, after more than three decades of research and development efforts, clinical success has yet to be realized. Successful delivery of DNA is a crucial first step in attaining safe and effective gene therapeutics. While vectors based upon recombinant viruses have shown high delivery and transfection efficiencies, they may also pose certain health risks to patients, can be difficult to target to cell or tissue types of interest, and present difficulties for large-scale manufacturing. Non-viral vectors look to offer a safer alternative and can be engineered to more effectively treat a specific cell type, tissue, or pathology, but these vectors are still plagued with low transfection levels and cannot provide adequate and sustained levels of gene expression. Continued efforts focus on producing next generation non-viral vectors that safely deliver therapeutic transgenes with the efficiency of their viral counterparts.

Many barriers exist in the successful trafficking of these non-viral complexes to the nucleus. Current evaluations of non-viral gene delivery treatments in more clinical settings often focus on a single barrier at a time, and as a result, may not lead to an overall improvement in gene delivery. Concurrently, more quantitative or systematic *in vitro* experiments may not correlate well with *in vivo* data. Our combined approach of quantitative vector trafficking and expression experiments coupled with computational simulation of vector specific mathematical models that describe every step of the gene delivery process has shown that a systems level approach can glean insight into the most rate-limiting steps for a given vector and generate hypotheses for future vector development and improvement.

These studies have been extended to primary liver cultures, coupled with device development to attain a more clinically relevant model system and more spatial resolution to study intracellular vector trafficking and localization. A larger perfused 3-D liver bioreactor has been built that allows for long-term culture of primary hepatocytes that more closely mimic hepatic phenotype than in conventional 2-D cultures and for multiplexed quantitative measurement that is not possible in animal models. A newly constructed density gradient electrophoresis device can separate vesicular organelles and track vector dynamics throughout the cell. These systems have provided more comprehensive data sets which show that vectors behave differently in different culture systems and that different vectors show unique cell trafficking dynamics. These results lend insight for future vector screening methodologies and provide vector specific mathematical models for primary cell transfection that can lead to further optimization of the polymer vectors studied in this work, which can contribute to the development of more efficient next generation *in vivo* delivery agents.

Advisors: Linda Griffith and Douglas Lauffenburger

Acknowledgements

I owe a great deal of gratitude to my advisors, Linda Griffith and Doug Lauffenburger, without whom this work would not have been possible. Thank you for providing me with exceptional support and guidance throughout this thesis work. I truly appreciate the freedom that you gave me to explore different avenues while also providing helpful guidance when I needed it. The opportunities you gave me to pursue ideas independantly as well as to travel for collaboration and to share my work with a number of different audiences greatly helped in shaping me into the researcher and person that I am today. I also feel extremely lucky to have had the chance to work with you and other exceptional people in the Biological Engineering Department as this new discipline and program was still being actively developed at MIT. I would also like to thank my former advisor at Johns Hopkins, Jim Harden, whose enthusiasm and guidance played a large role in fostering my initial love for research and applied science as an undergraduate and formed the basis for my training as a graduate student. I am also very grateful to my thesis committee members: Jay Han, Alex Klibanov and Scott Manalis. You all provided excellent feedback and guidance that kept my work focused and productive. You were always extremly positive and supportive, and truly helped me in shaping my thesis.

I had countless friends and mentors during my time at MIT, and it's difficult to thank everyone fully. I am particularly indebted to Anand Sivaraman, Kevin Janes, Karel Domansky, Csani Varga, and Bart Hendriks for their advice and guidance both inside and outside of the lab when I first arrived at MIT and began my thesis work. I owe a special thank you to Bart Hendricks, who went out of his way to provide me with computational modeling assistance at the end of my thesis work which led to very rewarding conclusions that would have been otherwise unattainable. I also am deeply indebted to Jennifer Fang, who worked with me for over three years and helped me in making great improvements to our experiemental methods and performed a lot of the work with me that made the final data discussed in this thesis possible. I also want to thank the talented UROPs and visiting students that I've had the opportunity to teach and work with over this time including David Jackson, Nathan Etassami, and Cynthia Chang. A special thanks goes to Bonnie Huang for being an exceptional visiting student and helping to perform a good deal of work in characterizing the giant liver bioreactor with me. I would also like to thank my collaborators outside of the lab. Mini Thomas from the Klibanov lab and Greg Zugates from the Langer lab provided me with the next generation polymer vectors that made for highly interesting studies and results in my thesis work. Brendan Harley in the Yannas lab was also very helpful in work to develop novel scaffolds for our reactor systems.

I had an amazing experience at MIT due to the wonderful people that I was able to interact with inside and outside of the lab. Collaborators and friends in the lab included Anand, Joe M., Karel, Walker, Dan D., Aran, Csani, Bart, Kevin, Vivian, Ley, Ben, Joe S., Albert, Megan, Neil, Ale, Shawdee, Nick, Lisa, Kathryn, John W., Bree, Corey, John B., Alexandria, Laura, Emily, Ricardo, Katy, Ajit, Brent, Matt and Ta. Thanks for making the Griffenburger domain such an enjoyable place to work everyday. I'd like to especially thank Ben for being an excellent colleague in the lab who has taken on a lot of resonsibility to keep moving things forward in the group, and to Joe M. and Albert for being great officemates over all these years. I'd also like to thank as many of my friends and classmates that I've had outside of the lab as well, who have made my time at MIT all the more enjoyable – Eric, Sri, Ale, Nick, Ty, Jon, Ryan, Rouzey, Ricardo, Reshma, Diana, Kathryn, Danielle, Seth, Kirk,

Mike S., Sid, Robert, Geoff, Jeb, Mark, Brent F., Andrew, Vic, Jason, Barry, Brian, HD, Jared and all of my other ski buddies, hockey friends, BE people and housemates that are too numerous to list but all had a huge impact on my life over the last five years. You are all great people.

Last but certainly not least, I would like to thank my family. You had the most to do with this accomplishment. I primarily owe this success to your caring and support over the years, and I dedicate this thesis work to you. I would like to thank my brother Gavin and sister Ali for all the fun times we had growing up, and especially to Ali for being such an amazing friend during my time in Boston. I owe my deepest thanks to my parents, who dedicated themselves to making sure that I always had the best education and opportunities, even when they weren't readily available. Without your dedication, this upstate NY kid would have never made it to MIT! And lastly I would like to sincerely thank Maxine for all of her love and support over the last five years. You have been and are my best friend and you have made this such a happy and enjoyable time in my life. Thank you!

Table of Contents

List of Tables and Figures

Chapter 1

Chapter 2

Chapter 3

Chapter 4

Chapter 5

Chapter 1

Introduction and Background

1.1 Gene Therapy

Gene therapy can be broadly defined as a therapeutic approach that seeks to treat or prevent diseases by adding, correcting, or replacing genes [1]. Through the delivery of DNA or RNA to desired cell types, this strategy has the potential to treat a number of disorders by leading to the expression of wild-type or recombinant proteins that have a curative effect [2] or by modulating RNA expression levels to remedy aberrant gene expression [3, 4].

Some of the most obvious benefactors of this form of treatment are single gene inherited disorders such as sickle cell anemia, hemophilia, acquired immune disorders, familial hypercholesterolemia, muscular dystrophy and cystic fibrosis [5-12], where transfection and expression of an appropriate transgene without the deleterious mutation could effectively cure the disease. Gene therapy may also be used to develop recombinant therapies for diseases that involve many genes. For instance, unwanted gene expression profiles may be altered in cancer cells, cancer cells can be targeted and altered to illicit an anti-tumor immune response, or cytokines may be expressed that make it easier for targeted cells to be treated with a pro-drug [13-16]. Recombinant multi-gene therapies could also be adapted for heart disease and diabetes along the same lines where intervention may be required at multiple checkpoints to achieve the desired remediation of cell or tissue phenotype [9, 17, 18]. Chronic infectious diseases, including HIV, herpes and hepatitis, also stand to benefit from gene therapy [19-23]. Delivery of DNA vaccines could prevent the onset of infection altogether [24, 25], while the expression of small RNA fragments and recombinant proteins could shut down viral gene expression or enzyme function to slow disease progression in already infected patients and allow parallel treatment strategies to work more effectively [21, 26-29]. DNA vaccines also offer the potential to attain safer and more stable methods of storing, distributing and expressing antigens that could allow for robust and affordable prophylactics for third world countries and more efficient distribution during impending large scale epidemics that would not be possible with traditional attenuated viruses and protein based vaccines [30].

After the inception of gene therapy in the early 1970's, research in the field greatly accelerated in the 1980's with the discovery of restriction endonucleases and the arrival of PCR

amplification methods [2, 31]. With progress in the following decade and eventual completion of the human genome project at the turn of the century, more and more information has become available for gene therapy approaches to exploit. Additionally, greater understanding of small RNA based regulation of gene expression in recent years continues to offer increased flexibility and application for gene therapy platforms. However, after more than thirty years of research and nearly two decades of clinical trials, long-term clinical success has yet to be attained [32-34]. To date, no clinical trials have received full approval, with only a handful of restricted approvals issued for orphan drugs in the U.S. and Europe [35-38], and the few

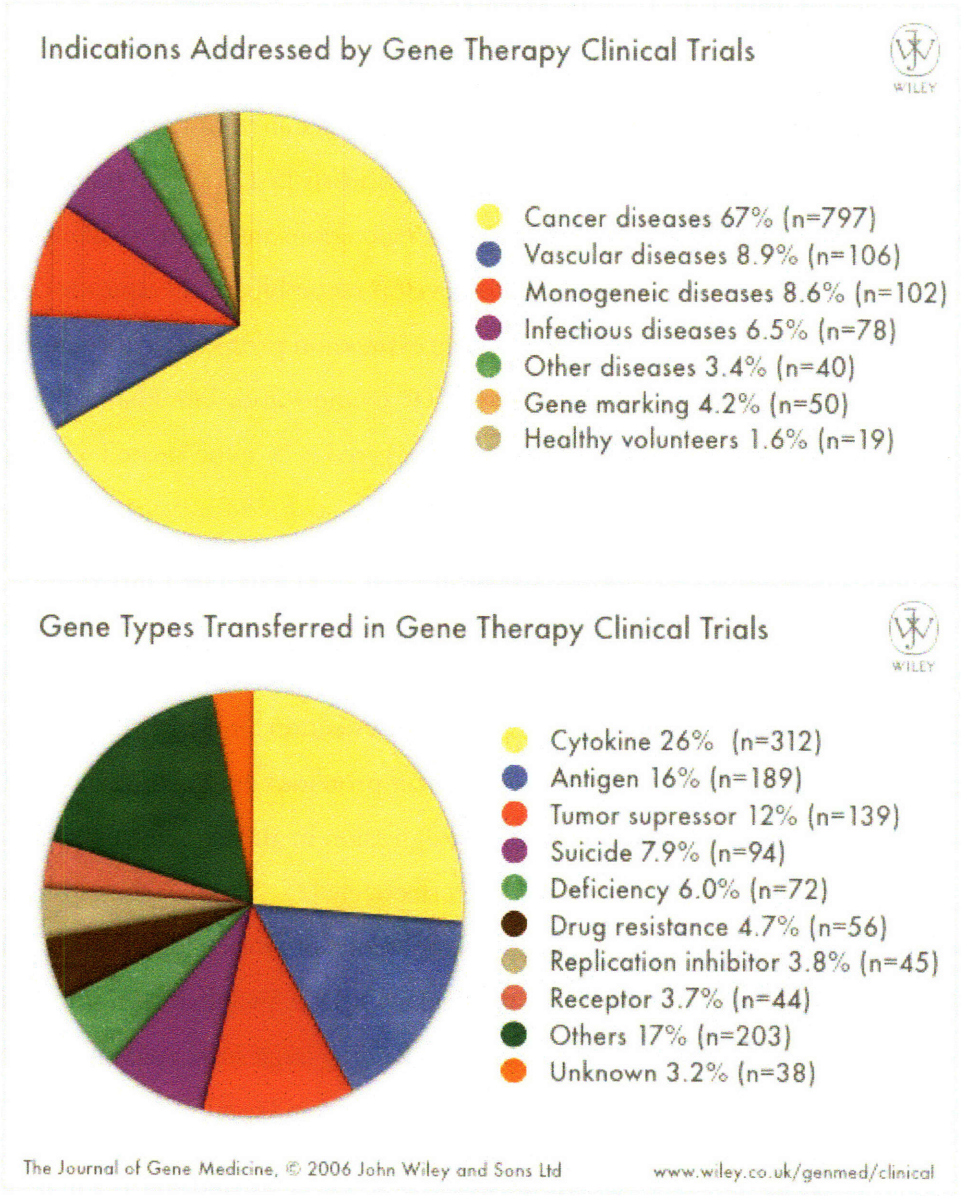

Figure1.1: Overall breakdown of disease indications and gene types used in all documented gene therapy clinical trials to date, worldwide [34].

recent early successes have resulted in tragic consequences such as development of leukemia [39-41]. Very few gene therapy trials have been able to progress into Phase III studies, and due to many of these setbacks and adverse complications, the number of approved trials has decreased significantly in recent years from the peak at the turn of the century.

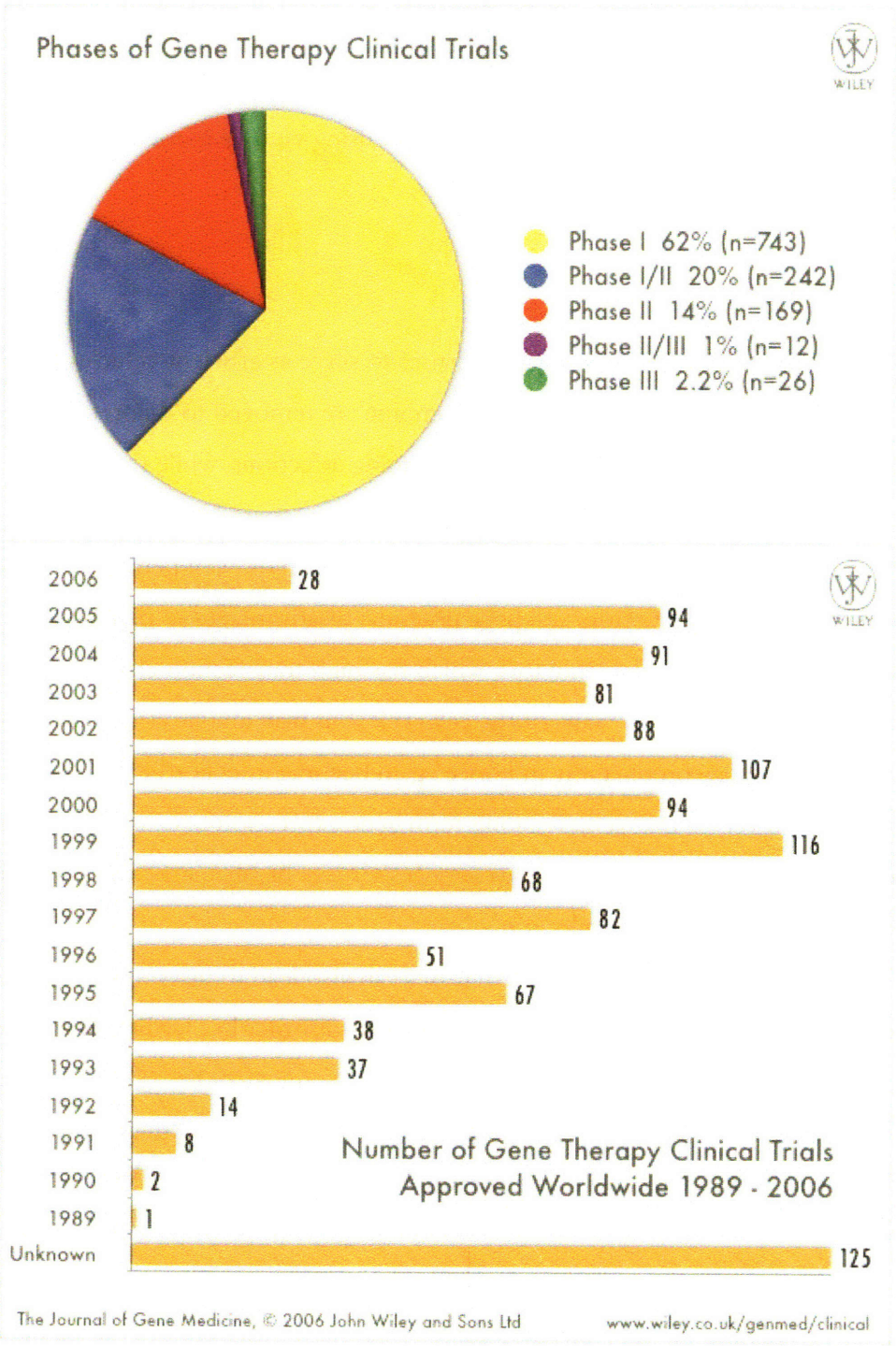

Figure 1.2: Distribution of worldwide gene therapy clinical trials by current or ending phase and by year [34].

1.2 Gene Therapy Strategies: Delivery Methods and Vectors

For gene therapy to be successful, a transgene or multiple transgenes must be safely delivered to the nucleus and lead to therapeutic gene expression without any dangerous side effects. Cells can either be transfected *in vivo* by administering various gene formulations to the patient, or cells can be removed from the patient, transfected *ex vivo* to attain the desired phenotypic change, and then reinserted to have their desired effect [1, 2, 42]. Either of these strategies can be theoretically accomplished by using viral or non-viral transfection methods.

1.2.1 Viral Vectors

Viral gene therapy utilizes modified viruses to serve as efficient vehicles for DNA delivery [33, 43]. Specific regions of the viral genome are removed to theoretically render the viral vectors incapable of replicating and becoming infectious, while the desired transgenes are inserted in their place. In general, viral vectors are highly efficient in delivering their gene payload, and normally lead to long term or even permanent gene expression. However, viral vectors still pose potential disadvantages to patients [44]. Common viral vectors include adenovirus, which has high transfection efficiency both in vivo and ex vivo on cells in any stage of the cell cycle, but may invoke strong immune responses or undergo recombination and once again become infectious [43, 45]. Retrovirus is an effective viral vector that achieves long-term gene expression in *ex vivo* transfections with a relative low immune response; however, this virus is highly inefficient *in vivo* and is unable to transfect non-dividing cells [43].

In addition to recombination, retroviruses can also lead to insertional mutatgenesis and more serious complications, potentially curing one disorder but leading to another [33, 46-48]. Lentiviruses have been studied for their ability to transfect hematopoietic stem cells, but they still have potential for infection and concerns exist regarding their immunodeficiency virus origins [49-51]. All three of these vectors share the common limitation that they can only carry a limited amount of gene material (usually less than 8 kb), making some multi-gene approaches unfeasible. This setback may be addressed by herpes virus carriers, which have a high payload capacity, although these vectors can be highly immunogenic and potentially toxic [43, 52]. Adeno-associated vectors look to provide high

in vivo transfection efficiency and prolonged gene expression with a low immune response, but are hampered by even smaller carrying capacity (less than 4.5 kb) and can also pose the risk of insertional mutagenesis and infection [43, 45, 53, 54]. Although this list is not exhaustive, it can be seen that while at first sight viral vectors may appear to be the perfectly evolved gene delivery vehicles, each vector possesses a set of advantages and disadvantages that makes it potentially suitable for certain applications, but not without risks.

1.2.2 Non-viral Vectors: Naked DNA and Facilitated Delivery

The simplest non-viral alternative for gene delivery is the introduction of naked plasmid or oligomeric DNA to cells [55, 56]. DNA plasmids can carry virtually unlimited payloads, are noninfectious, and do not pose immunogenic risks, while oligomers are also relatively safe and are cheap to produce. However, these advantages are tempered by the fact that delivery of naked DNA is plagued with low transfection efficiency, and the minimal levels of gene expression that do result are normally very short-lived [57]. This transient expression can be prolonged via "gene gun" delivery or intramuscular injection of plasmid, which slows the rate of plasmid degradation, but these approaches are only applicable to a limited number of disorders [58-62]. Some of the most exciting and recent progress in non-viral gene therapy has been in the development of technologies that actively enhance the delivery of naked DNA. Electroporation, which subjects cells and tissue to very short pulses of a high voltage electric field, serves to reversibly permeabilize the plasma membrane, facilitating plasmid transport to the cytoplasm and eventually the nucleus [63-66]. Although this treatment method has shown success in a number of pre-clinical trials, the long term effects and safety of this technique must be established before its clinical utility can be realized. Hydrodynamic delivery of plasmids has also developed into a useful technique to evaluate the curative potential of different plasmids in animal models. High pressure injection to the tail vein of mice or rats can lead to long term, efficient gene expression in the liver [66, 67], though limitations exist in completely scaling up this approach for humans, as injection volumes would have to be on the order of liters! Catheter guided balloons may be developed to close off portions of the liver, substantially minimizing the apparent volume for delivery [68], but such an approach may not be very appealing for patients when other options are available. In summary, while naked DNA delivery techniques may provide

increased safety, it is unclear as to whether these approaches will realize widespread application in gene therapy.

1.2.3 Non-viral Vectors: Molecular Conjugates

The use of synthetic, non-viral vectors as gene carriers provides another route for improving the transfection efficiency of RNA and plasmid and oligomeric DNA [1, 69, 70]. The first synthetic gene carriers studied in the early 1980's were traditional liposomes, which fused to the plasma membrane and delivered their DNA cargo into the cytoplasm [71, 72]. Cationic lipids and organic polymers such as polylysine came into use shortly thereafter, with some carriers incorporating ligands for cell specific uptake [73-75]. These carriers formed smaller, cationic particles with the negatively charged DNA, entering the cell through endocytosis and protecting the plasmids from degradation for more of the intracellular route to the nucleus. However, most of these non-viral complexes were still subjected to degradation within the lysosomal pathway, since no vesicular escape mechanism was in place for these carriers.

With the advent of polyethylenimine (PEI), this picture began to change [76]. With every third atom of this polymer being a protonatable nitrogen atom, PEI could serve as a buffering agent, or "proton sponge", in the acidic late endosomes and lysosomes. While the mechanism of endosomal or lysosomal escape remains to be definitively proven, this property of PEI certainly contributes to more efficient trafficking of complexes into the cytoplasm, increasing the chances for nuclear association and delivery. As a result, PEI has become one of the most widely studied non-viral vectors [77-94]. This discovery has also led to a new wave of synthetic vectors that seek to engineer polymer properties that increase endosomal lysis and escape due to pH sensitive functional groups, bind nuclear import proteins more efficiently with the incorporation of nuclear localization sequences, and increase vector lifetime *in vivo* by preventing serum protein aggregation with steric stabilizing agents such as polyethylene glycol (PEG) [95-97]. Hybrid vectors are also being designed which incorporate targeting ligands and other recombinant or viral capsid proteins to increase cell specific targeting and trafficking efficiency [69, 97-102]. Novel combinatorial chemistry approaches and reengineering of traditional cationic, amine containing polymers has also led to different classes of next generation gene delivery vehicles which are less toxic than traditional PEI vectors, but deliver their genetic payload far more efficiently[103-111].

However, these non-viral carriers still transfect cells with much lower efficiency and shorter expression times than their viral counterparts. It is hoped that with further refinements to both vector and plasmid properties, novel complexes can be developed that rival the efficiencies of viral vectors, while still remaining safe for patients and providing the versatility to be tailored to a multitude of very specific disorders.

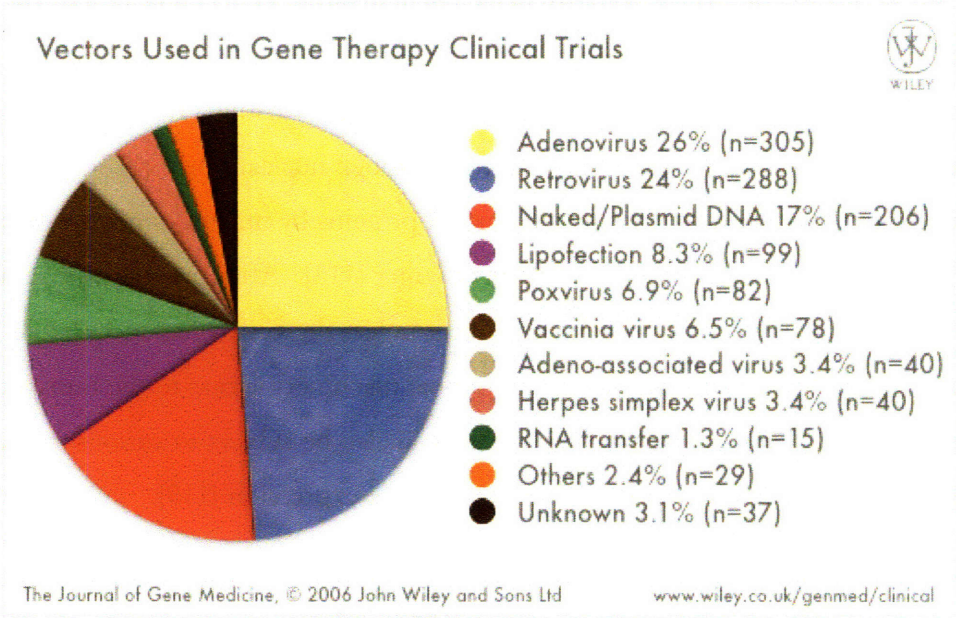

Figure 1.3: Breakdown of gene therapy vector types used in gene therapy clinical trials to date. As can be seen above, the vast majority of trials are focused on viral vectors, followed by roughly one quarter of trials using more traditional first generation non-viral techniques such as lipofection and naked DNA transfer. More progress needs to be made on next generation non-viral carriers so that they are not only safe, but also increasingly effective and more attractive for clinical application.

Motivation and Significance of Thesis Work

1.3 Non-viral Carriers Face Multiple Extracellular and Intracellular Barriers

In order for efficient transfection to be accomplished, a non-viral vector/plasmid complex must overcome a number of barriers on its way to the nucleus [112, 113]. First, whether *in vivo* or *in vitro*, the complex must travel via convection or diffusion to the surface of the cells that require treatment. The complex must be resistant to aggregation in the presence of serum proteins, while also having low immunogenicity. These properties are essential for a carrier to have high safety and efficacy *in vivo*. The complex must then bind to the cell surface and be internalized, either through a specific ligand-receptor interaction leading to receptor

mediated endocytosis, or via non-specific interactions with cell surface proteoglycans such as syndecans followed by fluid phase endocytosis [114, 115].

After internalization, the complex is trafficked from coated pits to early endosomes, where it may then be recycled or shipped further down the pathway to the acidic late endosomes and lysosomes. It is crucial that the complex have some form of vesicular escape mechanism, so it can enter the cytoplasm before degradation occurs within these late vesicles. The complex must then travel to the nucleus, with any prematurely unpackaged DNA being subjected to rapid degradation rates due to the presence of cytosolic nucleases [116]. DNA segments larger than 100 bp cannot freely diffuse through nuclear pores [117], so the complex or plasmid alone must then bind to nuclear import proteins by utilizing a nuclear localization sequence since most transgenes are 3 kb pairs or larger [113]. After nuclear pore complex formation and import, gene expression can't occur unless the vector has successfully unpackaged from the plasmid, giving transcriptional machinery access to the transgene [118]. After successful nuclear delivery, non-viral DNA can also be subject to various mechanisms of gene silencing, which can result in highly transient gene expression [119].

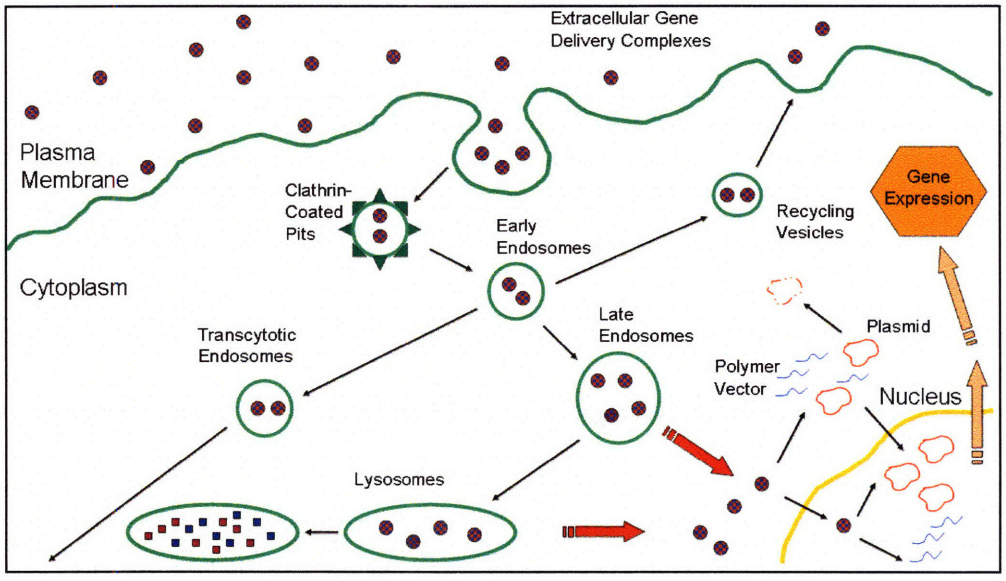

Figure 1.4: Non-viral vectors face multiple barriers multiple barriers on the way the successful nuclear delivery and transgene expression. Since non-viral complexes are usually on the order of 100 to 500 um in diameter and cannot freely diffuse across the plasma membrane, they must rely on the endocytic pathway for cellular uptake and intracellular trafficking to the nucleus.

In general, a majority of past research on both viral and non-viral fronts has been of a more clinical and qualitative nature. Studies would mainly focus on overcoming one barrier at a time and merely evaluate resultant gene expression levels and duration for some dosing level of a given viral or non-viral formulation. In the case of viral vectors, which have evolved complex mechanisms to efficiently surpass all of these barriers, this methodology can still yield some useful outcomes. However, in the context of non-viral vectors that must be designed from the ground up to overcome each barrier, this approach can be detrimental and inefficient. Changing the physical properties of a vector may be favorable for one barrier, but actually hinder overall efficiency by making it more difficult to accomplish another step in the delivery process. Past work has shown binding and internalization at the cell surface [120, 121], endosomal escape [122-124], transport in the cytoplasm [116, 125], nuclear import [126-131], and vector unpackaging [118] to all be potentially rate-limiting steps in the delivery process. The most important message to take away from these conclusions is that the rate-limiting step and significance of other major barriers can depend heavily on the specific vector/plasmid complex used and the particular cell type being studied.

1.4 New Experimental Approaches Can Glean Insight for Vector Design Properties

Quantitative and systematic studies of gene delivery may be advantageous to tackle this multiple-barrier scenario. Past work in our group has shown that taking a computational modeling approach combined with quantitative experiments for gene delivery analysis can provide a powerful predictive tool for gene carrier development and refinement [113]. By adjusting model parameters to fit quantitative experimental data, sensitivity analyses can be performed to determine what steps are most rate limiting for a specific complex. Parameter spaces can also be varied in a systematic manner in simulations that reveal how multiple vector properties could be adjusted to give the most optimal gene expression profiles. However, current models are experimentally limited due to the small number of subcellular fractions that can be studied quantitatively. Many processes are lumped together, and as a result, a good deal of mechanistic information regarding the intracellular dynamics of gene delivery is lost.

This systems level analysis was extended more recently by coupling quantitative whole cell and nuclear trafficking data from a variety of vectors, both viral and non-viral, with a more refined mathematical model [132]. Additional experimental data from the literature was used to build a more comprehensive model that could more accurately describe many of the

aforementioned intracellular delivery barriers. Vector dependent parameters were fit to the respective data sets to acquire specific models for Adenovirus, PEI25, PEI2, and a next generation branched PEI called PEI2C12, Lipofectamine, and naked plasmid DNA.

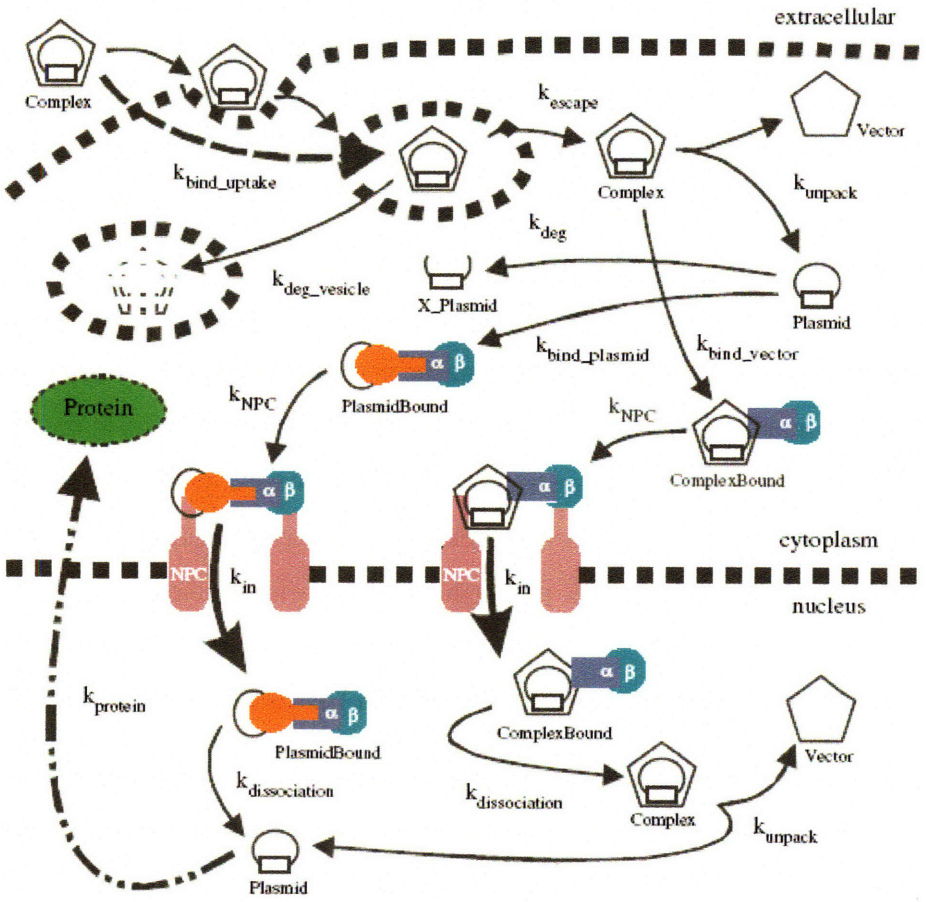

Figure 1.5: Schematic representation of the first order rate processes involved in intracellular trafficking and delivery of plasmid to the nucleus via a gene delivery vector. These steps were included in a mathematical model of ordinary differential equations, and the model was fit to experimental data for each vector by varying rate constant values that were dependent on the vector properties. Simulations could then be run with each vector specific model to gain mechanistic insight for that carrier [132].

Sensitivity analyses were then run on each these vector specific models to gauge which steps were most important for the vector to achieve successful gene delivery and maximal transgene expression. Some of the most important conclusions from this analysis were that different vectors did in fact have different rate limiting steps within the same cell type (in this case, the C3A hepatocarcinoma cell line). Some of these conclusions made mechanistic sense due to what was expected of the carrier from its structure and inherent chemical properties. While other results were less intuitive, they did make physical sense and generated interesting

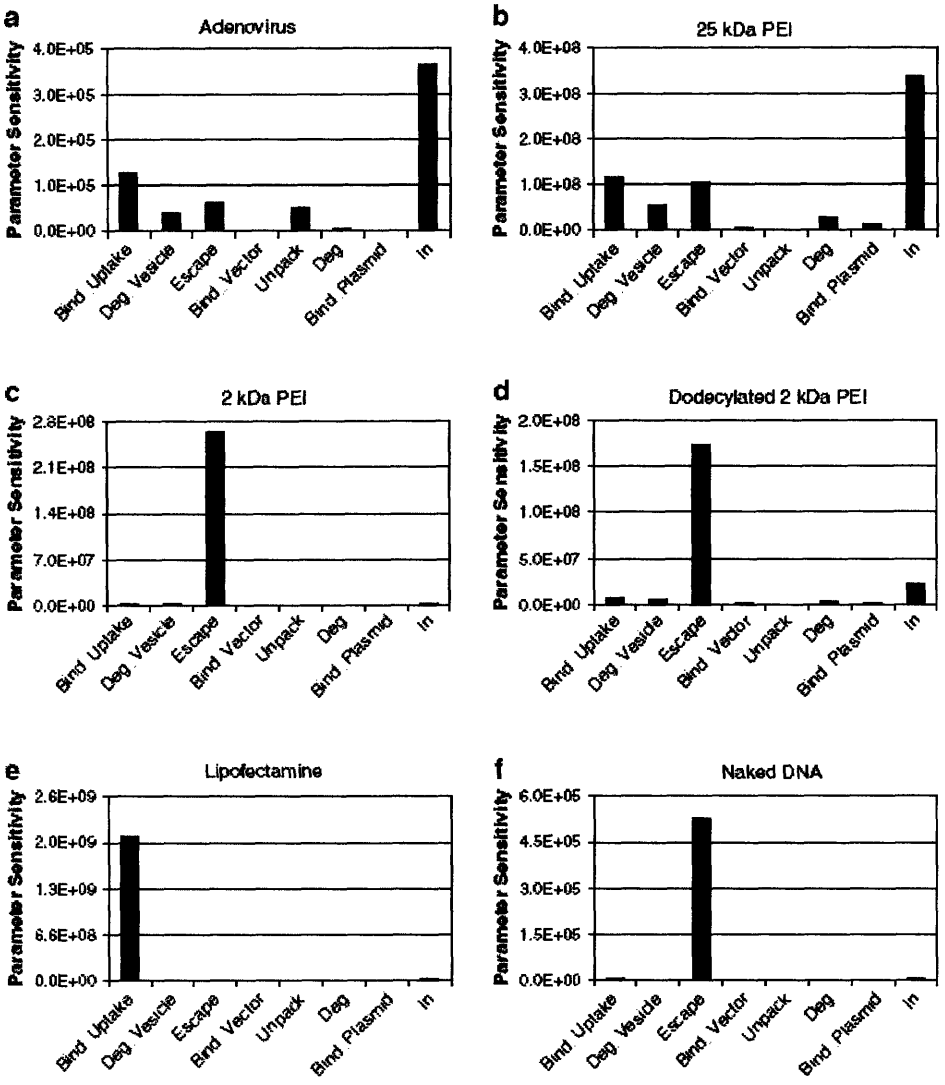

Figure 1.6: Sensitivity analysis results for each vector specific mathematical model. Parameter sensitivities were evaluated for delivery steps that were dependent on vector properties. A high sensitivity value implies that a step may be potentially rate limiting in the delivery process, revealing here that different vectors have different rate limiting steps [132].

hypotheses for further experimental study and refinement. Interestingly, overall results for some of the vectors differed significantly from those seen in other cell types. For instance, PEI2C12 greatly outperformed traditional PEI25 in the Cos-7 monkey kidney cell line, but this phenomenon was not observed in the C3A cell line. This observation lends credence to the idea that vectors should be evaluated on a cell type by cell type basis, as the intrinsic phenotype of a cell can affect the delivery efficiency of a given carrier. Furthermore, this supports the need for more efficient methods of quantitatively screening novel vector performance in primary cell types and more *in vivo* like experimental models, since cell lines can differ greatly from their original primary cell source.

1.5 Experimental Goals for Improved Gene Delivery Analysis

To further improve on these findings and build more accurate and predictive mathematical models, increased subcellular resolution must be obtained to more accurately identify potentially important barriers and gain additional understanding of the gene delivery process for specific non-viral complexes. Progress has also been made in systematically producing and screening novel non-viral vectors in a more high-throughput manner, increasing the chances for the discovery of new chemical moieties that have desirable properties for gene therapy [133, 134]. While this work is significant, improvements in screening are needed that will be able to determine why novel vectors show increased transfection efficiencies. Comparing gene expression levels in conventional two-dimensional cell line cultures will identify the best performing vectors in that cell line, but likely won't correlate with vector performance *in vivo* in animal models and patients. While animal models and clinical studies can reveal overall vector safety or efficacy, it can be very difficult to acquire quantitative, mechanistic data, and therefore, it is once again difficult to understand why or why not a gene therapy vector was successful or how it could be further improved. The knowledge gained from better screening in a more in vivo like experimental system that still allows for quantitative analysis will allow for more intelligent refinements in subsequent vector iterations, potentially resulting in highly efficient carriers.

1.5.1 Increased Spatial Resolution for Intracellular Trafficking Experiments

A major goal of this thesis work is to develop a method to better study the intracellular trafficking of non-viral gene delivery vectors. Different groups have attempted to track PEI transport within the endosomes and lysosomes of single cells via different imaging and fluorescence detection strategies [90-94]. The fact that these studies have actually brought about conflicting observations and reopened the debate over the mechanism of PEI-mediated gene delivery highlights the fact that a more quantitative method of analysis would be beneficial in examining these processes. Other efforts have focused on utilizing novel fluorescence techniques to more quantitatively track the pH environment of non-viral complexes [135], but this approach only allows analysis of a limited portion of the overall delivery route and leaves some uncertainty of the actual location of the complex. Conducting a more comprehensive, and not merely quantitative, analysis could allow for the validation of

mass action kinetic models for more accurate prediction of vector behavior and insight for improvement.

After reviewing a myriad of potential subcellular fractionation methods, it has been concluded that an approach utilizing density gradient electrophoresis (DGE) could yield the desired intracellular resolution, while still meeting the sensitivity demands of quantitative downstream assays. DGE exploits differences in both the density and charge of proteins, cells and organelles by driving electromigration of charged species through a viscous medium that varies in density in the same dimension as the applied electrical potential [136]. As a result, this methodology is exceptionally useful for separating and collecting different classes of endosomes and lysosomes, which have differential surface protein expression and membrane composition, leading to diverse and distinct density and charge properties [137-141].

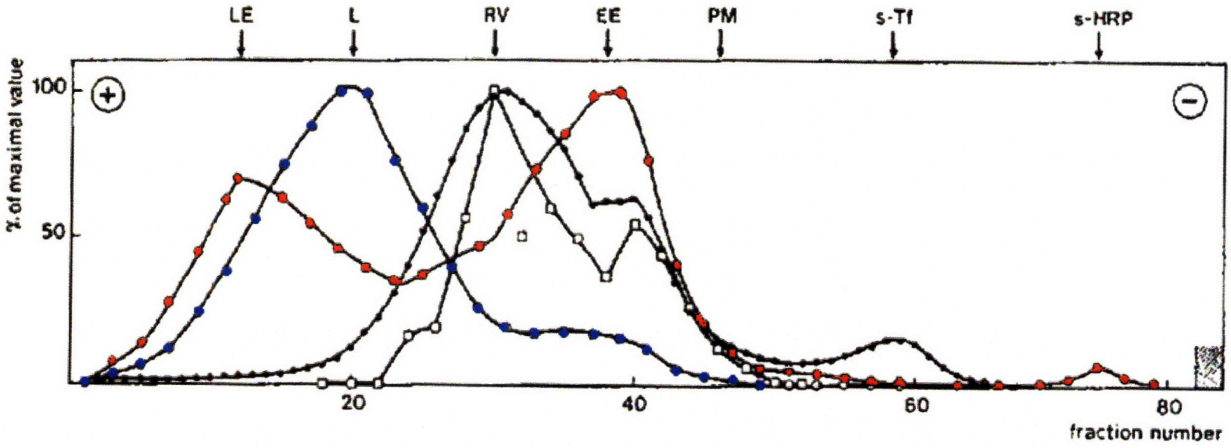

Figure 1.7: Separation potential of density gradient electrophoresis (DGE) columns: a typical fractionation pattern of organelles from labeled Mel Juso cells performed on an early density gradient electrophoresis prototype. LE = Late Endosomes, L = Lysosomes, RV = Recycling Vesicles, EE = Early Endosomes, PM = Plasma Membrane, s-Tf = soluble transferrin, s-HRP = soluble HRP. Fraction 1 was at the top of the DGE column at the beginning of the separation run and fraction 80 at the bottom of the column [142].

More conventional methods such as density gradient centrifugation or free flow electrophoresis perform separations based on either density or charge differences alone [143]. As a result, these techniques cannot separate endosomal subpopulations or robustly deal with the slight intrinsic variability of each vesicle type, while requiring multiple runs on the same sample to achieve the same number of fractions with high resolution [143, 144]. Meanwhile, microfluidic bioseparation devices have shown proof of principle to sort vesicular organelles, but don't provide efficient recovery methods or enough material to support downstream

assays [145]. A functional DGE device will be built based on the work of Ab Tulp and coworkers at the Netherlands Cancer Institute (NKI) [142, 146-148]. Two prototypes were constructed that performed efficient, one-step separation of vesicular organelles in a number of cell lines, allowing all organellar fractions to be collected with high resolution from the same sample. It is hoped that a similar device can be adapted and optimized to separate the same organelles from primary rat hepatocytes.

1.5.2 A More *In Vivo*-like System to Study Vector Delivery and Expression Efficiency

While successful implementation of DGE on non-virally transfected cells can provide a wealth of information on the intracellular mechanisms of gene delivery, there is no guarantee that this data will lead to clinically applicable conclusions. Oftentimes, as previously mentioned, experimental results acquired from a cell line in 2-D culture do not correlate well with those seen in *in vivo* tissue or primary cells in general [149]. As a result, a requisite first step in furthering these experimental approaches is to move experiments into the appropriate primary cell types of interest. Optimizing DGE experiments in primary hepatocytes should offer a number of insights into the intracellular delivery mechanisms of different vectors in a cell type that is highly relevant in *in vivo* gene therapy approaches. The liver performs many important functions in the uptake and processing of xenobiotics in the body. Additionally, it serves as an attractive organ target for a number of gene therapy applications [150-158]. However, the two-dimensional culture formats that are optimal for throughput and sample processing when studying vector trafficking do not reflect the complex three dimensional tissue structure and cell type interactions that exist in native liver. When primary cells cultured in 2-D on either adsorbed collagen monolayers or collagen gels are transfected with a gene therapy vector, every cell in the culture has equal access to vectors in the culture medium. These cultures are also static, and in the absence of flow, particles simply sediment on the cells and are endocytosed.

This is not the case in *in vivo* liver, where a complex hierarchy of cell types and overall tissue organization means that not every cell has equal access to a therapeutic that is large enough that it must rely on endocytosis for cell uptake. Additionally, some of the cell types in native liver, such as Kupffer cells, may preferentially take up the vector and degrade it before the desired target cells, hepatocytes, have access to significant vector uptake. Furthermore, primary hepatocytes cultured in traditional two-dimensional formats quickly dedifferentiate

and lose liver specific phenotype. Therefore, it is difficult to carry out long term gene delivery and expression analyses in these systems to gauge primary cell success of vectors. It should be noted that liver structure and function and the role of specific cell types is reviewed in great detail in the thesis introductions of Anand Sivaraman and Albert Hwa, and the reader is referred to these documents for further background information on the liver [159, 160].

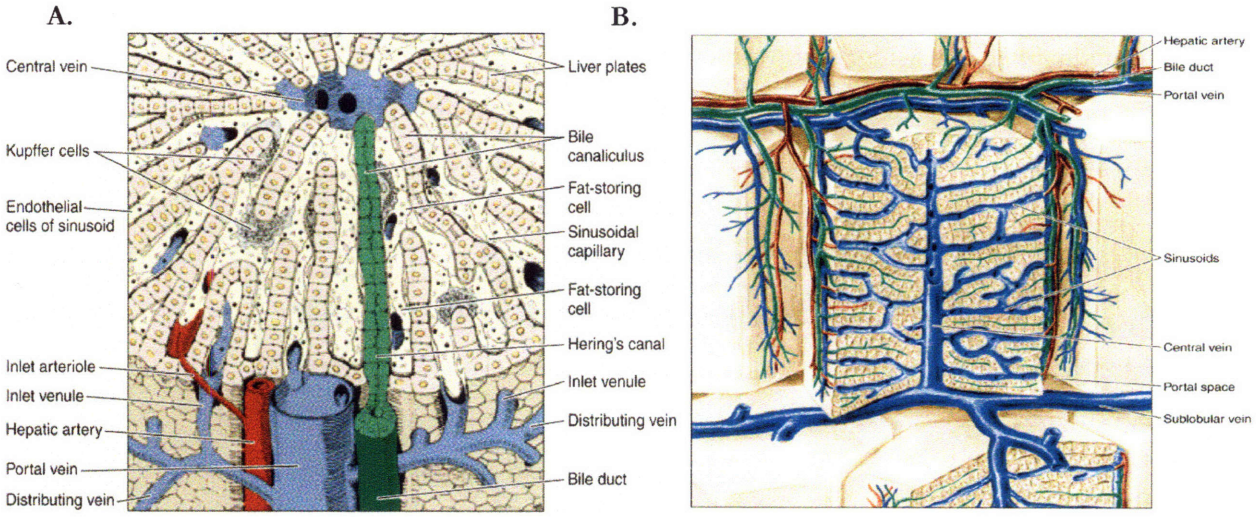

Figure 1.8: Schematic representations of the 3-D structure and hierarchy of the liver. A) Cell arrangement of the sinusoidal flow conduits in a liver lobule. B) Vascularization of one liver portal triad unit. C) Detailed schematic of a sinusoid cross section highlighting the complex interaction of multiple cell types. Cell types are as follows: H, Hepatocytes; EC, Endothelial Cells; SC, Stellate Cells; KC, Kupffer Cells; P, Pit Cells. Images A and B are taken from Junqueira and Carneiro, Basic Histology, a text and atlas, p. 333, Figure 16-11. Image C is taken from Wake *et al.* 1997. Images originally appeared in the thesis of Anand Sivaraman, © Massachusetts Institute of Technology.

Ideally, the gap between cell line and animal model studies must be filled with an experimental system that can foster cells or tissue in a manner that promotes *in vivo*-like tissue structure and phenotypic expression, while also facilitating quantitative study in greater temporal and spatial resolution. It is hoped that studying non-viral gene delivery in a three-dimensional, perfused liver bioreactor that has been previously developed in the Griffith lab will generate more clinically relevant data. This bioreactor has been shown to facilitate the reorganization of primary rat hepatocytes and hepatic spheroids into tissue with liver-like

morphology and phenotype, and greatly prolongs the time that these primary cells can be cultured *in vitro* [161, 162]. As mentioned previously, liver itself is a common target organ for *in vivo* gene therapy strategies [163], so this system has the potential to provide an excellent, controllable test bed for the improvement of non-viral vectors for a wide variety of clinical applications. The system also utilizes serum containing perfusion medium, which can provide an additional test for how a vector may perform in vivo. Multiple reactors can be seeded and repeatedly form consistent tissue structures, allowing for numerous transfection runs from the same primary cell source that can be analyzed at different time points or for multiple vectors.

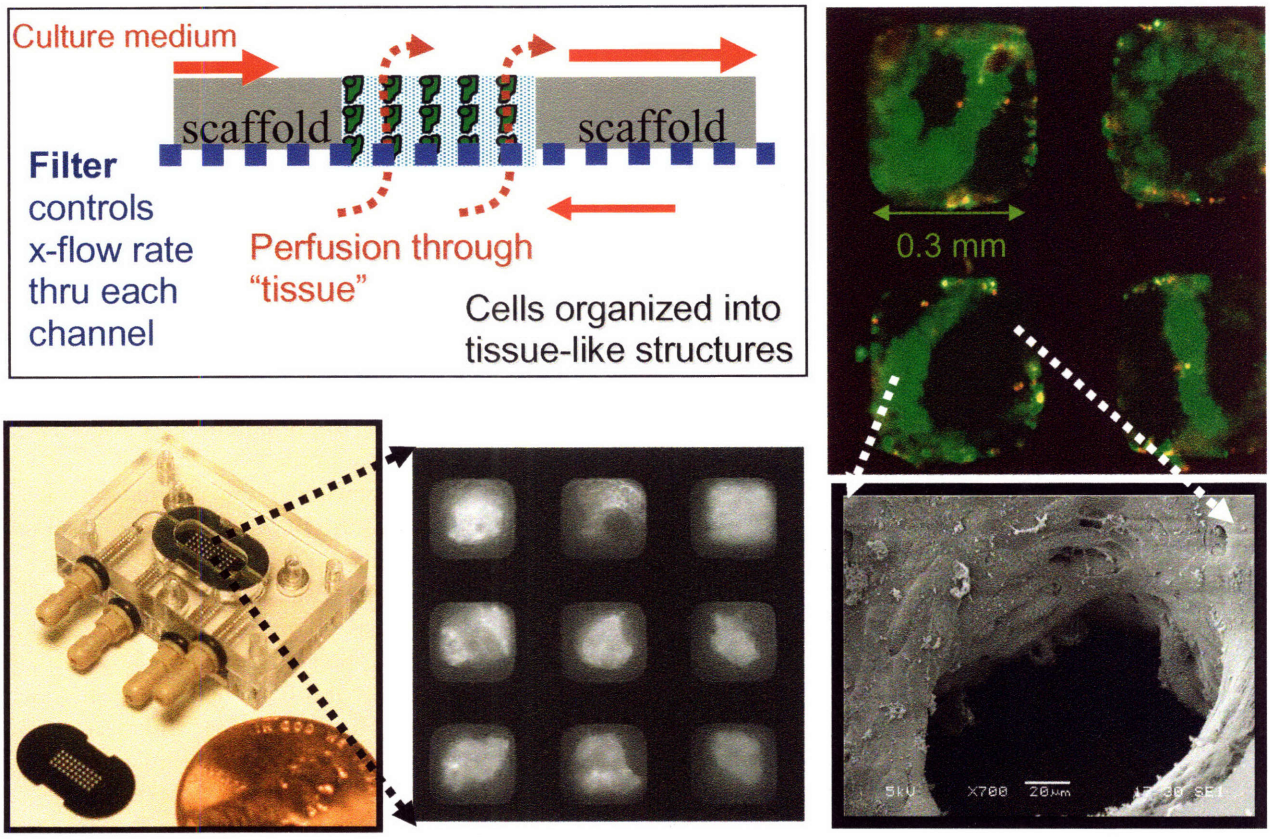

Figure 1.9: The perfused 3-D Milli-F liver bioreactor. Hepatocytes in the reactor channels are perfused with culture medium and form tissue structures that remain viable over long term culture with enhanced liver phenotype as compared to traditional in vitro culture formats.

By combining quantitative DGE trafficking studies in short term two-dimensional cultures relevant to the time scales of nuclear delivery of gene therapeutics and long term delivery efficiency and expression assays in the liver bioreactor to compare differences between 2-D and 3-D systems of primary cells, it is hoped that both mechanistic and clinical level lessons can be learned about non-viral vector performance and knowledge can be gained on design properties of these vectors that can potentially be enhanced.

1.6 Overall Thesis Objective and Specific Aims

The overall goal of this thesis work is to develop and optimize devices and methods for a combined experimental and modeling approach for the quantitative analysis of the dynamics of non-viral gene delivery in primary liver cultures. Successful implementation of this dual strategy should provide added insight and refinement in identifying the major barriers to successful non-viral gene delivery in a more clinically relevant experimental system. To achieve this end goal, the specific aims of this thesis are:

1. Develop an improved experimental method for subcellular fractionation to permit higher-resolution quantitative measurement of vector dynamics in primary hepatocytes.
    a. This will require the fabrication of a density gradient electrophoresis device that exploits charge and density differences in cellular organelles, thus allowing for more efficient post-transfection organellar separations. This fractionation method must ideally allow for early endosomal, late endosomal/lysosomal, nuclear and cytoplasmic fractions to be acquired from the same sample.
    b. The method must be repeatable and completely preparative to allow for reliable fraction identification and downstream quantification of DNA plasmid and polymer carrier. The approach must allow for large enough sample sizes for downstream assays to accurately measure vector and plasmid levels. Separation runs and cell lysis techniques will be specifically optimized for primary hepatocytes.

2. Perform transfection experiments with non-viral vectors and a canonical viral vector in primary liver cultures coupled with downstream assays to quantify intracellular trafficking and gene expression at time points of interest.
    a. Characterization and improvement of the scaled-up giant reactor will be performed in order to acquire a reliable experimental system that will provide cell numbers which satisfy the demands of the quantitative downstream assays. A more efficient transfection scheme will also be explored in this larger reactor set-up, and cell recovery from the reactor chip will be optimized.

b. Employ a series of non-viral gene delivery and post-transfection assays in short term 2-D cultures to determine vector/plasmid and plasmid levels in intracellular fractions recovered from DGE processing. Build trafficking time courses with increased spatial resolution for each vector.

3. Build an improved mathematical model that accounts for vector, plasmid and vector/plasmid complex dynamics by describing for each relevant species: Binding and internalization at the cell surface, vesicular trafficking and escape, nuclear localization and import, complex unpackaging, and transgene expression.
    a. The degree of subcellular resolution obtained via specific aim 1 and the availability of kinetic data for primary hepatocytes/related cell lines will dictate the complexity of the overall model and its individual components.
    b. Model parameters will be fit to the quantitative kinetic data acquired via specific aims 1 and 2 to make vector specific models. Sensitivity analyses will be performed on these to determine which processes are rate limiting for successful nuclear delivery, providing insight for potential improvement of a vector's physical properties and related efficiency. *In silico* model simulations over tractable parameter spaces could serve as a basis for optimization of transgene expression as a function of vector properties, and generate hypotheses for future experiments.

Chapter 2

Device Development and Optimization of Experimental Systems

2.1 Introduction

This chapter will discuss the initial development and refinement of the major experimental systems that were used throughout this thesis. Finalized systems and applications of the optimized experimental methods will be detailed in chapters three through five. The major goals of this stage of the overall thesis work were to build and optimize two devices that would make specific aims 1 and 2 experimentally feasible in primary hepatocytes.

The first device, a density gradient electrophoresis (DGE) column, was built in collaboration with researchers at the Netherlands Cancer Institute based on an earlier prototype that showed potential for separating the vesicular organelles of the endocytic pathway at the desired subcellular spatial resolution [142, 147, 148]. Modifications, which will be discussed below, were made on a newly built device in the hopes of achieving enhanced separation and more consistent and efficient runs. It should be mentioned that a good deal of the assay development and optimization was performed in collaboration with Jennifer Fang, a BE masters student whose thesis centered on testing a large matrix of cell culture conditions, cell lysis and lysate processing techniques, and DGE run parameters to arrive at the optimization of hepatocyte organelle separation and fraction identification. A comprehensive summary of our joint assay development work has been described in Jennifer's thesis, as well as a more extensive review on the selection of an appropriate separation method from the available options. For brevity this chapter will highlight essential work and findings only, and the reader is referred to her thesis for further details [164].

The second device to be used in this work is a scaled up, perfused 3-D liver bioreactor for gene delivery studies in a tissue engineered liver surrogate. Previous experiments have been performed in the lab to examine adenovirus gene therapy and delivery efficiency in the original, smaller liver bioreactor systems developed in the Griffith lab [161, 162]. However, these original systems only housed on the order of 10,000 to 20,000 cells, and a very high multiplicity of infection (usually an MOI of 1,000) was used to achieve detectable levels of

EGFP transgene expression by interrogation via two-photon microscopy. As was discussed in the introduction, non-viral vectors typically yield transgene expression levels that are many orders of magnitude below those of their viral counterparts. As a result, it would be very difficult to measure transgene expression levels with enough resolution to quantitatively compare the performance of different non-viral carriers. Additionally, an end goal of this and future work is to develop bioreactor systems that allow for easy recovery of cells. In the original bioreactor systems and experimental protocols, the reactor housing was optimized for high performance in situ imaging of the liver tissue, but it was difficult to quickly recover the cells for quantitative downstream assays. A new system with more total tissue can also provide enough material for multiple assays from the same reactor, thereby providing a very high-information content assay system. With enough material, cells could be recovered and used to recover RNA, DNA and protein from the same system, or assays could be performed at the subcellular level now that sensitivity requirements could be met.

With two viable experimental systems at hand, a last step in the assay development phase is to ensure that the systems not only work for primary hepatocytes in general, but also for hepatocytes transfected with gene therapy vectors. Just as important is the screening and identification of new and interesting non-viral vectors that are able to be studied in these systems. Moreover, the development of robust viral and non-viral transfection protocols are needed that allow for accurate comparison of the vectors and determination of appropriate dosage levels that are clinically applicable, allow for unbiased comparison between vectors and between 2-D and 3-D results, and don't simply achieve high transfection levels due to unrealistically high dosages. These considerations will be discussed at the end of each section and the chapter as a whole.

2.2 DGE Device and Protocol Development

This section describes the newly built DGE device, device characterization, assay development and proof of concept results showing a preparative separation method that can be used to study the intracellular dynamics of gene delivery. Chapters 3 and 5 discuss final applications for this device. This section will primarily discuss preliminary and end results and the steps that were taken to optimize the overall protocol for cell lysis, lysate preparation

and loading and the DGE run. For a detailed, step by step description of the DGE protocol, please see Appendix 4.

2.2.1 The Device: Component Descriptions and Initial Characterization

The DGE device was constructed in collaboration with the H4 Tumor Biology Division of the NKI. The device follows the same design principles of the Tulp DGE prototype seen below in figure 2.1, with some modifications made to improve separation potential and efficiency. Briefly, the separation column (s) and the upper and lower electrophoresis buffer chambers (I and II) were machined in one piece from a cylinder of polymethylmethacrylate (PMMA). The electrode holders (n and B) are also made from PMMA, but are removable to allow for easy cleaning and maintenance of the column and chambers. Circular platinum and palladium electrodes (Pt, anode and P, cathode) were machined with exactly the same diameter of the separation column to ensure a more constant current density throughout the column, which has been shown to enhance separation resolution in the previous prototype. A non-gassing palladium electrode is required in the lower chamber because bubbles generated by a traditional gassing electrode would cause hydrodynamic disturbances to the contents of the separation column. The membrane (m), which is secured by an O-ring (o) to the rounded bottom of the separation column, allows for the passage of ions and serves to connect the column electrically, but not hydrodynamically, to the lower buffer chamber. Standard banana clips are used to attach the electrodes to a power supply, which powers the device at 300 volts under constant current conditions at roughly 10

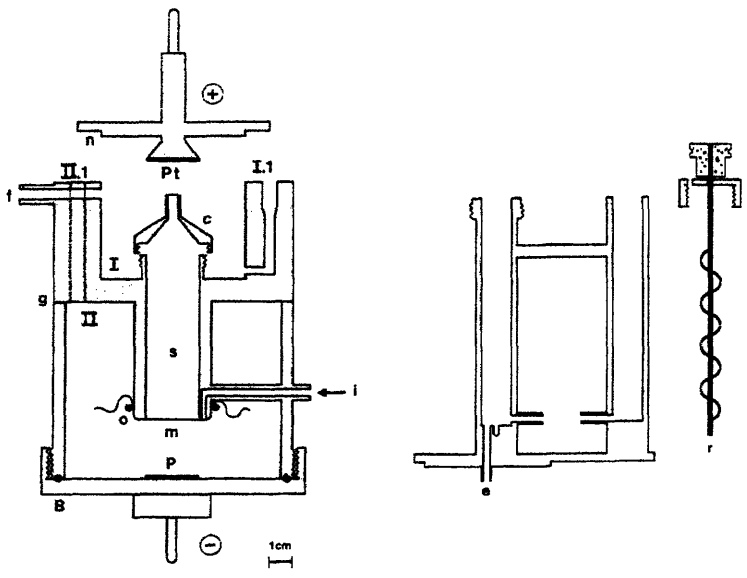

Figure 2.1: DGE prototype and gradient mixer. Schematic represents a cross section of the device, which is machined from cylinders of PMMA. [117]

milliamps. A multimeter is used to ensure that the current does indeed stay at 10 milliamps for the entire run, as this is crucial for repeatable, high-resolution separations since charged species maintain a constant electromigration velocity when driven by a constant current power supply. Since constant current conditions maintain migration speed but can lead to temperature increases and fluctuations, all runs must be performed in a cold room at 4°C to maintain density gradient integrity and sample band uniformity. The removable top cone (c) allows for precise and evenly distributed sample and density gradient introduction, as well as post-separation sample collection when outfitted with a capillary tube. A syringe pump is used to introduce separation media into the column via a specially designed inlet (i) that causes little disturbance to the column contents. The gradient mixer at the right of figure 2.1 consists of PMMA columns connected by a rubber tube at (v), and the mixing rod (r) is powered by a simple motor and variable voltage AC adaptor that can yield different mixing speeds for different stages of the gradient layering. The mixer base is fashioned such that it firmly interconnects with the top buffer chamber and allows for gradient introduction via the outlet (e) directly into the top cone.

In all DGE runs, a lower gradient, usually varying from 10-7% Ficoll, is layered in the column, and then the cell lysate is layered onto the column in a thin band of 6% Ficoll. Finally, a larger upper density gradient, usually varying from 5-0% Ficoll is layered over the sample. The top cone is then replaced by the electrode after the upper chamber (I) is filled with electrophoresis buffer. An electric potential is then applied to cause cellular organelles of different density and surface charge to migrate away from the initial sample band to different heights in the column. At the end of the run (usually 40-80 minutes) the upper electrode (n) is once again replaced with the cone (c), and a syringe pump can then be used to pump 10% Ficoll into the bottom of the chamber through the inlet (i) in order to elute the column contents through the cone and attach capillary tube and into a multiwell plate or fraction collector to acquire the separated organelles and assay for their location. Peristaltic perfusion pumps were built to continuously cycle electrophoresis buffer to and from inlet and outlet pairs for the upper (I.1 and f) and lower chambers (II.1 and II.1, one outlet occluded in view). This is especially important for the replenishment of the non-gassing palladium electrode in the bottom chamber. The device must also be completely level and free of vibration to yield the best separation results, so a vibration isolation platform is used under the device to ensure these optimal conditions.

One of the most significant changes that was made to the device was an increase in overall size in order to make a longer separation column. In the original prototype, the column measured 7 cm in length, but only 5 cm were actually usable since a water front co-migrates with cations across the bottom of the anion impermeable membrane during the course of a run. Traditionally, a 10% Ficoll cushion was left in the bottom 2 cm of the column and the initial sample band would migrate upwards into the upper 5% to 0% Ficoll density gradient that filled the remaining 5 cm of the column. Separation runs typically lasted 40 to 60 minutes, and the water front would remain below the 2 cm sample line during this short time. The new DGE device was designed with a column length of 12 cm, with buffer chambers, outlet and inlet sizes, and flow rates of buffer replenishment being scaled appropriately. This increased size was settled on due to empirical findings made by the Tulp lab and theoretical predictions that balanced sample band dispersion over the course of the run with overall separation potential between organellar cohorts for a given upper gradient length and overall separation column length [142].

Additionally, a more simple cellophane membrane that is permeable to both anions and cations replaced the original membrane, which was exclusively permeable to cations [142, 146]. Observation has shown that this new membrane significantly slows the rate of water co-migration into the bottom of the separation column, making for more usable column length and much longer run times. This will benefit the longer column as well in that more sizable density gradients can be used to potentially receive better organelle separation than that observed with the traditional 5% to 0% gradient of only 10-12 mL in total volume. Accordingly, a larger gradient mixer was also built, which can accommodate gradient layers of up to 30 mL. A larger upper orifice was also be incorporated in the upper electrode cap, so that O_2 and H_2 bubbles can be gently removed from the platinum electrode during operation, making for a more uniform electric field and better separations.

Some design flaws were discovered and remedied during the very initial characterization runs in cell lines that had been used with the previous prototype. Since the gradient mixer was made larger to accommodate the modified device, more air was present in the upper, unused portion of the mixing column. As a result, inserting the mixer caused a pressure disturbance great enough to distort the sample layer. While the newly designed upper electrode cap gave better access for the cleaning of air-bubbles during the separation run, it also allowed the electrode to move slightly during the cleaning, leading to more harm than

good for the uniformity to the electric field. The new openings in this electrode cap also gave the buffer in the upper chamber an alternate route of egress, and buffer merely spilled from the top of the chamber rather than from the small outlet tube. These circumstances led to a poor separation pattern, and the need for additional machining. To remedy the gradient mixer, two small holes were drilled in the top portion of the mixing column to expel air when the mixer is inserted. A groove was also cut into the motor housing and a stop pin was put on the outer surface of the column to put the mixing shaft tip at a more exact position further from the tube exit so the sample band would not be disturbed during upper density gradient administration. A removable clamp was machined from PMMA to keep the upper electrode steadfast during cleaning. The overflow problem was solved by simply boring the upper outlet tube to a larger diameter, so that it would pose less resistance to the exit flow.

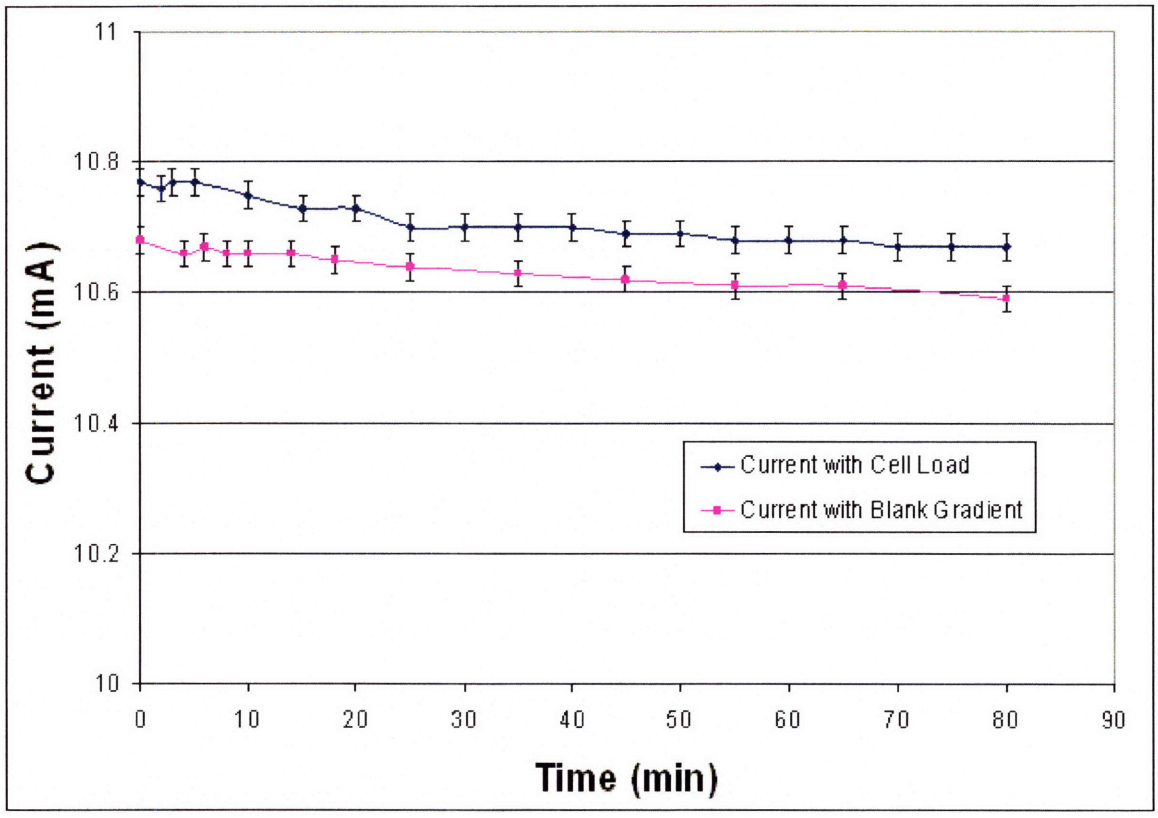

Figure 2.2: The new DGE device is able to maintain a constant current in the appropriate range over adequate separations times, both in the presence and absence of cell lysate. A commercially available electrophoresis power supply capable of running in a constant current mode with mAmp resolution is all that is required. This is a crucial feature of the device since migration velocity correlates directly with current, and constant organelle speeds allow for more effective and consistent separations.

With these modifications in place, the following run successfully recreated the separation pattern seen in previous experiments with the Mel Juso cell line. Odd fractions were assayed for β-Hex activity for lysosomal activity, HRP activity and total protein as can be seen in figure 2.4A. The HRP pulse-chase routine employed allowed for visualization of both early and late endosomal peaks. Fractionation experiments were then moved on to HepG2 cells, to evaluate the ability of the device to separate organelles in liver-like cells. Due to time constraints, only one run was performed on the HepG2 cells. Compared to past results obtained with the original DGE prototype, the system performed even better than expected (see figure 2.4B). Unfortunately, the second pulse of HRP was too long to effectively label the early endosomes, but the most surprising and positive results came from the fact that the late endosomal and lysosomal peaks were more than ten fractions apart from each other and very well separated from the total protein peak, which is where early endosomes normally localize to in DGE runs, whereas in the shorter column there had been no significant separation in HepG2 for these two subpopulations from the main peak (these runs were conducted in the very first DGE prototype [146], with only 3 cm of usable column and 40 minute runs). This set the grounds for further optimization in primary hepatocyte cultures.

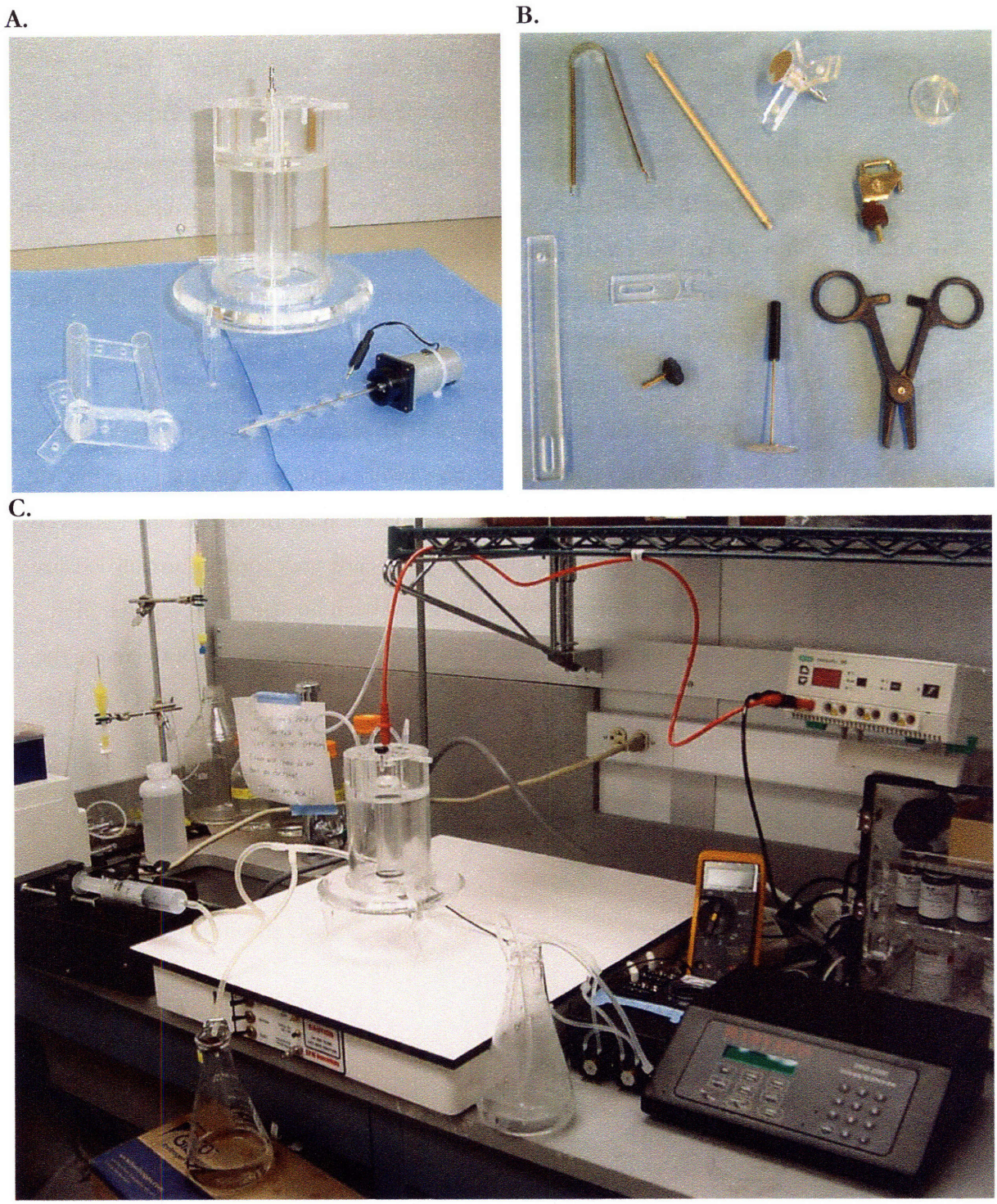

Figure 2.3: A) DGE device with palladium electrode base and platinum electrode at top. The gradient mixer is at the lower left and the mixing motor is at lower right. **B)** Peripheral components for the device, clockwise from top left: loading tweezers and extraction tool for ultracentrifuge, platinum electrode, top cone for sample loading and recovery, adjustable C clamp for lower waste tube between syringe pump and column, scissor clamps for gradient mixer connection tube, metal sieve to protect column contents during buffer addition/removal to upper chamber, clamp and screw for platinum electrode alignment, long arm to replace clamp to hold elution tubing during sample collection. **C)** Working device on vibration isolation platform and integrated with peripheral components, clockwise from left: syringe pump for chamber filling and sample collection, power supply, ammeter, syringe pump controller, peristaltic pumps for buffer circulation, buffer flask, and waste flask for gradient addition.

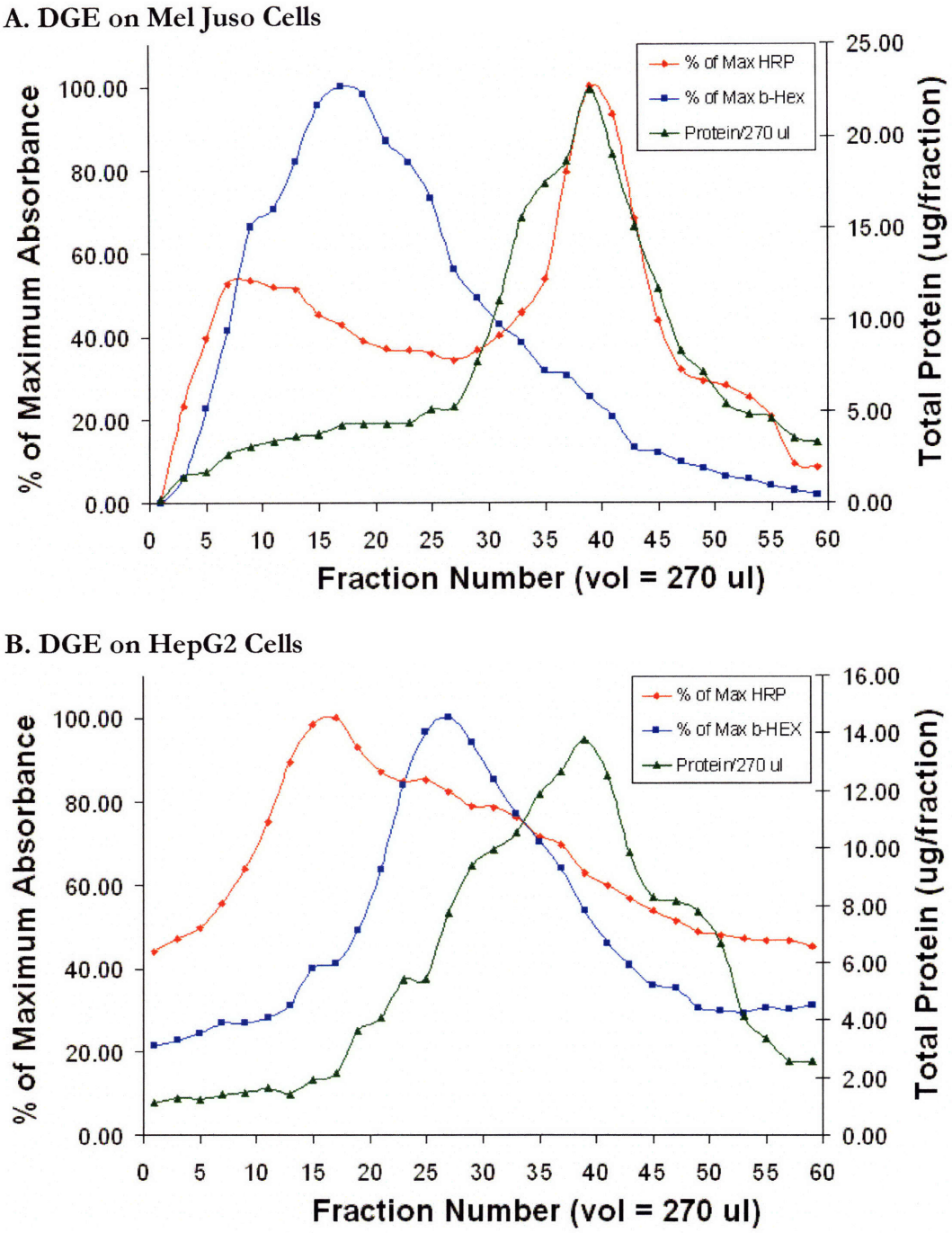

Figure 2.4: Results of initial characterization runs on cell line cultures using the original upper gradient length on the new column. **A)** Fractionation of Mel Juso cells, the most well characterized cell line on the earlier DGE prototype. Cells were pulsed with HRP for 4 minutes, chased with unlabeled media, pulsed again for 3 minutes to label both early and late endosomes (right and left HRP peaks). The β-Hex assay indicates the lysosomal peak, and the protein assay shows the main total protein peak the organelles migrated away from. This data exactly recapitulated what was seen in the earlier prototype, showing that the physical changes to the new device did not hinder separation with the original run conditions. **B)** Fractionation of HepG2 cells to gauge the potential for separation in liver like cells. The 4 minute, 27 minute, 7 minute pulse-chase-pulse regiment was not optimal to label the early endosomes, but this run showed excellent separation of late endosomes and lysosomes from the total protein peak. **Note:** Fraction 1 is at the top of the column and fraction 60 fraction 60 is at the bottom of the lower gradient at the end of the run. This holds in all subsequent DGE output plots.

2.2.2 DGE Optimization for Primary Hepatocyte Fractionation

After the initial characterization runs at the NKI and integration of new peripheral components to complete a new DGE set-up at MIT, characterizations runs were performed on primary rat hepatocytes to determine how the original protocol and run parameters would fare. Unfortunately, these first separations runs did not yield a desirable output. Fractions were assayed for β-Hex and total protein alone to simply see if a single lysosomal peak could be separated from the total protein peak. Unfortunately, multiple lysosomal peaks were observed at different locations in the column, and a significant portion of lysosomes was still stuck with the total protein peak (see Fig. 2.5).

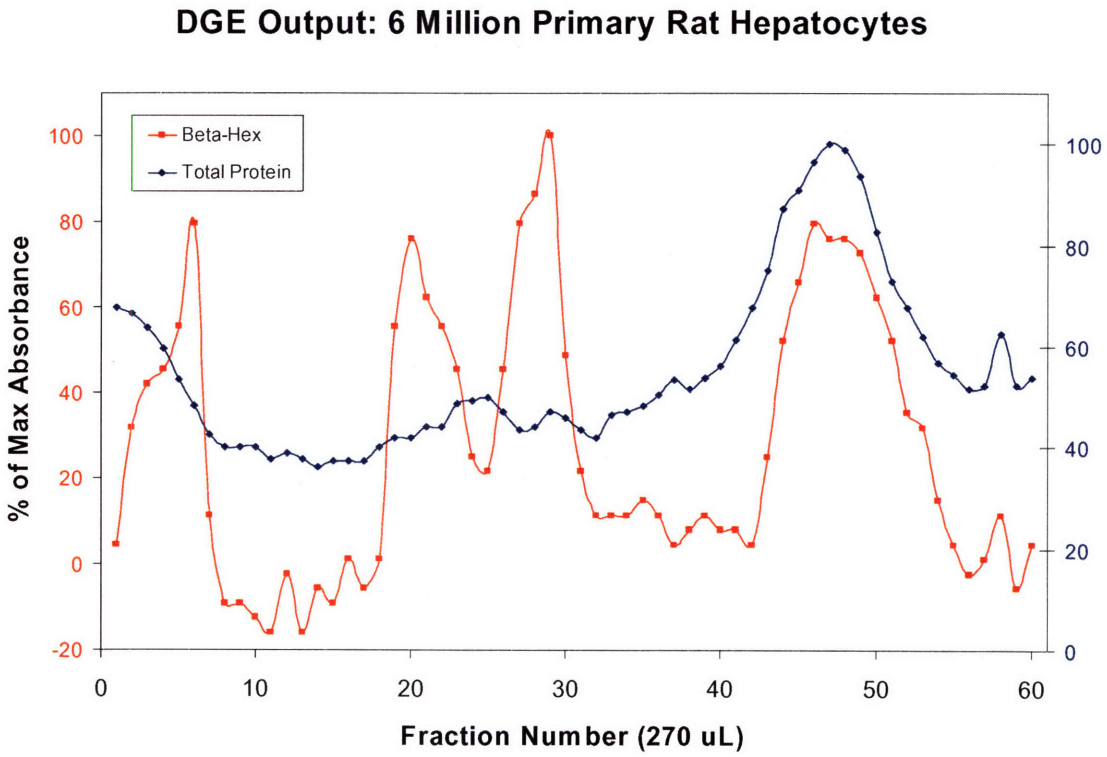

Figure 2.5: DGE output for an 80 minute run on 6 million hepatocytes plated on an adsorbed collagen monolayer. The same run conditions and gradients volumes (6 mL lower, .5 mL sample layer, 10 mL upper) were used as with the initial cell line runs.

This result suggested that both sample processing and DGE run parameters needed to be optimized for the primary cells. The rest of this section will summarize the changes that were made to the protocol in order to obtain acceptable resolution in the separation of early and late vesicular organelles from hepatocytes.

1) Cell Culture Conditions and Cell Number per Run

A modified protocol was developed for the preparation of adsorbed collagen monolayers (see Appendix 3). Drying the monolayers after the adsorption of collagen allowed for better cell adhesion and morphology and ultimately better DGE separations. There had been prior evidence in the literature that dried monolayers were superior for culturing primary cells such as hepatocytes [165-169]. This avoided the need to move experiments to collagen gels or gel sandwiches, which would have made cell collection and lysis far more difficult and could have potentially made time course studies for trafficking impossible with the desired temporal resolution. Successful separations were obtained with cultures of 24, 48 and 72 hours on these surfaces (with daily medium changes); however, DGE runs for final characterization and data sets were only performed on hepatocytes within 24 hours of seeding to make sure that data was obtained on cells that had undergone as little de-differentiation as possible and maintained cuboidal morphology and other traits of hepatic phenotype maintenance [164].

Fewer total hepatocytes were also loaded onto the column, due to the fact that primary hepatocytes have a greater amount of total protein per cell. For Mel Juso cells, the cell limit had been established at 10 million cells/DGE run. However, for hepatocyte runs approaching these numbers it seemed that the organelles were not escaping from the total protein peak efficiently and streaming effects may have been muddling the separation of the lysosomes. Experiments were moved to 60 mm dishes seeded with 2.4 million hepatocytes. Culture medium was also changed 4 hours post-seeding to remove debris and prevent overcrowding. Cutting down on debris significantly improved cell lysis steps and overall separation. Considering the wash step after seeding, washing during sample processing, retention of a small fraction of the whole cell lysate and post-nuclear spin supernatant, DGE runs successfully separated organelles for a column load of roughly 1-1.5 million primary hepatocytes.

2) Cell Lysis

Since hepatocytes have a larger diameter than HepG2 and Mel Juso cells, a larger gauge needle was settled on for cell lysis. Ultimately, a 21G x 2 inch needle was used with a 3 mL syringe. Cells were also collected in a greater volume of DGE buffer, as a more dilute

cell suspension was found to lyse far more efficiently. Cells were still allowed to swell on ice in hypotonic DGE buffer for 20 min before 12 expulsions through the syringe. As long as the tube was prechilled before collection, endocytosis was complete halted at the time points of interest regardless of this swelling time and a lysate with greater than or equal to 98% pure nuclei was consistently obtained. Cell washing and labeling steps, as well as cell collection and lysis technique specifics are highlighted in Appendix 4.

3) Cell Lysate Processing

After the nuclei are spun out of the cell lysate, the supernatant must be trypsinized in order to free up the different vesicular organelles from cytoskeletal filaments. The trypsin type used and the trypsinization time are highly important and can have different effects in different cell types [170]. After testing a number of trypsin types and digestion conditions, it was found that using Trypsin type XII A for six minutes was optimal. It was also found that adding cold PBS instead of DGE buffer to the supernatant after inhibition of the trypsin but before addition of extra protease inhibitors maintained organelle integrity and yielded a larger organelle pellet after ultracentrifugation.

4) Sample and Gradient Layering and Run Duration

One of the biggest advantages that this new DGE device provided was the flexibility to perform runs with larger density gradients or gradients over different ranges of Ficoll concentrations. The separation column length in the original prototype limited the lower gradient to be no more than 6 mL (3 mL of 10% and 3 mL of 7% Ficoll in each leg of the gradient mixer) and the upper gradient to be no more than 10 mL (5 mL of 5% Ficoll and 5 mL of DGE buffer with no Ficoll in mixer). Increased gradient lengths and run times were tested in the hopes of attaining wider separations between the different classes of organelles. The conditions that were found to give the best separations in primary hepatocytes were an eighty minute run at 10.6 mAmps and 300 volts (constant current mode), with 0.5 mLs of sample in 6% Ficoll layered between the original 6 mL 10-7% lower gradient and a much larger 25 mL 5-0% upper gradient. An optimized protocol was also developed which took advantage of the computer controlled syringe pump, variable rate power supply to the mixing motor, and more pliable tubing at the lower column inlet to ensure that the sample

layering and gradient introduction resulted in an extremely flat and thin sample layer, which greatly enhances separation potential in the device.

5) Sample Collection and Fraction Assays

A movable based was used to allow for easy collection of samples in small and large well 96 well plates. This allowed for a higher flowrate during sample collection while still providing careful control over fraction size to gauge what the optimal volume was to retain resolution between organelle subpopulations but reduce the total amount of assays to map the fractionation pattern. Assays were miniaturized so that throughput could be increased by reading fractions in a multiwell plate reader format.

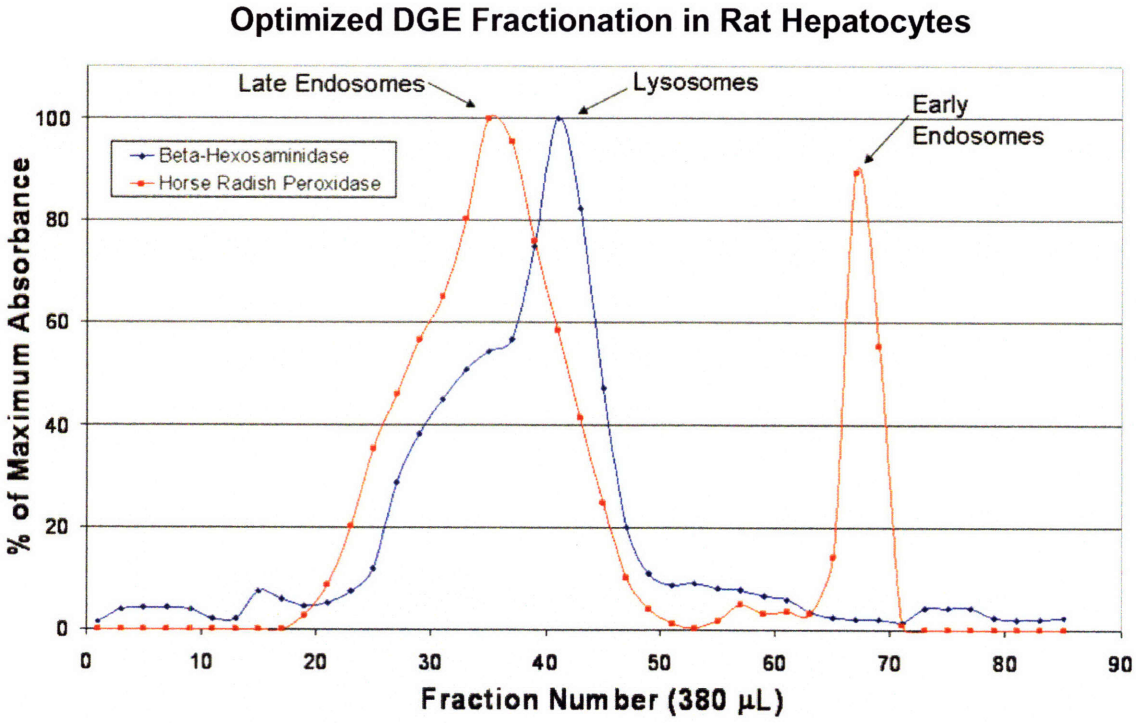

Figure 2.6: Fractionation pattern of primary hepatocyte organelles after optimization of the overall DGE protocol. Odd fractions were probed for HRP after a dual pulse chase pulse to label early and late endosomes. Optimal pulse chase pulse conditions were found to be 4 minute pulse – 15 minute chase – 3 minute pulse. Assay for β-Hexosaminidase shows the location of lysosomes after the DGE run. The DGE device successfully separates these three organelle types. Late pulse only and early pulse only DGE runs only show one HRP peak in the appropriate location, giving support that these peaks are indeed separate endosome sub-populations (see Chapter 3).

As can be seen in figure 2.6, optimization of this large panel of sample processing techniques and run parameters has achieved excellent separation of the organelles of interest on primary hepatocytes. This work was then extended to better fraction identification via various sample concentration techniques and western blotting for membrane proteins unique to early and late endosomes. While traditional protein precipitation techniques were not compatible with the separation buffer, the fact that DGE fractionation is completely preparative and keeps organelles intact after the run is complete was exploited to attain a novel concentration method. DGE runs were performed on HRP pulsed hepatocytes and the fractions comprised the second late vesicle HRP peak were recollected in an ultracentrifuge tube and spun down at 100,000 x G for an hour. This repelleted the organelles in those fractions, and the pellet was resuspended in sample buffer and run on an SDS-PAGE gel. A western blot was then performed where the late endosome fraction, the post-nuclear spin supernatant (PNS) (which should contain all vesicles) and the post-endosomal ultracentrifugation spin supernatant (which should only contain a small amount of broken vesicle membranes if any) were blotted with two antibodies. One antibody, anti-Rab9, is specific for late endosomes, while the other, anti-EEA1, is specific for early endosomes [164]. These antibodies were previously optimized for primary hepatocyte cell lysates [164]. In the late fractions sample, there was a strong Rab9 signal and no detection of EEA1 binding. This provided strong evidence that the late fraction exclusively contains late endosomes and that there are indeed two distinct endosomal populations separated by the DGE device.

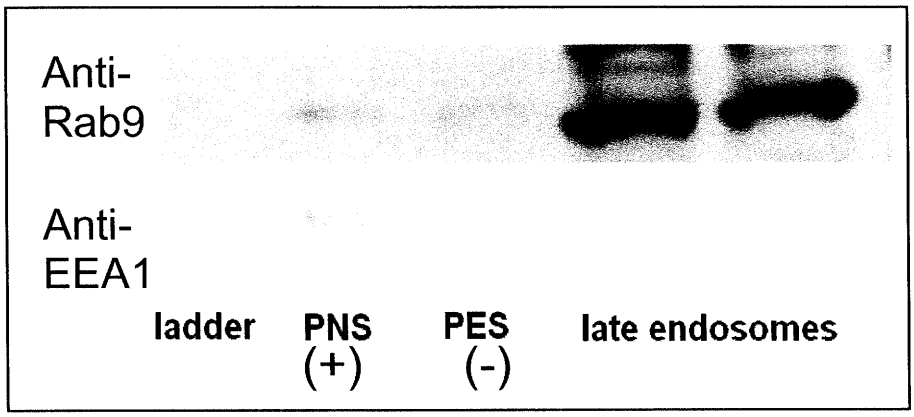

Figure 2.7: Western results probing for late and early endosomes in a positive control (PNS), a negative control (PES), and in vesicles spun down from the leftmost "late endosome" peak from HRP pulse-chase-pulse mapping of a DGE run. Rab9 is a Rab GTPase specific to late endosomes and EEA1 or early endosome antigen one, is a protein complex specific to early endosomes.

2.2.3 Feasibility of DGE Analysis for Gene Delivery Tracking

With robust separation of organelles optimized for primary hepatocytes, the remaining task at hand for assay development was to verify that this approach could truly be effective in measuring non-viral vector trafficking. The biggest question that remained was whether or not DGE would still work in the presence of cationic non-viral gene delivery complexes, or if the separation pattern would be greatly deflected by the addition of these dense, charged particles to the cells and organelles. Additionally, if an acceptable separation pattern is still attainable in transfected cells, can the delivered plasmids be recovered from the various cell fractions in a large enough amount that they could still be measured via real-time quantitative PCR.

Figure 2.8 shows that upon gene delivery with polyethylenimine/plasmid DNA gene delivery complexes and a standard HRP pulse-chase-pulse labeling, the DGE fractionation pattern results in organelle peaks that are a bit more spread out in width and shifted downward in the column slightly. The late endosome and lysosome peaks are also less well separated, likely due to the fact that NV complexes are building up in these vesicles and as a result there may be less of a difference in density between them. Overall, DGE fractionation is able to repeatedly separate a late and early vesicular fraction such as this particular example, and as a result the approach should be able to provide increased spatial resolution in for quantitatively studying gene delivery trafficking dynamics.

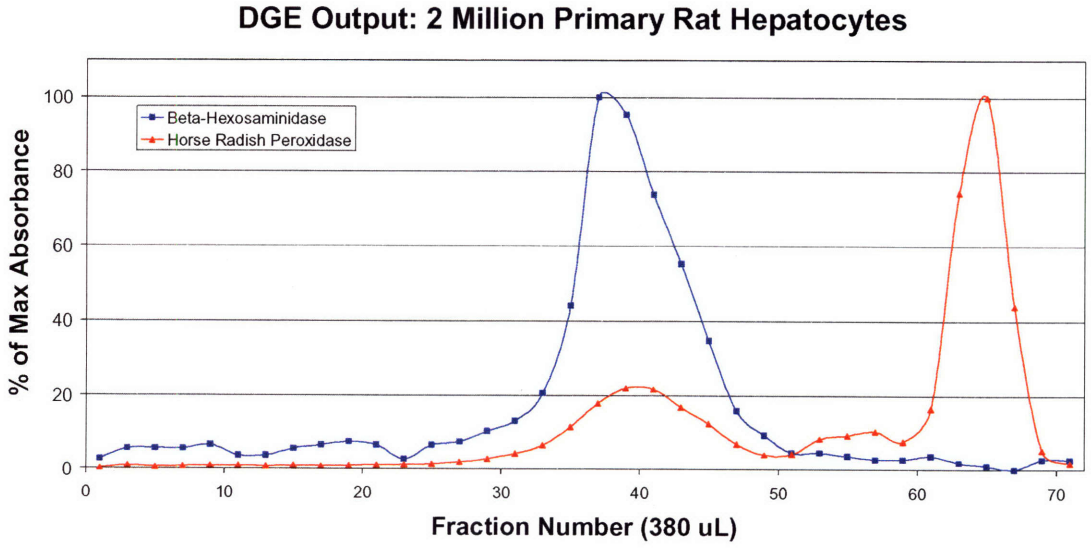

Figure 2.8: DGE fractionation pattern for a cell sample processed 40 minutes after delivery with a PEI25 non-viral gene delivery vector complexed with plasmid DNA at an N/P ratio of 20. 10 ug of total DNA was delivered to the cells at a concentration of 5 ug/mL of HGM.

The fact that the DGE device was able to achieve more than thirteen 380 uL fractions of separation between the fractions containing the late and early vesicular peaks in the presence of gene delivery vector provided an added advantage for future experiments as well. Instead of taking these smaller volume fractions in a conventional 96 well plate, fewer larger fractions could be taken in a deep well plate and still allow for enough resolution to separate the two cohorts. This significantly cut down on the amount of samples that had to be processed for DNA purification and real-time PCR.

In the end, it was determined that twenty four 1.25 mL fractions could be collected for each run. This accounted for the entire volume of the upper and lower density gradients and the original sample band volume, and still provided adequate separation between the late and early peaks. As a result, DNA could be purified from each fraction instead of only probing alternating fractions. Therefore, with a simple volume correction calculation, all plasmids were accounted for in actual measurement and could simply be added up to determine the total number of plasmids in each vesicle type. This method is far less error prone than probing a few fractions and then devising an integration function to interpolate the total number of plasmids in each vesicle, which would have been the required method if a larger number of fractions were required to achieve the desired spatial resolution. This higher volume also provided enough material to perform these assays in multiplicate in order to ensure the most accurate measurements possible, while also allowing for enough material to assay for β-Hex activity in every fraction to provide absolute certainty that the lysosomal peak separated well in each run and that plasmids were being mapped to proper vesicle type.

A DNA purification protocol was optimized using a high-throughput 96 well plate format to purify delivered plasmids from four full runs at once. A previously optimized Taqman primer and probe set and protocol were then used to quantify the number of delivered gWiz β-Gal plasmids in each fraction by comparing the cycle threshold numbers of each sample to a plasmid standard curve. Figure 2.9 shows two example of these preliminary plasmid mapping experiments, which showed that DGE could be used to quantitatively track plasmid delivery dynamics in primary hepatocytes.

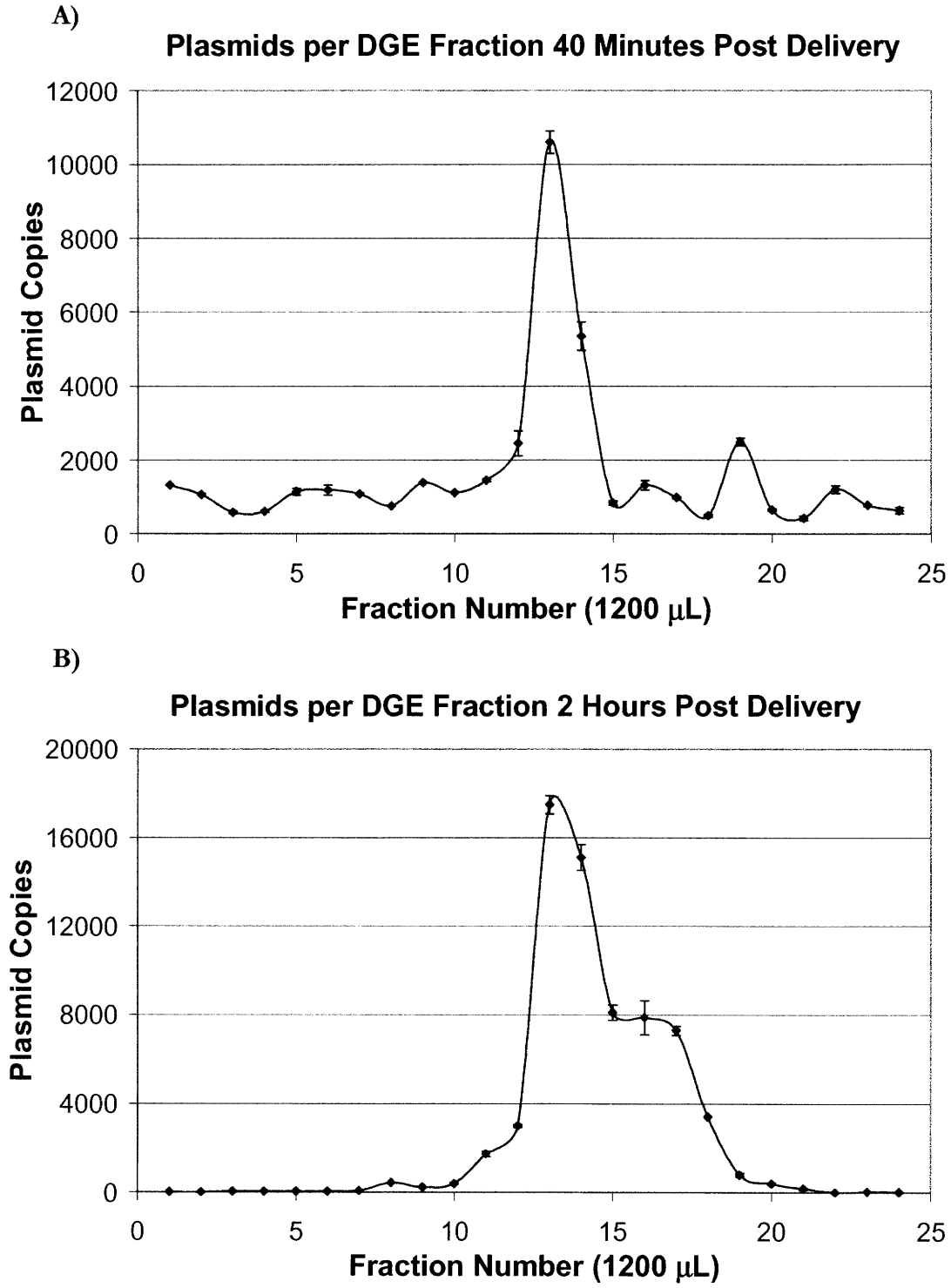

Figure 2.9: Quantitative real-time PCR measurement in larger DGE fractions to track plasmid trafficking **A)** 40 minutes after and **B)** 2 hours after transfection with a PEI 25 vector complexed with gWiz β-Gal Plasmid at an N/P ratio of 20. 10 ug of plasmid DNA in 2 mL of HGM was delivered to 2 million hepatocytes for both cases. At 40 mins post delivery, it can be seen that most plasmids have already trafficked to the late vesicles with a small amount remaining in the early vesicles. At 2 hours nearly all of the plasmid has built up in the late vesicles and these unescaped complexed have caused the late fraction to shift lower in the separation column.

2.3 Optimization of a Scaled-up 3-D Liver Bioreactor

As was discussed in the chapter introduction, the development of a larger perfused liver bioreactor is necessary to meet the needs of a number of experiments including the quantitative evaluation of non-viral gene delivery carriers. At the beginning of this thesis work, a "giant" liver bioreactor was in its nascent stages of development. This new reactor, seen below in figure 2.10, was scaled up from the previously designed Milli-F reactor using basic design principles. The giant reactor houses one thousand 300x300x230 um square channels in its scaffold as compared to the forty channels of the same size in the Milli-F reactor. Combined with a removable top window to allow for easier and more efficient seeding, this reactor has the potential to culture on the order of one million cells, which would meet the sensitivity demands of a number of new assays and experimental strategies.

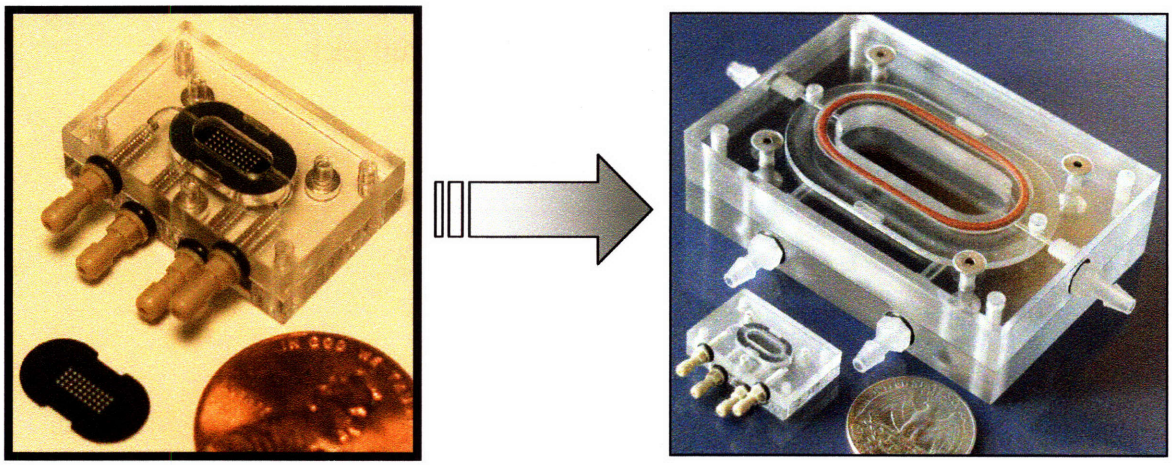

Figure 2.10: The scaled up giant reactor next to its smaller predecessor, the original Milli-F reactor.

Design principles and microscopic design parameter considerations to recapitulate the essential elements of the *in vivo* liver microenvironment in an *in vitro* system for the original Milli-F reactor have been extensively covered in previous work in our lab [161, 162, 171]. Since the giant reactor employs a scaled up array of channels that remain at the same length scale for each functional channel unit, many of these findings and work carry over to the new system. This new reactor still utilized a dual perfusion pump system that supplied the flow of culture medium into the upper and lower reactor chambers to control the flow rate of the media over and through the channels of the cell containing scaffold, the middle filter and the bottom support scaffold. Since the channels were the same size of those of the Milli-F scaffold and there were simply more of them, oxygen and nutrient diffusion

limitations were the same within each functional unit of the reactor. Under the assumption that the middle filter provided the main resistance to perfusion flow and therefore dictated a uniform flow rate through every channel, flow rates were linearly scaled up to keep the per channel flow and residence time in the upper chamber the same as that in the Milli-F.

Initial runs in the new system, however, proved problematic. The increased number of cells in the system led to a good deal of debris in the fluidic circuit after both seeding and reversal of crossflow. There also appeared to be recirculation of medium occurring in the upper flow chamber. These issues compounded in the build-up of pressure in the system. Peristaltic pumps would break down, and if they were able to continue operating, pressure would build up enough to crack the silicon scaffolds. The traditionally used inline filters were unable to handle the debris load after the crossflow change and usually resulted in prematurely ended runs with no crossflow if the scaffolds didn't crack. It is universally accepted in past work in our lab that reactors seeded with day three hepatocyte spheroids should be cultured for an additional 4 days in the bioreactor before liver phenotype and tissue structure and reorganization have reached a more in vivo like state suitable for performing assays of interest. Since these new reactors could not consistently reach day seven of culture post isolation, a number of improvements needed to be made to achieve a viable system.

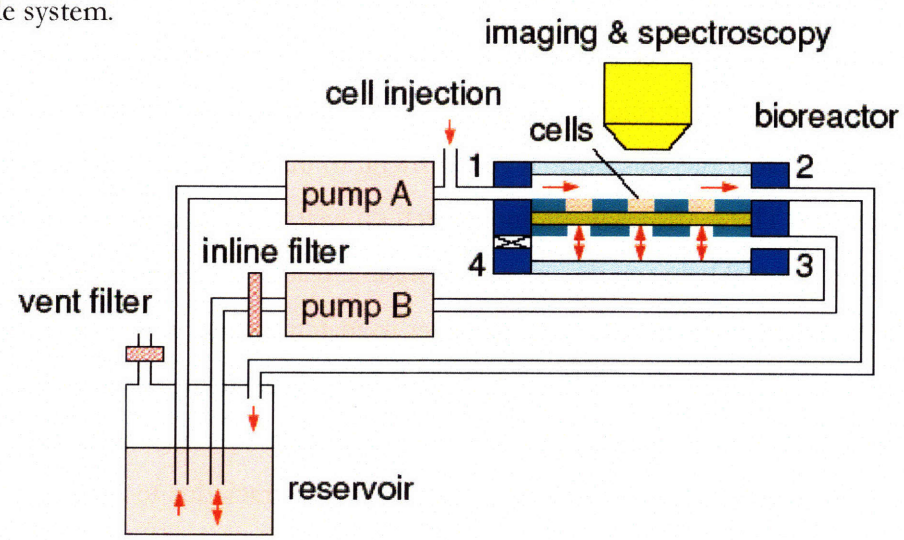

Figure 2.11: General schematic for the Milli-F reactor fluidic system and reactor pocket components [160]. Two peristaltic pumps drive the flow of culture medium over the top of and through an upper cell holding scaffold and a lower support scaffold. A 5 um filter is sandwiched between the two scaffolds to provide precise and uniform control over the rate of perfusion flow through the tissue aggregates in the upper scaffold channels and to aid in the retention of cells during initial seeding, cell attachment to the scaffold walls, and tissue reorganization. The giant reactor follows the same general scheme with some modifications that will be described in subsequent sections.

2.3.1 Improvements for the Giant Reactor Culture System

A number of modifications were made to the physical components of the giant reactor, as well as to the steps of the seeding and maintenance protocols, in order to achieve a viable scaled up liver surrogate for gene delivery studies and other applications that required a higher cell number. These improvements are summarized in this section. For a detailed assembly, seeding and maintenance protocol, please refer to Appendix 6.

1) Materials Changes

A number of new materials and parts were adapted for components of the fluidic circuit and reactor pocket. One significant problem with the original set-up concerned the scaffold material and alignment issues of the scaffolds in the reactor pocket. While silicon wafers with etched channels provided an excellent scaffold for the smaller reactor versions, they provided a number of problems in the giant reactor. First of all, due to the physical area of exposure available at the MIT facilities for etching these scaffolds from a master wafer, only two giant reactor scaffolds could be made at a time (as compared with 30-50 scaffolds at a time for the smaller reactors), making them very costly and tedious to fabricate. In order to ensure uniform crossflow through the channels, the top, cell containing scaffold and the bottom, support scaffold need to be perfectly aligned. To accomplish this, scaffolds were machined with very stringent tolerances to exactly match up with the width and length of the reactor pocket. Practically, this made it very difficult to insert the scaffolds into the reactor pocket however. The scaffolds would not match up well with the different gasket materials used to create a seal between the upper and middle reactor body pieces and the lower and middle body pieces (It had been much easier to match up and peel off the gaskets without breaking the scaffolds in the small reactor due to the much smaller aspect ratio of the original scaffolds). This either broke the scaffolds, or significantly delayed assembly time. If assembly was successful, the scaffolds would frequently crack due to the aforementioned pressure buildups.

These problems were solved by moving to polycarbonate scaffolds to seed cells in a more flexible material that could deal with initial pressure fluctuations without breaking and also be easier to load into the reactor pocket. Drilling methods did not provide enough precision for proper alignment, so channel fabrication was performed via laser machining.

Designs for a blocking mask were sent to a laser machining company (J.P. Sercell and Associates), and different exposure times were tested to assess overall cost with precision. A longer exposure time at a lower power causes less warping in the polycarbonate and therefore more precision for alignment, but is also more tedious and costly. Scaffolds were tested at 16, 23, and 28 minutes of exposure with the appropriate power levels to finish etching in that span. Alignment holes were also etched in the sides of the scaffold that would fit exactly over new alignment pins in the reactor pocket. This alignment strategy was now possible with the more flexible polycarbonate. It was found that all 28 minute scaffolds aligned well with at least one other scaffold in the group, and roughly half of the 23 minute scaffolds aligned well in specific pairings. None of the 16 minute scaffolds aligned particularly well. This approach yielded 8 pairs of usable scaffolds. The scaffolds were easy to assemble, aligned well in the reactor pocket, and sealed up well with new silicone gaskets.

Changes were also made to the reservoir, tubing, and connectors in order to decrease pressure buildup and recirculation of debris in the system. Larger diameter connectors were used to decrease the chances of clogging and the required pressure drop. Similarly, larger tubing was also used for connecting tubing and peristaltic tubes. The larger peristaltic tubes also decreased the amount of work the pump had to expend for a given flow rate. This decreased wear on both the pumps and the tubes. Additionally, the inlet tubes on the inside of the reservoir cup were shortened such that they would pick up less of the unseeded cells and debris that would build up on the reservoir floor, thus cutting down on the amount of debris being recirculated in the system.

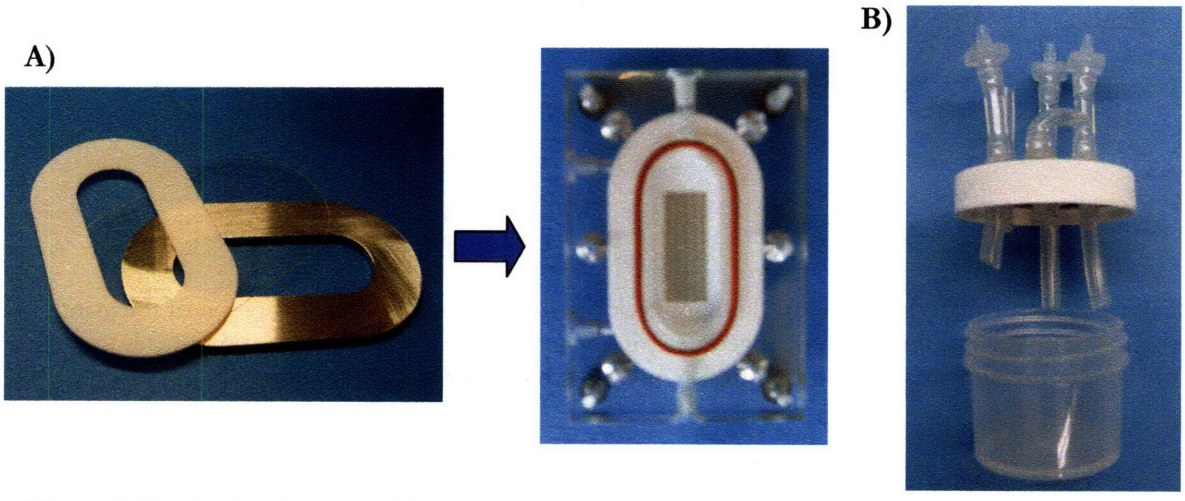

Figure 2.12: A) New laser machined polycarbonate scaffolds and silicone gaskets and **B)** larger tubing and connectors and shorter inlet and outlet reservoir tubes helped to significantly improve the performance of the giant reactor.

2) Improved Flow Chamber Geometry

It was also suspected that simply proportionally scaling up the flow chamber volumes and inlets and outlets to a lesser extent may have created non-uniform or recirculating flow in the upper chamber. Computational fluid dynamics simulations were performed in Femlab to investigate this suspicion. Simulations revealed that flow was breaking down in the upper chamber and that some recirculation was occurring at the outlet end of the chamber (see figure 2.13). As a result new geometries were tested in Femlab to find inlet and outlet designs that would allow for uniform flow over the scaffold array over the range of velocities that could be used in the new set-up. A new design was settled on that showed improved uniformity in flow over the cells, quelled high velocities before the scaffold array, and maintained straight streamlines into and out of the upper chamber (see figure 2.14).

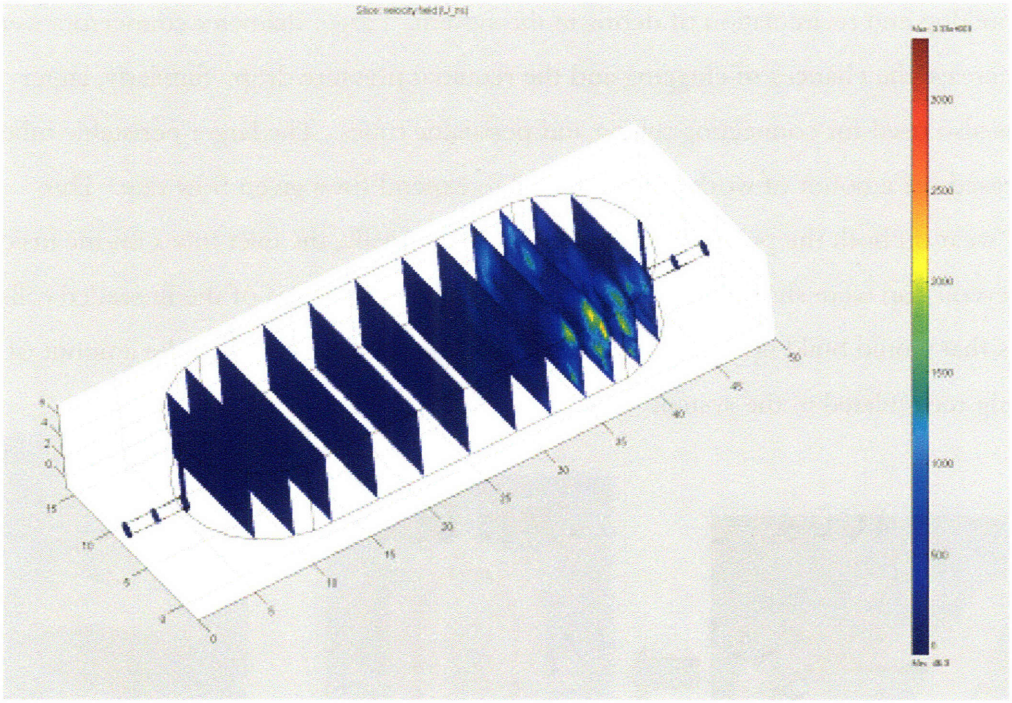

Figure 2.13: Femlab simulation of fluid flow velocity distribution in the first iteration of the giant reactor. The original upper chamber geometry in the giant reactor led to recirculation of culture medium in the upper chamber and complete breakdown of flow at high velocities.

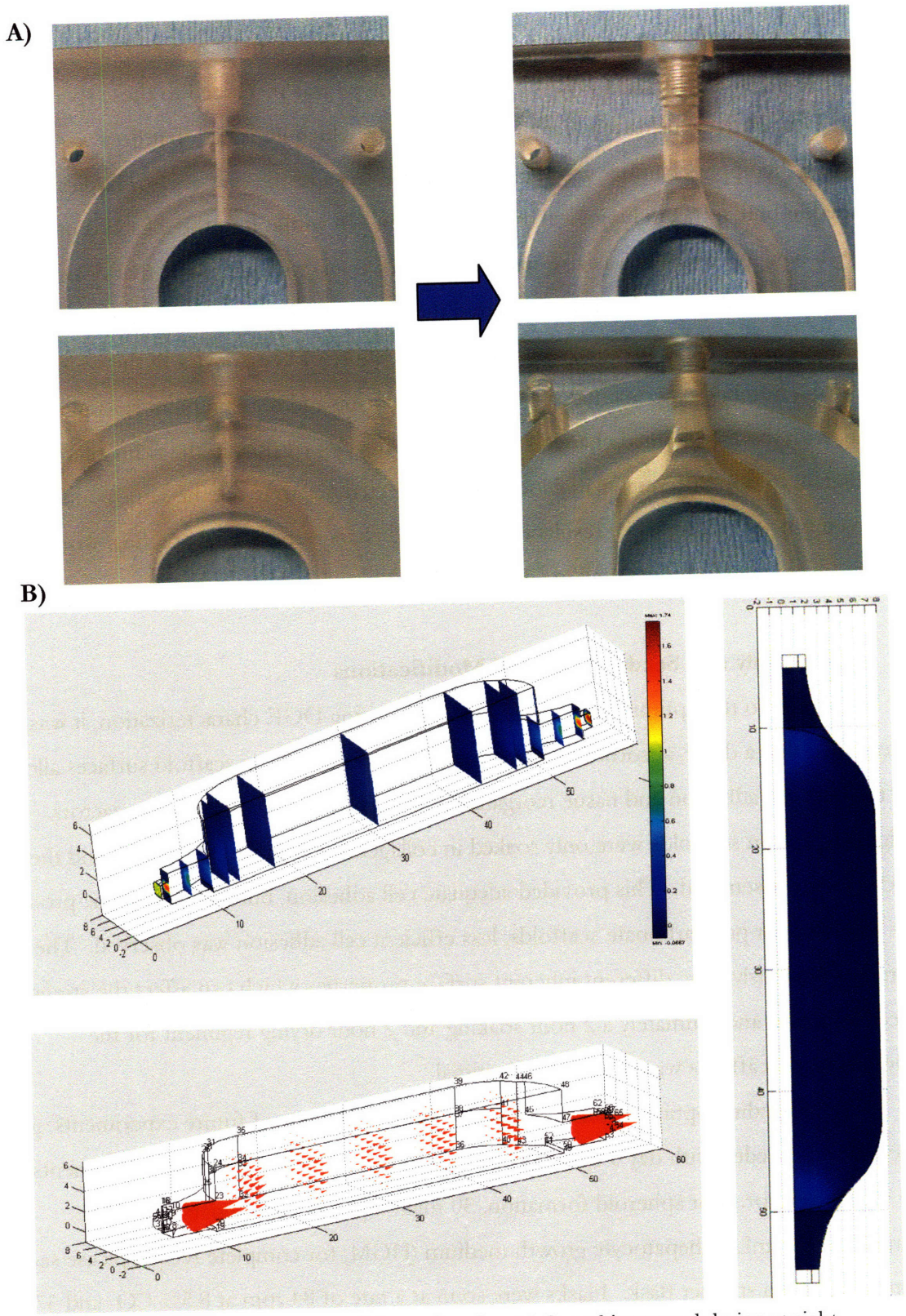

Figure 2.14: A) Original giant reactor inlet and outlet at left, and improved design at right. **B)** Femlab CFD simulation results for the new design, CCW from top: The new geometry results in uniform fluid flow over the scaffold array with high velocity quelled before the channel containing area of the scaffold. Streamlines indicate that no recirculation is occurring, and velocity is very uniform and non-zero just above the cell bed. Reactor body was cut in half for faster computation.

These modifications appeared to completely resolve recirculation and flow uniformity issues for the giant reactor. A new prototype was machined to these specs and evaluated qualitatively using dye tracking experiments, which indicated that flow was indeed uniform in the upper chamber with no recirculation. As a result, new reactor bodies were machined in bulk to begin biological characterization. In addition to the inlet and outlet changes a new top window was also machined with a thicker middle insert that decreased the upper chamber volume and in turn decreased the residence time for the medium in the upper chamber, which is advantageous for general culture of hepatocytes in the system as well as for a number experimental applications for dosing and measurement sensitivity. In general, with these combined changes, there is fully developed flow in the main chamber such that all cells in different spatial locations in the channel array see the same conditions at any given time in culture. The results of this second change and arrival at a final working system are covered in more detail in Chapter 4.

3) Assembly and Seeding Protocol Modifications

Similar to the optimization for 2-D cultures during DGE characterization, it was determined that a dried, adsorbed collagen monolayer on the upper scaffold surfaces allowed for the best cell adhesion and tissue reorganization in hepatocyte seeded giant reactors. Originally, silicon scaffolds were only soaked in collagen solution for 30 minutes and then reactors were assembled. This provided adequate cell adhesion, but when the same protocol was followed for polycarbonate scaffolds, less efficient cell adhesion was observed. The two materials obviously have different inherent surface properties which can affect the strength of cell adhesion and ultimately a 2 hour soaking and 2 hour drying regiment for the polycarbonate scaffolds was found to be optimal.

In all seeding optimization experiments and the majority of future experiments, giant reactors were seeded with day 3 spheroids to maintain consistency with past experiments in the Milli-F reactor. For spheroid formation, 30 million primary rat hepatocytes were cultured in 100 mL of hepatocyte growth medium (HGM, for complete recipe, please see Appendix 2) in a spinner flask. Flasks were spun at a rate of 84 rpm at 8.5% CO_2 and 37°C for 3 days. One important rule in giant reactor seeding is to avoid overseeding. A single giant reactor should not be seeded with more than 2 million cells. It is difficult to count actual cell numbers in spheroids or to accurately count spheroids themselves and thus some

estimating is necessary. If spheroids are size fractionated between 100 and 300 um in size for seeding, the efficiency of cell recovery has been estimated to be roughly 20%, meaning that for 30 million cells seeded into a spinner flask, 6 million cells will be recovered in seedable spheroids. If the size range is extended to between 50 and 300 um in size, then recovery is closer to 35-40%. This will ensure that roughly 10-12 million seedable cells will be recovered. The second size range was settled on ultimately, but some initial characterization runs were performed with the 100 to 300 um size range of spheroids being seeded. A general rule that should be followed is to seed three reactors per spinner flask for the 100 um cutoff and 5-6 reactors per spinner flask with the 50 um cutoff.

Seeding is also far more efficient if BSA containing media is used to prime the system after assembly and is also used to resuspend and seed the recovered spheroids. In albumin free medium, the spheroids aggregate considerably and reduce the number of cells that can be pipetted into the channels. With BSA in the medium, it is completely safe to repeatedly pipette the cell suspension up and down over the scaffold channels with moderate downward crossflow turned on to ensure the most even seeding of the channels. Some initial characterization runs were performed with albumin free medium to compare results and liver phenotype in the system to previous albumin free data in the Milli-F. However, subsequent experiments described in Chapter 4 use HGM with BSA. Additionally, a medium and reservoir cup change 2 hours after seeding greatly helps in reducing debris and extra cells from the system if slight overseeding has occurred. For full details on the optimized seeding protocol, please see Appendix 6.

4) Maintenance Protocol Modifications

After 24 hours of culture in the reactor, crossflow direction is normally changed. After seeding, a downward crossflow is maintained at a flow rate of 1 mL/min, or 1 uL/min/channel (which was the same rate used in the Milli-F). This helps to retain the cells in the channels as they attach to the walls and begin to reorganize. After 24 hours, the crossflow is reversed to an upward direction at the same flowrate to remove dead and unattached cells and other debris from the channels. This reversal in cross flow means that medium is now pumped from the reservoir into the bottom flow chamber. If the freed cells and debris circulating in the system get pumped into the lower chamber and up against the bottom of the filter, crossflow can get blocked. To make certain that this perfusion flow is

maintained for the duration of the culture, an in-line filter is placed on the crossflow line before it gets to the reactor, thereby screening out debris and only sending clean medium to the bottom chamber.

In the Milli-F reactor, a 25 mm 0.8/0.2 um dual syringe filter disc was placed in the crossflow line. This filter could last up to 3 days before the risk of clogging arose. With the increased amount of cells and debris circulating in the giant reactor fluidics, this filter would sometimes clog in a matter of hours. To resolve this problem, a strategy was adopted where three different filters of decreasing pore size were placed in sequence in the cross flow line. A chain consisting of a 5 um filter, a 1.2 um filter, and a 0.8/0.2 um filter (now at a larger 32 mm diameter size) were place in the crossflow line upon flow reversal. Additionally, media was changed in a new reservoir cup before adding in the filter chain. In the Milli-F, the in-line filter was added, flow was turned on, and the filters were primed for an hour before media was change. This was too risky for the giant reactor, so filter chains are primed with fresh media on a separate pump before adding them to the crossflow line so that the media can be immediately changed and less debris initially gets stuck in the filters. This new set-up was able to maintain consistent crossflow with no clogging or leaking for up to four days. Typically, filters were changed every three days to guarantee no adverse events. It was also seen that with anything less than the three filters during the first three days after crossflow reversal, leaking would occur in the crossflow line, indicating clogging and reduced or no crossflow.

Typically, culture medium was changed just prior to seeding (after priming), at the time of crossflow change, and every 2 days thereafter. In the case of overseeding, media could also be changed 2 hours post seeding as was previously mentioned. In general this equates to a lower medium/cell ratio than that achieved in the Milli-F, since there is an order of magnitude more cells but only slightly more HGM in the giant reactor. Presently, with the advent of the new multi-well liver bioreactor system, the giant reactor has an intermediate medium/cell ratio since the most frequently used iteration of the multi-well system holds between 500,000 to 800,000 cells per well with an order of magnitude less medium. Future studies need to be performed to address potential issues that arise from these discrepancies.

5) Recovery of Cells from the Giant Reactor

As was mentioned in the chapter introduction, another desirable feature of this new system was to optimize the rapid recovery of cells from the reactor in order to perform various quantitative assays of interest. Within the context of this thesis work, a major goal was to optimize cell recovery to quantitatively measure transgene expression after gene delivery via different vectors to compare efficiencies in 2-D vs. 3-D culture systems. Depending on speed of recovery and temporal resolution needed for intracellular trafficking studies, experiments could also be performed to study intracellular trafficking in 3-D as well.

For the brunt of experiments performed in the Milli-F system, either in situ imaging was performed to probe a fluorescent reporter of interest, or metabolism or general cell phenotype was measured by probing for molecules in the medium flowing out of the reactor outlet. In the case that cells did need to be recovered from the reactor, the entire chip would be removed and submerged in a lysis or recovery buffer, for instance, in the case of RNA extraction, a scaffold could be removed, submerged in Trizol and frozen. In the case of the giant reactor, the polycarbonate scaffolds are not compatible with Trizol and can be damaged by multiple rounds of freezing and thawing. Therefore, it is desirable to find a method to extract whole cells from the giant reactor channels, pellet them, and then place them in the appropriate lysis buffer.

A number of methods were examined, including different calcium free buffers, collagenase, and EDTA buffers. The most rapid method of recovery was obtained with Dispase, a bacterial analog of trypsin. Reactors could be quickly disassembled with the upper, cell-containing scaffold placed in a 10 cm Petri dish. Dispase could then be pipetted on top of the cell array (usually 3 mL per scaffold was sufficient), the plate could be incubated at 37°C for 5 minutes, and after this brief incubation, cells could be gently pipetted out of the channels, collected in a centrifuge tube, and spun down (see figure 2.15). Protocols were optimized for RNA purification and quantification of β-Gal expression via a delivered reporter plasmid from recovered and pelleted cells.

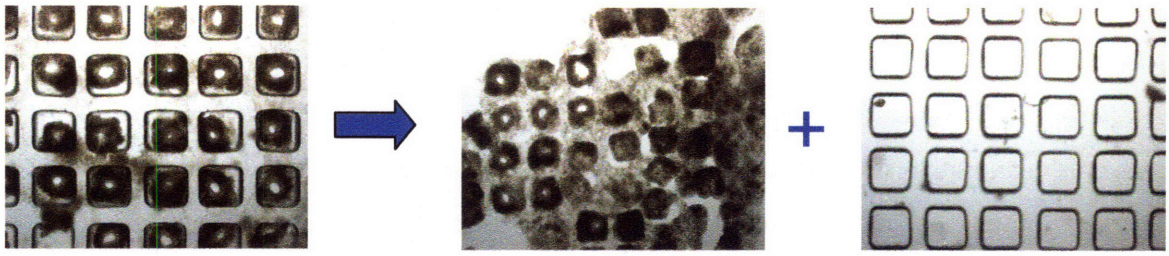

Figure 2.15: Incubation in Dispase allows for rapid recovery of tissue from the scaffold channels. As can be seen at left, addition of Dispase and incubation at 37°C for five minutes already loosens tissue structures from the channel walls, and with gentle pipetting the channels are completely cleaned.

2.3.2 Characterizing a Functional Giant Reactor System

With all of the initial design problems addressed in the giant reactor, the next step in characterizing the system was to gauge its ability to foster 3-D liver tissue cultures with more *in vivo* like phenotype than conventional 2-D culture systems. Qualitatively, tissue reorganization and morphology over time were evaluated via light microscopy. The primary quantitative metric that was used in this evaluation was to measure the mRNA expression levels of transcripts indicative of liver specific phenotype via RNA purification, cDNA generation and quantitative real-time, reverse transcriptase PCR. mRNA levels for a number of cytochrome P450 enzymes, phase II metabolic enzymes, liver specific transcription factors, membrane transporters and nuclear receptors were quantified in giant reactor cultures and then compared to *in vivo* liver slices, isolated hepatocytes, 2-D collagen sandwich cultures and the Milli-F reactor. Previous microarray experiments had shown this pool of genes to be the most significantly upregulated in liver tissue versus other tissue types from *in vivo* rat samples [160].

These quantitative comparisons of relative gene expression levels provided a good deal of information. Direct comparison between the two bioreactor systems revealed whether or not design changes from the scale up significantly affected giant reactor performance. Comparison of giant reactor transcript levels to 2-D cultures and *in vivo* liver slices also allowed a gene by gene assessment of the maintenance of hepatic phenotype in gauging whether or not the reactor providing a more in vivo-like culture system than the conventional collagen sandwich cultures, which serve as the current gold standard for *in vitro* primary hepatocyte studies [172].

A)

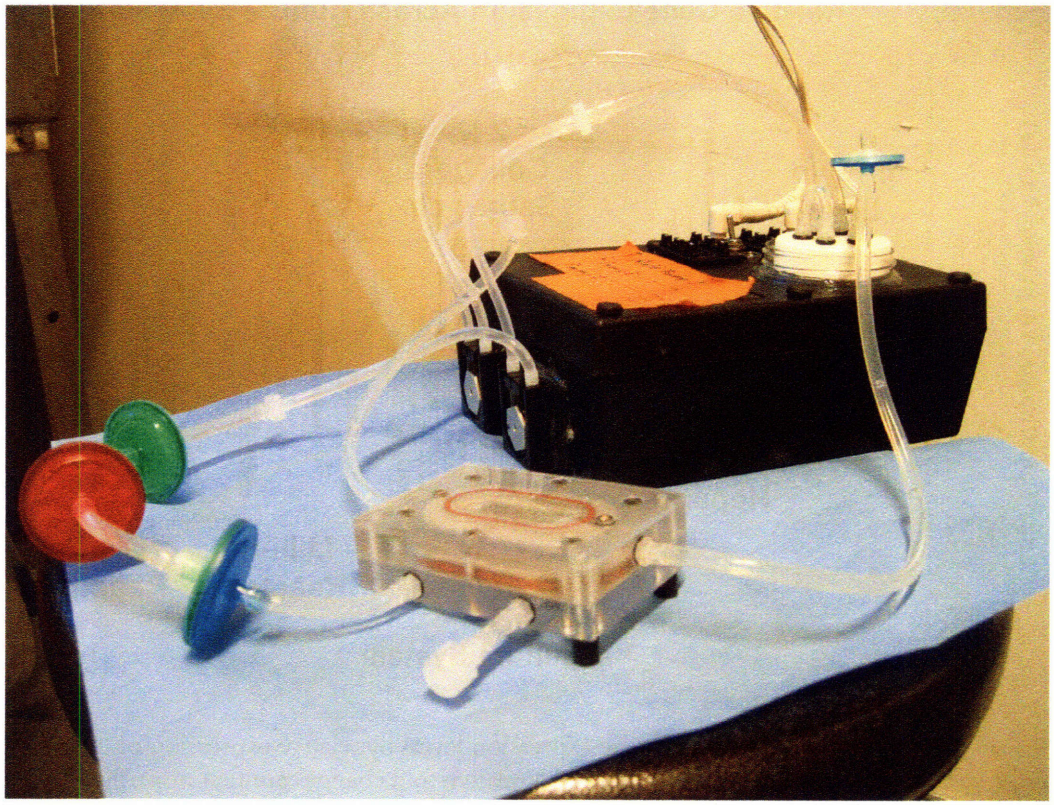

B)

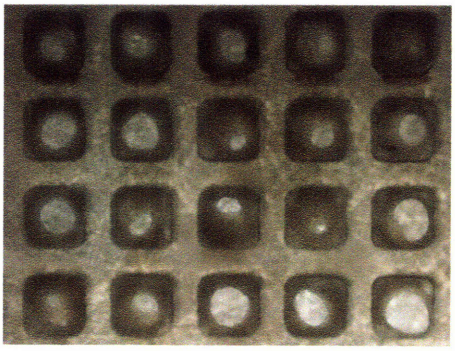

Figure 2.16: A) Final giant reactor system with peristaltic pumps, fluidics and in-line filters in the crossflow line feeding the lower chamber. Reactor feet are only used on the outlet end of the reactor to prevent build-up of air bubbles in the upper flow chamber. **B)** *In situ* light microscopy image of liver tissue structure under optimal seeding and maintenance conditions at seven days post isolation. Tissue attachment and overall morphology is comparable to that seen in silicon scaffolds and in the Milli-F reactor.

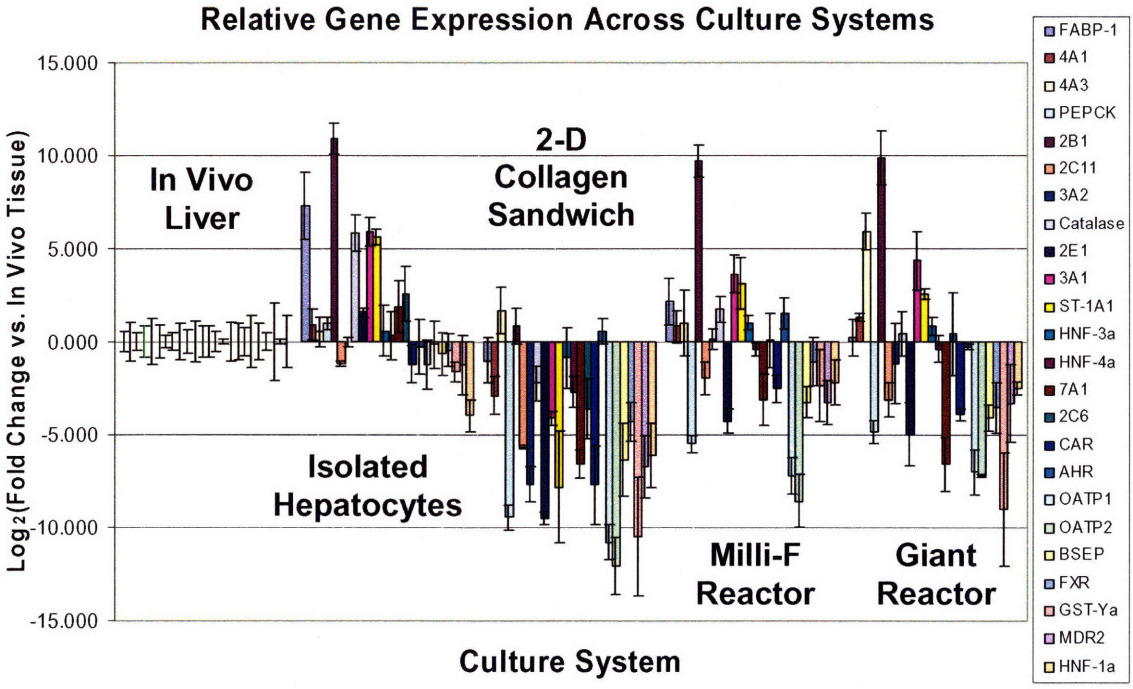

Figure 2.17: Initial comparison of gene expression levels by relative expression of liver specific mRNA transcripts across culture systems. All relative fold changes are first normalized the amount of 18s ribosomal RNA in that sample and then normalized to transcript levels in *in vivo* liver slices. Liver slices were submerged in Trizol and homogenized immediately after removal from the animal, isolated hepatocytes were lysed in Trizol immediately after perfusion isolation, and collagen sandwiches and both reactor cultures were taken down at day y after isolation and lysed in Trizol. Please see appendices for detailed RNA purification, cDNA generation, and RT-PCR protocols.

Results for the initial gene expression comparison were promising. The giant reactor compared fairly well with the Milli-F results, with some genes being slightly more upregulated/less downregulated than in the Milli-F and others less upregulated/more downregulated than in the Milli-F. Overall, the expression patterns between the two systems were comparable, and both systems were less downregulated as compared to 2-D collagen gel sandwiches at day 7 in culture. Further optimization in the system was now continued to obtain more efficient seeding and to develop a viable gene delivery and detection protocol. Further expression analysis on the final iteration of the giant reactor is discussed in Chapter 4.

2.3.3 Optimizing Transfection Protocols in the Giant Reactor

Initial attempts to perform gene delivery and transgene expression experiments in the giant reactor were largely unsuccessful. These poor results were traced to the in-line filters in the crossflow line, which provided a good deal of surface area for non-viral complexes to adsorb to. A modified protocol was developed where giant reactors were seeded with day 3 spheroids, crossflow was reversed at 24 hours, and then the inline filter chain was left in the crossflow line for 3 days. At day 7, the crossflow filter chain was removed and replaced with a silastic tube. Since the crossflow line was filterless now, the direction of crossflow was changed back to 1 mL/min downward to prevent clogging the lower chamber during gene delivery. Non-viral complexes were then prepared following each vector specific complexation protocol, added to 6 mLs of HGM and added to the reactor reservoir. DNA was delivered at a concentration of 5 ug/mL to keep conditions consistent with 2-D transfection protocols, thus allowing for unbiased comparison of 2-D and 3-D gene delivery efficiencies for a given vector.

HGM with and without BSA was evaluated for transfections. The presence of BSA in the medium can lead to aggregation and sedimentation of non-viral particles, while its absence can cause increased adsorption of the particles to the surfaces of the tubing, reservoir and reactor parts. Empty reactors were transfected with complexes in each type of medium, and a small volume of medium was taken from the reactor outflow every hour for the first four hours of delivery. DNA was purified from each aliquot, and the amount of plasmid DNA copies per unit volume of medium was determined via quantitative Taqman real-time PCR. Results of this experiment showed that depletion of complexes in the circulating media was more a function of adsorption rather than aggregation and sedimentation (see figure 2.18). Reactors transfected with BSA containing medium retained relatively constant levels of plasmids in the circulating flow, while BSA free replicates all showed a decrease in circulating plasmids over time. The fact that such a small media volume was being mixed by inflow to the reservoir by both the outlet tube and the crossflow line (and that the intake tubes in the reservoir being very close to the floor in these set-ups) meant that complexes were being retained in the circulated media and didn't stay sedimented on the floor.

As a result, all future transfection experiments were performed with BSA containing HGM. Using the modified transfection protocol described above, reactors were transfected

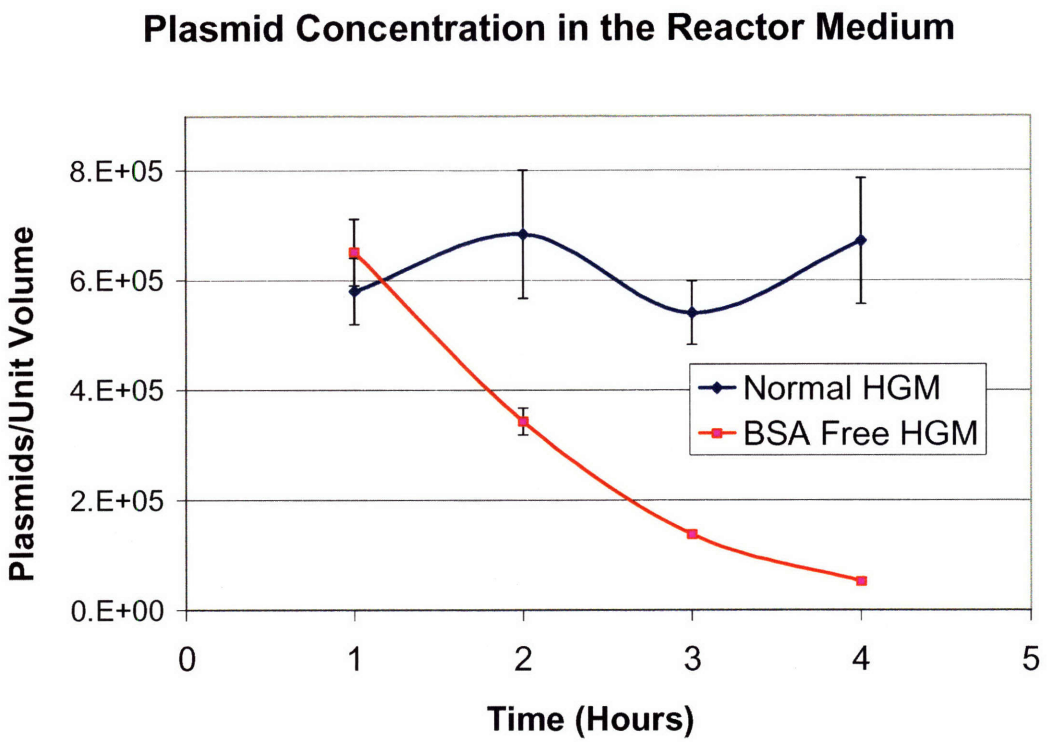

Figure 2.18: Effect of BSA on the maintenance of constant circulating concentrations of non-viral particles. Giant reactors assembled and primed with medium with and without BSA were dosed with PEI25/gWiz β-Gal plasmid non-viral complexes at an N/P ratio of 20. Plasmid concentration was then measured in the reactor outflow over time via real-time PCR.

on day 7 and taken down on day 9 to measure transgene expression levels 48 hours after delivery. Cell scaffolds were incubated in Dispase for 5 minutes, collected and pelleted, resuspended in reporter lysis buffer, and assayed for β-Galactosidase activity levels (see Appendix 13). Preliminary tests with PEI25 vectors showed detectable levels of gene expression over controls, paving the way for future studies with next generation vectors (see figure 2.19).

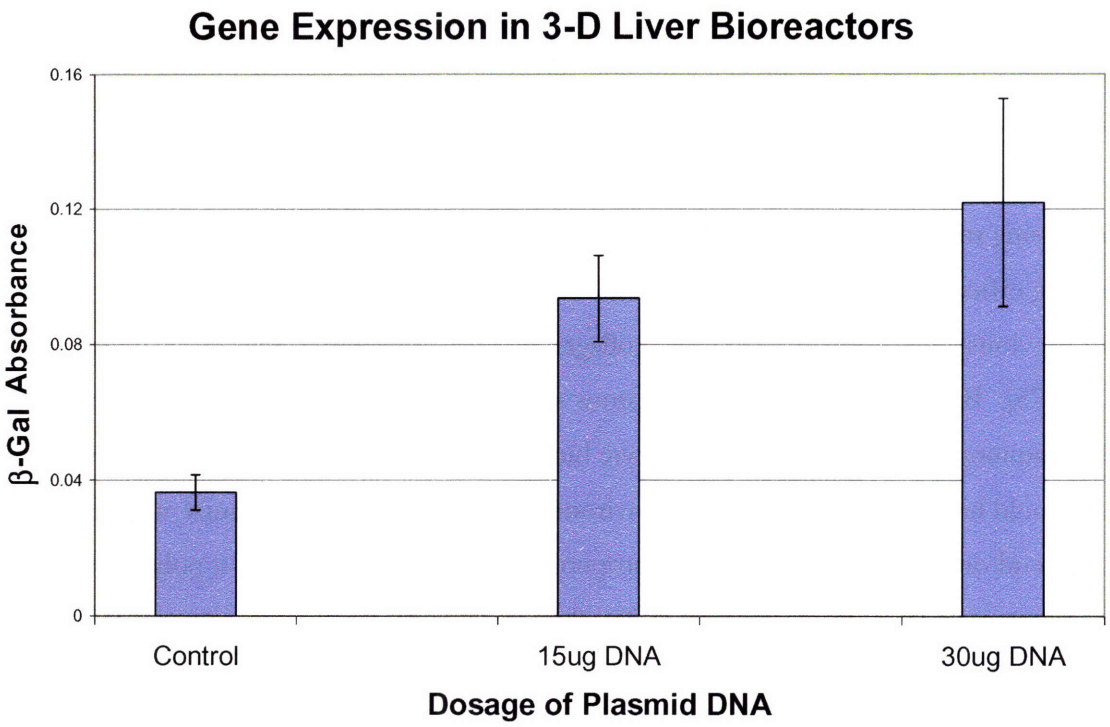

Figure 2.19: β-Galactosidase transgene expression 48 hours after gene delivery of two amounts of total plasmid DNA. gWiz b-Gal plasmids were complexed with PEI25 at an N/P ratio of 20, added to 6 mL of BSA containing HGM in each giant reactor reservoir. β-Gal absorbance was normalized to total protein.

2.3.4 Extension of Polycarbonate Scaffold Machining and Processing

All remaining experiments in this thesis work are performed in the optimized systems as described above. However one limitation of this iteration of the giant reactor system lies in the fact the laser machined polycarbonate scaffolds are expensive and aligned pairs are in low supply in the lab. Additionally, spheroid formation and seeding is still relatively inefficient in terms of the number of cells that are wasted in reactor seeding. This will become an important factor when reactor studies are moved to other cell types, such as human hepatocytes, where cells are usually in scarce supply. Work was performed to look at solutions for these problems.

In summary, new cooled drilling methods were adapted to successfully reduce polycarbonate warping. Along with the use of the new alignment hole strategy in the sides of the scaffold, this greatly reduced alignment issues. By drilling multiple scaffold blanks in a stack, a batch of ten to twenty scaffolds could be acquired that were completely interchangeable as top and bottom scaffolds in the giant reactor pocket. The walls of these

new circular channels obviously had different surface properties due to the new processing technique, but provided good cell adhesion and are currently being used in another study in the Griffith lab.

To address the issue of variation in channel surface properties due to different processing methods or batches, as well as explore methods of single cell seeding to increase seeding efficiency, a collaboration with the Yannas lab was undertaken to adapt a method to put previously developed freeze-dried collagen-gag scaffolds within these drilled channels [173-175]. By forming a flexible and porous strut network of collagen and different glycosaminoglycans relevant in hepatocyte binding and signaling throughout the channel, cells could have a consistent scaffold environment to bind to and reorganize without having to depend on the actual structure and properties of the scaffold wall, be it polycarbonate or any other material. This could potentially allow for consistency in experiments across scaffold materials and eliminate dependence on spheroid formation for cell seeding. These pre-treated scaffolds would also

A method was developed to consistently form these freeze-dried scaffolds within the drilled channels and sterilize the scaffolds without compromising their structure. Initial experiments in the giant reactor showed promise for single cell seeding; however, more work needs to be performed to find a consistent priming method for these scaffolds, since air can sometimes become trapped in the freeze dried collagen structures and build up during culture. Some of the progress from these projects is highlighted in figure 2.20.

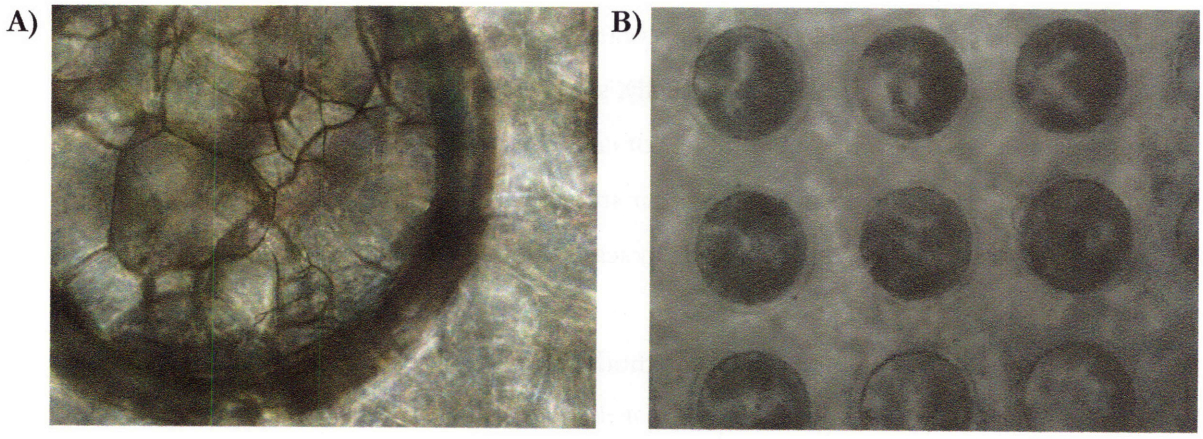

Figure 2.20: A) Freeze-dried collagen-gag scaffold structure within on the newly drilled polycarbonate channels. The channel diameter is 300 um, so most features are on the order of 50-100 um. **B)** Day 6 tissue structures formed from single cell seeding of rat hepatocytes into a drilled array of channels with collagen-gag matrix. Cells take over the matrix during the culture and form nodules of tissue.

2.4 Selection of Vectors for Gene Delivery Studies

While unmodified polyethylenimine (PEI25) vectors served as an excellent first vector to test for proof of concept studies in trafficking and 3-D transfection assays, they also posed many problems in the move to primary cell systems. PEI25, the high molecular weight version of this cationic polymer, has been well studied in *in vitro* gene delivery experiments [70, 76, 77, 80, 82, 83, 93, 176], typically in cell lines. In a number of culture systems and animal models, and even in cell lines, the toxicity of traditional PEI vectors has been documented [177]. In the primary hepatocyte culture systems used in this thesis work, especially in the 2-D adsorbed collagen cultures, PEI25 proved to be highly toxic and had a pronounced effect on the membrane integrity of primary hepatocytes, as discovered by an LDH release assay that is not typically used in general toxicity screens of gene therapy vectors. This caused binding and uptake and trafficking experiments in primary hepatocytes to be highly variable and largely unrepeatable with PEI25. It is important to note that a lower N/P ratio than 20 may have results in lower toxicity effects, but if this vector were to be used in future mechanistic studies, it was desirable to keep this ratio consistent with past cell line studies [132] for a direct mechanistic comparison between hepatic cell lines and primary hepatocytes. Lowering this N/P ratio would increase particle size and change a number of the physical properties of the complexes, making mechanistic comparisons impossible.

These PEI vectors were also highly vulnerable to the presence of BSA in the medium when used in static 2-D transfections. Without the presence of mixing as is the case in the reactor systems, these particles sediment onto cells and are taken up via fluid phase endocytosis. It was seen that in the presence of BSA in static cultures, cells would aggregate and likely become too large to be taken up into cells, making for vastly different uptake dynamics in the different medium formulations (see figure 2.22). Displaying serum stability in the presence of albumin and other serum proteins is a crucial first step in demonstrating that a vector may have *in vivo* efficacy. As a result, finding vectors that perform well in more *in vivo* like medium formulations was a goal in this work in order to perform experiments that could study more clinically relevant therapeutics mechanistically. These issues made it necessary to identify new vectors to use in the final quantitative trafficking studies.

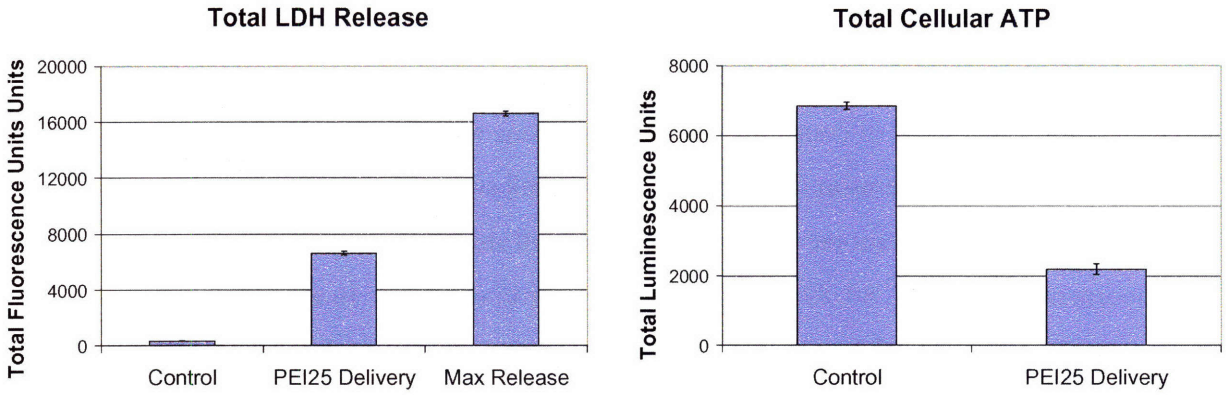

Figure 2.21: Toxicity assays to gauge the effect of PEI25 delivery on primary hepatocytes. The LDH release assay measures general membrane integrity and shows that PEI25 is just below half as disruptive as the addition of a strong lysis buffer for the maximum LDH release case. Total cellular ATP provides a measure of the overall metabolic health of the hepatocytes, and PEI25 delivery cuts this metric to one third of that for untreated cells. Cells were dosed with PEI25/gWiz β-Gal plasmid complexes at an N/P ratio of 20 and a concentration of 5 ug DNA/mL of media.

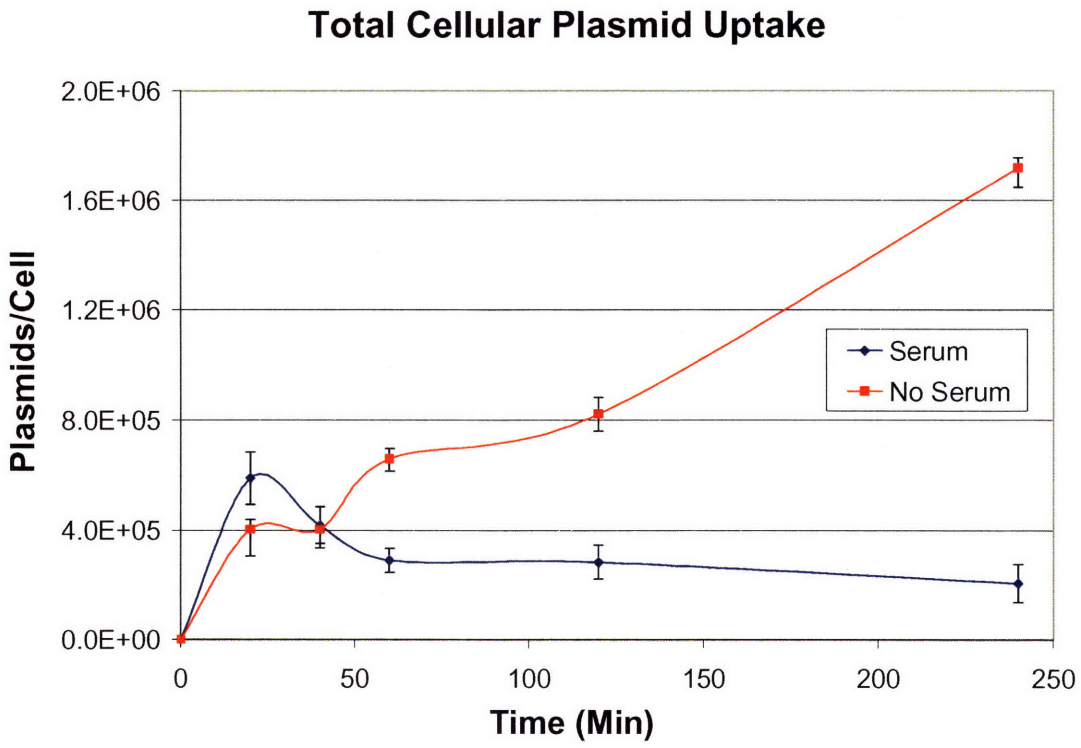

Figure 2.22: Plasmids uptake dynamics with a PEI25 vector are highly sensitive to the presence of serum proteins such as BSA.

A number of next generation polymers were screened for expression efficiency and toxicity in primary hepatocytes. These included next generation PEI based carriers developed in the Klibanov lab, as well as a new class of poly(β-amino ester)s from a polymer library that was generated in the Langer lab using high throughput combinatorial chemistry approaches [103-105, 108, 109]. All of these vectors displayed increased efficacy and decreased toxicity when compared to PEI25 in previous studies, and it was a matter of finding carriers that displayed these desired properties in our primary cell systems as well. These polymers were used to complex gWiz β-Gal plasmid DNA and transfect primary hepatocytes. Three assays were performed on each sample at both 4 hours and 24 hours to gauge toxicity. A traditional MTT metabolic activity assay and a total cellular ATP assay gave a metric for the overall metabolic health of the cells, and an LDH release assay gave information on the integrity of the plasma membrane. For specific toxicity assay protocols, please refer to Appendix 14. Gene expression was also quantitatively measured at 24 hours to compare efficacy. Previous to the wide-scale screening, optimal N/P ratios were determined for maximal gene expression in primary hepatocytes for the linear PEI22 and cross-linked PEI polymers (data not shown).

Of the panel of polymers tested, the small cross-linked PEI and the poly(β-amino ester) C32-7 (see figure 2.23) provided the best mix of membrane integrity, high expression and maintenance of metabolic activity at the early and late time points. A summary slide of these assay results at 24 hours can be seen in figure 2.24. It was decided that these vectors would be good candidates to explore mechanistic trafficking differences in comparison with one another and with adenovirus gene delivery (see chapters 3 and 5). These three vectors are also compared to traditional vectors such as naked DNA and PEI25 in terms of gene expression efficiency in 2-D and 3-D cultures (see chapter 4).

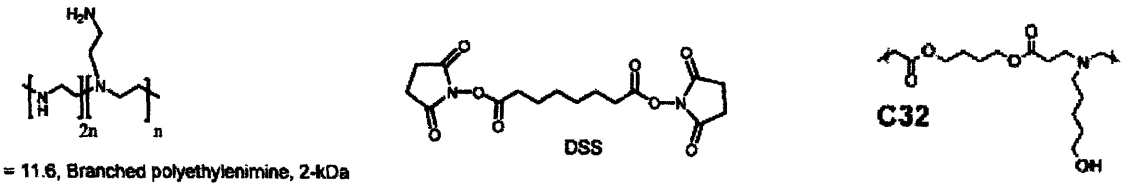

Figure 2.23: Structures of the two next generation cationic polymers to be studied. Small cross-linked PEI consists of low MW 2 kDa PEI cross-linked together with DSS [108]. C32-7, generally referred to as C32 in the literature and the remainder of this document, results from the Michael addition of an amine group with a hydroxylated carbon chain into an ester backbone [103]. Both molecules contain protonatable amine group that can act as proton sponges in lysosomes and aid in vesicular escape, but overall structural differences may lead to mechanistic differences in trafficking.

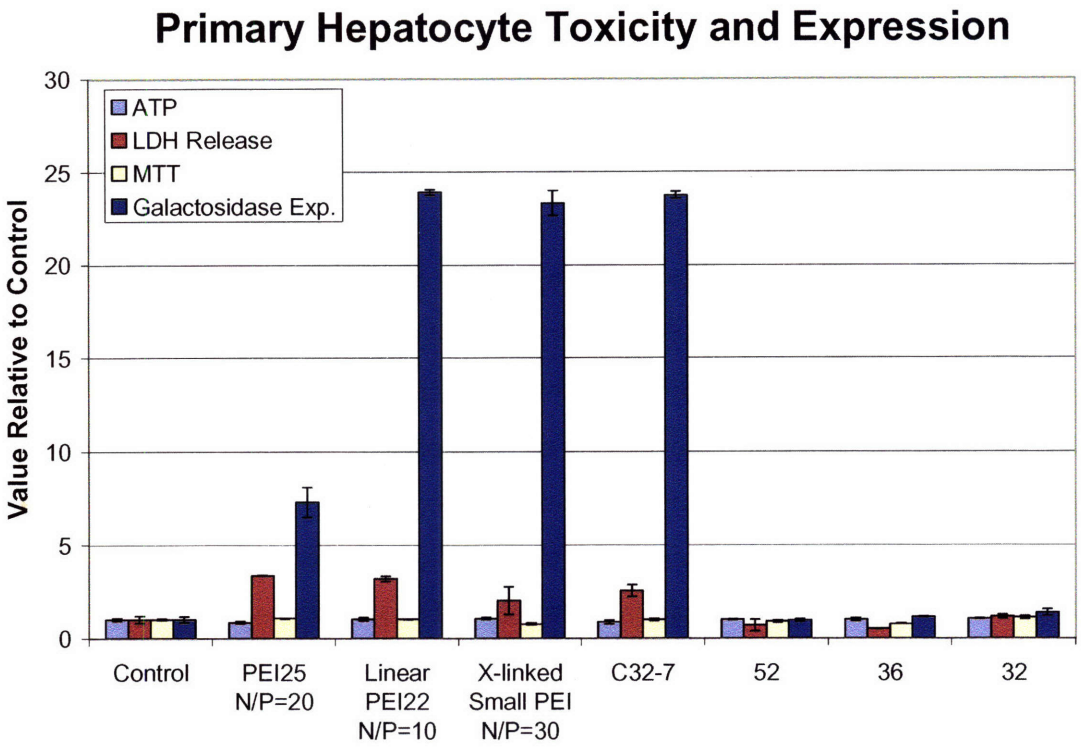

Figure 2.24: Summary of 24 hour toxicity and gene expression results for candidate PEI based vectors and poly(β-amino ester)s C32-7, 52, 36, and 32. Cells were dosed with 5 ug/mL at the indicated N/P ratios for the PEIs and at a polymer/DNA mass ratio of 100:1 for the poly(β-amino ester)s.

Interestingly, similar screens were performed in Cos-7 and HepG2 cell lines in preparation for a high throughput uptake and expression study for a number of C32 and other poly(β-amino ester) variants, and these cells were largely insensitive to the toxic effects of the different polymers. LDH release levels were three to four fold lower in these cell lines than they were in primary hepatocytes for the same vectors and metabolic activity was fairly constant in all cases (data not shown). Additionally, the 36 poly(β-amino ester) vector studied above was inefficient in primary hepatocytes, yielding gene expression levels barely above the untreated control cases, but was highly efficient in both Cos-7 and HepG2 transfections [178]. These findings reinforce the importance of moving vector screening into primary cells and into the specific cell type of interest for analyses that can truly reveal whether or not a vector could perform well for a clinical indication of interest.

Chapter 3

A Density Gradient Electrophoresis Approach to Quantitatively Measure Intracellular Trafficking of Non-viral Therapeutics

3.1 Introduction

For a gene therapy vector to be successful, a transgene must be safely delivered to the nucleus and lead to therapeutic levels of gene expression without any dangerous side effects. Recombinant viral vectors are the current gold standard for attaining highly efficient gene transfer and expression, but carry along with them certain risks and limitations. While non-viral vectors look to offer a safer alternative with enhanced versatility, these synthetic vehicles fail to achieve levels of expression or delivery efficiency to be considered as viable clinical options in most cases.

In order for efficient transfection to be accomplished, a non-viral vector/plasmid complex must overcome a number of barriers on its way to the nucleus [112, 113]. In general, a majority of past research on both viral and non-viral fronts has been of a more clinical and qualitative nature. Quantitative or mechanistic studies would mainly focus on overcoming one barrier at a time and merely evaluate resultant gene expression levels and duration for some dosing level of a given viral or non-viral formulation. In the case of viral vectors, which have evolved complex mechanisms to efficiently surpass all of these barriers, this methodology can still yield some useful outcomes. However, in the context of non-viral vectors that must be designed from the ground up to overcome each barrier, this approach can be detrimental and inefficient. Changing the physical properties of a vector may be favorable for one barrier, but actually hinder overall efficiency by making it more difficult to accomplish another step in the delivery process. Past work has shown binding and internalization at the cell surface [120, 121], endosomal escape [122-124], transport in the cytoplasm [116, 125], nuclear import [126-131], and vector unpackaging [118] to all be potentially rate-limiting steps in the delivery process. The most important message to take away from these conclusions is that the rate-limiting step and significance of other major barriers can depend heavily on the specific vector/plasmid complex used and the particular cell type being studied.

Quantitative and systematic studies of gene delivery can be advantageous to tackle this multiple-barrier scenario [113, 132, 179-182]. Past work has shown that taking a computational modeling approach combined with quantitative experiments for gene delivery analysis can provide a powerful predictive tool for gene carrier development and refinement [113, 181]. Fitting mathematical models to quantitative data can allow for unbiased analysis that can generate insights about the data that is not readily appreciated by crude inspection of individual time courses or end point analyses. This can immediately drive new hypotheses as to why a vector is or isn't successful, while also allowing for more intelligent design of future investigations.

One setback that hinders these efforts is the lack of tools that can provide rich quantitative data with the spatial and temporal resolution needed to build truly accurate and informative models. As a result, many analyses tend to lump multiple intracellular processes into single steps and multiple organelles into a single compartment. While model fits can then be more accurate and or true to what little quantitative data can be acquired, overall conclusions usually can't pinpoint what is specifically important in the overall process for a given vector. The multiple delivery steps that occur in the endocytic vesicles and cytosol are often a victim of these lumped approaches. Imaging can provide some information to help in understanding intracellular trafficking and nuclear import [181, 183]. However, imaging approaches are usually semi-quantitative at best and it is difficult to discriminate between organelle types without sophisticated labeling techniques which hinder analysis throughput. They also measure phenomenon on a cell by cell basis and don't always reflect what is truly going on in the population of cells as a whole. Approaches are needed that compliment these imaging techniques and provide quantitative data on a populational level.

We have developed a subcellular fractionation method employing an improved density gradient electrophoresis (DGE) device based on past work that demonstrated the ability of this approach to separate the organelles important in gene delivery uptake and trafficking [142, 147, 148, 184]. This method is completely preparative and allows for quantitative measurement of delivered plasmids not only in these organelles, but also in whole cell, nuclear, and cytoplasmic fractions of the same sample, allowing for data sets with enhanced spatial resolution. Past studies have developed rigorous methods to quantitatively monitor vesicular trafficking, but were unable to extend measurement to other compartments [94, 135].

DGE exploits differences in the charge and density properties of different organelles in the same dimension, allowing for separation of organelle subpopulations while also making for highly efficient collection and measurement of these organelles. More conventional methods such as density gradient centrifugation or free flow electrophoresis are either tedious or costly and perform separations based on either density or charge differences alone [143]. As a result, these techniques cannot easily separate endosomal subpopulations or robustly deal with the slight intrinsic variability of each vesicle type, while requiring multiple runs on the same sample to achieve the same number of fractions with high resolution, causing sample loss between steps and making it difficult to be truly quantitative [143, 144]. Meanwhile, microfluidic bioseparation devices have shown proof of principle to sort vesicular organelles with excellent resolution, but don't yet provide efficient recovery methods or enough material to support presently available downstream assays [145, 185, 186]. DGE has the potential to handle cell numbers that satisfy the sensitivity demands of current assays to faithfully map organelle separation patterns and measure plasmid delivery.

Furthermore, a goal in this work is to move studies to more clinically relevant experimental systems. Quantitative work in cell lines is more repeatable and potentially easier to perform with greater throughput, but screening new vector chemistries in these systems may not correlate well with results obtained in animal models, which do not lend well to quantitative analysis, or the ultimate clinical application. Here, we show proof of concept for this approach to separate the vesicular organelles in primary liver cells that are important in the trafficking of gene therapy vectors. This work is then extended to a next generation Poly(β-amino ester) non-viral vector, C32 and an enhanced polyethylenimine vector, small cross-linked PEI. These cationic polymers have previously been shown to be highly effective next generation synthetic vehicles [103, 105, 108], and we explore the potential for this DGE approach to quantitatively study the dynamics of the vesicular trafficking of these carriers in order to glean further mechanistic insight into their success as gene delivery agents.

3.2 Materials and Methods

3.2.1 DGE Device and Peripheral Set-up

The DGE device was machined from a cylinder of poly(methyl methacrylate) (PMMA). All peripheral components for the device such as the loading cone, electrode holders, clamps and custom gradient mixer were also machined from PMMA. Custom electrodes were machined from platinum and palladium to have the same diameter as the separation column, thereby ensuring the most uniform current density. Peristaltic pumps (Instech Laboratories, Plymouth Meeting, PA) were used to constantly replenish the upper and lower chambers with fresh buffer. Silicone O-rings, clamps, tubing and connectors were purchased from McMaster Carr, USA. A cellophane membrane (Amersham Biosciences, USA) separated the lower buffer chamber from the separation column, allowing for hydrodynamic but not electrical isolation of the column. A computer controlled syringe pump (Harvard Apparatus, Holliston, MA) was used in tandem with the gradient mixer to load and elute the column contents. A standard electrophoresis power supply in constant current mode (Bio-Rad Power Pac 300, Bio-Rad, USA) was used to drive the migration with current levels monitored by an ammeter. The column was set-up on a vibration isolation platform (Kinetic Systems, Boston, MA) in a 4°C cold room to minimize the effects of thermal fluctuations and vibrations in the column.

3.2.2 Primary Cell Isolation and Culture

Primary cells were isolated from male Fisher rats weighing 150-180 gm using a modified version of the Seglen 2-step collagenase procedure as previously described [161, 162]. Blendzyme Type III (Roche, USA) was used for digestion instead of collagenase. Cells that were released by the digestion were suspended in DAG (DMEM (Sigma-Aldrich, USA), Albumin, Gentamycin) and spun and washed twice at 50g for 3 minutes. The final pellet was resuspended in HGM, as described previously [161, 162, 187], to yield a 95% or greater pure suspension of hepatocytes. The final cell viability was determined by trypan blue exclusion, and cells were only used if viability was in the 89-95% range. Cells were seeded in 60 mm tissue culture dishes treated with a dried adsorbed collagen monolayer. Collagen type I from rat tail (BD Biosciences, Bedford, MA) was diluted in sterile 1x PBS at a concentration of 30 ug/mL. Plates were incubated with 3 mL of this solution for 2 hours,

then aspirated and allowed to dry in a sterile hood for two hours prior to seeding. Cells were seeded in 3 mL of HGM at a density of 800,000 cells/mL immediately after isolation. Medium was changed 4 hours post-seeding to eliminate dead and unattached cells and debris, while ensuring 90-95% confluency. All experiments were performed within 24 hours of seeding to ensure the best maintenance of hepatocyte phenotype.

3.2.3 Cell Labeling and DGE Fractionation of Primary Hepatocytes

Cells were placed on ice to halt endocytosis and washed once with cold PBS++ (1x PBS with 1 mM $MgCl_2$ and $CaCl_2$). Pre-warmed HGM containing 2 mg/mL horseradish peroxidase (HRP) was added to the cells and the dish was returned to 37°C for 4 minutes. Cells were returned to ice, washed again, and given unlabelled medium for 15 minutes at 37°C to chase the first HRP pulse into the late endosomes. Cells were then returned to ice, washed, and pulsed with HRP for an additional 3 minutes to label early endosomes. Cells were then returned to ice, washed, and scraped and collected in 3 mL of hypotonic DGE buffer (250 mM sucrose, 10 mM acetic acid, 10 mM triethanolamine, and 1 mM Na EDTA). Cells were placed on ice briefly and allowed to swell and were then mechanically lysed by passing the suspension through a 21G x 2 inch needle 12 times. Lysis was evaluated to be $\geq$ 98% efficient with no whole cells typically visible and nuclei left fully intact. This mechanical lysis technique eliminated the need for detergent based lysis buffers and allowed for rupture of the plasma membrane while keeping all other organelles of interest intact. Nuclei were spun out of the suspension, and the supernatant was treated with trypsin for 6 min at 37°C and then returned to ice. Trypsin inhibitor and the protease inhibitors aprotinin, leupeptin and PMSF were added to the lysate. The lysate was spun for one hour at 100,000g to recover all organelles. The organelle pellet was resuspended in 0.5 mL of 6% Ficoll (Amersham Biosciences, USA) in DGE buffer and was layered in the DGE column between a lower linear density gradient of 6 mL ranging from 10% -7% Ficoll, and an upper linear density gradient of 25 mL ranging from 5%-0% Ficoll. Migration of the organelles was driven by an electric potential at 10.6 mAmps and 300 volts for 80 minutes in constant current mode. The top electrode was replaced by a cone and tube to elute off the column contents into a multiwell plate at the desired fraction volume. All reagents were purchased from Sigma-Aldrich, USA unless otherwise noted.

3.2.4 DGE Fraction Mapping Assays and Western Blotting

Fractions were assayed in a multiwell format to determine the location of the organelles of interest after the separation. HRP activity was determined by mixing 100 uL of each fraction with 200 uL of an O-dianisidine substrate reagent. Samples were incubated for 1 hour at room temperature and absorbance was read at 455 nm. β-Hexosaminidase, an endogenous enzyme in lysosomes, was assayed by adding 150 uL of a P-nitrophenyl-N-acetyl-β-D-glucosiminide substrate reagent to 60 uL of each fraction. Samples were incubated at 37°C for 1 hour, the reaction was stopped by adding 90 uL of a 2 M glycine buffer at pH 10 and absorbance was read at 405 nm.

Western blots were performed by labeling and fractionating cells by DGE and identifying the fractions which contained late endosomes and lysosomes by the HRP and β-Hex peaks. These fractioned were pooled together and spun at 100,000g for 1 hour to re-pellet the intact, separated organelles. The organelle pellet was resuspended in sample buffer, run on a 7.5% SDS-PAGE gel (Bio-Rad, USA) and transferred to a Sequi-Blot PVDF membrane. The membrane was blocked with non-fat dry milk and incubated with primary antibodies anti-EEA-1 (Mouse IgG, BD Biosciences, Bedford, MA) or anti-Rab9A (Goat IgG, Santa Cruz Biotechnologies, Santa Cruz, CA) overnight at 4°C at a dilution of 1:250, and in the appropriate HRP-conjugated secondary antibody (Santa Cruz Biotechnologies, Santa Cruz, CA) for 1 hour at room temp at a dilution of 1:2,500. Blots were developed by adding 1 mL of Western Lightning reagent (Perkin Elmer, Boston, MA) and imaging on a Kodak developer (Kodak, Rochester, NY).

3.2.5 Plasmid, Polymers, and Non-viral Complex Formation

Plasmid gWiz-β-Galactosidase (Gene Therapy Systems, San Diego, CA) encodes the enzyme β-galactosidase controlled by the human cytomegalovirus (CMV) promoter. The plasmid DNA was purchased purified and ready for use from a contract plasmid manufacturing company (Aldevron, Fargo, ND). 25kD PEI was purchased from Sigma-Aldrich (St Louis, MO). The C32 and small cross-linked PEI polymers were synthesized as described previously [103, 104, 108].

For transfection via PEI25, polymer and DNA were diluted to the appropriate concentrations in sterile water and combined at an N/P ratio of 20. Polymer was added to

DNA and left at room temperature for 20 minutes to allow for formation of complexes. For C32, polymer and DNA were diluted in sterile filtered sodium acetate buffer, pH 5.4, and combined at a polymer mass/DNA mass ratio of 100. For the cross-linked PEI, polymer and DNA were diluted in sterile water and were mixed at room temperature for 10 minutes at an N/P ratio of 30. All complexes were added to HGM at a DNA concentration of 5 ug/mL. Non-viral particle size was determined via dynamic light scattering using a ZetaPALS Zeta Potential Analyzer with ZetaPALS Particle Sizing Software Version 2.3 (Brookhaven Instruments Corporation, Holtzville, NY). Number averaged particle diameters were determined over a lognormal distribution for each PEI vector/plasmid complex. The 25kD PEI complexes measured 228.3 ± 47.6 nm in diameter, the C32 complexes were 152.0 ± 4.2 nm, and the cross-linked PEI complexes were 167.5 ± 8.2 nm in diameter.

3.2.6 DNA Isolation and Taqman Quantitative PCR

Plasmid DNA was purified from each fraction of a given DGE run using the DNEasy 96 Tissue Kit (Qiagen, Valencia, CA). Plasmid quantification was performed using the MJR Chromo 4 (Bio-Rad, USA). β-Galactosidase plasmid forward and reverse primers and probe were designed using Primer Express Software (Applied Biosystems) and yielded sequences for forward primers, reverse primers, and dual labeled probes. Two sets of forward and reverse primers with probe were ordered and tested for optimal efficacy, as determined by widest spread of linear standard curve range and steepest slope of standard curve (Applied Biosystems, Foster City, CA). The resulting primers and probe spanned an 80bp region in the β-Gal coding region of the plasmid and had sequences: forward primer (5'-TTA CAG GGC GGC TTC GTC T-3'), reverse primer (5'-TAA GCC GAC CAC GGG TTG-3'), and dual labeled probe (5'-6FAM-CTG GGT GGA TCA GTC GCT GAT TAA ATA TGA TG-TAMRA-3'), used at concentrations of 400nM/400nM/25nM, respectively. PCR cycle conditions were 50°C for 2 min, 95°C for 10 min, followed by 40 cycles of 95°C for 15 s and 60°C for 1 min. In order to normalize samples to a per cell basis, genomic DNA was also purified from a whole cell sample from each DGE run. Taqman primers and probe were similarly designed to quantify the rat GAPDH gene which spanned an 80bp region with the following sequences: forward primer (5'- TGG GAT AGC CAG TGC TCT TA -3'), reverse primer (5'-ACA GGA GAT GGG TTG GAA CT -3'), and dual labeled

probe (5'-6FAM-TGA GCC ATC ATC ATC TCC GCT G-TAMRA-3'). The primers and probe were used at concentrations of 900nM/900nM/225nM, respectively. PCR cycle conditions were 50°C for 2 min, 95°C for 10 min, followed by 40 cycles of 95°C for 15 s and 54°C for 1 min.

3.2.7 Transfection and Trafficking Assays

Cells were washed and complexes were added in 2 mL of HGM at 5 ug DNA/mL. At the post-delivery time point of interest, plates were removed from 37°C, placed on ice to halt endocytosis and subjected to the DGE collection, lysis prep, and separation protocol without HRP labeling. DGE fractions were assayed for β-hexosaminidase activity to determine the location of the late vesicles (since late endosomes and lysosomes were found to colocalize on the column when transfected with these gene delivery vectors). Real-time PCR was performed on each fraction, and plasmid quantities in the fractions corresponding to the late vesicles were summed and normalized to the cell number as determined from the rat GAPDH amplification and comparison to a standard curve. Similarly, the smaller plasmids peaks that were measured to the right of the late vesicle peak and were negative for β-hexosaminidase activity were summed to determine the amount of plasmids in early endosomes for each time point. Triplicate runs were performed at each time point to build the late and early vesicle trafficking time course. To determine nuclear localization of plasmids, nuclei were spun down at 1000g after cell samples were lysed for DGE run preparation. Nuclear pellets were frozen, resuspended in PBS and purified for plasmid and genomic DNA as described above, and subjected to Taqman real-time PCR for plasmid and cell number quantification.

3.3 Results

3.3.1 An Improved Density Gradient Electrophoresis Device

A DGE device was designed and built based on work by Tulp and coworkers that reported an early prototype which showed the potential for high resolution separation of cellular organelles and laid the ground work for the empirical and theoretical principles of device design and operation [142, 147]. Figure 3.1A shows a schematic of the assembled device, which consists of a separation column that is surrounded by an upper and lower buffer chamber that contain custom machined platinum and palladium electrodes. Cell lysates are layered onto the column between lower and upper linearly varying density gradients of Ficoll. Migration of the organelles is driven by an electric potential under constant current conditions, which ensures constant migration speeds of the various organellar cohorts at a given position in the column and allows different organelle types to migrate up or down the column as tight horizontal bands. Different cohorts will experience differential acceleration as they escape from the initial sample band from buoyancy effects and electromigration due to the fact that different organelle types have different density and charge characteristics [142]. After an electrophoresis run of 40-80 minutes, multiple organelle bands separate to different vertical locations in the column. Since separation is performed in only one dimension, organelles can be easily collected by eluting the column contents into fractions of a given volume, which is dictated by the desired resolution. Therefore, this approach is completely preparative and allows for multiple assays to be performed on intact organelles in the collected fractions.

The device body and peripherals were machined following the same design principles as the earlier device (see figure 3.1B for a detailed description of components). In order to obtain potentially higher resolution separations, the new device was designed to be 70% larger overall with significantly more usable column length than its predecessor. A limitation to the old device lied in the fact that there was only 6 cm of usable length in the separation column. While other improvements had allowed for longer runs in the range of 60-100 minutes in this prototype, large density gradients could not be layered to take advantage of this and achieve better separations. Our new prototype has a usable column length of over 11 cm, which can potentially maximize the potential for differential acceleration and overall separation distance between different organelles, while also being within suitable size limits

such that band broadening of organelle cohorts over time does not significantly affect resolution [142]. A custom gradient mixer was also built that allows for linear density gradients of up to 35 mL to be carefully layered onto the separation column. This provides more freedom in optimizing gradient lengths and concentrations as well as run parameters to achieve the best possible separations for the organelle and cell types of interest, in this case, endosomes and lysosomes in primary rat hepatocytes. New device peripherals such as a computer controlled syringe pump and a vibration isolation platform were also integrated in the current set-up to allow for more consistent results with the best possible resolution for the given run conditions.

3.3.2 Subcellular Fractionation of Primary Hepatocytes

A large panel of gradient lengths and ranges, run conditions, and cell collection and lysis steps were examined in order to find the optimal set of conditions for endosome and lysosome fractionation for primary rat hepatocytes. The best results were obtained when 500 uL of the processed organelle suspension was layered between a lower Ficoll density gradient of 6 mL varying from 10-7% Ficoll and an upper gradient of 25 mL from 5-0%. Organelle migration was driven for 80 minutes at a constant current of 10.6 mAmps, and 85 fractions were collected in 380 uL increments and assayed for organelle distribution (see figure 3.2). Prior to lysis and fractionation, hepatocytes were subjected to a pulse chase pulse routine with horseradish peroxidase (HRP) to label both early and late endosomes. An endogenous marker enzyme for lysosomes, β-hexosaminidase (β-Hex), provided an assay target for these vesicles. The late endosomes (leftmost HRP peak) and lysosomes migrate significantly further up the column than early endosomes, with the late endosomes localizing to fractions 21-47 and the primary lysosomal peak at fractions 37-49. The lower shoulder on the left side of the lysosomal peak has been shown to be maturing β-Hex with lower levels of activity in late endosomes and endoplasmic reticulum compartments [142, 170]. Both of these cohorts are significantly separated from early endosomes, which localize in fractions 63-71. This separation pattern has been found to be repeatable for cell loads of up to 1 mg of lysate total protein, allowing for fractionation of up to 4 million primary hepatocytes.

To confirm that the HRP peaks did in fact represent two homogeneous endosomal subpopulations, fractions 21-47 were pooled together and subjected to ultracentrifugation to repellet the separated organelles. The organelle pellet was resuspended in sample buffer and

subjected to western blotting with primary antibodies specific to late (anti-Rab9 GTPase) and early endosomes (EEA-1, early endosome antigen 1). The pelleted organelles gave a strong Rab9 signal and no EEA-1 signal, denoting a pure population of late endosomes in these fractions (see figure 3.3). To reinforce these findings, cells were also labeled with a single HRP pulse followed by a chase with unlabeled medium or with a single short pulse with no chase to label only late or early endosomes, respectively. In both cases, a single HRP peak resulted in the appropriate location (see Figure 3.4).

With excellent separation between late and early vesicles and the ability to separate late endosomes and lysosomes further if desired by optimizing runs with slightly longer gradients or run times and smaller fractions, it remained to be seen if the introduction of charged gene delivery complexes would significantly deflect the fractionation pattern. To explore this question, primary hepatocytes were transfected with cationic polymer/plasmid complexes and simultaneously labeled with HRP as previously described with the same concentration of non-viral complexes in the pulse and chase media. While there was a small degree of broadening of the peaks overall, and the build-up of complexes in late endosomes and lysosomes caused these vesicles to co-localize more significantly and shift slightly downward in the column, DGE fractionation still provided excellent separation of late and early vesicles (see figure 3.5). Since DGE fractionation resulted in over 11 380 uL fractions of separation between early and late vesicles, much larger fractions could be taken with the desired resolution still achieved in future trafficking studies.

3.3.3 Quantitative Non-viral Trafficking Studies

To quantitatively evaluate the vesicular trafficking dynamics of the C32 poly(β-amino ester) and small cross-linked PEI vectors, multiple DGE runs were performed on transfected hepatocytes at different time points after administration of the complexes. Hepatocytes were placed on ice to halt endocytosis, lysed and fractionated at 10, 20, 40, and 60 minutes after transfection. Separated organelles were collected in 24 fractions of 1.25 mL. DNA was purified from each fraction, and the amount of delivered plasmids per fraction was determined using Taqman real-time PCR. Plasmid numbers were then normalized to a per cell basis by performing Taqman real-time PCR for rat GAPDH genomic DNA copies from a whole cell aliquot from each replicate. Data was then

compared to β-Hex mapping of the fractions (Figure 3.6), and the appropriate late vesicle containing fractions were summed to acquire the total number of plasmids present in late endosomes and lysosomes.

Figure 3.6A shows representative per cell plasmid distributions over the collected DGE fractions at each time point for the C32 vector. Plasmids have already trafficked to the late vesicles within 10 minutes of delivery and build up significantly at 20 and 40 minutes. With each ensuing time point up to 40 minutes it can be seen that the vesicles become denser due to the build-up of complexes in these vesicles and the late vesicle localized plasmids shift slightly lower in the column. By 60 minutes after transfection, significantly fewer plasmids are detected and the peak localizes back to a higher position in the column.

A clearer picture of the quantitative trafficking time course in early and late vesicles can be seen when late vesicle negative and positive fractions are summed for each replicate and averaged together (see figure 3.7). Both vectors show a similar trend in early vesicle dynamics, though more plasmids seem to be delivered or accumulated in these compartments for the PEI vector. The C32 vector shows dynamic entry and exit of plasmids in the late vesicles with nearly 1,000 plasmids per cell trafficked into these compartments by 10 minutes, and a peak of over 1,500 plasmids per cell in these vesicles is reached by 20 minutes. After this point, processes such as endosomal and lysosomal escape as well as degradation can lead to the decreasing trend that is seen in the data. Conversely, the cross-linked PEI vector demonstrates a more linear trafficking profile in the late vesicles, and steadily builds up to nearly 12,000 plasmids per cell at 1 hour post delivery, suggesting potentially different uptake and escape kinetics at these delivery steps.

While these vectors demonstrate different vesicular kinetics for the same dose of plasmid DNA, they do ultimate result in nearly identical delivery of plasmids to the nucleus. Each carrier achieves greater than 100,000 plasmids per cell at or in the nucleus at 1 hour post transfection (Figure 3.8). Once again, the C32 vector appears to deliver its DNA payload faster than the cross-linked PEI vector, which shows a more gradual nuclear delivery but achieves the same degree of overall efficiency over the time span studied in this work.

3.4 Discussion and Conclusions

Quantitative and systematic approaches to studying non-viral gene carriers can offer a good deal of insight into why vectors are efficient or inefficient at a mechanistic level. Monitoring dynamic uptake and intracellular delivery processes in various quantitative and semi-quantitative experimental formats can answer many questions regarding these physical steps. However, in this complex multi-step delivery process, coupling systems level analysis with these approaches can result in additional information and conclusions not apparent from experimental observation alone. Fitting mathematical models to quantitative data sets is particularly useful in this context. Models can reveal delivery steps that are not intuitively rate limiting by visual inspection, but actually play a crucial role in successful nuclear delivery and transgene expression for a specific vector chemistry in the cell type of interest. Model analyses and simulations can drive mechanism based development of next generation carriers by generating new hypotheses for the intelligent design of vectors, and can also account for the effects that a potential change could have on all or many delivery steps and the ensuing degree of overall success.

However, for a model to be instructive, it must be trained with the right information and with accurate information. One of the major current limitations to these systems level approaches is the lack of tools that can provide rich, quantitative data sets at the intracellular level. We have developed a density gradient electrophoresis (DGE) approach that allows for the quantitative analysis of intracellular trafficking in primary liver cells. The liver plays a number of highly important roles in systemic *in vivo* gene therapy [151, 152, 154, 156, 158], and it hoped that with assay development in primary hepatocytes, quantitative data can be generated which will contribute to future models that can better reflect how a vector will perform in clinical application.

We have developed an improved DGE device that allows for the separation and recovery of the cellular organelles important in gene delivery (Figure 3.1). This device was based on past work that showed excellent proof of principle for high resolution organelle fractionation in a human melanoma cell line [142]. DGE provides a number of advantages over other currently available approaches. Other widely used subcellular fractionation techniques are unable to perform one step separation of endosomal subtypes, and usually require centrifugation or flow routines that can last on the order of 12 to 24 hours and result in sample loss. By exploiting both charge and density differences in the same dimension, our

device is able to separate organelles from cell lysates in 80 minutes while allowing for easy sample collection in less than 10 minutes. Other approaches that utilize two modes of separation usually do so in two dimensions, which complicates sample collection for quantitative assays, and these methods usually use substrates that make it impossible to separate large intact organelles. Buffers and reagents used in this DGE method are completely compatible with downstream techniques such as DNA purification and western blotting, and this device is able to process cell quantities that meet the sensitivity demands of currently available assays such as real-time PCR. Additionally, the sequential processing steps in our approach allow whole cell, nuclear, and cytoplasmic fractions to be collected in addition to the vesicular organelles from the same sample. This allows for quantitative measurement of the comprehensive cellular distribution of delivered plasmids.

Modifications made in our new device have allowed for more flexibility in optimizing separations for different cell types and for increased precision, repeatability, and overall ease of use. Cell lysis, lysate processing, and DGE run conditions have been optimized for primary rat hepatocytes to achieve excellent separation of late and early vesicles involved in non-viral complex uptake and trafficking. Cell labeling techniques and western blotting were performed to confirm repeatability of the fractionation pattern and separation of specific endosomal subtypes (Figures 3.2, 3.3, and 3.4). Late endosomes migrate upward in the column (towards the positive anode) slightly faster than lysosomes and both organelle types separate significantly from early endosomes.

Characterization of the device was extended to gauge separation ability for non-virally transfected cells. Cationic complexes have the potential to change both the charge and density characteristics of organelles and could therefore significantly alter the distribution of organelles in the column. Delivery of cationic PEI25 complexes decreased the upward migration of the late endosomes and caused minor broadening of the organelle peaks (Figure 3.5). However, excellent separation was still attained between late and early vesicles. Intensity of the late vesicle HRP peak relative to the early peak was diminished. This was most likely due to the fact that the PEI complexes were escaping from these vesicles and causing leakage of HRP into the cytosol.

For the particular application of separating and collecting late vesicles to measure vector trafficking, the DGE device provided more than enough resolution with the previously optimized conditions, such that fraction size could be significantly increased.

Early and late vesicles could still be separated and collected, but with significantly fewer total samples to assay. This made quantification of delivered plasmids in a given organelle fraction more experimentally feasible for multiple vectors and time points. DNA purification and real-time PCR, as well as organelle mapping, could be performed on every fraction due to the increased amount of material in each fraction and decreased number of overall samples. Simply summing the relevant fractions for a total vesicular plasmid amount could now be performed, rather than relying on integration methods that estimated total plasmid amounts from a subset of fraction measurements or by mixing adjacent fractions, which would have introduced more uncertainty and error into the quantitative measurements. This proof of concept paved the way for more in depth studies of vector trafficking for next generation non-viral therapeutics.

C32 is a next generation cationic vector that has been shown to be the most efficient non-viral delivery agent from a new combinatorial chemistry library of poly(β-amino ester)s [106]. Small cross-linked PEI has also demostrated enhanced transfection ability over traditional PEI vectors while offering lower overall toxicity [108]. In our primary hepatocyte culture systems, these vectors yielded highly efficient transfection levels and reduced toxicity as compared to more traditional vectors such as PEI25 (data not shown). We extended a more in depth analysis utilizing DGE fractionation and DNA quantification via Taqman real-time PCR to study the dynamic trafficking of plasmids in late vesicles via C32 transfection. Hepatocytes were transfected with C32 complexes and were lysed and fractionated at 10, 20, 40 and 60 minutes after transfection. Larger 1.25 mL fractions were collected from the DGE column after the run, making it possible to purify DNA from every sample and perform triplicate real-time PCR to accurately quantify the amount of plasmid in each fraction of every replicate.

Representative DGE column distributions at each time point already give some hint to the trafficking dynamics of the vectors, as is detailed for a series of C32 replicates (Figure 3.5). Plasmids are rapidly trafficked into the cell, with a significant of amount of plasmids already detected in the fractions specific to late vesicles. Plasmids build up in these late compartments significantly at 20 and 40 minutes, and due to this accumulation, cause the prominent late vesicle peaks in the DGE column to shift downward slightly. This is most likely due to an increase in organelle density from the presence of the particles, though the positive zeta potential of the particles can lessen the overall negative charge of the organelles

and lessen electromigration towards the anode. However, it is thought that the lipid bilayer of the organelles buffers the charge effects of the particles and that a change in peak location is mainly caused by density effects. By 60 minutes post delivery, a decrease of peak height is seen and the peak shifts upward in the column. Endosomal and lysosomal escape of C32 complexes is the most plausible explanation for this combined decrease in magnitude and upward shift and lends merit to the hypothesis that increased density caused this shift more than a change in zeta potential. If a decrease and shift is seen, it is thought that the decrease in magnitude in late vesicle plasmids is more due to endosomal escape for this vector and less to vesicular degradation, since significant degradation and minimal escape would have retained similar contents and overall charge inside the vesicles and should have resulted in similar column distribution. Additionally, the tighter fraction distribution of the plasmid peaks at 40 and 60 minutes potentially suggests vesicles with a more homogeneous distribution of complexes within the vesicles or a more pure population of a given late vesicle subtype, denoting that some vesicles were more likely to allow escape earlier on and others required more build-up of complexes before escape could be possible. Since the C32 polymer is thought to utilize the proton sponge mechanism for escape from late endosomes and lysosomes, this makes mechanistic sense. For instance, more acidic lysosomes may allow for faster vesicle swelling and rupture due to increased activity of ion pumps and water channels, leaving behind less acidic late endosomes that require a higher build-up of polymer before vesicle escape can occur. Conversely, complexes may build up to level significant for escape sooner in late endosomes than in lysosomes, allowing for some early rupture of late endosomes before fusion and progression to lysosomes. Future studies that identify run conditions that provide greater resolution between these vesicle subtypes could help in answering these questions, as well as coupling this quantitative approach with systematic data analysis or qualitative imaging data.

While examining this raw data can generate interesting mechanistic hypotheses, it is difficult to pinpoint a correct explanation due to the multiple barriers and events that exist at this stage of the gene delivery process. Averaging the summed late vesicle distributions over time can yield a quantitative time course that can be potentially more useful and accurate to this end in future analyses and also give a clearer overall picture for generating hypotheses and making polymer to polymer comparisons (figure 3.7). For the C32 vector, total late vesicular plasmids peak at 20 minutes and begin to decrease, supporting the plausibility of

early escape from some of these compartments, and showing substantial decreases by 60 minutes. This gives direct quantitative evidence that rapid vesicular trafficking and escape could contribute to this polymer being such an efficient carrier, however, it should be acknowledged that complex unpackaging and plasmid degradation can also contribute to this decrease. Although this vector does rely to some extent at least on the proton sponge mechanism, its slightly more hydrophobic character than traditional vectors such as PEI may lend to faster disruption of vesicle membranes or more efficient binding and uptake at the cell surface for enhanced early trafficking. The small cross-linked PEI has a more linear profile for late vesicle trafficking and shows significantly more build-up in these compartments than the C32 vector. However, the fact that this vector ultimately achieves the same number of nuclear plasmids suggests that vesicle escape may not be ultimately be a rate limiting step for this vector, suggesting that other steps may require attention to further optimize this carrier.

These individual contributions can be parsed out by using these quantitative trafficking data sets to fit mathematical model parameters that describe these individual steps. Future work will focus on generating quantitative vesicle trafficking sets for a number of vectors to compare mechanistic differences in these delivery steps that are difficult to extract from the data without this higher level analysis. Furthermore, since this DGE device and experimental approach also allows for the recovery of whole cell, cytoplasmic, and nuclear fractions, comprehensive quantitative data sets can be built following these same principles. These high information content data sets can be used to constrain parameter fits to the experimentally measured total cellular distribution of plasmids and not just the early or late vesicle trafficking data sets alone. This preliminary characterization and proof of principle work has shown our approach to be robust in attaining quantitative trafficking data from primary hepatocytes from multiple animals. Extension of these methods should provide more rigorous and accurate mechanistic data and models that can drive the improvement of next generation non-viral therapeutics.

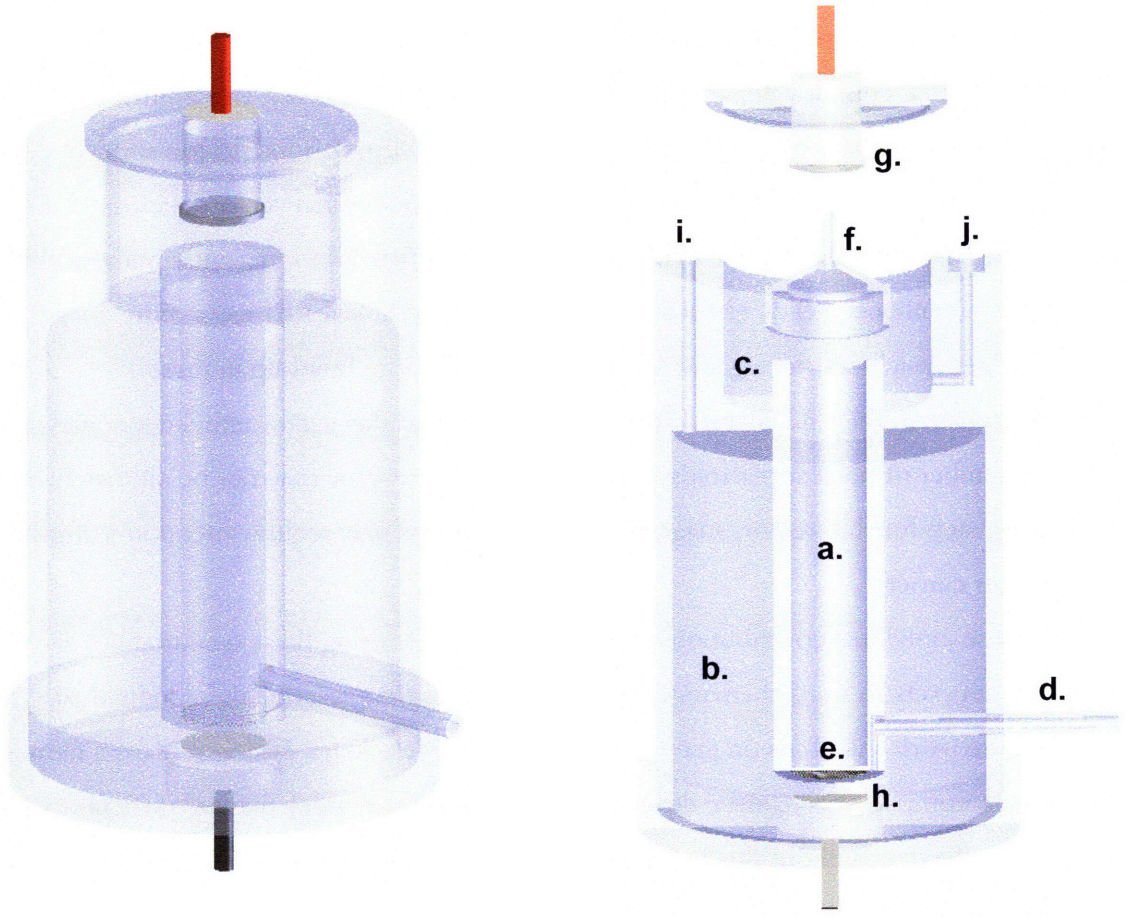

Figure 3.1: A) Schematic of the assembled density gradient electrophoresis device. **B)** Mid-plane view of the device. The separation column (a) is situated within the outer device cylinder with makes up the lower (b) and upper (c) buffer chambers. An inlet (d) connects to a computer controlled syringe pump for control over loading steps and eluting fractions out of the top of the column at the end of the run. A cellophane membrane (e) is held over the bottom of the separation column with an O-ring and makes up the floor of the column, connecting it electrically but not hydrodynamically to the lower buffer chamber. A removable cone attachment (f) allows for uniform gradient and sample layering and is reincorporated with a capillary tube connected to it at the end of the run for precise control of fraction collection. The platinum anode (g) locked onto the top chamber during the separation run, and the palladium cathode (h) is seated in a removable based that allows for cleaning of the device and seals off the lower chamber with an O-ring. Ports (i) and (j) (second set of port occluded by view, allow for peristaltic tubes to add and remove electrophoresis buffer during runs to keep the buffer fresh and make separation runs more consistent.

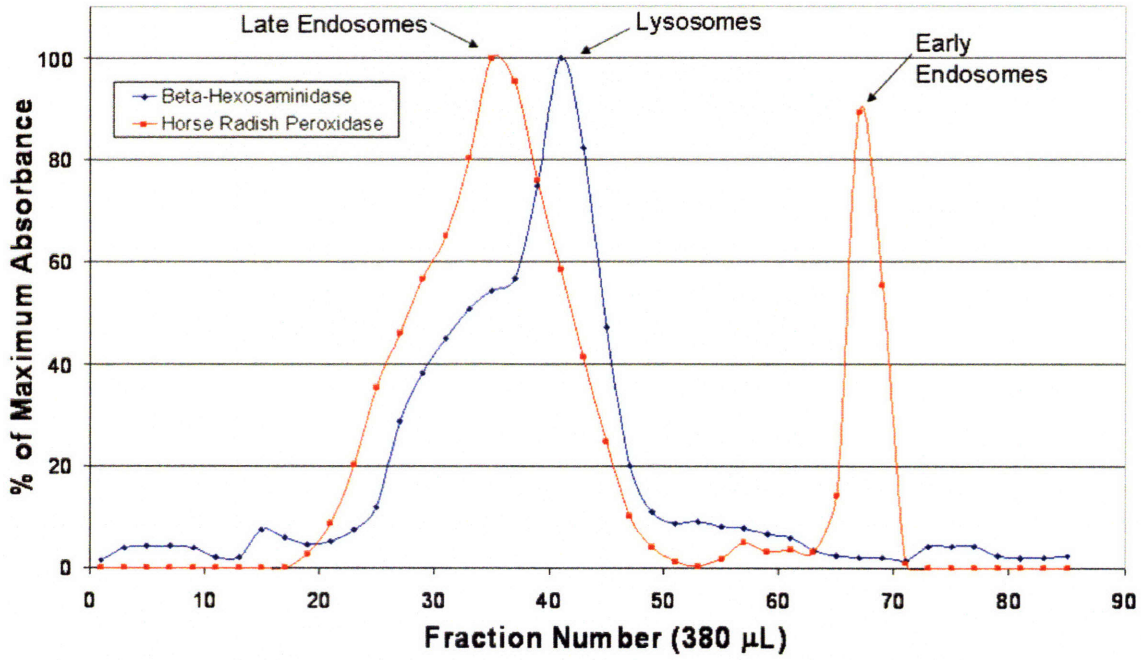

Figure 3.2: Optimized DGE fractionation pattern of endosomes and lysosomes in primary rat hepatocytes. 380 uL fractions were eluted off of the column and collected in a 96 well plate after an 80 min separation run, with fraction 1 being at the top of the column and fraction 85 being at the bottom of the lower density gradient. Prior to lysis and fractionation, cells were subjected to a dual pulse chase pulse of horse radish peroxidase (HRP) to label early and late endosomes. Odd fractions were assayed for HRP to determine the location of these endosomes after the DGE run, and an assay for β-hexosaminidase shows the location of lysosomes. The DGE device successfully separates these three organelle types.

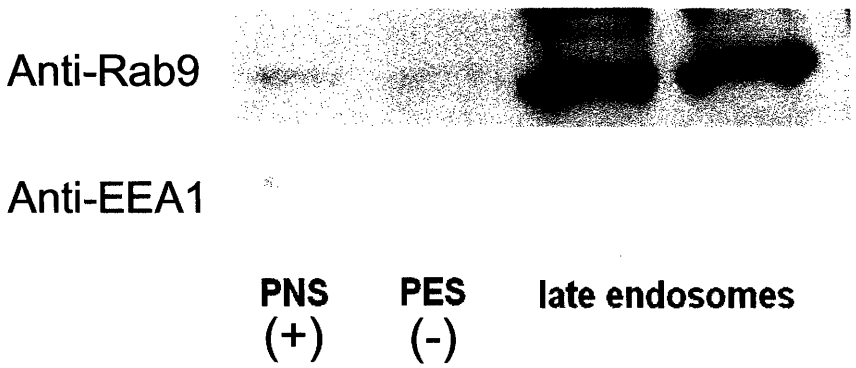

Figure 3.3: Western blot results probing for late and early endosomes in a positive control (PNS, post nuclear supernatant after 1000xg spin of lysate, which should contain all endosomes), a negative control (PES, post endosomal supernatant after 100,000xg spin of lysate), and in vesicles spun down at 100,000xg from fractions comprising the leftmost late endosome peak in figure 3.2 A). Rab9 is a Rab GTPase specific to late endosomes and EEA1, or early endosome antigen one, is a protein complex specific to early endosomes. It should be noted that there is a faint signal in the negative control due to a small fraction of broken endosomal membranes that remain in the supernatant after ultracentrifugation.

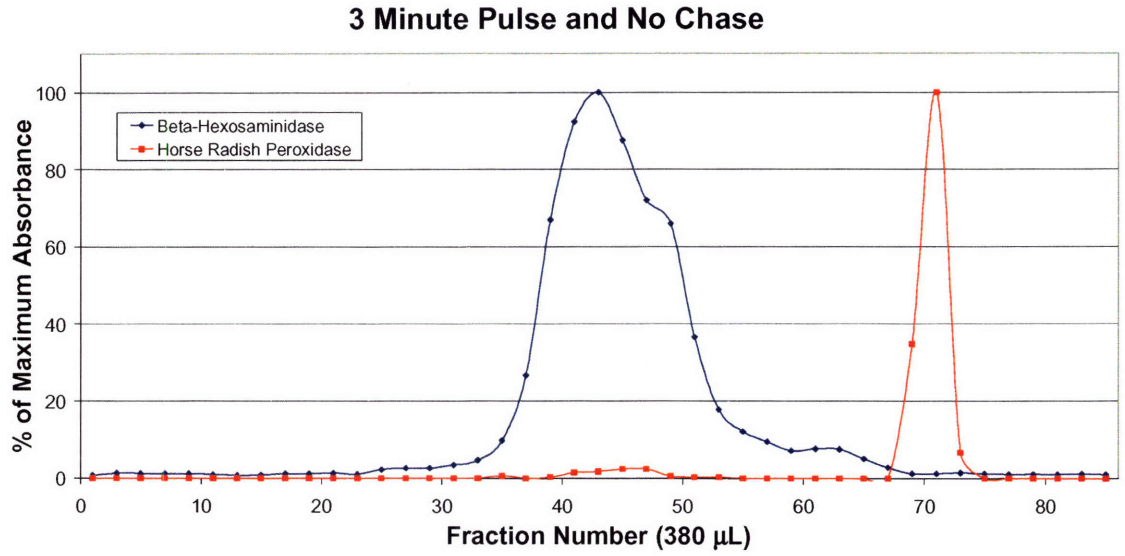

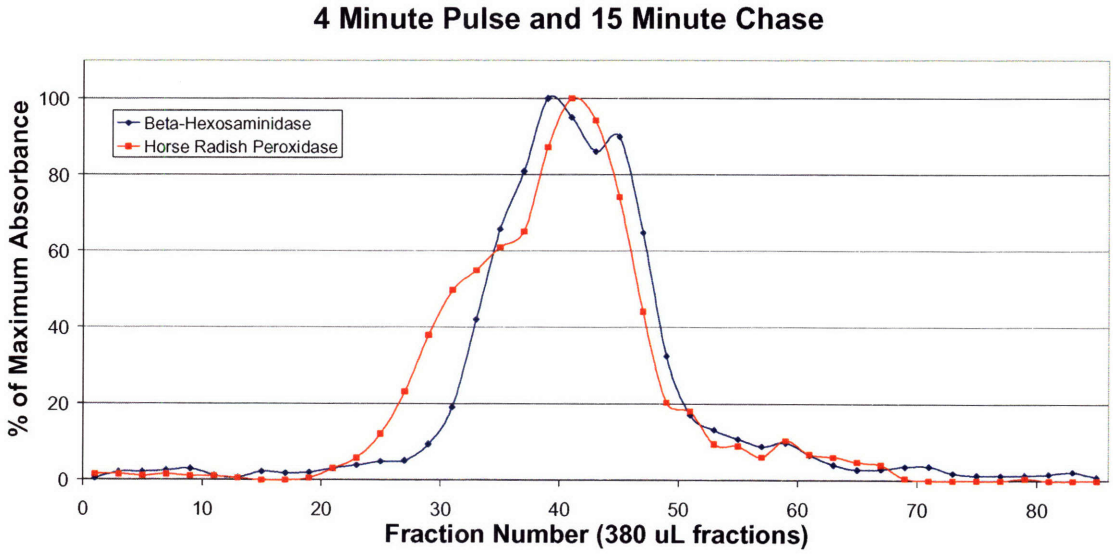

Figure 3.4: Pulse chase characterization of DGE fractionation of primary hepatocytes. Primary hepatocytes were subjected to a single short early HRP pulse immediately followed by lysis or a pulse of HRP followed by an unlabelled media chase to label only late vesicles before lysis. DGE runs yielded unique peaks for the two labelling approaches.

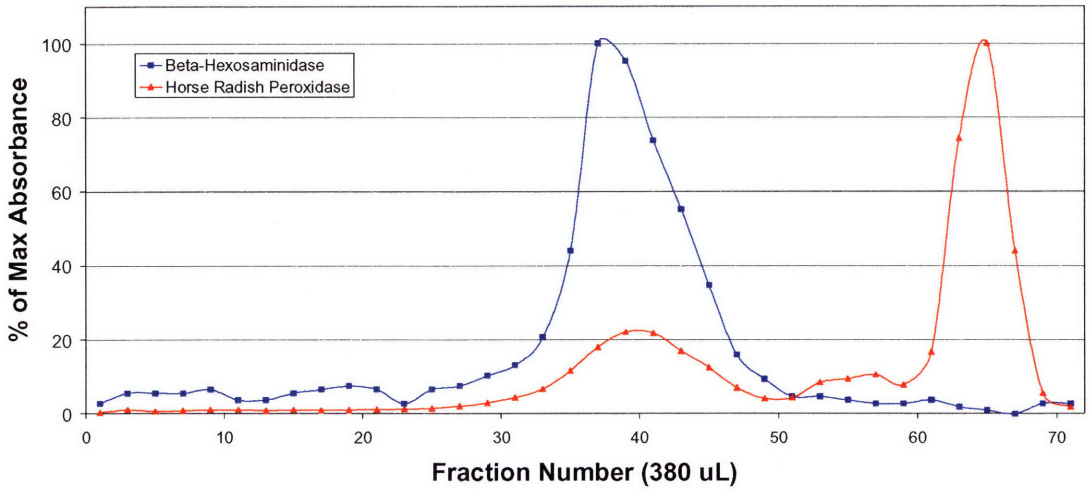

Figure 3.5: Effect of non-viral gene delivery via cationic polyplexes on the DGE fractionation pattern. Primary hepatocytes were simultaneously HRP labeled and transfected with a polyethylenimine non-viral vector (PEI25) complexed with gWiz β-Gal plasmids at an N/P ratio of 20 were lysed 40 minutes after delivery. Organelles were separated by an 80 minute DGE run and 380 uL fractions were collected in a 96 well plate. Gene delivery broadens peaks and causes the late vesicles to shift downward slightly in the column, but this approach still provides excellent separation between late and early vesicles.

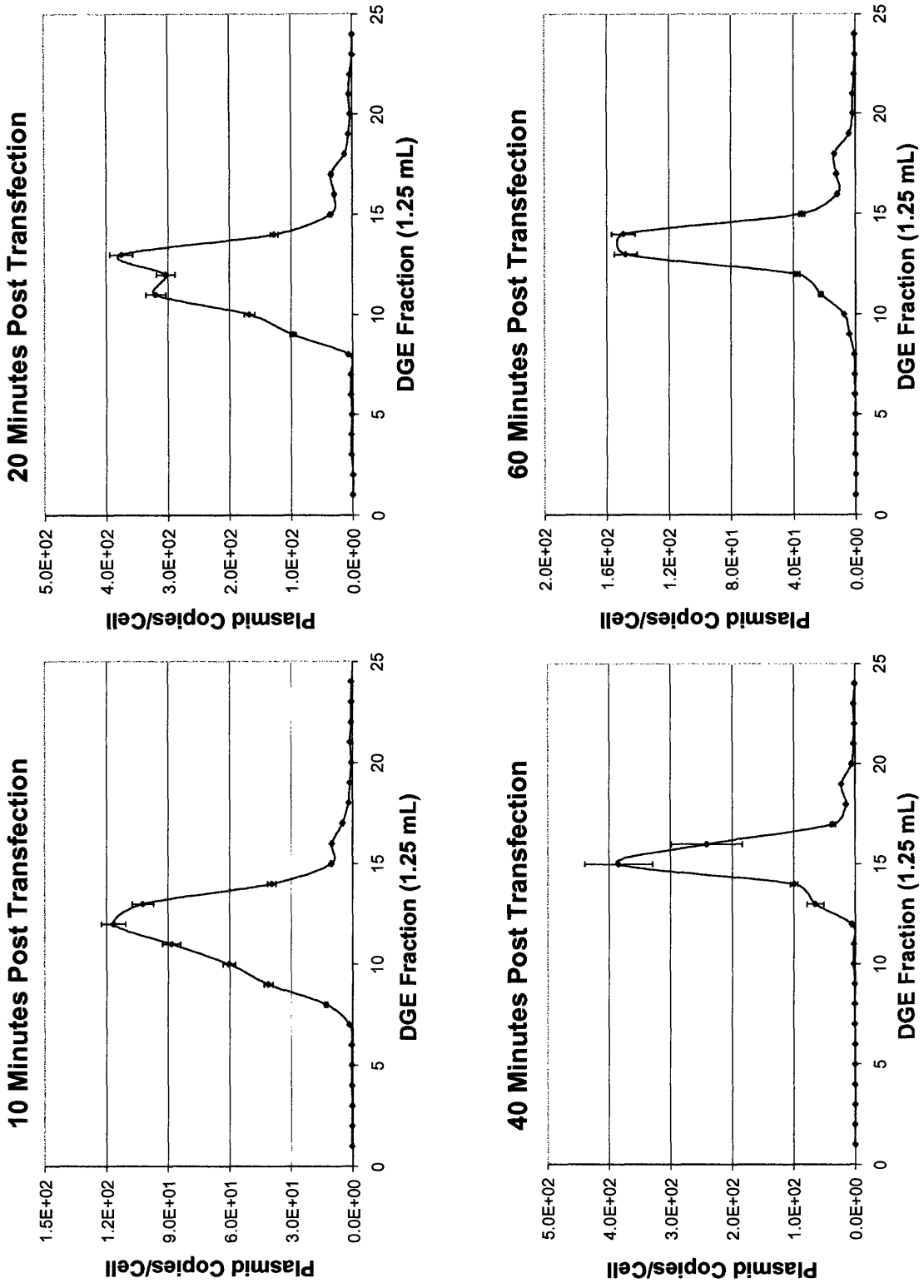

Figure 3.6A: Plasmid mapping of vector trafficking via DGE. Please see the complete figure caption on the following page.

Figure 3.6: A) Plasmid mapping of vector trafficking via DGE. Primary hepatocytes were transfected with C32 complexes at a plasmid to cell ratio of 5e5 plasmids per cell. At the indicated time points after administration of the complexes, cells were collected on ice, lysed and fractionated in an 80 minute run on the DGE column. 24 fractions of 1.25 mL were collected, with fraction 1 representing the top of the column at the end of the run and fraction 24 representing the bottom portion of the lower density gradient. DNA was purified from each fraction, and quantified on a per cell basis using Taqman real-time PCR. Please note the difference in y axis scales in order to best visualize the plasmid peak at each time point. B) Plasmid peaks overlayed with β-hexosaminidase signal to indicate the late vesicle containing fractions (see next page).

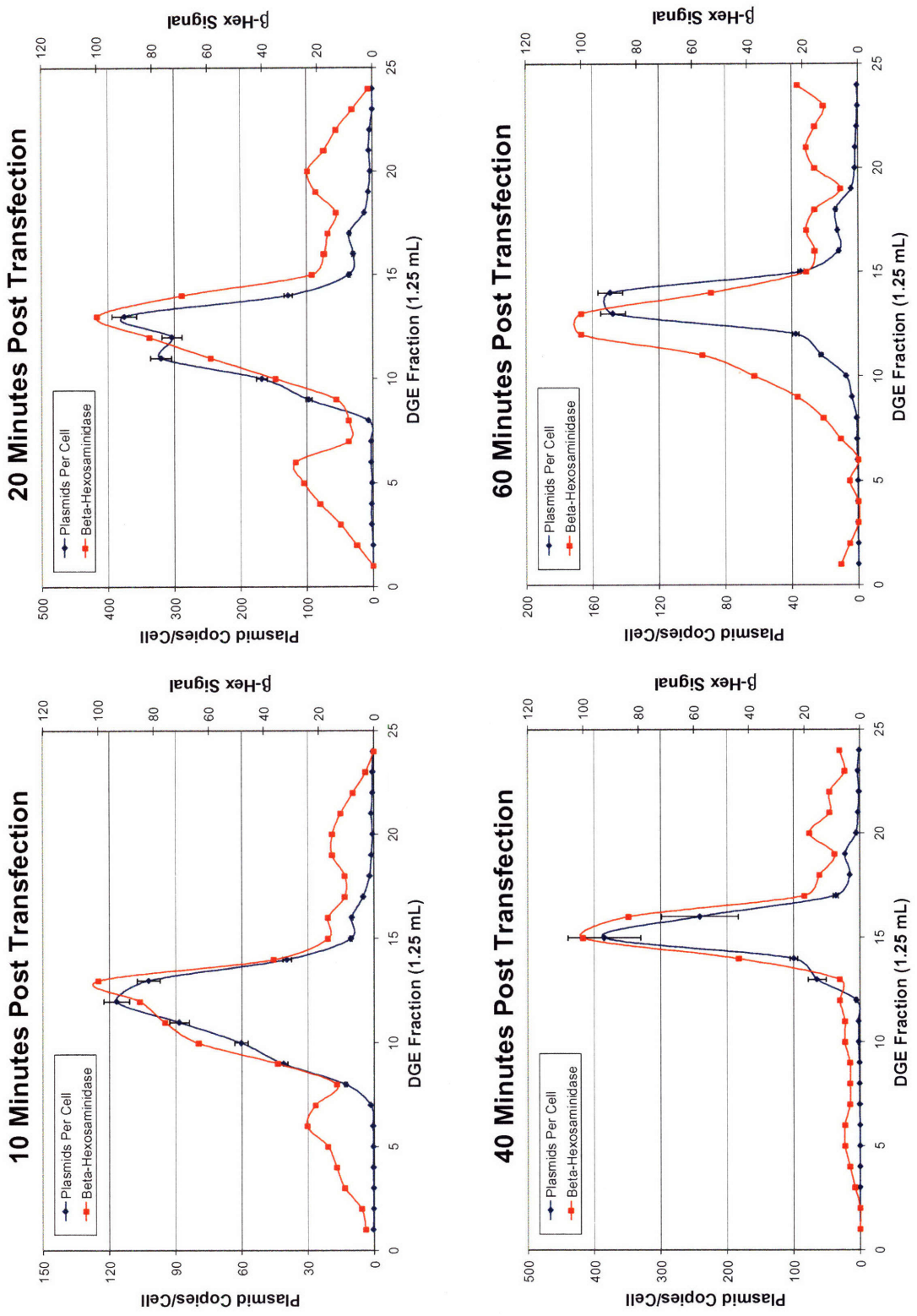

Figure 3.6B: Plasmid mapping of C32 vector trafficking via DGE with β-hexosaminidase peaks overlayed on the plasmid peaks.

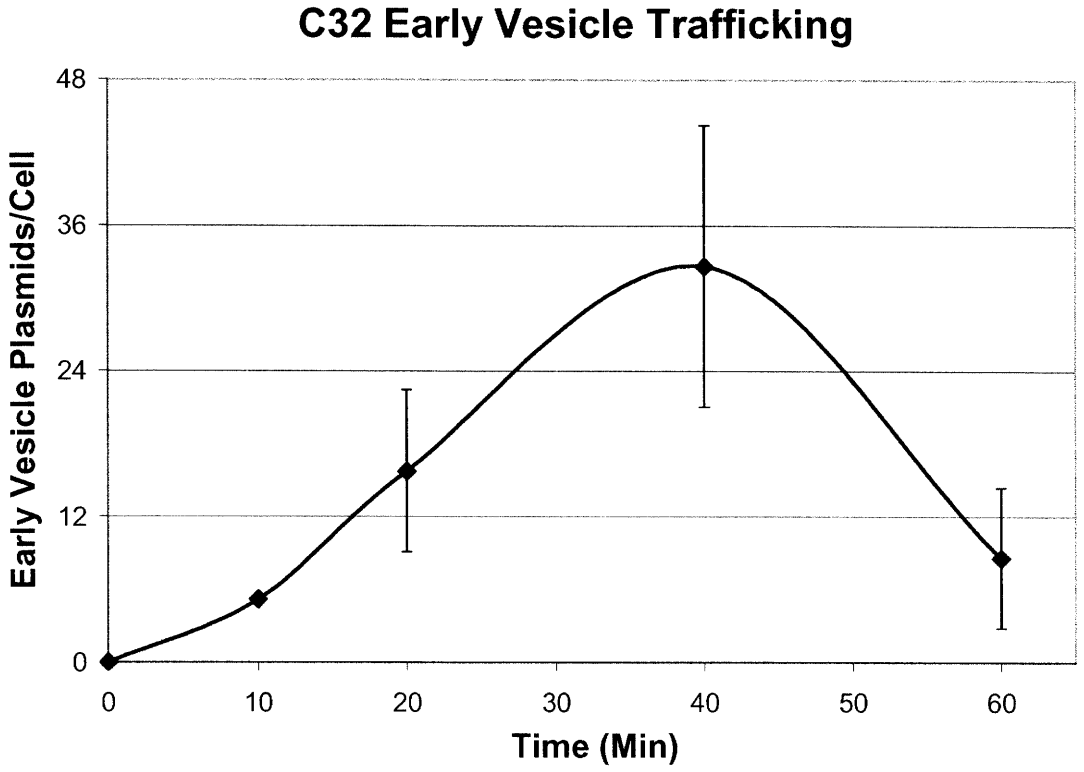

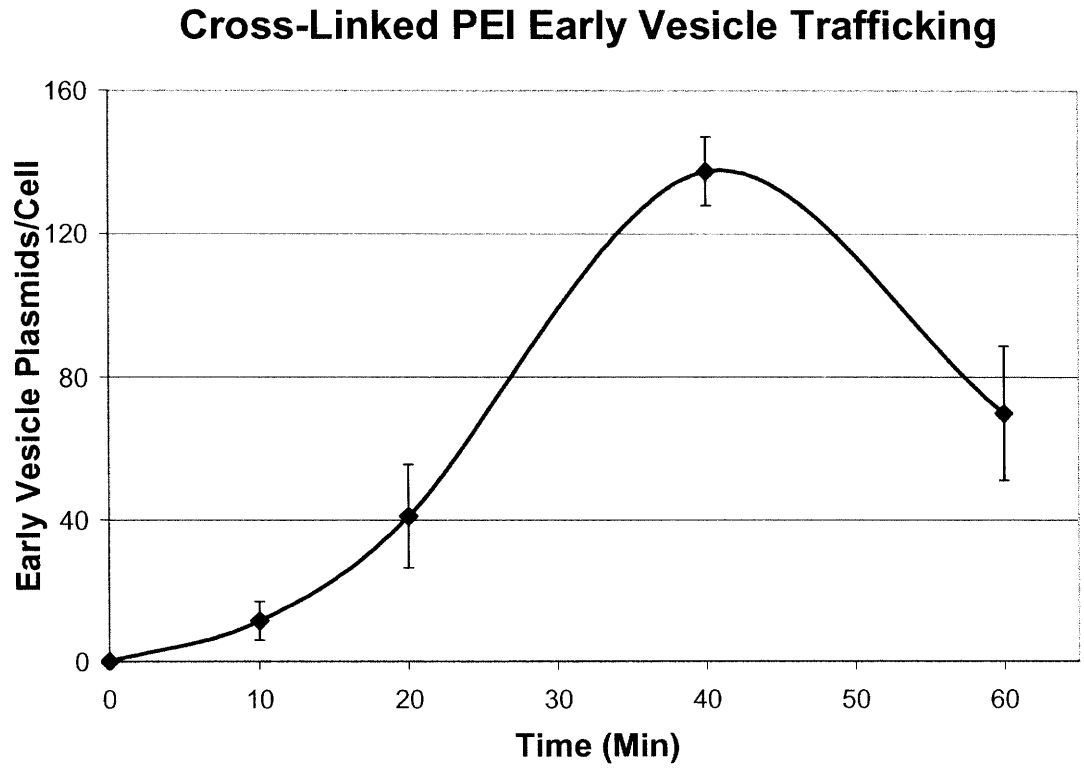

Figure 3.7A: Early vesicle plasmid trafficking time courses for the C32 and small crosslinked PEI non-viral vectors during the first hour after transfection (see full caption on page 98).

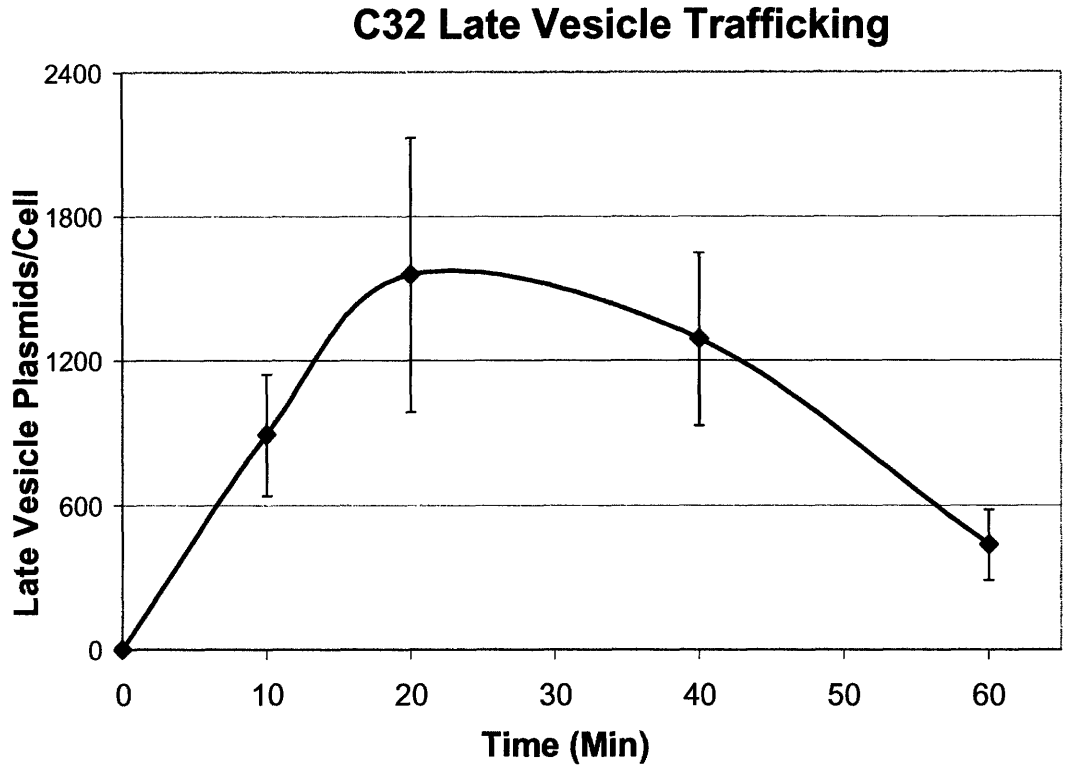

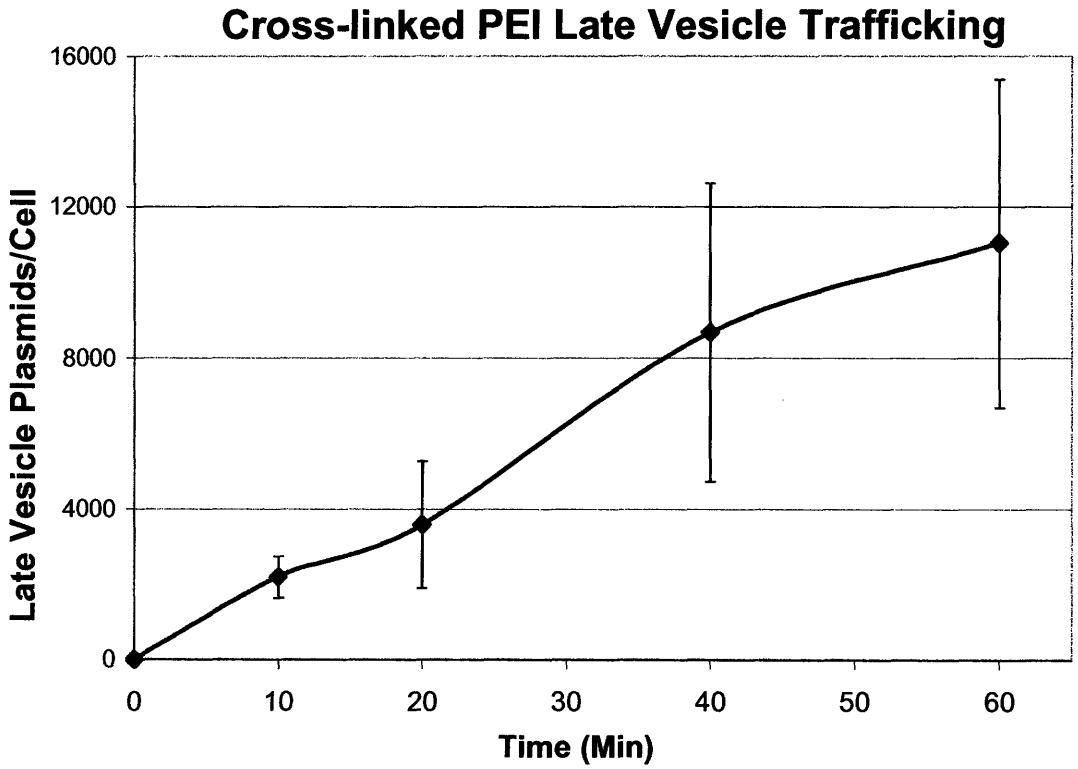

Figure 3.7B: Late vesicle plasmid trafficking time courses for the C32 and small crosslinked PEI non-viral vectors during the first hour after transfection (see full caption on the next page).

Figure 3.7: Quantitative early (A) and late (B) vesicle trafficking time courses for C32 and small cross-linked PEI delivered plasmids. Per cell plasmid amounts were summed for late vesicle containing fractions via β-hexosaminidase mapping for each time point replicate and averaged to show the total per late vesicle per cell plasmid levels over the first hour of delivery. Similarly, the smaller plasmid peaks to the right of the β-hex peaks where early endosomes have been shown to localize were summed to determine early endosomal replicates.

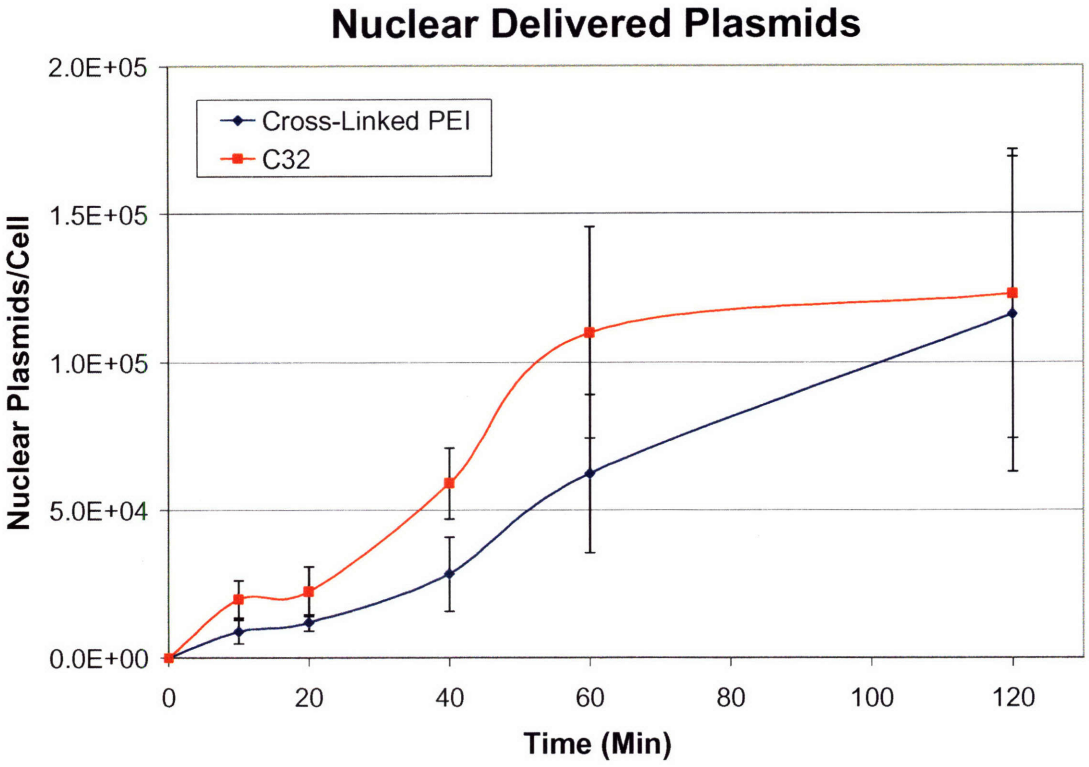

Figure 3.8: Nuclear trafficking of C32 and small cross-linked PEI delivered plasmids in primary hepatocytes. Cells were transfected, and at the time points of interest, mechanically lysed. Nuclei remained intact during lysis and were pelleted and assayed for total per cell plasmid content.

Chapter 4

A 3-D Perfused Liver Bioreactor for the Study of Non-viral Gene Therapy Vector Performance

4.1 Introduction

New approaches in tissue engineering are important for a number of applications. While an ultimate goal in this field is to replace specific organ tissues to address unmet clinical needs, current and future approaches can also be applied to the development of *in vitro* systems that can advance our understanding of the biological processes important in tissue morphogenesis and organ function [188]. The liver is a particularly attractive candidate for such approaches. Primary hepatocytes quickly lose many of their liver specific functions when removed from the liver and cultured in standard formats [172]. Systems that are able to foster the important 3-D microenvironment of the liver, including rebuilding the architecture of homo and heterotypic cell-cell interactions, providing physiologically accurate mechanical cues, and delivering the proper spectrum of molecular factors and stimuli over time, can provide experimental surrogates that better reflect in vivo observations while allowing for more quantitative and multiplexed analysis. Such systems could advance understanding of basic liver biology and development, while also providing more useful information for applied toxicology studies and mechanistic studies of xenobiotic delivery.

A number of improved *in vitro* model systems have been developed in the attempts of recapitulating some degree of the 3-D architecture and functional behavior of *in vivo* liver. These systems and approaches have been reviewed extensively in the context of the degree liver function that can be maintained for specific systems and how these systems can be applied to the drug development process [171]. Notable approaches that move away from more traditional liver slices, microsome preparations and standard 2-D cultures include a number of quasi 3-D seeding approaches in basement membrane and extracellular matrix components, employing novel co-culturing strategies, and 3-D bioreactor systems [189-197].

We have previously developed a three dimensional perfused microarray bioreactor that allows for long term culture of primary hepatocytes and better maintenance of liver specific phenotype [161, 162, 171]. This system provided adequate mass transfer of nutrients and oxygen to cells in functional flow channel units that allowed for the reorganization of primary hepatocytes into 3-D tissue structures. These tissue structures are

maintained at the relevant length scales and mechanical flow environment representative of a liver capillary bed *in vivo*. Initial versions of this reactor system focused on configurations that allowed for precise *in situ* imaging of the tissue units within the cell scaffold, but contained relatively few channels in the array. This allowed for comprehensive evaluation of the tissue over time and provided many insights into ways in which design parameters and device components could be further optimized. This microreactor demonstrated improved maintenance of metabolic function and overall liver phenotype compared to traditional cultures. The system has been applied to drug metabolism and enzyme induction studies [171] and has showed the potential for providing more in vivo like cell interaction seen in the liver parenchyma.

An advantage of this system is that these functional channel units are scalable in number to provide reactors that can hold more total tissue. While imaging and metabolism studies were suitable for the original system, additional applications which required more material to meet the sensitivity demands of various quantitative assays or required the purification of RNA, DNA and protein from the same sample for high information content analyses were not feasible. One application of interest in our current work is to use the perfused liver microreactor as a more clinically relevant in vitro test bed for novel non-viral gene therapy vectors. The liver plays many important roles in *in vivo* gene therapy, and it has been seen in past work that novel carriers that perform well in 2-D cell line models of liver don't necessarily translate this success to in vivo animal models or primary cell cultures. Past work in the original reactor was able to detect GFP based transgene expression from adenovirus delivery at relatively high multiplicities of infection via two-photon microscopy [162]. However for non-viral vectors, which typically yield levels of gene expression that are orders of magnitude below that of their viral counterparts, more cells are needed to quantitatively measure significant differences in transgene expression from different carriers. This motivated the design of a scaled up version of the perfused liver microreactor.

Here we describe the design and fabrication, characterization and initial applications of a new perfused liver bioreactor which has been significantly scaled up from its predecessor. This reactor still utilizes the same original channel size and geometry in the cell scaffold but has employed new chamber designs, components and scaffold fabrication techniques to achieve a much larger array of channels. Flow rates can be carefully controlled such that shear stresses and nutrient and oxygen delivery rates are equivalent to the original

system, allowing for viable primary tissue with well characterized morphological behavior that can be maintained in long term culture. An analysis of liver specific phenotypic gene expression is described that compared this new system with other culture systems, and initial characterization is extended to explore the utility of this system as a test bed for the quantitative evaluation of novel non-viral therapeutics.

4.2 Materials and Methods

4.2.1 Primary Liver Cell Isolation

Primary cells were isolated from male Fisher rats weighing 150-180 gm using a modified version of the Seglen 2-step collagenase procedure as previously described [161, 162, 171]. Blendzyme Type III (Roche, USA) was used for digestion instead of collagenase. Cells that were released by the digestion were suspended in DAG (DMEM (Sigma-Aldrich, USA), Albumin, Gentamycin) and spun and washed twice at 50g for 3 minutes. The final pellet was resuspended in hepatocytes growth medium (HGM), as described previously [161, 162, 171, 187], to yield a 95% or greater pure suspension of hepatocytes. The final cell viability was determined by trypan blue exclusion, and cells were only used if viability was in the 89-95% range. Cells were kept on ice and seeded into 2-D plates or spinner flasks within 10 minutes of the isolation.

4.2.2 Reactor Design, CFD Simulations, Machining, and Components

A number of main flow chamber geometries were conceived and tested for uniform flow profiles in Comsol v3.1 (Comsol, Inc., Burlington, MA). Geometries of the flow chamber were extruded to 3-D, meshed and run with an incompressible Navier Stokes model in the Comsol Multiphysics package. The Navier Stokes equation was non-dimensionalized and Reynolds numbers were simulated that represented the range of flow rates that would be used in the chamber, as well as simulations $\pm$ one order of magnitude from this range to ensure robust operation. The geometry that yielded the most uniform flow and easiest machining was chosen. The three main body pieces for the reactor were machined from polycarbonate based on this design and tested with qualitative dye tracking experiments. Satisfactory results were observed, and these pieces were mass produced for

biological characterization studies. All compartments were fabricated by standard CNC machining. The fluidic ports in the compartments were fitted with commercially available polypropylene connectors (Ark-Plas Products, Flippin, Arkansas). The overall size of the 3-compartment bioreactor housing was approximately 78 x 54 x 21 mm.

Oblong scaffold blanks were cut out of a 230 um thick sheet of polycarbonate (McMaster-Carr, Dayton, NJ). In each blank, a 20 x 50 array of microchannels was micromachined using a 9X molybdenum mask on an IX-1000 industrial workstation equipped with a KrF excimer laser lasing at 248 nm (J. P. Sercel Associates, Hollis, NH). The entire channel array was scanned with a mask scanning technique to minimize localized heating of the scaffold. Two alignment holes were also laser-machined in the scaffold. The holes were used to accurately position the scaffold in the bioreactor pocket furnished with a pair of Dowel pins. This arrangement ensured precise co-registration of the microchannels in the cell-holding and support scaffolds. Peristaltic tubes and pumps (Instech Labs, Inc., Plymouth Meeting, PA) were integrated in to custom dual pump boxes with digital potentiometers to control pumps rates. 13.5 V AC adaptors and power jack connectors were purchased from Radio Shack. With the exception of 5 um Durapore filters for the reactor chamber (Millipore, Billerica, MA) and inline syringe filters (Pall, USA), all other components and raw materials were obtained from McMaster Carr including O-rings, screws, tubing, silicone sheets for punching custom gaskets, reservoirs, and stainless steel for custom retaining rings.

4.2.3 Preparation of 2-D Collagen Gel Sandwich and Adsorbed Collagen Cultures

Collagen sandwich cultures were prepared as explained in previous methods [171]. 35 mm 6-well plates were coated with 600 uL of a collagen solution and allowed to gel overnight at 37°C and 8.5% CO_2. Cells were seeded at 50,000 cells/cm^2 in HGM at a concentration of 500,000 cells/mL. Cells were incubated overnight, the medium was aspirated, and a top layer of 300 uL of collagen solution was evenly distributed in each well to form a top gel layer for an hour. 1 mL of HGM was then added to each well and changed daily thereafter.

For 2-D transfection experiments, cells were seeded in 60 mm tissue culture dishes treated with a dried adsorbed collagen monolayer. Collagen type I from rat tail (BD Biosciences, Bedford, MA) was diluted in sterile 1x PBS at a concentration of 30 ug/mL.

Plates were incubated with 3 mL of this solution for 2 hours, then aspirated and allowed to dry in a sterile hood for two hours prior to seeding. Cells were seeded in 3 mL of HGM at a density of 800,000 cells/mL immediately after isolation. Medium was changed 4 hours post-seeding to eliminate dead and unattached cells and debris, while ensuring 90-95% confluency. All experiments were performed within 24 hours of seeding to ensure the best maintenance of hepatocyte phenotype.

4.2.4 Preparation of 3-D Hepatocyte Spheroids

30 million isolated primary rat hepatocytes were added to 100 mL of HGM in a 500 mL spinner flask (BellCo, NJ, USA) on a spinner table and spun at 85 rpm [198]. The cells formed spheroidal aggregates and were collected after 3 days of culture just prior to reactor seeding. Spheroids in the 100-300 um size range were retained by using the appropriately sized filter meshes (Sefar America, Kansas City, MO). This fraction was spun down at 50g for 3 minutes, and gently resuspended in 20 mL of fresh HGM to reduce debris in the seeding. We have previously shown better maintenance of functional tissue phenotype in perfused microreactor systems seeded with spheroids as opposed to single cells [161, 162].

4.2.5 Assembly, Seeding, and Maintenance of the Liver Bioreactor

Polycarbonate reactor body pieces and scaffolds were sterilized by soaking in 70% ethanol for 30 minutes, followed by a rinse in sterile 1x PBS. All other reactor components were sterilized via autoclaving. Prior to assembly, the upper cell holding scaffold was treated with collagen to promote cell attachment. The scaffold was soaked in a 30 ug/mL solution of collagen (Type 1 form rat tail, BD Biosciences, USA) in 1x PBS for 2 hours at 37°C, and then aspirated and allowed to dry in a sterile dish for 2 hours. The 5 um middle filter was coated with 1% BSA (Sigma, St. Louis, MO) for 30 minutes and then rinsed in PBS. Sterile components were assembled into the reactor body in the order seen in Figure 4.2. The inlet and outlet connectors were then connected to the tubing and reservoir and loaded onto the dual peristaltic pump box. Reactors were primed with 25 mLs of HGM (which contains 2 g/L of BSA) for one hours to passivate the inner surfaces of the bioreactor and tubing and to eliminate any air bubbles from the system. Medium was changed just prior to seeding.

To seed spheroids into the channels, the upper chamber was partially drained and the top window was removed. A moderate downward crossflow was turned on (1-2

mL/min range) and 3-4 mLs of the spheroid suspension was gently pipetted over the scaffold array. The reactor was gently rocked as the crossflow helped pull the spheroids into the channels. The cell suspension was repipetted up and down in the reactor chamber to drop over the channel array if seeding looked uneven after visual inspection. Crossflow was turned off and the top window was then returned to the reactor body. Main flow was turned on at 3 mL/min and the reactor was held at an incline with the outlet end up to remove air from the chamber and expel any unseeded spheroids into the reservoir. Downward crossflow was then turned on at 1 mL/min to help retain seeded cells in the channel and subject cells to physiological levels of shear stress and nutrient and oxygen delivery [161, 162]. Medium was changed 2 hours post seeding to remove unseeded cells and debris from the reservoir.

After 1 day of the culture in the bioreactor, spheroids have attached to the channel walls and begun to spread and rearrange. Therefore, downward crossflow is no longer needed to retain the cells in the channels. The crossflow is reversed to an upward direction at 1 mL/min at this point to remove unattached cells and debris and is maintained in this direction for the duration of the culture. Now that the crossflow pump was sending medium into the lower reactor chamber, there existed the danger of pumping these freed cells and debris in to the lower chamber and clogging the underside of some channels in the support scaffold. This would cause uneven perfusion flow in some of the channels, which is usually kept constant across all channels due to the 5 um filter between the upper cell scaffold and lower support scaffold providing the primary resistance to flow. To maintain constant flow in all channels, chain of in-line filters was placed in the crossflow line between the pump and the lower reactor chamber. Since this new reactor system contained significantly more cells, there is more debris initially in the circulation after crossflow change, therefore 3 filters are required in series to prevent the reactor from clogging – a 5 um filter, a 1.2 um filter and a 0.8/0.2 filter. This set-up was able to maintain constant flow over long term culture. The filter chain was primed with HGM prior to the crossflow change, and medium was changed 1 hour after crossflow change as well to removed most of the debris. After crossflow reversal, medium was changed every 2 days, and filter chains were changed every 3 days. Cultures were maintained in an incubator at 37°C and 8.5% CO_2.

4.2.6 RNA Isolation and cDNA Generation

Total RNA was recovered from 2-D collagen gel sandwich cultures and 3-D liver reactor cultures at 7 days post-isolation. For 2-D sandwich cultures, 1 mL of TRIzol® (Invitrogen, Carlsbad, CA) was added to each well, and the well contents were homogenized with a 25G needle, collected in an Eppendorf tube, and frozen at -80°C. For 3-D bioreactor cultures, giant reactors were disassembled and the cell scaffold was placed in a 10 cm Petri dish and incubated in 3 mL of Dispase (BD Biosciences, USA) for 5 minutes at 37°C. Tissue was collected in the bottom of the dish via gentle pipetting through the channel array, transferred to a 15 mL centrifuge tube, and pelleted at 50g for 3 minutes. Supernatant was removed with a pipette, and the cell pellet was resuspended in 1 mL of TRIzol®, transferred to an Eppendorf tube and frozen at -80°C. For Milli-F reactors, scaffolds were placed directly in an Eppendorf tube containing 1 mL of TRIzol® and frozen. Samples were then thawed and any remaining tissue attached to the channel walls was washed off of the scaffolds and lysed with a 25G needle. For isolated hepatocytes, 1 million cells were pelleted at 50g for 3 minutes immediately after the perfusion. Supernatant was removed and cells were resuspended in 1 mL of TRIzol® and similarly frozen. For *in vivo* rat liver slices, 1 slice of each of the four lobes was removed and placed in 5 mL of TRIzol®. The liver pieces were then broken up using a tissue homogenizer at high speed and frozen at -80°C. 1 mL of the total 5 mL was processed for total RNA recovery.

To recover RNA, samples were thawed on ice and 200 uL of chloroform was added to separate the RNA from an organic phase containing DNA and protein. Samples were mixed by inverting and vortexing and then spun at 12,000g for 15 minutes at 4°C to fully segregate the aqueous and organic phases. RNA was then cleaned and concentrated using the Qiagen RNEasy Mini kit (Qiagen, Valencia, CA) and stored at -80°C. For conversion to cDNA, RNA samples were thawed on ice, and sample concentrations and purity were determined using a NanoDrop (NanoDrop Technologies, Wilmington, DE) and evaluating the A260 and A260/A280 ratio. 200 ng of total RNA was brought to a volume of 8 uL with DEPC water (Qiagen). 1 uL of amplification grade DNAse I (Invitrogen) and 1 uL of DNAse I of 10x DNAse I buffer were added and incubated for 15 minutes at room temperature to eliminate any genomic DNA contamination. The enzyme was then inactivated by adding 1 uL of 25 mM EDTA (Invitrogen) and incubating at 65°C for 10 minutes. 9 uL of a master mix solution containing 1 uL of DEPC water, 2 uL of a 5mM

dNTP mix (Qiagen), 2 uL of a 10 uM stock of random hexamer primers, 2 uL of 10x RT Buffer (Qiagen), 1 uL of Omniscript RT® solution (Qiagen, 40 units activity/uL), and 1 uL of a 1:10 RNAse inhibitor dilution in 1x RT buffer (Ambion, 1 unit activity/uL stock). The samples were mixed, spun down and incubated at 37°C for 1 hour for the reverse transcription reaction to occur. Samples were then spun down and stored at -80°C.

4.2.7 Primers and RT-PCR

Primers specific for genes indicative of maintenance of liver phenotype in hepatocytes were designed using mRNA or cDNA sequences from the NCBI database in the primer3 software at the Whitehead Institute (http://frodo.wi.mit.edu/cgi-bin/primer3/primer3_www) and have been previously described [171]. mRNA expression studied in this work used the following primers: 18s (5-GCAATTATTCCCCATGAACG-3 forward and 5-GGCCTCACTAAACCATCCAA-3 reverse), FABP-1 (5- CCAGAAAGGG AAGGACATCA-3 forward and 5- GTCTCCAGTTCGCACTCCTC-3 reverse), PEPCK (5-ATACGGTGGGAACTCACTGC-3 forward and 5- TGCCTTCGGGGTTAGTTATG-3 reverse), Catalase (5- ACATGGTCTGGGACTTCTGG-3 forward and 5- CCATTCGCAT TAACCAGCTT-3 reverse), HNF3a (5-TCAACGCTTGTTTCGTCAAG-3 forward and 5-TCACACTTGAAGCGCTTTTG-3 reverse), HNF-4a (5-CTGAGACTCCACAGCC ATCA-3 forward and 5-CTAGATGGCTTCCTGCTTGG-3 reverse), CAR (5-GGAG GACCAGATCTCCCTTC-3 forward and 5-GACCGCATCTTCCATCTTGT-3 reverse), AHR (5-ACTACACGCCAGACCAGCTT forward and 5-ATTCATTGCCAGGA AACCAG-3 reverse), OATP-1 (5-AACCCTGAAATGTGGTCAGC-3 forward and 5-GCAGGCAGATAGCTTGATCC-3 reverse), OATP-2 (5-CAATTCGGTATCCCCA CATC-3 forward and 5-CTGCACATCCAACACCAATC-3 reverse), BSEP (5-CCAC CAGAACATGACAACG-3 forward and 5-CCCAGTGATGACCCATAACC-3 reverse), FXR (5-ATGTCCGGAGTTCTGTCAGG-3 forward and 5-GCCTCTGCTCGATGTC CTAC-3 reverse), GST-Ya (5-CTTGGCAAA AGACAGGACC-3 forward and 5-GTTTT GCATCCATGGGAAGC-3 reverse), MDR2 (5-CTTTGTGGTGGGGACAC TCT-3 forward and 5-CCAAGAAGACCAGCGAGAAC-3 reverse), and HNF1a (5-GCCATCTG GGTGGAGATAAA-3 forward and 5-ACCAGTCCCACAGTG TCCTC-3 reverse).

For quantitation of mRNA expression levels, 1 uL of cDNA was added to 25 uL of SYBR Green 2x Master Mix (Qiagen), 21 uL of DEPC water, and 1.5 uL each of the forward and reverse primers. A Chromo4 real-time PCR detection system (MJ Research, Waltham, MA) was used with Opticon Monitor 3 software to run standard Qiagen SYBR Green RT-PCR annealing and melting protocols. Melting curves were analyzed to ensure primer specificity and threshold levels were kept consistent between runs for accurate comparison between genes and culture systems. The ribosomal RNA 18s has been found to be constant relative to total RNA and cell number across these 2-D and 3-D cultures systems, and was therefore used to internally normalize each gene before replicates were averaged or expression levels were compared between systems.

4.2.8 Plasmid, Polymers, Virus and Non-viral Complex Formation

Plasmid gWiz-β-Galactosidase (Gene Therapy Systems, San Diego, CA) encodes the enzyme β-galactosidase controlled by the human cytomegalovirus (CMV) promoter. The plasmid DNA was purchased purified and ready for use from a contract plasmid manufacturing company (Aldevron, Fargo, ND). 25kD PEI was purchased from Sigma-Aldrich (St Louis, MO). The small cross-linked PEI and the C32 polymer were synthesized as described previously [105, 106, 108]. The adenovirus serotype 5 with E1 and E3 deletions encoding β-galactosidase under a CMV promoter was purchased from Vector Core (University of Michigan, Ann Arbor, MI).

For transfection via PEI25 and small cross-linked PEI, polymer and DNA were diluted to the appropriate concentrations in sterile water and combined at an N/P ratio of 20 and 30, respectively. Polymer was added to DNA and left at room temperature for 20 minutes PEI25 and 10 minutes for the small cross-linked PEI to allow for formation of complexes. For C32, polymer and DNA were diluted in sterile filtered sodium acetate buffer, pH 5.4, combined at a polymer mass/DNA mass ratio of 100, and left at room temperature for 5 minutes before adding to prewarmed medium. All complexes and naked DNA were added to HGM at a DNA concentration of 5 ug/mL. For adenovirus, a master stock was thawed on ice and diluted 1:100 in a 10% glycerol in 1x PBS buffer to make frozen working stock aliquots. The appropriate amount of particles were added for a multiplicity of infection of 20 assuming that there were 1 million cells seeded in the reactor

cultures and 2 million cells in 2-D cultures. Non-viral particle size was determined via dynamic light scattering using a ZetaPALS Zeta Potential Analyzer with ZetaPALS Particle Sizing Software Version 2.3 (Brookhaven Instruments Corporation, Holtzville, NY). Number averaged particle diameters were determined over a lognormal distribution for each vector/plasmid complex. The 25kD PEI complexes measured 228.3 ± 47.6 nm in diameter, the small cross-linked PEI complexes were 167.5 ± 8.2 nm, and the C32 complexes were 152.0 ± 4.2 nm.

4.2.9 Transfection and Gene Expression Assays

For 2-D transfections, cells were seeded and washed on adsorbed collagen monolayers as described above and cultured overnight. Cells were then transfected with naked DNA, non-viral vectors, or adenovirus in 2 mLs of HGM at the appropriate concentrations noted above. Cultures were maintained for 48 hours and then transfection medium was removed, and cells were washed and collected in 1x Reporter Lysis Buffer (Promega, Madison, WI) and β-Galactosidase transgene expression levels were measured in the cell lysate using an absorbance based assay kit (Promega). Transgene expression levels were normalized to total protein in each sample, using a BCA Total Protein Assay kit (Pierce, Rockford, IL).

For 3-D transfection, liver bioreactors were seeded as described above and maintained for 4 days (Day 7 post isolation). To ensure that the inline filter chain did not lead to significant vector adsorption and loss, the crossflow was reversed back to 1 mL/min downward through the channels. This allowed for removal of the filter chain without the danger of clogging the system or developing uneven flow through the channels. Medium was aspirated from the reservoir cup, and 6 mLs of medium at the appropriate concentration for each vector was added. Reactor cultures were maintained with 3 mL/min of main flow across the upper chamber and downward crossflow of 1 mL/min for 48 hours. Giant reactors were disassembled and the cell scaffold was placed in a 10 cm Petri dish and incubated in 3 mL of Dispase for 5 minutes at 37°C. Tissue was collected in the bottom of the dish via gentle pipetting through the channel array, transferred to a 15 mL centrifuge tube, and pelleted at 50g for 3 minutes. Supernatant was removed with a pipette, and the cell pellet was resuspended in 1 mL of 1x Reporter Lysis Buffer and processed, assayed and normalized as above for the 2-D samples.

4.3 Results

4.3.1 Reactor Design and Fabrication

An exploded view of the large reactor can be seen in Figure 4.1. The reactor body consists of three main polycarbonate pieces. All scaffold components fit precisely into a pocket on the bottom side of the middle piece. Two silicone gaskets and a silicone O-ring with a stainless steel retaining ring provide a seal around the outer edges of the primary scaffold components, creating an upper and lower flow chamber when the top window and base are screwed into the middle piece. The top window of the reactor body can be easily removed after assembly and priming to efficiently seed cell spheroids into the channels of the top scaffold via pipetting. The 5 um hydrophilic Durapore filter (Millipore) is sandwiched between the cell holding scaffold and lower support scaffold to provide constant flow resistance across the scaffold array, regardless of how many cells are seeded into each individual channel. This results in uniform crossflow in all channels. This filter also helps to retain cells in the channels initially after seeding. The cell scaffolds were also machined from polycarbonate, using a laser machining technique that allowed for the precise cutting of 1000 300x300x230 um channels without warping. The channels were arranged in a 20x50 array. By machining two alignment holes at the sides of the scaffold away from the channel array and seating two alignment pins in the reactor body pocket, precise co-registration between the cell scaffold and the support scaffold was consistently achieved and allowed for uniform perfusion flow for all scaffold pairs. The polycarbonate scaffolds stayed well aligned under a large range of flow rates, and were much easier to handle and insert into the reactor pocket due to their flexibility and compatibility with the gaskets than the silicon scaffolds used in the original reactor system.

The overall fluidic circuit for the reactor is controlled by a dual peristaltic pump (Figure 4.2). Main flow is controlled by pump A which replenishes the upper chamber and drives flow over the scaffold surface and out of the upper chamber outlet for reoxygenation of medium in the tubing and medium reservoir. Pump B controls the crossflow, and can send flow to or from the lower reactor chamber to create perfusion flow either upward or downward through the channels. The upper and middle body components were also designed to have an injection port at the inlet and outlet of the upper flow chamber so that media could be directly sampled from the reactor, probes could be inserted for monitoring oxygen, and drugs or gene vectors could be administered without opening the reservoir or

detaching any tubing. Media flow rates in the main chamber were adjusted such that the scale-up of main flow and of upper chamber volume and scaffold surface area would yield the same scaffold shear stresses as previously modeled [162]. Per channel perfusion cross flow rates were maintained at the same rate as the original system. To insure that the cell scaffold experienced a uniform velocity field and shear stresses across the entire channel array, different upper flow chamber geometries were designed and subjected to computational fluid dynamics simulations at the desired flow rates. The optimal design, which yielded uniform velocity and no recirculation of flow over the channel array (Figure 4.3), was machined as a prototype and tested before mass production via standard CNC machining. Figure 4.4 shows a fully assembled giant reactor with the optimal inlet and outlet geometries. The upper laser machined scaffold can be seen through the top window, which still allows for *in situ* light microscopy of the channels during culture.

4.3.2 Reactor Seeding, Tissue Reorganization and Maintenance of 3-D Cultures

A 95% pure fraction of isolated rat hepatocytes was cultured in a spinner flask for 3 days to form spheroidal aggregates. Prior to assembling reactors, the top cell holding scaffold was treated with collagen to promote cell attachment and the Durapore filter was treated with 1% bovine serum albumin (BSA) to prevent cell adhesion and potential clogging of perfusion flow in the channels. Reactors were then assembled and primed with HGM to passivate all of the inner surfaces of the fluidics circuit. Spheroids were sized fractionated to acquire aggregates with diameters in the 100-300 um range. It had been previously shown that seeding reactors with spheroids as opposed to single cells resulted in superior tissue morphogenesis and function [162]. These spheroids were pelleted and resuspended in fresh HGM, and medium was also changed in the primed reactors. The fact that this new reactor has a removable top window makes for fast and efficient seeding of the channels. Channels were evenly packed with spheroids in under 1 minute. For the first 24 hours of culture, downward crossflow was maintained at a rate of 1 mL/min, or 1 uL/channel/min, with a main flow of 3 mL/min. This helped retain the cells in the channels as they began to attach to the collagen coated walls. By 24 hours, cells attached very well to the channels walls and had already begun spreading and reorganizing. Cross-flow was then reversed in an upward direction at the same flow rate. This expelled debris from the channels as well as any dead or unattached cells, leaving viable adhesive cells that could further reorganize. The cross

flow line was outfitted with a chain of in-line filters to prevent clogging of the channels due to debris build-up in the lower flow chamber against the support scaffold channels.

These 3-D cultures were typically maintained until day 7 post isolation before experiments were performed. The tissue in the channels showed extensive attachment to the walls and formation of annular tissue structures at this point (Figure 4.5). The polycarbonate scaffolds demonstrated excellent retention of tissue under these flow conditions. At day 7 post isolation, an average of just over 1 million viable cells were recovered from the channels of each large reactor, as determined by total RNA measurements and RT-PCR of 18s ribosomal RNA, followed by comparison to a standard curve. This is a vast increase over the original Milli reactor system, which usually housed an average of 40,000 cells. A protocol was developed that allowed for efficient recovery of these cells for various downstream quantitative assays. Incubation of the cell scaffold in Dispase (BD Biosciences), a bacterial amino-endo peptidase, for 5 minutes effectively loosens the tissue structures from the channel walls. Intact cells can be collected by gently expelling them from the channels via gentle pipetting after this short incubation. Cells can then be pelleted and frozen or processed for any number of assays.

4.3.3 Quantitative Comparison of Liver Phenotype via RT-PCR

In order to more definitively gauge the maintenance of liver phenotype in this new system, quantitative RT-PCR was performed to measure the level of liver specific mRNA transcripts in comparison with *in vivo* liver, freshly isolated hepatocytes, standard 2-D collagen gel sandwich cultures, and the original Milli microreactor system. This analysis could answer a number of questions including how the reactor compared to in vivo transcript levels, if this new system was superior to traditional 2-D cultures in maintenance of hepatic phenotype, and also if the changes made to scale up the reactor significantly changed its performance from its smaller predecessor.

RNA was isolated from in vivo liver slices and isolated hepatocytes immediately after surgery and isolation, and from day 7 cultures for the collagen sandwich and liver bioreactor cultures. cDNA was generated from each RNA sample and optimized primer sets for genes indicative of liver specific function were quantified via real-time SYBR Green PCR. A microarray analysis using Affymetrix Rat Genome Array (U34A) Gene Chips had previously been performed to identify which genes were most significantly upregulated in liver tissue in

comparison with other tissues [171] and a subset of these genes were examined in this study. For each culture system, normalized replicates were averaged for these genes and then all data was normalized to the *in vivo* liver transcript levels (Figure 4.6). The genes tested represented a panel of liver enriched transcription factors: HNF-1a, HNF-3a, and HNF-4a; membrane transporters and general metabolism genes: FABP-1, BSEP, Catalase, MDR2, OATP-1, and OATP-2; phase II metabolic enzymes: GST-Ya; and liver enriched nuclear receptors: CAR, AHR, and FXR. In general, it could be seen that the large reactor maintains more upregulated liver phenotype at the transcript level than 2-D collagen sandwich cultures, and that the overall pattern of expression for this new system is comparable to the original microreactor, suggesting that scaling up the system did not significantly alter the hepatocyte culture at the functional level.

4.3.4 Transfection Experiments in 2-D and 3-D Culture Systems

2-D adsorbed collagen monolayer and 3-D Giant reactor cultures were transfected as described in sections 4.2.8 and 4.2.9 with five gene therapy vectors: naked plasmid DNA, traditional PEI25 complexes, next generation non-viral complexes small cross-linked PEI and poly(β-amino ester) C32, and a canonical viral vector, adenovirus serotype 5. All delivered the same β-galactosidase transgene under the same CMV promoter. Samples were lysed and quantitatively assayed for transgene expression at 48 hours after transfection. Normalized replicates were averaged and then globally normalized to the respective PEI25 expression level in each culture system (Figure 4.7).

The Giant reactor provided enough transfected cells to detect PEI25 expression well above control levels, which was not possible due to signal to noise limitations in the original Milli reactor system. Naked DNA yielded expression that was slightly above control levels in 2-D transfections, but was not significantly different from the control in the 3-D system. In 2-D, the small cross-linked PEI transfected primary hepatocytes with 80 times the efficiency of PEI25 and yielded expression that was almost half that of adenovirus, which gave 170 times the expression of the PEI25 vector. Meanwhile, the C32 vector was slightly less efficient but still gave high expression in 2-D, with over 30 times the gene expression of PEI25. Interestingly, in 3-D this trend was reversed between the next generation non-viral vectors. The small cross-linked PEI transfection resulted in a slightly more than 3 times the gene expression of PEI25 in the Giant reactor, while the C32 vector provided a nearly 7 fold

increase in expression. The adenovirus was once again the most efficient vector in the 3-D system, giving a 20 fold increase over the PEI25 levels.

4.4 Discussion and Conclusions

Here we describe a new, scaled up perfused liver bioreactor for maintenance of primary liver cultures in a 3-D microenvironment. This new "Giant" reactor is based on the same design principles as a previously developed system that demonstrated the ability to culture primary hepatic cells in 3-D tissue structures over longer periods of time than conventional 2-D cultures with improved maintenance of liver phenotype and function [161, 162, 171]. While the previous system focused on providing high resolution imaging capabilities with less total cells in each culture, our new system provides added versatility for performing multiple experiments on the same reactor as well as housing enough cells to perform a number of quantitative assays with higher sensitivity demands.

The functional channel units in the cell scaffold that provide a substrate for attachment and reorganization of primary liver tissue, as well as a controllable platform for perfusion flow, were kept consistent with our previous design. This allowed for careful control of the levels of shear stress and oxygen and nutrient delivery that showed the best results previous for tissue morphogenesis and enhanced phenotypic function. Operation parameters were optimized to yield a system which robustly recreated these conditions in the context of a larger fluidic circuit and reactor chamber. These conditions, as well as optimal reactor chamber geometries, were validated via a number of computational fluid dynamics simulations and qualitative dye tracking experiments in early prototypes. These studies, coupled with computational analysis in our previous work [162], confirmed that cells throughout the larger cell array experienced uniform flow with no recirculation, physiological levels of shear stress, and more than adequate nutrient and oxygen delivery.

New features were incorporated in this design to allow for faster and more consistent seeding over the larger array of channels in the cell scaffold. A three part reactor body was employed to allow for direct addition of cells via pipetting, as dependence on the original hydrodynamic seeding technique could not achieve uniform cell seeding over the larger 1000 channel array. This dramatically sped up the seeding procedure and also

increased seeding efficiency, with 5 fold less total cell spheroids (on a per channel basis) required per reactor to attain fully seeded channels. This improvement provided the benefit of increasing the number of total reactors that could be seeded for each spheroid preparation and also paved the way for future design work in systems that aim to culture human liver cells, where seeding efficiency is of the utmost importance since cell supplies can be quite scarce as compared to an animal source.

New machining approaches were adopted to use scaffold materials that were more practical for the size and assembly constraints of the larger system. Scaffolds achieved precise channel alignment for uniform crossflow, and their mechanical properties allowed for faster reactor priming and assembly without the danger of breaking that existed with silicon scaffolds. An optimized collagen treatment protocol was devised in order to achieve comparable cell adhesion for the polycarbonate channel walls as compared to the original silicon scaffolds. The polycarbonate scaffolds successfully recreated the qualitative cell adhesion and tissue reorganization observed in the original system. These scaffolds demonstrated excellent retention of cells, consistently providing over 1 million cells per reactor at the relevant time points. This provides for more than enough material to purify RNA, DNA, protein and metabolites from the same sample, allowing for simultaneous characterization for a given experimental applications at many levels. Increased cell seeding and retention over the culture period also results in increased debris in the fluidic circuit, especially at early time points following crossflow reversal. New protocols were adapted to efficiently handle this debris and maintain culture well beyond the previously established time period over which the hepatocytes stabilize to more *in vivo*-like hepatic function and morphology, which is typically day 7 post isolation for most applications [171].

Optimized protocols for the fast recovery of intact cells from the polycarbonate scaffolds also provide another degree of flexibility for this system. Cells can be collected and pelleted and then subjected to smaller volumes of lysis or assay buffer in order to attain a higher degree of sensitivity for hard to measure molecules. This has also allowed proof of concept for subcellular fractionation approaches to study intracellular trafficking and distribution of therapeutics, as well as uptake and metabolism studies for drugs such as non-viral gene therapeutics that have much higher temporal resolution than is possible in animal models. Due to the success of polycarbonate as a scaffold material, work is also underway to mass produce large polycarbonate scaffolds via novel drilling approaches. This would

provide low cost scaffolds that would essentially be disposable and facilitate a number of new experiments that would require directly placing the scaffolds in more abrasive lysis or assay buffers, as well as allow for sectioning of multiple scaffolds to study cell morphology and distribution throughout the 3-D tissue structures. With such a large scaffold array, some channels could also be prepared for sectioning and various imaging analyses while another portion of the culture could be subjected to functional assays, corroborating these data from the same sample and gaining a greater understanding of the underlying mechanisms involved in tissue morphogenesis for a given seeding condition or cell type distribution.

In order to more broadly characterize liver phenotype in the new system, an RT-PCR approach was utilized to quantitatively measure the mRNA expression levels for a panel of liver enriched genes responsible for a wide variety of hepatocyte specific functions. The genes tested included liver enriched transcription factors, membrane transporters and general metabolism genes, phase II metabolic enzymes, and liver enriched nuclear receptors. Gene expression patterns were compared between the new "Giant" reactor and its predecessor, the smaller Milli-F reactor, to determine if the design and parameter changes made in scaling up the system had a significant affect on the on the overall maintenance of liver phenotype. Overall, the patterns compared favorably in nearly all cases. Both 3-D systems were significantly less downregulated compared to 2-D collagen sandwich cultures relative to the in vivo levels, suggesting enhanced *in vitro* maintenance of hepatic phenotype.

The giant reactor was particularly effective in maintaining the expression levels of the hepatocyte nuclear factor (HNF) family of transcription factors. Liver specific gene expression is thought to be controlled primarily at the transcriptional level [199]. The HNFs play an important role in promoting a variety of liver specific gene expression, and many liver specific genes have promoter sites for multiple HNFs [200-202]. HNF4α and HNF1α are considered to be two of the most important transcription factors in this class, coupled with other HNF variants, they are thought to play an important role in the expression of cytochrome p450 enzymes. HNF4a regulates metabolism of fatty acids, glucose and cholesterol, it plays a role in multiple biosynthesis processes, and also factors into liver development [203-209]. Gene expression of HNF1α, HNF3α, and HNF4α were all maintained at close to *in vivo* levels (Figure 4.6), suggesting a solid foundation for liver specific function for this new 3-D culture system. The fact that the majority of the downstream metabolism and transport related genes that were measured, such as BSEP (bile

salt export pump), the OATPs (organic anion transporter polypeptides), MDR2 (multiple drug resistance 2 P-glycoprotein) and GST-Ya (glutathione S-transferase Ya), are also upregulated corroborates with the upregulated transcriptional control elements. Two genes, FABP-1 (fatty acid binding protein 1) and catalase, showed moderate downregulation from 2-D levels. Interestingly, the transcript levels for both of these genes were brought back to in vivo levels when reactors were run without bovine serum albumin (BSA) in the medium. In general, this RT-PCR approach can be used to examine the effects of medium formulations or operating parameters on gene expression patterns in order to optimize the 3-D system for the specific application of interest. In the case of these studies, however, BSA was left in the medium, since this serum protein plays an important role in non-specific adhesion to gene therapy vectors, potentially changing their physical properties and/or causing non-viral particle aggregation. By leaving BSA in the system, the 3-D reactor would serve as a more *in vivo*-like test bed for new gene therapy vectors.

As a potential first application for this new reactor system, 2-D and 3-D transfections experiments were carried out to examine the gene delivery efficiency of novel non-viral gene therapy vectors in comparison to a viral vector and an established non-viral carrier. It was hoped that this study would first show if gene expression would be quantitatively measurable with the higher number of cells in the scaled up reactor, and secondly, if it could provide insight as to whether or not relative gene delivery efficiencies could change as a function of the culture system used to study the vector. PEI25 vectors, for which gene expression levels were difficult to quantitatively measure in the cell numbers provided by the original microreactor system, provided significant levels of β-Galactosidase transgene activity over no dose and naked DNA controls. This vector was set as the benchmark for comparison for the next generation non-viral carriers and the adenoviral vector. The small cross-linked PEI vector performed exceptionally well in 2-D transfections, giving an 80 fold increase in gene expression, and perhaps more impressively, was only a little under 2 fold less efficient than the adenovirus in 2-D. The C32 vector, which had been shown to be highly efficient in Cos-7 and HepG2 cell line, yielded less transgene expression than the cross-linked PEI vector but still greatly outsurpassed the PEI25 vector with a 30 fold improvement in 2-D expression.

The most interesting results from this study came from the comparisons between the 2-D and 3-D experiments. In 3-D tissue transfections, it was expected that the gene delivery

vectors would likely be less efficient on the basis of transgene expression per total DNA dose. This could be explained by the fact that not every cell in the culture is readily accessible to the complexes in the medium. Vectors would have to carry their DNA payload through the tissue structures, be it through vessels structures that can sometimes form in the tissue due to the presence of a small fraction of non-parenchymal cells such as endothelial cells in the hepatocyte isolate or through matrix proteins that are secreted by the hepatocytes as they reorganize in the channels. Additionally, non-viral complexes may aggregate over time in the fluidic circuit, and either become too large to be endocytosed by the cells or potentially sediment in the reservoir with increased size. This decreased overall efficiency was observed, but what was more unexpected was that the two next generation non-viral vectors gave resulting expression levels that were opposite the case seen in 2-D transfections. In the liver bioreactor, the small cross-linked PEI was doubled in efficiency by the C32 vector, while the cross-linked PEI had more than doubled the C32 efficiency in 2-D. A number of explanations for this phenomenon can be postulated. For instance, the C32 may stay more stable in the fluidic loop over time and result in more prolonged delivery, whereas in the 2-D case, the complexes sediment onto every cell and can be easily endocytosed. Additionally the slightly more hydrophobic character may allow the C32 to bind to cell membranes more efficiently under flow conditions.

While significant mechanistic analysis would be required to prove or disprove these or other theories, the primary conclusion that can be made from this initial study is that the success of a gene therapy vector can depend heavily on the system in which it is tested. While quantitative and mechanistic studies of vector delivery, the majority of which are performed in cell lines in 2-D cultures, can be useful to understand why or why not a vector is efficient, they may be irrelevant in many cases when extending these therapeutics to clinical applications. This strengthens the need to study vectors in pre-clinical animal models, though simply relying on these models will not necessarily drive vector development significantly. This is due to the fact that quantitative and mechanistic analysis is highly difficult to conduct in animal models. If a vector is marginally effective in a given animal model, it is difficult to deduce why it was effective, or more importantly, how it can be made more effective. It is now clear that endpoint level screening alone will not result in many non-viral vectors that are as effective as their viral counterparts. Approaches in rational design of vectors show promise for improved carriers, but experimental systems that allow

for quantitative analysis are needed that more faithfully mimic the in vivo environment and cell phenotypes that a vector will need to contend with. These systems can provide feedback that will be more useful in designing functionality to overcome various barriers to expression. Our scaled up liver bioreactor provides a new system where such work can be performed. By combining quantitative intracellular level assays for gene vector trafficking and expression coupled with qualitative imaging analysis in this system, it is hoped that mechanistic data can be generated that drives the development of efficient vectors for in vivo liver gene therapy applications.

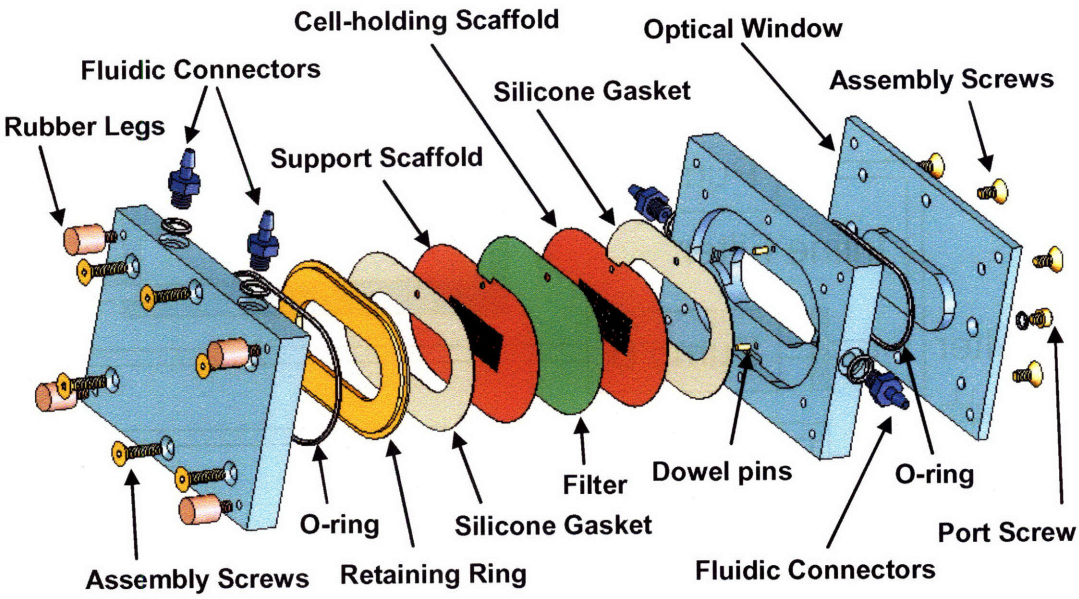

Figure 4.1: Exploded view of the Giant reactor components. All internal components fit over the alignment pins in the central pocket. The three polycarbonate body pieces screw together to form an upper and lower flow chamber around the cell holding scaffold, the middle filter, and the lower support scaffold.

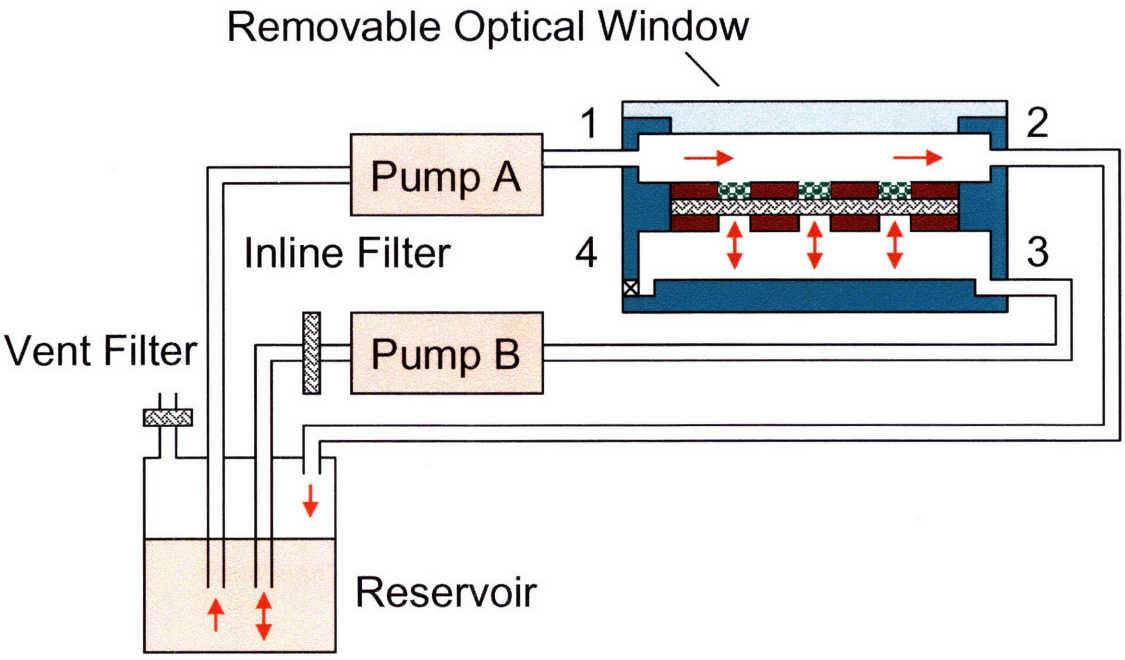

Figure 4.2: Fluidic circuit for the giant reactor. Two peristaltic pumps drive the flow of medium to and from the reactor inlets and outlets. Medium is reoxygenated in the reservoir cup and the tubing. Pump A controls the main flow over the top of the scaffold in the upper flow chamber, and pump B controls the perfusion flow, or cross flow, through the scaffold channels. The direction of the crossflow can be run either upward or downward through the channels at different stages of the culture. An inline filter is placed in the crossflow lined when pump B sends media from the reservoir to the lower flow chamber to prevent clogging.

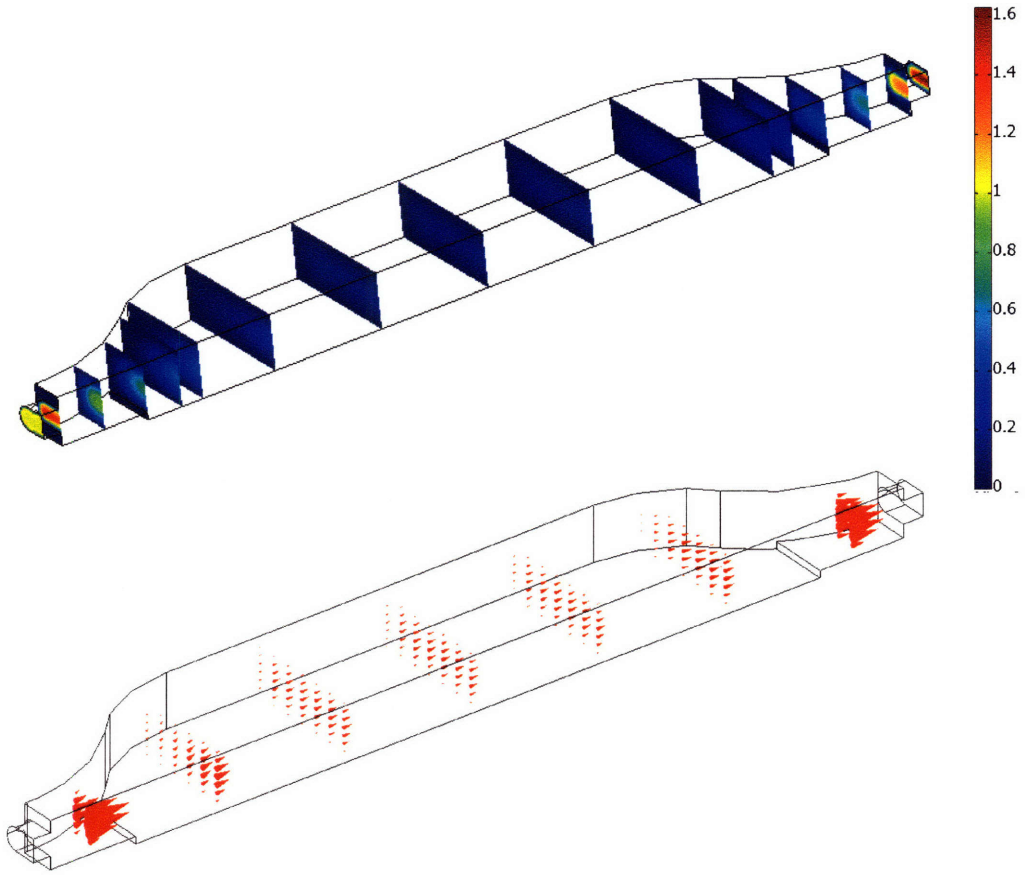

Figure 4.3: Computational fluid dynamics simulation of flow in the upper chamber of the giant reactor. The cell scaffold is exposed to a uniform velocity field that remains consistent over the entire channel array. High velocities are tempered shortly after chamber entry. Streamlines indicate no recirculation in the system. Velocity is normalized to the value at the inlet. Only half of the upper chamber was modeled due to symmetry to speed computation.

A)

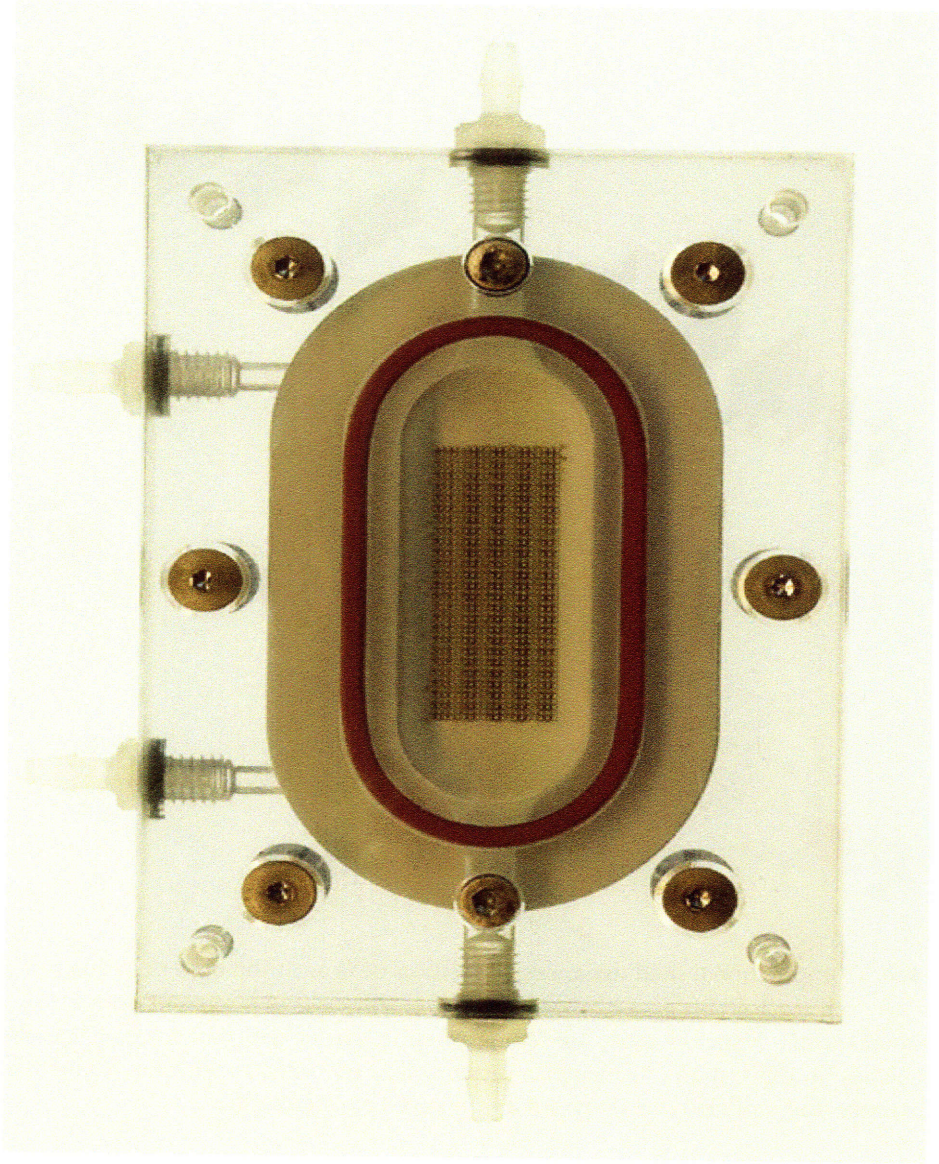

Figure 4.4: A) Top view of an assembled Giant reactor containing a laser machined polycarbonate scaffold with an array of one thousand 300x300x230 um channels. The overall size of the 3-compartment bioreactor housing is approximately 78 x 54 x 21 mm. **B)** The top window is easily removed from the assembled reactor to seed cells into the channel array. (See next page.)

B)

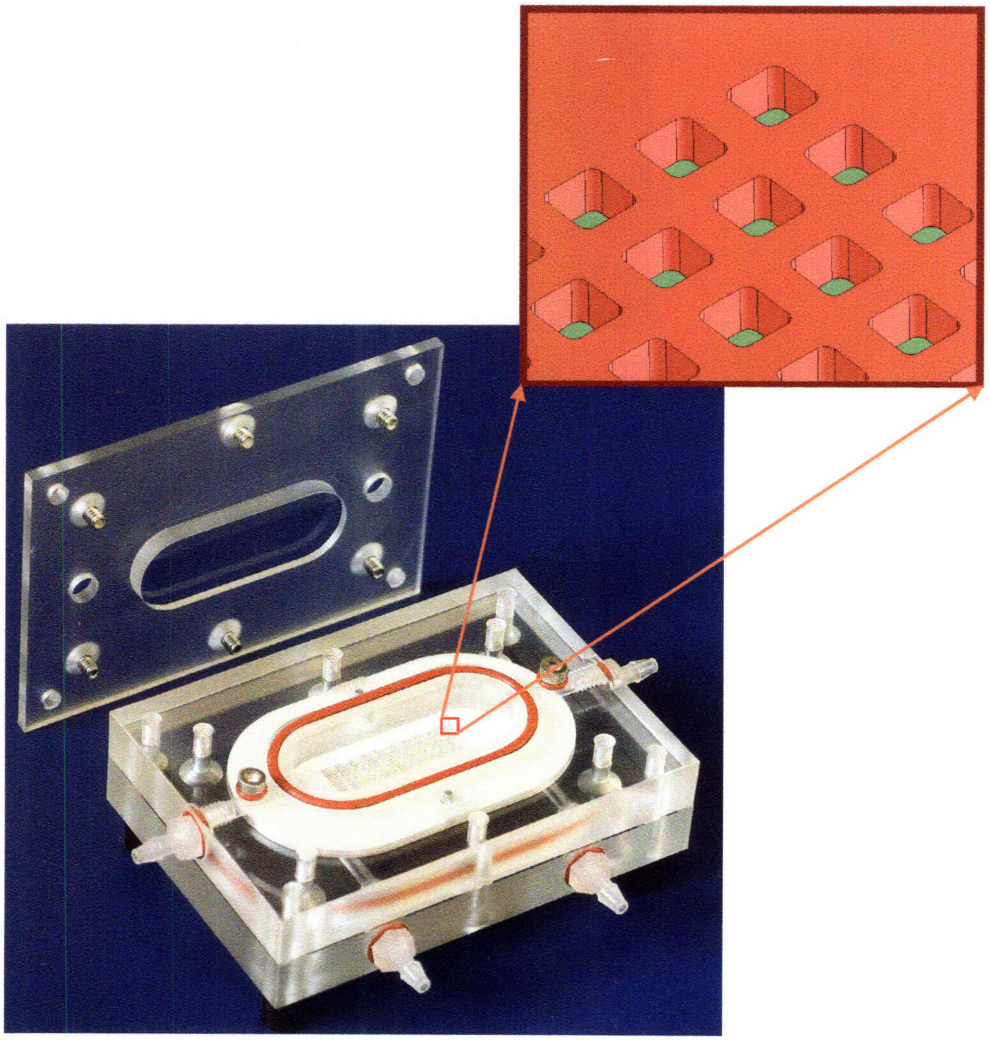

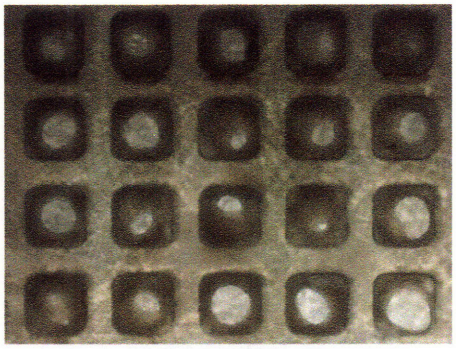

Figure 4.5: In situ light microscopy image of reorganized liver tissue structures in the channels of the collagen treated polycarbonate scaffold seven days after hepatocyte isolation.

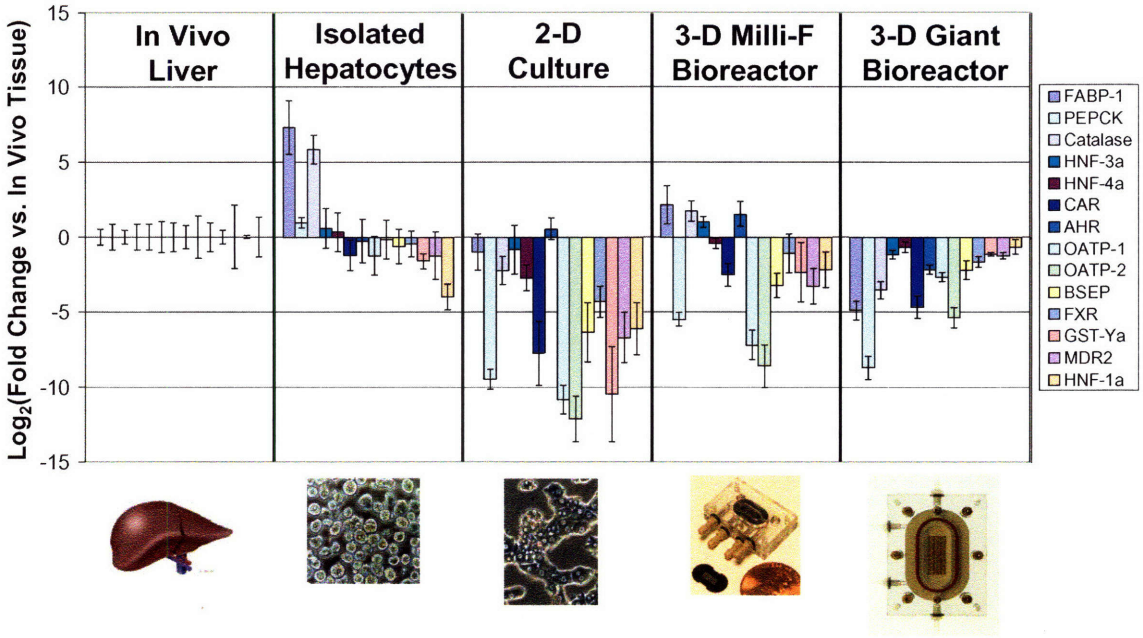

Figure 4.6: Relative liver specific gene expression across culture systems. RNA was purified from in vivo liver slices, freshly isolated hepatocytes, day 7 post isolation collagen gel sandwich cultures, day 7 post isolation Milli-F 3-D liver bioreactor cultures, and day 7 post isolation 3-D Giant Reactor cultures. cDNA was generated from RNA and RT-PCR was used with optimized primers to quantify previously determined liver enriched genes. Samples were internally normalized to ribosomal RNA 18s levels. Replicates were then averaged and globally normalized to *in vivo* expression levels to show the log fold 2 upregulation or downregulation of each transcript relative to native liver. *In vivo* and isolated hepatocytes samples were performed in quadruplicate, and 2-D and 3-D cultures systems in triplicate. RT-PCR was performed in technical triplicate.

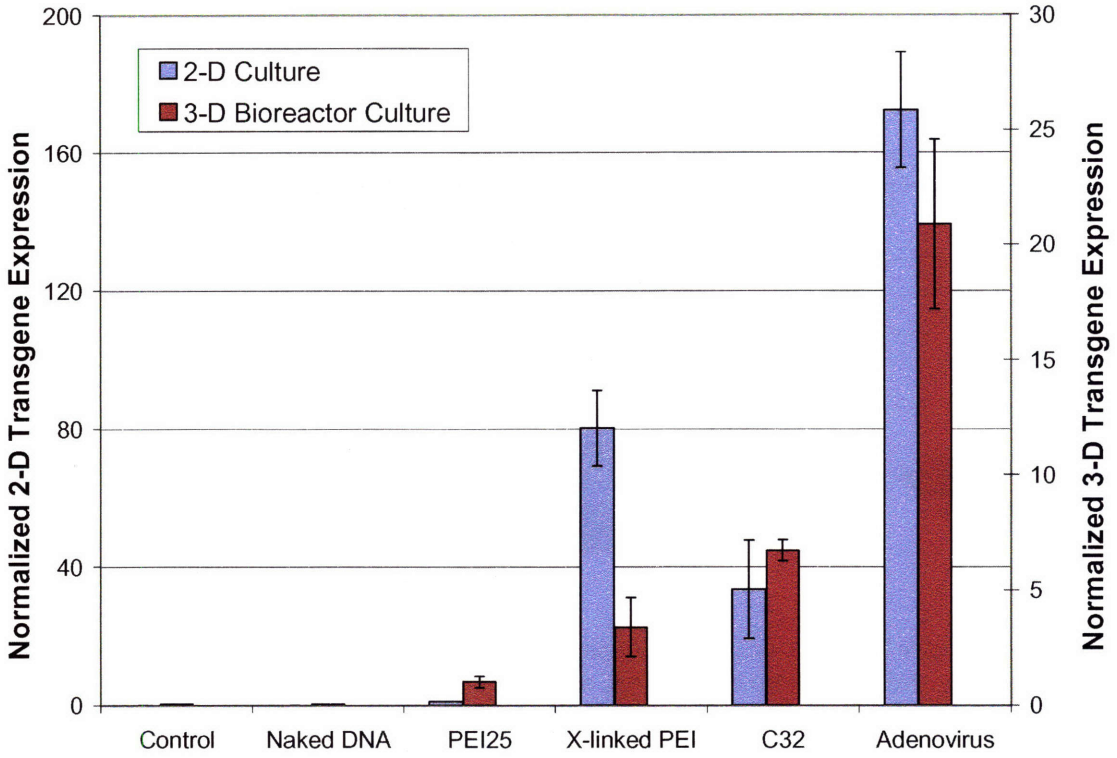

Figure 4.7: Transgene expression levels 48 hours after gene delivery to hepatocytes cultured in 2-D on adsorbed collagen monolayers and in 3-D in the liver bioreactor. Left axis denotes 2-D expression levels relative to PEI25, and right axis denotes relative 3-D expression levels. All 2-D and 3-D transfections were performed in experimental and technical triplicate.

Chapter 5

Quantitative Comparison of Next Generation Non-viral Gene Therapy Vectors with a Canonical Viral Vector: Quantitative Intracellular Trafficking Studies and Modeling Analysis

5.1 Introduction

As discussed in Chapter 3, mathematical modeling approaches and quantitative, mechanistic analysis in general can provide added insight for non-viral gene therapy vector development. However, it is apparent that new models must be developed that are more accurate and informative if this approach is to truly drive the rational design of vectors that are as efficient as viral carriers while offering the benefits of enhanced flexibility and overall safety.

To date, most mathematical models that have been applied to the study of non-viral gene therapy have utilized a compartmentalized, pharmacokinetics based approach [113, 132, 179, 182, 210]. In order to obtain accurate model fits, many compartmentalized models and quantitative studies must abstract the level of spatial detail in cellular compartmentalization and overall steps to a point where lumped parameters and model simulations are not successful in identifying rate limiting steps or in generating biologically relevant hypotheses [179, 183]. One way to potentially get around this problem is to collect rate information for specific steps from the literature [113]. However, this is potentially dangerous, since some processes are vector dependent and also most likely cell type dependant, so information must be chosen with care, taking into account the system and cell type the data was generated in and considering how the previous observation will translate into the application of interest.

Other attempts have explored the idea of integrating elements of stochasticity in model simulations of gene delivery and using single cell imaging data to corroborate model predictions [181]. While this certainly lends merit to the overall effort of improving gene therapy models, and may be advantageous to better describe certain portions of the delivery pathway, more immediate progress may be made by utilizing methods that allow for more quantitative analysis on a populational level. Efforts to this extent have been made in examining millions of transfected cells via FACS-based analyses but to date have mainly focused on isolated portions of the delivery pathway [135] or more generally on end metrics

of gene expression or insensitive toxicity assays [176, 211]. Approaches that could offer true compartmentalized quantitative measurement for a large number of cells may build data sets that can lead to model structures that can more robustly deal with populational variation within a cell or tissue type and also address the need for data that can help to fit parameters that describe hard to measure intracellular rate processes

The work in this chapter looks to extend the methods established and described in Chapter 3 to a more complete and rigorous analysis of vector trafficking. The primary goal is to mechanistically compare two next generation non-viral vectors, the previously introduced small cross-linked PEI and C32 poly(β-amino ester), with a canonical viral vector. While it has already been seen in Chapter 4 that these new vectors achieve highly efficient gene transfer and transgene expression in primary hepatocytes compared to more traditional non-viral vectors, it is interesting to explore if these carriers reach these results with any notable differences at the intracellular level. It is hoped that by employing the novel methods developed in this thesis work to build quantitative trafficking data sets with higher spatial resolution than was previously available, more accurate mathematical models can be created that can allow for extended analysis on vector performance and delivery mechanisms.

5.2 Materials and Methods

5.4.1 Primary Cell Isolation and Culture

Primary cells were isolated from male Fisher rats weighing 150-180 gm using a modified version of the Seglen 2-step collagenase procedure as previously described [161, 162]. Blendzyme Type III (Roche, USA) was used for digestion instead of collagenase. Cells that were released by the digestion were suspended in DAG (DMEM (Sigma-Aldrich, USA), Albumin, Gentamycin) and spun and washed twice at 50g for 3 minutes. The final pellet was resuspended in hepatocytes growth medium (HGM), as described previously [161, 162], to yield a 95% or greater pure suspension of hepatocytes. The final cell viability was determined by trypan blue exclusion, and cells were only used if viability was in the 89-95% range.

Cells were seeded in 60 mm tissue culture dishes treated with a dried adsorbed collagen monolayer. Collagen type I from rat tail (BD Biosciences, Bedford, MA) was diluted in sterile 1x PBS at a concentration of 30 ug/mL. Plates were incubated with 3 mL of this solution for 2 hours, then aspirated and allowed to dry in a sterile hood for two hours prior to seeding. Cells were seeded in 3 mL of HGM at a density of 800,000 cells/mL immediately after isolation. Medium was changed 4 hours post-seeding to eliminate dead and unattached cells and debris, while ensuring 90-95% confluency. All experiments were performed within 24 hours of seeding to ensure the best maintenance of hepatocyte phenotype.

5.4.2 Plasmids, Polymers, Virus and Non-viral Complex Formation

Plasmid gWiz-β-Galactosidase (Gene Therapy Systems, San Diego, CA) encodes the enzyme β-galactosidase controlled by the human cytomegalovirus (CMV) promoter. The plasmid DNA was purchased purified and ready for use from a contract plasmid manufacturing company (Aldevron, Fargo, ND). The small cross-linked PEI and C32 polymers were synthesized as described previously [105, 106, 108]. The adenovirus serotype 5 with E1 and E3 deletions encoding β-galactosidase under a CMV promoter was purchased from Vector Core (University of Michigan, Ann Arbor, MI).

For transfection via small cross-linked PEI, polymer and DNA were diluted to the appropriate concentrations in sterile water and combined at an N/P ratio of 30. Polymer was added to DNA and left at room temperature for 10 minutes to allow for formation of complexes. For C32, polymer and DNA were diluted in sterile filtered sodium acetate buffer, pH 5.4, combined at a polymer mass/DNA mass ratio of 100, and left at room temperature for 5 minutes. Both complexes were added to HGM at a DNA concentration of 5 ug/mL. Adenovirus particles were diluted in a 10% glycerol in 1x PBS buffer to make working stocks, and the appropriate amount of particles was added to the media to achieve a multiplicity of infection of 20. Non-viral particle size was determined via dynamic light scattering using a ZetaPALS Zeta Potential Analyzer with ZetaPALS Particle Sizing Software Version 2.3 (Brookhaven Instruments Corporation, Holtzville, NY). Number averaged particle diameters were determined over a lognormal distribution for the two complexes. The small cross-linked PEI complexes measured 167.5 ± 8.2 nm in diameter, while the C32 complexes were 152.0 ± 4.2 nm.

5.4.3 Quantitative Trafficking Assays

Hepatocytes were transfected with 2 mLs of medium at the complex and virus concentrations indicated above. Cells were collected and fractionated at 10, 20, 40, 60 and 120 minutes after transfection. At each time point of interest, the transfected plate was placed on ice to halt endocytosis, scraped, lysed and subjected to DGE fractionation as described in Chapter 3 (see section 3.2.3). After mechanical lysis, 400 uL of the whole cell lysate was aliquoted and frozen for plasmid quantification and normalization. After the nuclear spin, 400 uL of the supernatant was similarly retained. The total volume of the whole cell lysate and the post-nuclear supernatant were carefully measured to calculate total plasmids for each fraction based on the aliquot values. After completion of each DGE separation run, 24 1.25 mL fractions were collected and frozen.

Total plasmids were quantified in whole cell, nuclear, cytoplasmic, and all DGE fractions via Taqman real-time PCR. Organelle mapping assays were also performed on DGE fractions as described previously in Chapter 3 to determine the location of late and early vesicle fractions for each run. The relevant fractions were summed and these early and late vesicle quantities were subtracted from the post-nuclear supernatant quantity to

determine the total amount of free cytosolic plasmids. Total collected cell number for each sample was determined via real-time PCR quantification of the rat GAPDH gene as described below and comparison to a standard curve. All five fractions, whole cell, nuclear, cytosolic, early vesicular, and late vesicular, were normalized to a per cell basis. Normalized triplicate replicates were averaged for each fraction and time point to build the quantitative trafficking time courses.

5.4.4 DNA Isolation and Taqman Quantitative PCR

Plasmid DNA was purified from each fraction of a given DGE run using the DNEasy 96 Tissue Kit (Qiagen, Valencia, CA). Samples from each cell fraction were pooled in a round bottomed collection plate (Qiagen) for cell lysis. 200 uL of whole cell lysate and post-nuclear supernatant were used from each sample, while the entire nuclear pellet was resuspended in 150 uL of room temperature PBS and added to the collection plate. A multiwell pipette was used to thoroughly mix the contents of all DGE fractions, and 200 uL of each fraction was added to the collection plate. Samples were lysed for 30 minutes at 70°C, and then subjected to the standard Qiagen purification protocol. Plasmid quantification was performed using the MJR Chromo 4 system (Bio-Rad, USA). β-Galactosidase plasmid forward and reverse primers and probe were designed using Primer Express Software (Applied Biosystems) and yielded sequences for forward primers, reverse primers, and dual labeled probes. Two sets of forward and reverse primers with probe were ordered and tested for optimal efficacy, as determined by widest spread of linear standard curve range and steepest slope of standard curve (Applied Biosystems, Foster City, CA). The resulting primers and probe spanned an 80bp region in the β-Gal coding region of the plasmid and had sequences: forward primer (5'-TTA CAG GGC GGC TTC GTC T-3'), reverse primer (5'-TAA GCC GAC CAC GGG TTG-3'), and dual labeled probe (5'-6FAM-CTG GGT GGA TCA GTC GCT GAT TAA ATA TGA TG-TAMRA-3'), used at concentrations of 400nM/400nM/25nM, respectively. PCR cycle conditions were 50°C for 2 min, 95°C for 10 min, followed by 40 cycles of 95°C for 15 s and 60°C for 1 min. In order to normalize samples to a per cell basis, genomic DNA was also purified and quantified from a whole cell sample from each DGE run. Taqman primers and probe were similarly designed to quantify the rat GAPDH gene which spanned an 80bp region with the following sequences: forward primer (5'- TGG GAT AGC CAG TGC TCT TA -3'), reverse primer

(5'-ACA GGA GAT GGG TTG GAA CT -3'), and dual labeled probe (5'-6FAM-TGA GCC ATC ATC ATC TCC GCT G-TAMRA-3'). The primers and probe were used at concentrations of 900nM/900 nM/225 nM respectively. PCR cycle conditions were 50°C for 2 min, 95°C for 10 min, followed by 40 cycles of 95°C for 15 s and 54°C for 1 min.

5.4.5 Computational Modeling and Analysis

A linear system of ordinary differential equations (ODEs) was formulated to describe the intracellular delivery processes involved in vector uptake, trafficking, vesicular escape, degradation, unpackaging, and nuclear binding and uptake (Figure 5.1 and 5.2). This model structure was based on a previously developed ODE model [113] which has been experimentally validated in quantitative C3A cell line transfection experiments [132], but employed some added steps and more freedom to fit model parameters due to availability of more experimental data per vector in this current study. Rate constants that described delivery steps that are inherently dependant on the physical properties of the polymer or viral vector were subjected to parameter fitting routines to build vector specific mathematical models. Model simulations and parameter fitting routines were initially performed in Matlab (The Mathworks, Natick, MA), but were unable to provide acceptable model fits. Analysis was moved to Jacobian (Numerica Technology, LLC, Cambridge, MA) for more rigorous parameter estimation and sensitivity analysis capabilities. First, a graphical structure for the model steps was built in Teranode (Teranode Corporation, Seattle, WA). This model structure was then converted to SBML format and imported into Jacobian.

Predefined functions were used in Jacobian to perform parameter estimation by simultaneously fitting model parameters to all data sets for a given vector. After parameter fits were attained with minimized residuals, model simulations were also performed within Jacobian to assess the quality of the fit to each time course. Predefined sensitivity analysis functions were carried out in Jacobian to determine the delivery steps that had the greatest potential effect on the number of free nuclear plasmids achieved by each vector. Jacobian calculates instantaneous sensitivities and also outputs the integral of the time course, which is reported in the results section. Multistart algorithms were also employed to explore over four thousand parameter fits and ensuing sensitivity analyses to ensure that the best possible model fits were being attained. Principal component analyses on these larger data sets were performed in Matlab, using a predefined function in the Statistics Toolbox. All Matlab and

Jacobian code, as well as the Teranode model structure used in these model fits and analyses, can be found in Appendix 15.

5.3 Results

5.3.1 Mathematical Model

A linear system of differential equations was used to describe the intracellular gene delivery processes illustrated in Figure 5.1. This model was adapted from a previously developed system of equations [113, 132], with added steps and species due to the fact that more compartments could be experimentally monitored. Each step in the delivery pathway is approximated as a first order mass action rate process and follows the vector/plasmid non-viral complex or free plasmid from cell binding and uptake through to nuclear import and transgene expression from unpackaged plasmids in the nucleus. Overall, the model contains 17 ordinary differential equations, with 6 model parameters being dependent to some extent on vector chemistry and physical properties: k_{Bind_Uptake}, $k_{Traffic}$, k_{Escape}, $k_{Deg\_Vesicle}$, k_{Unpack}, and k_{Bind_Vector} (Figure 5.2).

A full model description, as well as the rational for inclusion, combination and omission of the various steps in the delivery process has been previously discussed [113, 132]. Additionally in this new model, the internalization and trafficking rate processes have been modified slightly since plasmids can now be quantified in early endosomes and in late endosomes/lysosomes. The uptake process is described as entry into the cell into these early vesicles, with a new vector dependent rate constant, $k_{Traffic}$, describing the progression into late vesicle compartments. Since the experimental data showed the majority of the delivered plasmid to accumulate in these late vesicles, even at relatively early time points, it was rationalized to limit the process of vesicular escape to the late vesicle compartments. However, it is not out of the question that vectors may escape from early compartments, and alternate model structures that can account for this and other processes may be examined in future analyses and model extensions. This model structure was successfully implemented in Teranode and imported into Jacobian for all forthcoming model fitting and data analysis.

5.3.2 Quantitative Trafficking Time Courses

To examine intracellular trafficking of plasmids with higher spatial resolution, primary hepatocytes were transfected with small cross-linked PEI, C32, and adenovirus vectors and processed for subcellular fractionation at multiple time points during the first two hours of gene delivery. Density gradient electrophoresis (DGE) was implemented in conjunction with high throughput DNA purification and quantitative Taqman real-time PCR to separate and recover early and late vesicle fractions and subsequently quantify plasmid trafficking over time. During the lysis and processing of each sample for DGE fractionation, other cell fraction aliquots were retained such that plasmids could also be quantitatively tracked in whole cell, cytosolic and nuclear fractions at each time point, allowing for a highly comprehensive analysis of cellular plasmid distribution.

Trafficking time courses can be seen in Figure 5.3. All three vectors show highly efficient cell uptake and nuclear delivery. The C32 vector appears to traffic its genetic payload to the nucleus faster than the adenovirus or PEI vectors which show a more gradual increase in nuclear associated plasmids. However, at the 120 minute time point the two non-viral vectors have delivered roughly the same amount of plasmid to the nucleus. The non-viral vectors both deliver just under 50% of the total available per cell extracellular plasmids within 2 hours, since the 10 ug of total DNA in the initial dose equates to roughly $5x10^5$ plasmids per cell. Once again, the C32 polymer displays slightly faster overall uptake kinetics, but levels off after 60 minutes and decreases slightly at the last time point, which is possibly due to degradation. Meanwhile, the PEI vector shows fairly linear uptake kinetics over the entire time course. The adenovirus is even more efficient, with nearly 75% of the dose per cell being taken up at 2 hours. The virus is taken up very quickly at first, and then the uptake rate slows at the late time points, most likely due to the fact that there is less of an extracellular excess of viral vector since a fairly low multiplicity of infection (MOI) was used in these experiments. This MOI was maintained at a low level since higher dosages have been shown to cause adverse affects in primary hepatocytes in 2-D culture. As was seen in gene expression results in Chapter 4, this is still more than enough vector though, since adenovirus is highly effective at maintaining transgene expression once the viral DNA has been delivered at the nucleus.

Figure 5.3B shows only the vesicular time courses in order to better evaluate the qualitative dynamics of trafficking in these compartments. The early endosome trafficking

looks fairly uninteresting for all of the vectors. A near constant level of plasmids is maintained that is much lower in magnitude than the amount of plasmids seen in the late vesicles. This result agrees with general observations in primary hepatocyte trafficking in the endocytic pathway, which is highly active. In optimizing pulse chase regiments for labeling only early endosomes in primary hepatocytes, pulses had to be kept to 3 minutes or less to keep signal only in early endosome DGE fractions. It appears that these vesicles may quickly and repeatedly form and cycle the internalized complexes to the late vesicle compartments, such that their instantaneous quantity of plasmid is not exceptionally high but their overall contribution to uptake and trafficking is significant. Substantially different dynamics are seen in the late vesicle fractions. The C32 vector achieves a very rapid pulse of plasmids into the late compartments with an early peak at the 20 minute time point. The decrease thereafter could suggest efficient escape, vesicular degradation, or a combination of the two processes. The cross-linked PEI vector once again shows a more consistent build up of plasmids, and the adenovirus shows more of an intermediate dynamic between those of the two non-viral carriers.

5.3.3 Vector Specific Model Fits to Experimental Data

While the quantitative trafficking time courses showed some interesting mechanistic differences between the three vectors, they can provide more utility for overall analysis through the creation of vector specific mathematical models. All quantitative data was imported into Jacobian, and estimation functions were used to systematically vary the values of the vector dependent rate constants: k_{Bind_Uptake}, $k_{Traffic}$, k_{Escape}, $k_{Deg\_Vesicle}$, k_{Unpack}, and k_{Bind_Vector}, while all other rate constants in the model were held constant. Parameter sets were determined which best fit the experimental data for each vector. Model fits with these optimized parameter sets can be seen in Figure 5.4.

The parameter values which gave the best fits for each vector are listed in Table 5.1. Additional mechanistic insight regarding the specific steps represented by the fit parameters can be postulated from these results. The C32 vector seems to be the most efficient carrier at cell binding and uptake, and possibly related to this also shows the fastest trafficking rate constant for trafficking into the late vesicles. While these were fairly intuitive conclusions from the experimental data, other results of the fits were not. For instance, according to the model fits, the small cross-linked PEI actually undergoes endosomal escape an order of

magnitude faster than the C32 and Ad5 vectors, which may have seemed counterintuitive when only considering the late vesicle trafficking time courses. Interestingly, adenovirus unpackages more slowly than the PEI vector, but faster than the C32 vector, yet overall shows slower vesicular degradation than both non-viral vectors.

5.3.4 Parameter Sensitivity Analysis

Vector specific models were subjected to parameter sensitivity analyses in Jacobian to determine what steps in the gene delivery process could be rate limiting for each vector. While vector specific parameter values can suggest where a vector is efficient or inefficient at a given step relative to other vector, it does not necessarily indicate whether or not that step is potentially rate limiting for the overall success of nuclear plasmid delivery. Sensitivity analyses take into account the contribution of all steps when a given parameter is varied as well, so consideration can be given to parameters that were not varied for the fits and stay relatively constant for all of the vectors.

The previously discussed model fits were the best possible fits for a set of initial parameter guesses and other constraints placed on the fitting routine. These guesses and constraints were determined by using a multistart script which ran a matrix of over 4,500 initial guesses and conditions for each vector that were input to the fitting routine. The fits were then ranked ordered and the top 5% of model fits were examined. The parameter values for each vector specific model general fell into a very tight range around the best fit values that are reported in table 5.1. However, in order to ensure that sensitivities weren't biased by this specific parameter fit, a similar recursive fit was run on the top 500 fits for each vector, to ensure that model parameter sets that were only slightly less good at describing the experimental data didn't show vastly different sensitivities and contest the validity of the best fit.

Figure 5.5 shows the overall average sensitivity values for each parameter and vector. Sensitivities were incredibly consistent over all of the parameter sets, as denoted by the relatively tight standard deviations. The most sensitive or potentially rate limiting steps for all three vectors are k_{Bind_Uptake} and k_{In}, the steps representing cell entry and nuclear import. All three vectors were also sensitive to binding nuclear import machinery and unpackaging to some extent. Adenovirus showed some sensitivity to vesicular degradation, while both polymers were largely insensitive to this step. The virus was also somewhat sensitive to

endosomal/lysosomal escape, with the PEI vector being less sensitive and the C32 vector being fairly insensitive to this step.

With all three vectors displaying sensitivity to multiple steps, and the largest discrepancies between vector sensitivities existing at moderate steps, a principle component analysis was performed on the parameter value and sensitivity values for the top 500 fits for each vector (Figure 5.6). Principle component analysis provides an efficient way to visualize, analyze and compare higher dimensional data by collapsing the contributions or multiple parameters or variable onto new coordinates, the basis vectors of which define the "new" combinatorial dimensions that show the greatest variation in the overall data set. Data sets were normalized and collapsed onto two principle components. Clustering was seen to some extent for the vector specific parameters, denoting that they were more similar to each other than to the parameters, but overall there was still a fairly random distribution overall which made this first pass analysis difficult to interpret. However, the most interesting results came from the principle component analysis of the sensitivity values. The sensitivities for each vector collapsed to three primary, unique clusters. This suggests that the vectors do indeed have unique sensitivities that depend on a weighted subset of the model parameters and therefore, steps in the gene delivery process. This result warrants more in depth future analysis on the makeup of these principle components and the implications they can have for vector development.

5.4 Discussion and Conclusions

We have demonstrated a combined experimental and modeling approach that provides a more comprehensive mechanistic analysis for the intracellular trafficking of gene therapy vectors. This approach has been directly applied to primary hepatocytes in order to generate quantitative data sets that describe the dynamics of gene delivery for an adenoviral vector and two next generation cationic polymer vectors. These new cationic polymers have been previously shown to be highly efficient carriers, and methods that provide insight into their success could translate to a better overall understanding of how to approach rational design of new carriers. It is generally more difficult to generate repeatable quantitative data in primary cells as compared to immortalized cell lines, but the methods developed in these studies were robust enough to deal with animal to animal and isolation to isolation differences in the hepatocytes. This was important in the context of our end goals of driving

future development for in vivo liver gene therapy, as it is becoming increasingly apparent that vectors should be evaluated in their primary cell or tissue type of interest to truly gauge if they can be useful for clinical application.

With increased spatial resolution in the cellular compartments that play an important role in uptake and transport to the nucleus, mechanistic differences could be observed in the delivery processes of the individual vectors. Additionally, these data sets provided the basis for more accurate mathematical model fits, which offer the potential and flexibility for more in depth analysis. Though direct observation of the experimental data was able to reveal some clues as to how vectors differed as delivery agents (Figure 5.3), more direct conclusions could be made from vector specific mathematical model fits and model analysis. Rate constants that described steps in the delivery process that are dependent on polymer or virus properties were fit to the experimental time courses. In these initial fits, model parameters were varied to best describe four simultaneous data sets: whole cell plasmids, cytosolic plasmids, total vesicular plasmids, and nuclear plasmids. It was found that separately fitting to all five time courses yielded inferior parameter fits, likely because information exists in multiple compartments for many of the rate constants. For instance, fitting endosomal escape and degradation parameters to the late vesicle time course alone is less accurate, since knowing the amount of plasmids that have already escaped and trafficked to the cytosol and nuclear compartments gives a more informative overall picture than just looking at how many plasmids are in the late vesicles at certain time points. Slightly non-intuitive results from overall parameter fits that are not immediately obvious when examining single time courses by eye show why it's powerful to fit to all data at once. Examination of the late time points in the C32 late vesicle time course suggested enhanced escape or increased vesicular degradation, but a comprehensive model analysis revealed that this was more likely due to enhanced uptake and trafficking relative to the other vectors. This conclusion began to make more physical sense when the nuclear, cytosolic and late vesicle time courses were all examined, a process which is done far more efficiently *in silico*.

Additionally, a total vesicle time course gave the best results for fitting in concert with the whole cell, cytosolic, and nuclear trafficking data (Figure 5.4). This was most likely due to the fact that the other four compartments greatly outweighed the early endosome compartment in plasmid per cell magnitudes, consequently giving them more overall weight in minimizing the residual error during the fitting process. More temporal resolution is likely

needed at early time points to accurately fit early endosome time course information, but as was discussed in the results, the low magnitude and rather constant dynamics of this compartment do make mechanistic sense in primary hepatocytes. Future analyses may focus on different model structures and fitting procedures that can utilize this information more effectively.

Overall, vector specific rate constants varied over five orders of magnitude and showed interesting differences at certain steps. As reported in the results section, interesting differences between vectors were seen in endosomal escape, unpacking and vesicular degradation steps that were not obviously apparent when examining the time courses. The enhanced uptake and binding ability of C32 could explain why it was able to attain increased success in 3-D transfections examined in Chapter 4, while the PEI vector may have greatly outperformed the C32 in 2-D cultures due to its increased ability to escape endosomes in a system where binding and uptake were less important.

Sensitivity analyses were carried out on all model parameters to surmise which steps in the overall delivery pathway could be rate limiting for successful delivery of nuclear plasmids (Figure 5.5). While the vector specific steps are obviously important to focus on since they can be directly addressed through chemical modifications to the vectors, all steps should be considered, since the overall model structure resulting from specific parameter fits can actually cause the processes with unvarying parameter values to also be more or less rate limiting. This was observed for all three vectors. The most sensitive step in all cases was nuclear import, followed again for all three vectors by cell binding and uptake. These results were encouraging when considering past analyses of less efficient vectors in the C3A cell line, where only the most efficient vectors showed sensitivity to nuclear import [132]. This suggests that both polymers are very efficient overall at navigating through the endosomal pathway and escaping efficiently, essentially building up at the entryway to the nucleus and waiting to get in. Achieving more efficient nuclear import could greatly enhance delivery efficiency, as well as finding more efficient ways to achieve cell uptake. There are many practical strategies that could be employed to address these enhancements. Incorporation of enhanced nuclear localization sequences on either the plasmid or the vector could allow for improved nuclear import [212]. Similarly, targeting moieties could be attached to the vector to allow for cell specific binding and increased uptake by triggering receptor mediated endocytosis events, rather than relying on nonspecific association with the plasma membrane

and internalization via general fluid phase endocytosis. In the specific context of primary hepatocytes, strategies could be pursued to target the asialoglycoprotein receptor for cell specific uptake. However, many efforts to date have been largely unsuccessful to this end. In general, careful consideration has to be taken for how incorporation of these cell and nucleus targeting groups will affect the overall structure and properties of the non-viral complexes.

Another observation that indicates vast improvement in these new vectors comes from looking at the relative magnitudes of the sensitivity values for the three vectors. In this study, the polymer sensitivity values are at the same order of magnitude as those for adenovirus. In our past comparison, adenoviral sensitivities were two to three orders of magnitude lower than those for all non-viral vectors examined. This suggests that the properties of the two next generation vectors have allowed them to become more efficient at overcoming all of the barriers in general. As a result, more intermediate sensitivity values are also observed, instead of the one or two blaringly sensitive steps that were observed for the less efficient non-viral vectors. The most interesting differences between vectors can be seen at these intermediate sensitivities, such as endosomal escape and vesicular degradation.

Since these vectors do have sensitivities to multiple steps, in order to maximally optimize a vector, further analysis may be required that takes multiple parameter contributions into account. While substantial improvements to new vectors could be made by addressing the common most sensitive steps for both vectors, looking at unique characteristics of each vector could lead to more customized improvements for each base chemistry. One method that can take this higher dimensional analysis and abstract it to an easier to digest format is principle component analysis, which can reduce complex, multidimensional data to a reduced set of basis vectors that are described by a combination of weighted contributions from the individual parameters. A preliminary principal component analysis was performed on the sensitivity values and the sensitivity contributions from the 11 analyzed parameters were collapsed to two principal components. Parameter data from hundreds of fits for each vector were fed into this analysis and surprisingly the points for each specific vector mapped together in distinct clusters. This suggested that each vector had a unique dependency on some combination of steps, and also gave clues to how similar one vector was to another in terms of how close their respective clusters were in this collapsed space. The two polymer vectors seem to be more similar to adenovirus than they

are to each other, which corroborates with the different trafficking dynamics that were seen for the two carriers. However, to truly gain insight from this approach and to gauge if these unique dependencies can actually translate to tractable physical approaches for vector improvement, more in depth analyses must be performed to better understand the breakdown of the principle components. Investigations into the how the overall model structure and parameter space affect the principle components and degree and localization of clustering can also be instructive. In general, this quantitative time course data and subsequent model analyses can generate a number of interesting hypotheses for future experimental efforts and extensions of model analysis and in silico simulation. These efforts have the potential to drive more rational vector design to improve non-viral delivery efficiency.

Figure 5.1: Mathematical Model Schematic

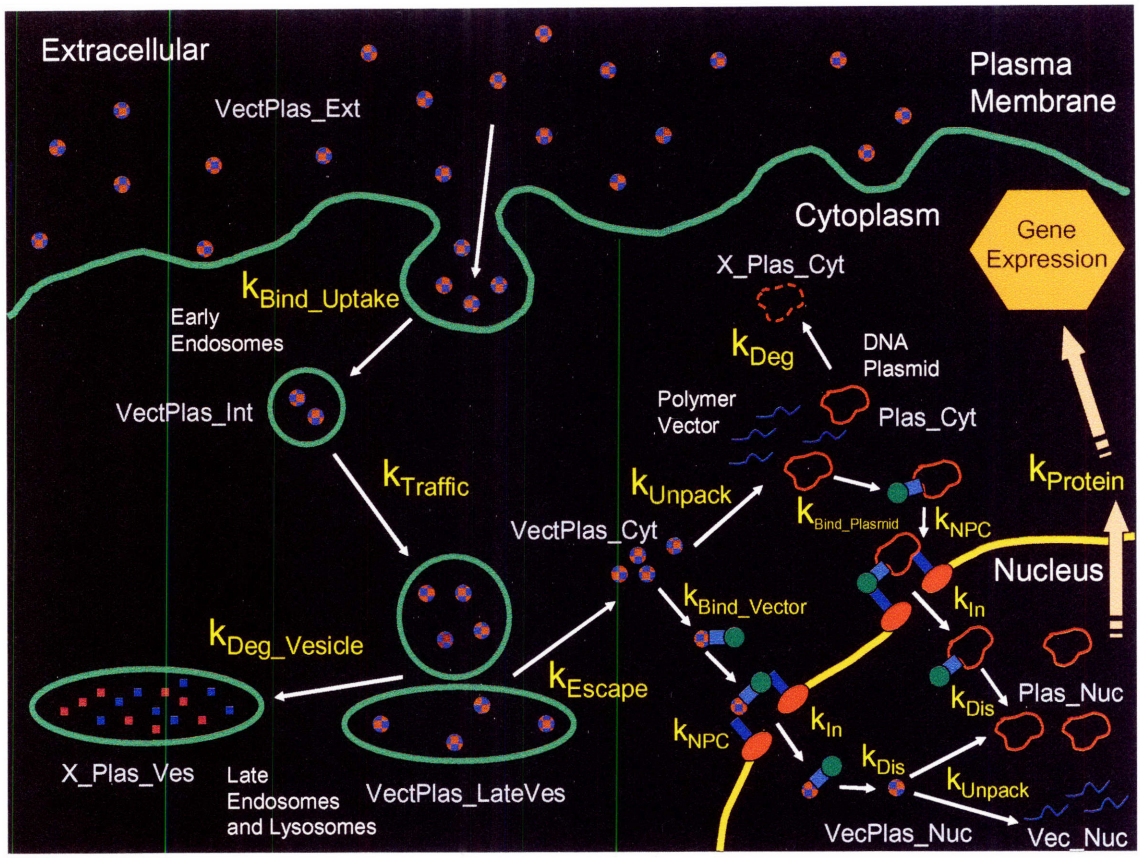

Figure 5.1: Mathematical model schematic depicting the intracellular delivery steps that are described in the mathematical model and the different species that can be measured via quantitative trafficking assays. Rate constants which describe various steps of the process are shown in yellow. Species are shown in blue. For clarity, species names were not shown for the multiple states that exist during nuclear import. These include VectPlasBound_Cyt, VectPlasBound_NPC, VectPlasBound_Nuc, PlasBound_Cyt, PlasBound_NPC, and PlasBound_Nuc.

$$\frac{d(VectPlas_{Ext})}{dt} = -k_{Bind\_Uptake} * VectPlas_{External} \quad (1)$$

$$\frac{d(VectPlas_{Int})}{dt} = k_{Bind\_Uptake} * VectPlas_{Ext} - k_{Traffic} * VectPlas_{Int} \quad (2)$$

$$\frac{d(VectPlas_{Late\_Ves})}{dt} = k_{Traffic} * VectPlas_{Int} - k_{Deg\_Vesicle} * VectPlas_{Late\_Ves} - k_{Escape} * VectPlas_{Late\_Ves} \quad (3)$$

$$\frac{d(X\_Plas_{Late\_Ves})}{dt} = k_{Deg\_Vesicle} * VectPlas_{Late\_Ves} \quad (4)$$

$$\frac{d(VectPlas_{Cyt})}{dt} = k_{Escape} * VectPlas_{Late\_Ves} - k_{Bind\_Vector} * VectPlas_{Cyt} - k_{Unpack} * VectPlas_{Cyt} \quad (5)$$

$$\frac{d(VectPlas_{Bound\_Cyt})}{dt} = k_{Bind\_Vector} * VectPlas_{Cyt} - k_{NPC} * VectPlas_{Bound\_Cyt} \quad (6)$$

$$\frac{d(VectPlas_{Bound\_NPC})}{dt} = k_{NPC} * VectPlas_{Bound\_Cyt} - k_{In} * VectPlas_{Bound\_NPC} \quad (7)$$

$$\frac{d(VectPlas_{Bound\_Nuc})}{dt} = k_{In} * VectPlas_{Bound\_NPC} - k_{Dissociation} * VectPlas_{Bound\_Nuc} \quad (8)$$

$$\frac{d(VectPlas_{Nuc})}{dt} = k_{Dissociation} * VectPlas_{Bound\_Nuc} - k_{Unpack} * VectPlas_{Nuc} \quad (9)$$

$$\frac{d(Plas_{Cyt})}{dt} = k_{Unpack} * VectPlas_{Cyt} - k_{Deg} * Plas_{Cyt} - k_{Bind\_Plasmid} * Plas_{Cyt} \quad (10)$$

$$\frac{d(Vect_{Cyt})}{dt} = k_{Unpack} * VectPlas_{Cyt} \quad (11)$$

$$\frac{d(Plas_{Bound\_Cyt})}{dt} = k_{Bind\_Plasmid} * Plas_{Cyt} - k_{NPC} * Plas_{Bound\_Cyt} \quad (12)$$

$$\frac{d(Plas_{Bound\_NPC})}{dt} = k_{NPC} * Plas_{Bound\_Cyt} - k_{In} * Plas_{Bound\_NPC} \quad (13)$$

$$\frac{d(Plas_{Bound\_Nuc})}{dt} = k_{In} * Plas_{Bound\_NPC} - k_{Dissociation} * Plas_{Bound\_Nuc} \quad (14)$$

$$\frac{d(Plas_{Nuc})}{dt} = k_{Unpack} * VectPlas_{Nuc} + k_{Dissociation} * Plas_{Bound\_Nuc} \quad (15)$$

$$\frac{d(X\_Plas_{Cyt})}{dt} = k_{Deg} * Plas_{Cyt} \quad (16)$$

$$\frac{d(Protein)}{dt} = k_{Protein} * Plas_{Nuc} \quad (17)$$

Figure 5.2: Mathematical model used to describe the rate processes discussed in the model schematic. Steps in the delivery process are modeled as first order rate processes, yielding a system of ordinary differential equations with the appropriate rate constants and species in each cellular compartment. VectPLas represents the intact non-viral complex, while Vect and Plas represent the unpackaged polymer or viral protein coat and the DNA plasmid or recombinant viral DNA containing the transgene, respectively. Subscripts denote the location and state of each species.

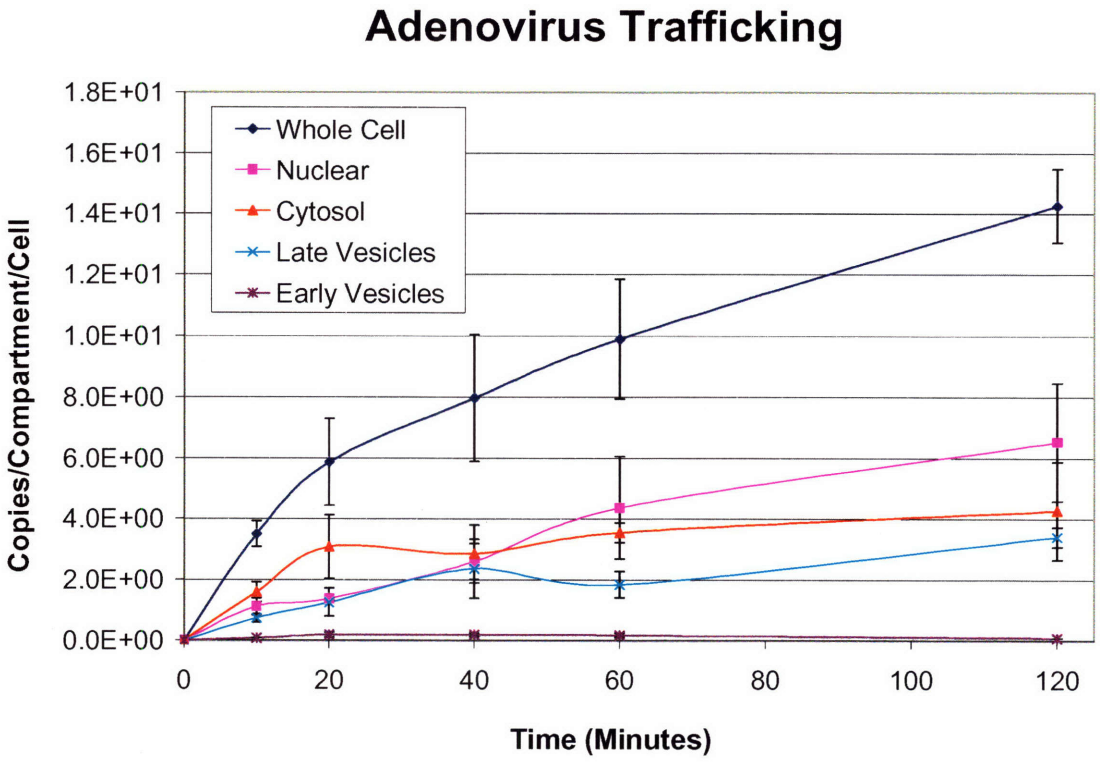
Adenovirus Trafficking
Copies/Compartment/Cell
1.8E+01
1.6E+01
1.4E+01
1.2E+01
1.0E+01
8.0E+00
6.0E+00
4.0E+00
2.0E+00
0.0E+00
0
20
40
60
80
100
120
Time (Minutes)
Whole Cell
Nuclear
Cytosol
Late Vesicles
Early Vesicles

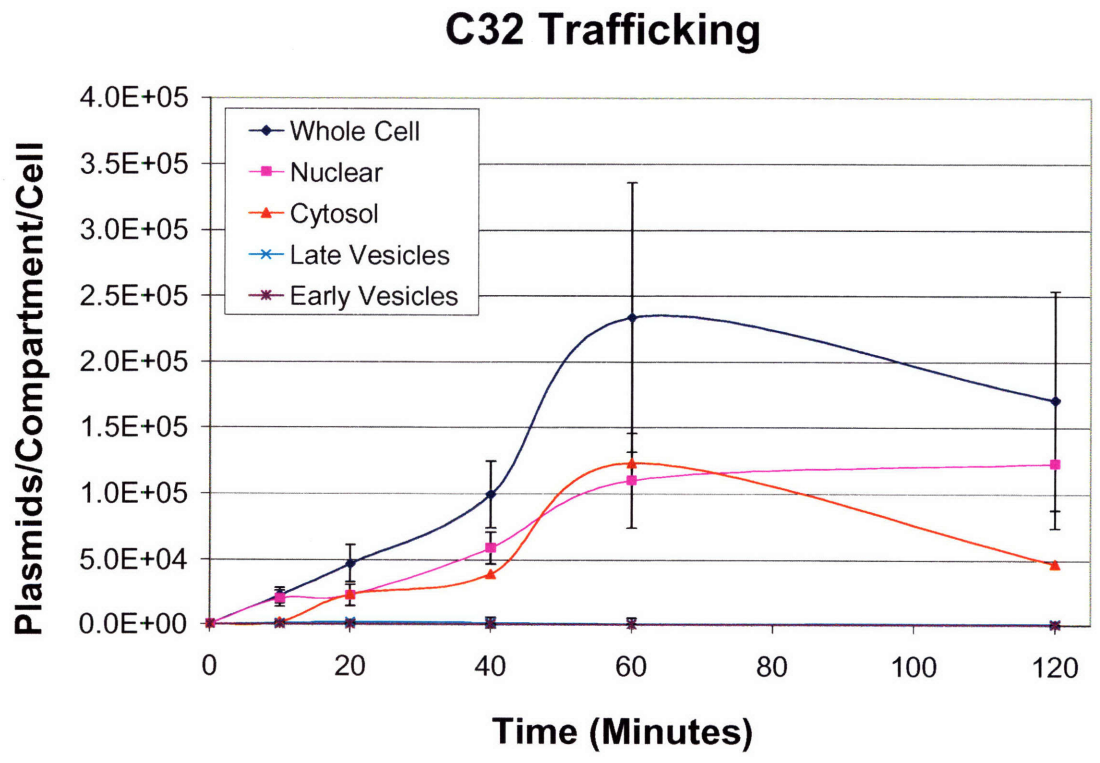
C32 Trafficking
Plasmids/Compartment/Cell
4.0E+05
3.5E+05
3.0E+05
2.5E+05
2.0E+05
1.5E+05
1.0E+05
5.0E+04
0.0E+00
0
20
40
60
80
100
120
Time (Minutes)
Whole Cell
Nuclear
Cytosol
Late Vesicles
Early Vesicles

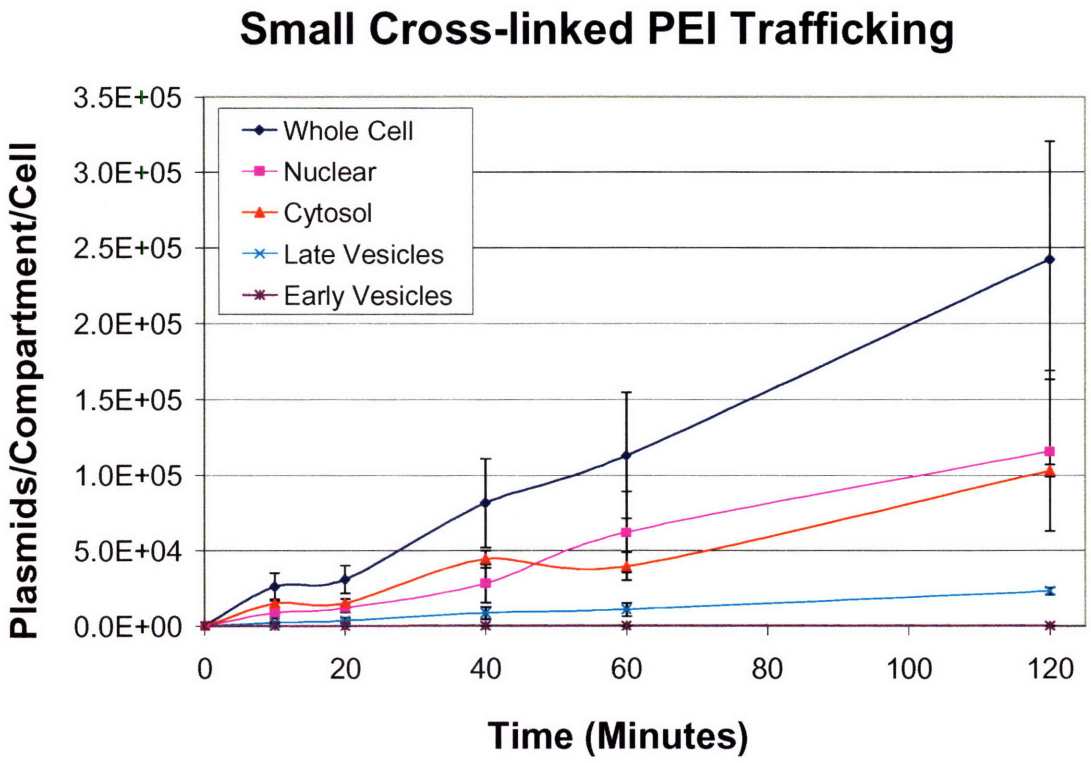

Figure 5.3 A): Quantitative trafficking time course data for Adenovirus, C32 and Small Cross-linked PEI with increased spatial resolution via DGE fractionation and quantitative Taqman real-time PCR.

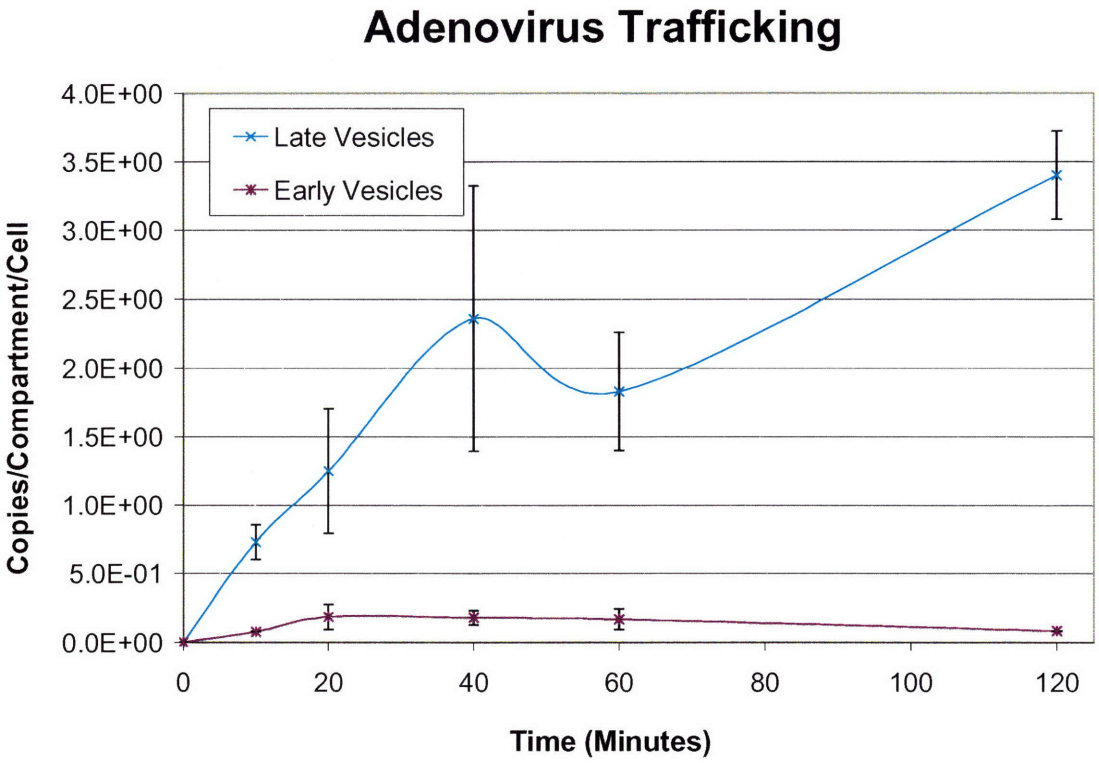
Adenovirus Trafficking
Late Vesicles
Early Vesicles
Copies/Compartment/Cell
4.0E+00
3.5E+00
3.0E+00
2.5E+00
2.0E+00
1.5E+00
1.0E+00
5.0E-01
0.0E+00
0
20
40
60
80
100
120
Time (Minutes)

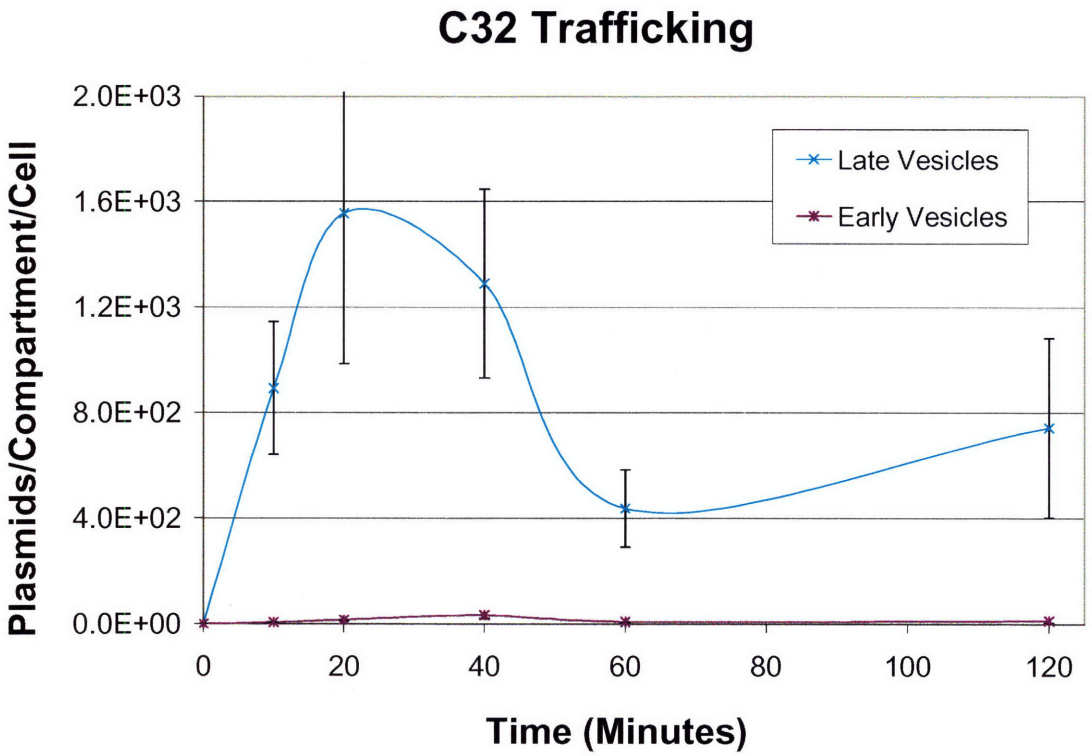
C32 Trafficking
Late Vesicles
Early Vesicles
Plasmids/Compartment/Cell
2.0E+03
1.6E+03
1.2E+03
8.0E+02
4.0E+02
0.0E+00
0
20
40
60
80
100
120
Time (Minutes)

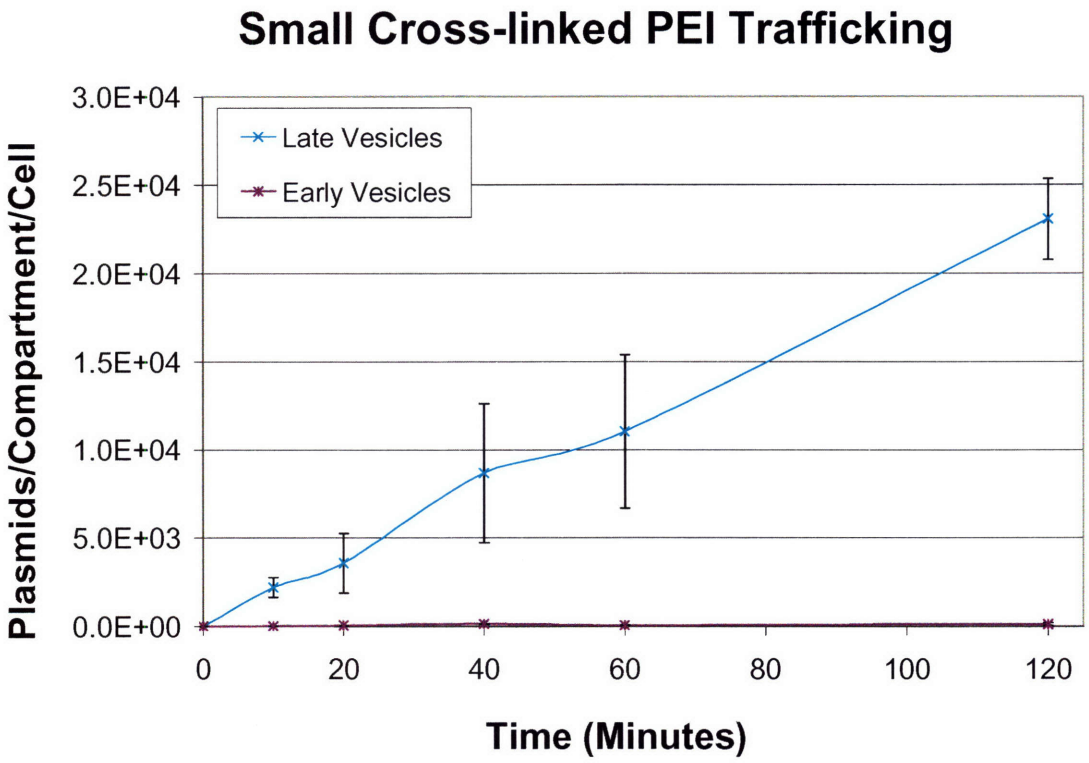

Figure 5.3 B): Abridged trafficking data set for early and late vesicle fractions to see a clearer picture of the vesicle dynamics of plasmid trafficking for the three vectors.

	X-Linked PEI	C32	Adenovirus
k_{Bind_Uptake}	5.14×10^{-3}	1.99×10^{-2}	1.17×10^{-2}
$k_{Traffic}$	9.50×10^{1}	1.07×10^{2}	1.17×10^{1}
k_{Escape}	9.50×10^{0}	9.15×10^{-1}	1.15×10^{0}
$k_{Deg\_Vesicle}$	9.99×10^{-1}	9.53×10^{-1}	3.84×10^{-1}
k_{Bind_Vector}	9.46×10^{-1}	2.99×10^{-1}	3.98×10^{-1}
k_{Unpack}	9.89×10^{-1}	2.79×10^{-1}	3.48×10^{-1}

Table 5.1: Vector Specific Parameter Values: Each first order rate constant is reported in units of min^{-1}.

Adenovirus

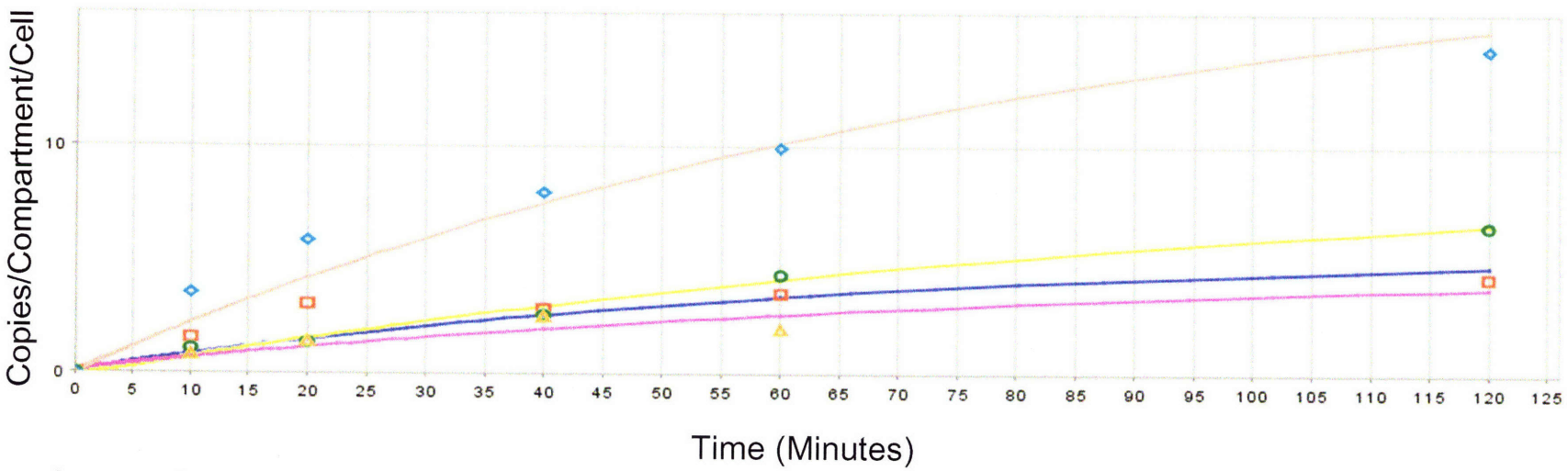

Legend

- Whole Cell Expt Data
- Whole Cell Model Fit
- Cytosol Expt Data
- Cytosol Model Fit
- Nucleus Expt Data
- Nucleus Model Fit
- Total Vesicles Expt Data
- Total Vesicles Model Fit

Small Cross-linked PEI

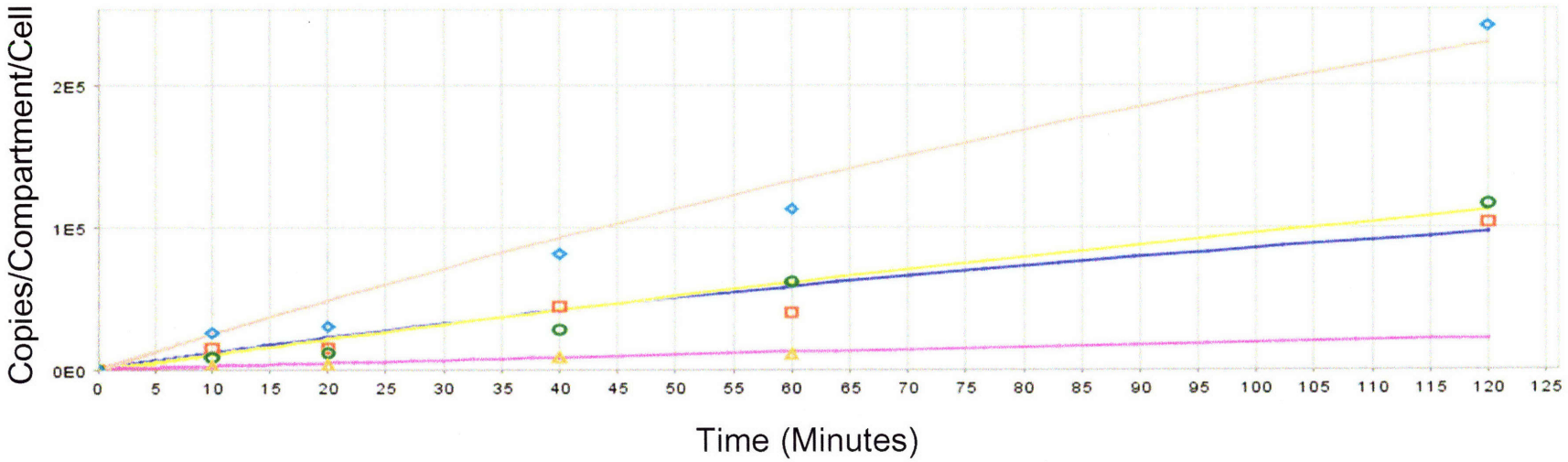

Legend

- Whole Cell Expt Data
- Whole Cell Model Fit
- Cytosol Expt Data
- Cytosol Model Fit
- Nucleus Expt Data
- Nucleus Model Fit
- Total Vesicles Expt Data
- Total Vesicles Model Fit

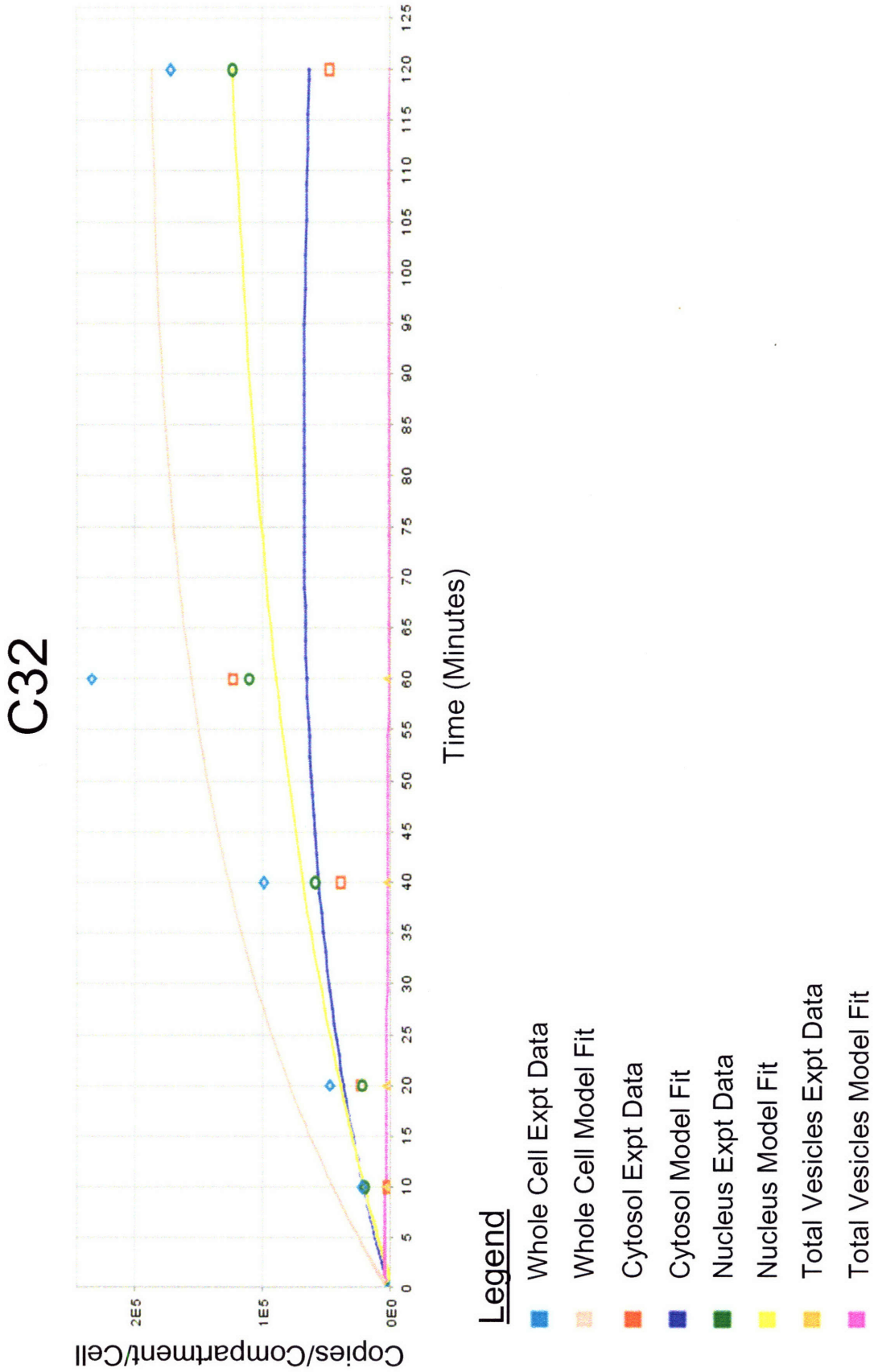

Figure 5.4: Vector specific model fits. Jacobian output for model simulations compared to experimental data after the parameter estimation routine is conducted.

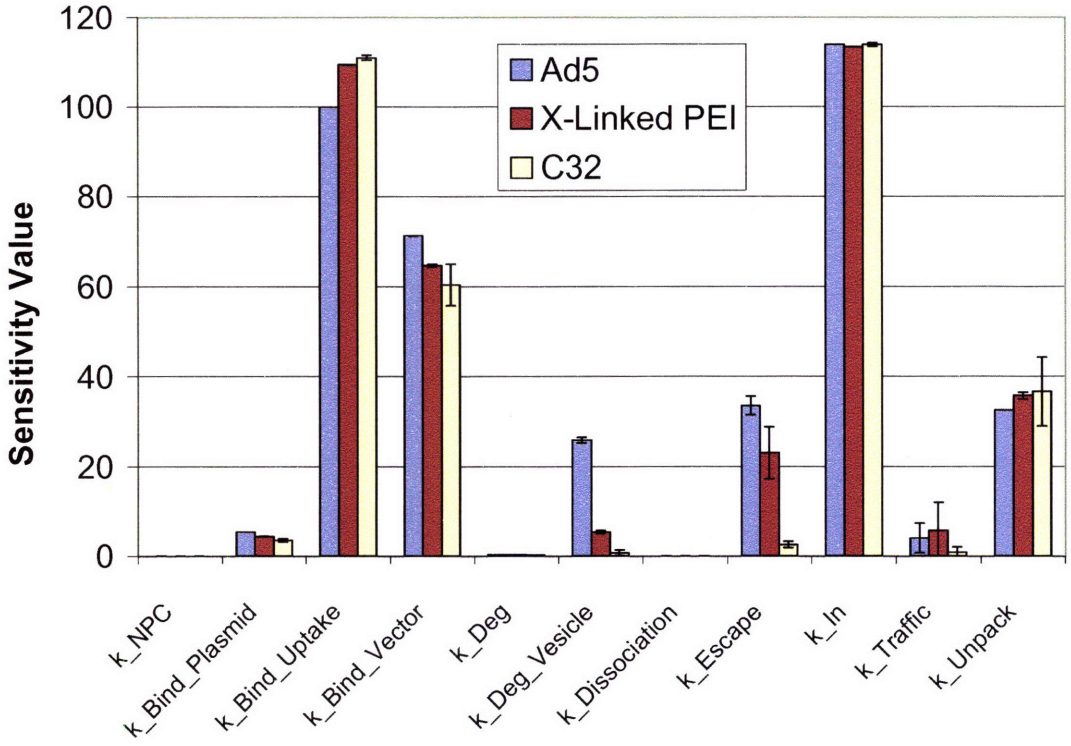

Figure 5.5: Parameter sensitivity analysis on the sensitivity of free nuclear plasmids for each vector specific parameter set from the multistart routine in Jacobian.

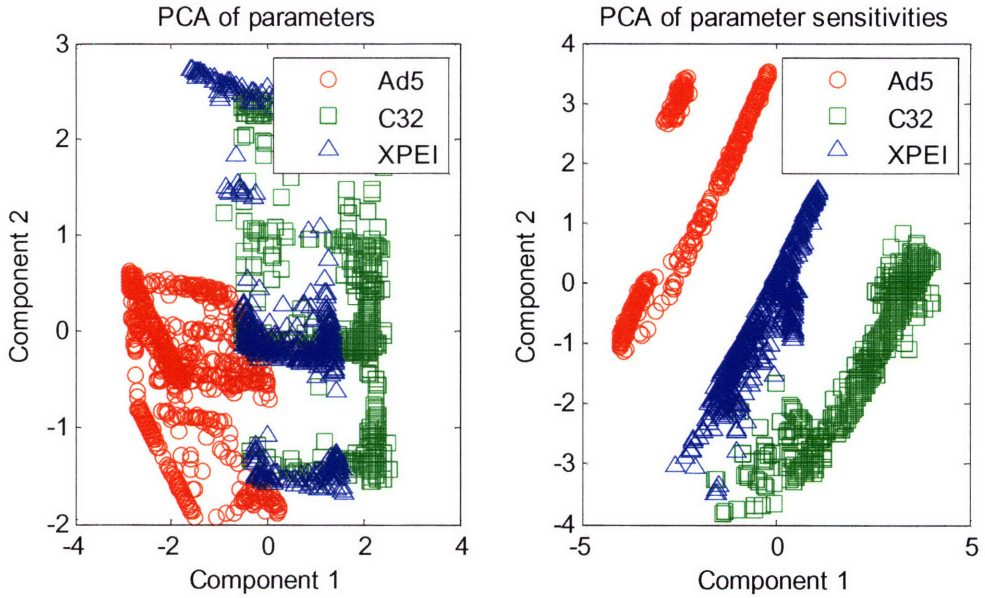

Figure 5.6: Principal component analysis of multiple model parameter fits and ensuing sensitivity analyses. Collapsing this multidimensional data to two combinatorially weighted vectors in 2-D space shows some interesting phenomena that can drive more in depth future analysis. Normalized sensitivities for each vector map to unique regions in this principal component space.

Chapter 6

Conclusions and Future Directions

Non-viral gene therapy holds a good deal of promise in providing safer gene delivery strategies with increased flexibility and application specific functionality. However, current non-viral vectors are inefficient compared to available viral carriers, and are largely underrepresented in gene therapy clinical trials today. Novel approaches for the rational design of non-viral vectors may be able to aid in the development of new vectors that safely transfect specific cell types with the efficiency of recombinant viruses. However, more tools are needed to provide quantitative, mechanistic information that can be used to improve vectors for specific applications. This thesis work aimed to provide new devices and assay methods that would contribute to this end, and specifically drive further development of non-viral vectors for primary liver cells.

An improved density gradient electrophoresis device was built and an optimized assay method was developed to successfully perform quantitative trafficking assays on primary hepatocytes, and provided further insight on the dynamics of gene delivery via next generation non-viral vectors. This approach was able to generate data sets that allowed for the creation of more comprehensive vector specific mathematical models. Additional analyses were performed with the models that can drive hypotheses for future experiments and for potential vector improvement. This more complete data set can also generally be used to train different mathematical model structures to improve these *in silico* analyses and learn more about parameter fitting techniques, sensitivity analyses, and principal component analyses in a well defined system.

In concert with this subcellular fractionation work, quantitative gene expression assays were moved into a new, 3-D perfused liver bioreactor that succesfully maintained enhanced liver phenotype of cultured primary hepatocytes and provided enough reorganized liver tissue to compare gene expression between novel and established vectors. It was hoped that this system would better reflect how a vector would perform *in vivo*, while still providing the ability to perform quantitative measurements. This system, when compared to 2-D transfection studies, provided very interesting results, revealing that vector success can be dependant not only on cell type but also on the culture environment. These preliminary

results make a strong argument for moving more vector studies into *in vitro* models that do a better job of recapitulating *in vivo* structure and phenotype.

This work served as a first step into exploring the utility of quantitative intracellular trafficking and gene expression studies in primary cells to learn more about how researchers can bridge the gap between cell line and animal studies to potentially develop better vectors or identify suitable applications for a given type of vector. Many direct extensions can be made in these systems to acquire more useful information for vector evaluation. One of the most obvious next steps is to fully combine the two main experimental approaches developed in this thesis work to study intracellular trafficking in primary hepatocytes that have an in-vivo like 3-D tissue structure and enhanced liver phenotype. The next generation vectors used in this study internalized and trafficked so efficiently that the overall time course had to be shifted to earlier time points than those used in our previous studies in C3A cells. This made it exceptionally difficult to acquire consistent data at the 10 and 20 minute time points in 3-D cultures. Additionally, when examining the quantitative time courses in Chapter 5, it can be concluded that an even earlier time point at 5 minutes post delivery may be useful in deciphering some of the early uptake and trafficking dynamics in the different compartments.

A new multiwell liver bioreactor that has been recently developed in the Griffith lab could address these issues quite effectively. In the current iteration of this new system, twelve cell scaffolds are assembled and seeded in an array of isolated wells within the reactor plate, and are all consistently perfused by a novel microfluidic pumping system. Preliminary work has been performed in this system with new scaffolds that have on the order of 800 channel units, meaning each well in the array would provide enough transfected cell material for expression or trafficking studies. Liver tissue in each well could be dosed with a vector/plasmid complex, and then individual scaffolds could be quickly recovered, washed and lysed for more accurate 3-D uptake assays with increased resolution. Without the risk of dedifferentiation that existed with performing multiple back to back DGE runs on the same batch of 2-D cultures, stabilized 3-D cultures could provide more throughput for performing full trafficking analyses as well. Overall this could allow for higher temporal resolution and the ability to compare more vectors more efficiently.

One of the primary limiting factors in this study that affected how many vectors could be examined and at how many time points was the rather long and involved process of

the DGE separation protocol. While this method did provide excellent separation over an order of magnitude faster than other available approaches, throughput was limited to one sample at a time, and at best, two runs could be performed in a day. Approaches that could multiplex this separation process would be highly beneficial to studying more vectors with better temporal resolution, yielding more informative quantitative data sets for model fitting and analysis. It appears that many efforts are on the verge of moving microfluidic separation systems that have achieved success with DNA and protein analytes to applications with cell organelles. This analysis would stand to benefit substantially from these developments, not only by gaining higher throughput and detection sensitivity, but also by potentially increasing the resolution of the overall separation and allowing for more detailed models to be accurately created.

The current data set generated from these studies can also be subjected to a number of mathematical model extensions. Different model structures can be explored that describe various steps in the delivery process with greater or less detail or additional steps altogether can be added which may explain alternate mechanisms. Analyzing goodness of model fits, sensitivity analyses and principal component analyses on these structures may help to reveal which structure is actually best, and suggest additional hypotheses into the nuances of the delivery mechanism for each vector. The gene delivery pathway provides a fairly linear and deterministic process as compared to many of the cell signaling networks that are often analyzed with these approaches. As a result, this data could provide an ideal training set for evaluating the utility of many of these approaches before applying the new techniques to more complicated or incomplete data sets and models.

Additionally, for models to become truly informative for non-viral vector development, more attention has to be given to the processes that occur after successful delivery of plasmids to the nucleus. It is becoming increasingly apparent that nuclear delivery may actually only represent half of the battle in attaining successful and safe non-viral gene therapies. Many novel non-viral carriers, including the vectors studied in this work, appear to deliver orders of magnitude more plasmid to the nucleus than viral vector yet still result in lower and less sustained transgene expression levels. Lessons need to be learned from viruses in regard to strategies for enhanced transcription factor recruitment and avoidance of gene silencing. Novel DNA constructs such as minicircle DNA coupled with integrase or transposase systems that achieve highly specific, site-directed insertion of

transgene into chromosomes that does not lead to aberrant expression of genomic DNA are attractive options that have emerged in recent times. It is hoped that further mechanistic study of these processes may lead to models that can lead to rational design of both components of the non-viral complex yielding a specific combination polymer and DNA that gives a highly safe and efficient therapy tailored for the clinical application of interest.

References

1. Huang, L., Hung, M.C., Wagner, E., ed. *Nonviral Vectors for Gene Therapy.* 1999, Academic Press: San Diego.
2. Templeton, N.S., Lasic, D.D., ed. *Gene Therapy: Therapeutic Mechanisms and Strategies.* 2000, Marcel Dekker: New York.
3. Weiler, J., J. Hunziker, and J. Hall, *Anti-miRNA oligonucleotides (AMOs): ammunition to target miRNAs implicated in human disease?* Gene Ther, 2006. **13**(6): p. 496-502.
4. Cullen, B.R., *Induction of stable RNA interference in mammalian cells.* Gene Ther, 2006. **13**(6): p. 503-8.
5. Weatherall, D.J., *Gene therapy: repairing haemoglobin disorders with ribozymes.* Curr Biol, 1998. **8**(19): p. R696-8.
6. Emery, D.W., et al., *Development of virus vectors for gene therapy of beta chain hemoglobinopathies: flanking with a chromatin insulator reduces gamma-globin gene silencing in vivo.* Blood, 2002. **100**(6): p. 2012-9.
7. Walsh, C.E., *Gene therapy Progress and Prospects: Gene therapy for the hemophilias.* Gene Ther, 2003. **10**(12): p. 999-1003.
8. Aiuti, A., et al., *Correction of ADA-SCID by stem cell gene therapy combined with nonmyeloablative conditioning.* Science, 2002. **296**(5577): p. 2410-3.
9. Khurana, R., J.F. Martin, and I. Zachary, *Gene therapy for cardiovascular disease: a case for cautious optimism.* Hypertension, 2001. **38**(5): p. 1210-6.
10. Griesenbach, U., et al., *Gene therapy progress and prospects: cystic fibrosis.* Gene Ther, 2002. **9**(20): p. 1344-50.
11. Ferrari, S., D.M. Geddes, and E.W. Alton, *Barriers to and new approaches for gene therapy and gene delivery in cystic fibrosis.* Adv Drug Deliv Rev, 2002. **54**(11): p. 1373-93.
12. Roberts, M. and G. Dickson, *The future of Duchenne muscular dystrophy gene therapy: shrinking the dystrophin gene.* Curr Opin Mol Ther, 2002. **4**(4): p. 343-8.
13. Curiel, D.T., W.R. Gerritsen, and M.R. Krul, *Progress in cancer gene therapy.* Cancer Gene Ther, 2000. **7**(8): p. 1197-9.
14. Lattime, E.C., Gerson, S.L., ed. *Gene Therapy of Cancer.* 1999, Academic Press: San Diego.
15. Pirollo, K.F., L. Xu, and E.H. Chang, *Non-viral gene delivery for p53.* Curr Opin Mol Ther, 2000. **2**(2): p. 168-75.
16. Mitchell, D.A. and S.K. Nair, *RNA transfected dendritic cells as cancer vaccines.* Curr Opin Mol Ther, 2000. **2**(2): p. 176-81.
17. Mahato, R.I., et al., *Cationic lipid and polymer-based gene delivery to human pancreatic islets.* Mol Ther, 2003. **7**(1): p. 89-100.
18. Xu, R., et al., *Diabetes gene therapy: potential and challenges.* Curr Gene Ther, 2003. **3**(1): p. 65-82.
19. Templeton, N.S., Lasic, D.D., ed. *Gene Therapy: Therapeutic Mechanisms and Strategies.* 2000, Marcel Dekker: New York. p. 535-548.
20. Cordelier, P., et al., *Inhibiting AIDS in the central nervous system: gene delivery to protect neurons from HIV.* Mol Ther, 2003. **7**(6): p. 801-10.

21. Cordelier, P., M.A. Zern, and D.S. Strayer, *HIV-1 proprotein processing as a target for gene therapy.* Gene Ther, 2003. **10**(6): p. 467-77.
22. Yokota, T., et al., *Inhibition of intracellular hepatitis C virus replication by synthetic and vector-derived small interfering RNAs.* EMBO Rep, 2003. **4**(6): p. 602-608.
23. Whitley, R.J. and B. Roizman, *Herpes simplex viruses: is a vaccine tenable?* J Clin Invest, 2002. **110**(2): p. 145-51.
24. Templeton, N.S., Lasic, D.D., ed. *Gene Therapy: Therapeutic Mechanisms and Strategies*. 2000, Marcel Dekker: New York. p. 549-568.
25. Pachuk, C.J., et al., *DNA vaccines--challenges in delivery.* Curr Opin Mol Ther, 2000. **2**(2): p. 188-98.
26. Morris, K.V. and J.J. Rossi, *Antiviral applications of RNAi.* Curr Opin Mol Ther, 2006. **8**(2): p. 115-21.
27. Rossi, J.J., *RNAi as a treatment for HIV-1 infection.* Biotechniques, 2006. **Suppl**: p. 25-9.
28. Sazani, P., M.M. Vacek, and R. Kole, *Short-term and long-term modulation of gene expression by antisense therapeutics.* Curr Opin Biotechnol, 2002. **13**(5): p. 468-72.
29. Little, S.R. and R. Langer, *Nonviral delivery of cancer genetic vaccines.* Adv Biochem Eng Biotechnol, 2005. **99**: p. 93-118.
30. Manthorpe, M., et al., *Plasmid vaccines and therapeutics: from design to applications.* Adv Biochem Eng Biotechnol, 2005. **99**: p. 41-92.
31. Kelly, E.B., *Gene Therapy and the Future*, in *Molecular Miracles*. 1998, Arc Mesa Educators: Triton Falls, NJ.
32. Marshall, E., *Gene therapy's growing pains.* Science, 1995. **269**(5227): p. 1050, 1052-5.
33. Thomas, C.E., A. Ehrhardt, and M.A. Kay, *Progress and problems with the use of viral vectors for gene therapy.* Nat Rev Genet, 2003. **4**(5): p. 346-58.
34. *Gene Therapy Clincal Trials Statistics, Updated July 2006.* **Volume**,
35. Gordon, E.M., et al., *First clinical experience using a 'pathotropic' injectable retroviral vector (Rexin-G) as intervention for stage IV pancreatic cancer.* Int J Oncol, 2004. **24**(1): p. 177-85.
36. Gordon, E.M., et al., *Pathotropic nanoparticles for cancer gene therapy Rexin-G IV: three-year clinical experience.* Int J Oncol, 2006. **29**(5): p. 1053-64.
37. Goyenvalle, A., et al., *[An opening in Duchenne muscular dystrophy: persistent therapeutic rescue of dystrophin by vectorized antisense mediated exon skipping in mdx mice].* Med Sci (Paris), 2004. **20**(12): p. 1163-5.
38. Goyenvalle, A., et al., *Rescue of dystrophic muscle through U7 snRNA-mediated exon skipping.* Science, 2004. **306**(5702): p. 1796-9.
39. Cavazzana-Calvo, M., A. Thrasher, and F. Mavilio, *The future of gene therapy.* Nature, 2004. **427**(6977): p. 779-81.
40. Fischer, A., S. Hacein-Bey-Abina, and M. Cavazzana-Calvo, *[Gene therapy of children with X-linked severe combined immune deficiency: efficiency and complications].* Med Sci (Paris), 2004. **20**(1): p. 115-7.

41. Hacein-Bey-Abina, S., et al., *A serious adverse event after successful gene therapy for X-linked severe combined immunodeficiency.* N Engl J Med, 2003. **348**(3): p. 255-6.
42. Kwon, Y.J. and C.A. Peng, *Engineering analysis of ex vivo retroviral transduction system.* Ann Biomed Eng, 2002. **30**(5): p. 731-42.
43. Robbins, P.D. and S.C. Ghivizzani, *Viral vectors for gene therapy.* Pharmacol Ther, 1998. **80**(1): p. 35-47.
44. Huang, L., Hung, M.C., Wagner, E., ed. *Nonviral Vectors for Gene Therapy.* 1999, Academic Press: San Diego. pp. 4-8.
45. Lai, C.M., Y.K. Lai, and P.E. Rakoczy, *Adenovirus and adeno-associated virus vectors.* DNA Cell Biol, 2002. **21**(12): p. 895-913.
46. Blaydes, S.M., et al., *Retroviral integration at the Epi1 locus cooperates with Nf1 gene loss in the progression to acute myeloid leukemia.* J Virol, 2001. **75**(19): p. 9427-34.
47. Kaiser, J., *Gene therapy. Seeking the cause of induced leukemias in X-SCID trial.* Science, 2003. **299**(5606): p. 495.
48. Baum, C., et al., *Side effects of retroviral gene transfer into hematopoietic stem cells.* Blood, 2003. **101**(6): p. 2099-114.
49. Logan, A.C., C. Lutzko, and D.B. Kohn, *Advances in lentiviral vector design for gene-modification of hematopoietic stem cells.* Curr Opin Biotechnol, 2002. **13**(5): p. 429-36.
50. Quinonez, R. and R.E. Sutton, *Lentiviral vectors for gene delivery into cells.* DNA Cell Biol, 2002. **21**(12): p. 937-51.
51. Loewen, N. and E.M. Poeschla, *Lentiviral vectors.* Adv Biochem Eng Biotechnol, 2005. **99**: p. 169-91.
52. Burton, E.A., D.J. Fink, and J.C. Glorioso, *Gene delivery using herpes simplex virus vectors.* DNA Cell Biol, 2002. **21**(12): p. 915-36.
53. Grieger, J.C. and R.J. Samulski, *Adeno-associated virus as a gene therapy vector: vector development, production and clinical applications.* Adv Biochem Eng Biotechnol, 2005. **99**: p. 119-45.
54. Grieger, J.C. and R.J. Samulski, *Packaging capacity of adeno-associated virus serotypes: impact of larger genomes on infectivity and postentry steps.* J Virol, 2005. **79**(15): p. 9933-44.
55. Huang, L., Hung, M.C., Wagner, E., ed. *Nonviral Vectors for Gene Therapy.* 1999, Academic Press: San Diego. pp. 7-11.
56. Herweijer, H. and J.A. Wolff, *Progress and prospects: naked DNA gene transfer and therapy.* Gene Ther, 2003. **10**(6): p. 453-8.
57. Lollo, C.P., M.G. Banaszczyk, and H.C. Chiou, *Obstacles and advances in non-viral gene delivery.* Curr Opin Mol Ther, 2000. **2**(2): p. 136-42.
58. Williams, R.S., et al., *Introduction of foreign genes into tissues of living mice by DNA-coated microprojectiles.* Proc Natl Acad Sci U S A, 1991. **88**(7): p. 2726-30.
59. Johnston, S.A., et al., *Mitochondrial transformation in yeast by bombardment with microprojectiles.* Science, 1988. **240**(4858): p. 1538-41.

60. Levy, M.Y., et al., *Characterization of plasmid DNA transfer into mouse skeletal muscle: evaluation of uptake mechanism, expression and secretion of gene products into blood.* Gene Ther, 1996. **3**(3): p. 201-11.
61. Martin, T., et al., *Plasmid DNA malaria vaccine: the potential for genomic integration after intramuscular injection.* Hum Gene Ther, 1999. **10**(5): p. 759-68.
62. Chang, Y. and G.J. Prud'homme, *Intramuscular administration of expression plasmids encoding interferon-gamma receptor/IgG1 or IL-4/IgG1 chimeric proteins protects from autoimmunity.* J Gene Med, 1999. **1**(6): p. 415-23.
63. Smith, L.C. and J.L. Nordstrom, *Advances in plasmid gene delivery and expression in skeletal muscle.* Curr Opin Mol Ther, 2000. **2**(2): p. 150-4.
64. Orr, R.M., *Technology evaluation: electroporation therapy, Genetronics Inc.* Curr Opin Mol Ther, 2000. **2**(2): p. 205-10.
65. Li, S. and M. Benninger, *Applications of muscle electroporation gene therapy.* Curr Gene Ther, 2002. **2**(1): p. 101-5.
66. Niidome, T. and L. Huang, *Gene therapy progress and prospects: nonviral vectors.* Gene Ther, 2002. **9**(24): p. 1647-52.
67. Liu, D. and J.E. Knapp, *Hydrodynamics-based gene delivery.* Curr Opin Mol Ther, 2001. **3**(2): p. 192-7.
68. Eastman, S.J., et al., *Development of catheter-based procedures for transducing the isolated rabbit liver with plasmid DNA.* Hum Gene Ther, 2002. **13**(17): p. 2065-77.
69. Luo, D. and W.M. Saltzman, *Synthetic DNA delivery systems.* Nat Biotechnol, 2000. **18**(1): p. 33-7.
70. Thomas, M. and A.M. Klibanov, *Non-viral gene therapy: polycation-mediated DNA delivery.* Appl Microbiol Biotechnol, 2003.
71. Fraley, R. and D. Papahadjopoulos, *Liposomes: the development of a new carrier system for introducing nucleic acid into plant and animal cells.* Curr Top Microbiol Immunol, 1982. **96**: p. 171-91.
72. Fraley, R., et al., *Liposome-mediated delivery of deoxyribonucleic acid to cells: enhanced efficiency of delivery related to lipid composition and incubation conditions.* Biochemistry, 1981. **20**(24): p. 6978-87.
73. Felgner, P.L., et al., *Lipofection: a highly efficient, lipid-mediated DNA-transfection procedure.* Proc Natl Acad Sci U S A, 1987. **84**(21): p. 7413-7.
74. Felgner, P.L., M. Holm, and H. Chan, *Cationic liposome mediated transfection.* Proc West Pharmacol Soc, 1989. **32**: p. 115-21.
75. Wu, G.Y. and C.H. Wu, *Receptor-mediated in vitro gene transformation by a soluble DNA carrier system.* J Biol Chem, 1987. **262**(10): p. 4429-32.
76. Boussif, O., et al., *A versatile vector for gene and oligonucleotide transfer into cells in culture and in vivo: polyethylenimine.* Proc Natl Acad Sci U S A, 1995. **92**(16): p. 7297-301.
77. Oh, Y.K., et al., *Polyethylenimine-mediated cellular uptake, nucleus trafficking and expression of cytokine plasmid DNA.* Gene Ther, 2002. **9**(23): p. 1627-32.
78. Morimoto, K., et al., *Molecular weight-dependent gene transfection activity of unmodified and galactosylated polyethyleneimine on hepatoma cells and mouse liver.* Mol Ther, 2003. **7**(2): p. 254-61.

79. Forrest, M.L. and D.W. Pack, *On the kinetics of polyplex endocytic trafficking: implications for gene delivery vector design.* Mol Ther, 2002. **6**(1): p. 57-66.
80. Thomas, M. and A.M. Klibanov, *Enhancing polyethylenimine's delivery of plasmid DNA into mammalian cells.* Proc Natl Acad Sci U S A, 2002. **99**(23): p. 14640-5.
81. Rudolph, C., R.H. Muller, and J. Rosenecker, *Jet nebulization of PEI/DNA polyplexes: physical stability and in vitro gene delivery efficiency.* J Gene Med, 2002. **4**(1): p. 66-74.
82. Pollard, H., et al., *Polyethylenimine but not cationic lipids promotes transgene delivery to the nucleus in mammalian cells.* J Biol Chem, 1998. **273**(13): p. 7507-11.
83. Ogris, M., et al., *DNA/polyethylenimine transfection particles: influence of ligands, polymer size, and PEGylation on internalization and gene expression.* AAPS PharmSci, 2001. **3**(3): p. E21.
84. Godbey, W.T., K.K. Wu, and A.G. Mikos, *Poly(ethylenimine)-mediated gene delivery affects endothelial cell function and viability.* Biomaterials, 2001. **22**(5): p. 471-80.
85. Godbey, W.T., K.K. Wu, and A.G. Mikos, *Size matters: molecular weight affects the efficiency of poly(ethylenimine) as a gene delivery vehicle.* J Biomed Mater Res, 1999. **45**(3): p. 268-75.
86. Godbey, W.T., et al., *Improved packing of poly(ethylenimine)/DNA complexes increases transfection efficiency.* Gene Ther, 1999. **6**(8): p. 1380-8.
87. Godbey, W.T., K.K. Wu, and A.G. Mikos, *Poly(ethylenimine) and its role in gene delivery.* J Control Release, 1999. **60**(2-3): p. 149-60.
88. Brissault, B., et al., *Synthesis of linear polyethylenimine derivatives for DNA transfection.* Bioconjug Chem, 2003. **14**(3): p. 581-7.
89. Huang, L., Hung, M.C., Wagner, E., ed. *Nonviral Vectors for Gene Therapy.* 1999, Academic Press: San Diego. pp. 192-204.
90. Godbey, W.T., et al., *Poly(ethylenimine)-mediated transfection: a new paradigm for gene delivery.* J Biomed Mater Res, 2000. **51**(3): p. 321-8.
91. Godbey, W.T., K.K. Wu, and A.G. Mikos, *Tracking the intracellular path of poly(ethylenimine)/DNA complexes for gene delivery.* Proc Natl Acad Sci U S A, 1999. **96**(9): p. 5177-81.
92. Bieber, T., et al., *Intracellular route and transcriptional competence of polyethylenimine-DNA complexes.* J Control Release, 2002. **82**(2-3): p. 441-54.
93. Kichler, A., et al., *Polyethylenimine-mediated gene delivery: a mechanistic study.* J Gene Med, 2001. **3**(2): p. 135-44.
94. Suh, J., D. Wirtz, and J. Hanes, *Efficient active transport of gene nanocarriers to the cell nucleus.* Proc Natl Acad Sci U S A, 2003. **100**(7): p. 3878-82.
95. Lynn, D.M., M.M. Amiji, and R. Langer, *pH-Responsive Polymer Microspheres: Rapid Release of Encapsulated Material within the Range of Intracellular pH.* Angew Chem Int Ed Engl, 2001. **40**(9): p. 1707-1710.
96. Cartier, R. and R. Reszka, *Utilization of synthetic peptides containing nuclear localization signals for nonviral gene transfer systems.* Gene Ther, 2002. **9**(3): p. 157-67.

97. Hagstrom, J.E., *Self-assembling complexes for in vivo gene delivery.* Curr Opin Mol Ther, 2000. **2**(2): p. 143-9.
98. Schaffer, D.V. and D.A. Lauffenburger, *Targeted synthetic gene delivery vectors.* Curr Opin Mol Ther, 2000. **2**(2): p. 155-61.
99. Varga, C.M., T.J. Wickham, and D.A. Lauffenburger, *Receptor-mediated targeting of gene delivery vectors: insights from molecular mechanisms for improved vehicle design.* Biotechnol Bioeng, 2000. **70**(6): p. 593-605.
100. Schwartz, J.J. and S. Zhang, *Peptide-mediated cellular delivery.* Curr Opin Mol Ther, 2000. **2**(2): p. 162-7.
101. Cashman, S.M., et al., *Intercellular Trafficking of Adenovirus-Delivered HSV VP22 from the Retinal Pigment Epithelium to the Photoreceptors-Implications for Gene Therapy.* Mol Ther, 2002. **6**(6): p. 813-23.
102. Heidel, J., S. Mishra, and M.E. Davis, *Molecular conjugates.* Adv Biochem Eng Biotechnol, 2005. **99**: p. 7-39.
103. Anderson, D.G., et al., *Structure/property studies of polymeric gene delivery using a library of poly(beta-amino esters).* Mol Ther, 2005. **11**(3): p. 426-34.
104. Anderson, D.G., S. Levenberg, and R. Langer, *Nanoliter-scale synthesis of arrayed biomaterials and application to human embryonic stem cells.* Nat Biotechnol, 2004. **22**(7): p. 863-6.
105. Anderson, D.G., D.M. Lynn, and R. Langer, *Semi-automated synthesis and screening of a large library of degradable cationic polymers for gene delivery.* Angew Chem Int Ed Engl, 2003. **42**(27): p. 3153-8.
106. Anderson, D.G., et al., *A polymer library approach to suicide gene therapy for cancer.* Proc Natl Acad Sci U S A, 2004. **101**(45): p. 16028-33.
107. Jon, S., D.G. Anderson, and R. Langer, *Degradable poly(amino alcohol esters) as potential DNA vectors with low cytotoxicity.* Biomacromolecules, 2003. **4**(6): p. 1759-62.
108. Thomas, M., et al., *Cross-linked small polyethylenimines: while still nontoxic, deliver DNA efficiently to mammalian cells in vitro and in vivo.* Pharm Res, 2005. **22**(3): p. 373-80.
109. Thomas, M., et al., *Full deacylation of polyethylenimine dramatically boosts its gene delivery efficiency and specificity to mouse lung.* Proc Natl Acad Sci U S A, 2005. **102**(16): p. 5679-84.
110. Mao, H.Q. and K.W. Leong, *Design of Polyphosphoester-DNA Nanoparticles for Non-Viral Gene Delivery.* Adv Genet, 2005. **53PA**: p. 275-306.
111. Zhang, X.Q., et al., *Galactosylated ternary DNA/polyphosphoramidate nanoparticles mediate high gene transfection efficiency in hepatocytes.* J Control Release, 2005. **102**(3): p. 749-63.
112. Huang, L., Hung, M.C., Wagner, E., ed. *Nonviral Vectors for Gene Therapy.* 1999, Academic Press: San Diego. pp. 11-16.
113. Varga, C.M., K. Hong, and D.A. Lauffenburger, *Quantitative analysis of synthetic gene delivery vector design properties.* Mol Ther, 2001. **4**(5): p. 438-46.
114. Gundelfinger, E.D., M.M. Kessels, and B. Qualmann, *Temporal and spatial coordination of exocytosis and endocytosis.* Nat Rev Mol Cell Biol, 2003. **4**(2): p. 127-39.

115. Gruenberg, J., *The endocytic pathway: a mosaic of domains.* Nat Rev Mol Cell Biol, 2001. **2**(10): p. 721-30.
116. Pollard, H., et al., *Ca2+-sensitive cytosolic nucleases prevent efficient delivery to the nucleus of injected plasmids.* J Gene Med, 2001. **3**(2): p. 153-64.
117. Ludtke, J.J., et al., *A nuclear localization signal can enhance both the nuclear transport and expression of 1 kb DNA.* J Cell Sci, 1999. **112 (Pt 12)**: p. 2033-41.
118. Schaffer, D.V., et al., *Vector unpacking as a potential barrier for receptor-mediated polyplex gene delivery.* Biotechnol Bioeng, 2000. **67**(5): p. 598-606.
119. Hong, K., J. Sherley, and D.A. Lauffenburger, *Methylation of episomal plasmids as a barrier to transient gene expression via a synthetic delivery vector.* Biomol Eng, 2001. **18**(4): p. 185-92.
120. Schaffer, D.V. and D.A. Lauffenburger, *Optimization of cell surface binding enhances efficiency and specificity of molecular conjugate gene delivery.* J Biol Chem, 1998. **273**(43): p. 28004-9.
121. Luo, D. and W.M. Saltzman, *Enhancement of transfection by physical concentration of DNA at the cell surface.* Nat Biotechnol, 2000. **18**(8): p. 893-5.
122. Cotten, M., et al., *High-efficiency receptor-mediated delivery of small and large (48 kilobase gene constructs using the endosome-disruption activity of defective or chemically inactivated adenovirus particles.* Proc Natl Acad Sci U S A, 1992. **89**(13): p. 6094-8.
123. Curiel, D.T., et al., *Adenovirus enhancement of transferrin-polylysine-mediated gene delivery.* Proc Natl Acad Sci U S A, 1991. **88**(19): p. 8850-4.
124. Plank, C., et al., *The influence of endosome-disruptive peptides on gene transfer using synthetic virus-like gene transfer systems.* J Biol Chem, 1994. **269**(17): p. 12918-24.
125. Lukacs, G.L., et al., *Size-dependent DNA mobility in cytoplasm and nucleus.* J Biol Chem, 2000. **275**(3): p. 1625-9.
126. Sebestyen, M.G., et al., *DNA vector chemistry: the covalent attachment of signal peptides to plasmid DNA.* Nat Biotechnol, 1998. **16**(1): p. 80-5.
127. Ludtke, J.J., M.G. Sebestyen, and J.A. Wolff, *The effect of cell division on the cellular dynamics of microinjected DNA and dextran.* Mol Ther, 2002. **5**(5 Pt 1): p. 579-88.
128. Brunner, S., et al., *Overcoming the nuclear barrier: cell cycle independent nonviral gene transfer with linear polyethylenimine or electroporation.* Mol Ther, 2002. **5**(1): p. 80-6.
129. Harel, A. and D.J. Forbes, *Welcome to the nucleus: CAN I take your coat?* Nat Cell Biol, 2001. **3**(12): p. E267-9.
130. Salman, H., et al., *Kinetics and mechanism of DNA uptake into the cell nucleus.* Proc Natl Acad Sci U S A, 2001. **98**(13): p. 7247-52.
131. Aplin, A.E. and R.L. Juliano, *Regulation of nucleocytoplasmic trafficking by cell adhesion receptors and the cytoskeleton.* J Cell Biol, 2001. **155**(2): p. 187-91.
132. Varga, C.M., et al., *Quantitative comparison of polyethylenimine formulations and adenoviral vectors in terms of intracellular gene delivery processes.* Gene Ther, 2005. **12**(13): p. 1023-32.

133. Akinc, A., et al., *Parallel synthesis and biophysical characterization of a degradable polymer library for gene delivery.* J Am Chem Soc, 2003. **125**(18): p. 5316-23.
134. Lynn, D.M., et al., *Accelerated discovery of synthetic transfection vectors: parallel synthesis and screening of a degradable polymer library.* J Am Chem Soc, 2001. **123**(33): p. 8155-6.
135. Akinc, A. and R. Langer, *Measuring the pH environment of DNA delivered using nonviral vectors: implications for lysosomal trafficking.* Biotechnol Bioeng, 2002. **78**(5): p. 503-8.
136. Tulp, A., *Density gradient electrophoresis of mammalian cells.* Methods Biochem Anal, 1984. **30**: p. 141-98.
137. Pol, A. and C. Enrich, *Membrane transport in rat liver endocytic pathways: preparation, biochemical properties and functional roles of hepatic endosomes.* Electrophoresis, 1997. **18**(14): p. 2548-57.
138. Pol, A., D. Ortega, and C. Enrich, *Identification and distribution of proteins in isolated endosomal fractions of rat liver: involvement in endocytosis, recycling and transcytosis.* Biochem J, 1997. **323 (Pt 2)**: p. 435-43.
139. Pfeffer, S., *Membrane domains in the secretory and endocytic pathways.* Cell, 2003. **112**(4): p. 507-17.
140. Ellinger, I., et al., *Different temperature sensitivity of endosomes involved in transport to lysosomes and transcytosis in rat hepatocytes: analysis by free-flow electrophoresis.* Electrophoresis, 2002. **23**(13): p. 2117-29.
141. Ellinger, I., H. Klapper, and R. Fuchs, *Fluid-phase marker transport in rat liver: free-flow electrophoresis separates distinct endosome subpopulations.* Electrophoresis, 1998. **19**(7): p. 1154-61.
142. Tulp, A., et al., *High resolution density gradient electrophoresis of cellular organelles.* Electrophoresis, 1996. **17**(1): p. 173-8.
143. Pasquali, C., I. Fialka, and L.A. Huber, *Subcellular fractionation, electromigration analysis and mapping of organelles.* J Chromatogr B Biomed Sci Appl, 1999. **722**(1-2): p. 89-102.
144. Kent, J., Personal Communication.
145. Lu, H., Personal Communication.
146. Tulp, A., D. Verwoerd, and J. Pieters, *Application of an improved density gradient electrophoresis apparatus to the separation of proteins, cells and subcellular organelles.* Electrophoresis, 1993. **14**(12): p. 1295-301.
147. Tulp, A., et al., *High performance density gradient electrophoresis of subcellular organelles, protein complexes and proteins.* Electrophoresis, 1998. **19**(7): p. 1171-8.
148. Tulp, A., et al., *High-resolution density gradient electrophoresis of proteins and subcellular organelles.* Electrophoresis, 1997. **18**(14): p. 2509-15.
149. Pampinella, F., et al., *Analysis of differential lipofection efficiency in primary and established myoblasts.* Mol Ther, 2002. **5**(2): p. 161-9.
150. Brunetti-Pierri, N. and B. Lee, *Gene therapy for inborn errors of liver metabolism.* Mol Genet Metab, 2005. **86**(1-2): p. 13-24.
151. Herzog, R.W., *Recent advances in hepatic gene transfer: more efficacy and less immunogenicity.* Curr Opin Drug Discov Devel, 2005. **8**(2): p. 199-206.

152. Hodges, B.L. and S.H. Cheng, *Cell and gene-based therapies for the lysosomal storage diseases.* Curr Gene Ther, 2006. **6**(2): p. 227-41.
153. Liu, F. and P. Tyagi, *Naked DNA for liver gene transfer.* Adv Genet, 2005. **54**: p. 43-64.
154. Nguyen, T.H. and N. Ferry, *Liver gene therapy: advances and hurdles.* Gene Ther, 2004. **11 Suppl 1**: p. S76-84.
155. Ponder, K.P., *Gene therapy for hemophilia.* Curr Opin Hematol, 2006. **13**(5): p. 301-7.
156. Prieto, J., et al., *Gene therapy of liver diseases.* Expert Opin Biol Ther, 2004. **4**(7): p. 1073-91.
157. Shin, E.C., et al., *Liver-directed gamma interferon gene delivery in chronic hepatitis C.* J Virol, 2005. **79**(21): p. 13412-20.
158. Xia, D., M.M. Zhang, and L.N. Yan, *Recent advances in liver-directed gene transfer vectors.* Hepatobiliary Pancreat Dis Int, 2004. **3**(3): p. 332-6.
159. Hwa, A., *Microvessel Structure Formation in a 3D Perfused Co-culture of Rat Hepatocytes and Liver Endothelial Cells.* Massachusetts Institute of Technology, Cambridge, MA, 2006.
160. Sivaraman, A., *A Microfabricated 3D Tissue Engineered "Liver on a Chip": High Information Content Assays for in vitro Drug Metabolism Studies.* Massachusetts Institute of Technology, Cambridge, MA, 2004.
161. Powers, M.J., et al., *Functional behavior of primary rat liver cells in a three-dimensional perfused microarray bioreactor.* Tissue Eng, 2002. **8**(3): p. 499-513.
162. Powers, M.J., et al., *A microfabricated array bioreactor for perfused 3D liver culture.* Biotechnol Bioeng, 2002. **78**(3): p. 257-69.
163. Arias, I.M., Boyer, J.L., Chisari, F.V., Fausto, N., Schachter, D., Shafritz, D.A., ed. *The Liver: Biology and Pathobiology.* 4th ed. 2001, Lippincott, Williams, and Wilkins: Philadelphia. pp. 941-962.
164. Fang, J., *Optimization of Organelle Fractionation Methods for Quantitative Analysis of Gene Delivery Trafficking Kinetics.* Massachusetts Institute of Technology, Cambridge, MA, 2006.
165. Dewez, J.L., et al., *Competitive adsorption of proteins: key of the relationship between substratum surface properties and adhesion of epithelial cells.* Biomaterials, 1999. **20**(6): p. 547-59.
166. Dewez, J.L., Y.J. Schneider, and P.G. Rouxhet, *Coupled influence of substratum hydrophilicity and surfactant on epithelial cell adhesion.* J Biomed Mater Res, 1996. **30**(3): p. 373-83.
167. Dupont-Gillain, C.C., et al., *Patterned layers of adsorbed extracellular matrix proteins: influence on mammalian cell adhesion.* Biomed Mater Eng, 2004. **14**(3): p. 281-91.
168. Dupont-Gillain Ch, C., et al., *Controlling the supramolecular organisation of adsorbed collagen layers.* J Mater Sci Mater Med, 2004. **15**(4): p. 347-53.
169. Jacquemart, I., et al., *Nanostructured collagen layers obtained by adsorption and drying.* J Colloid Interface Sci, 2004. **278**(1): p. 63-70.
170. Verwoerd, D., Personal Communication.

171. Sivaraman, A., et al., *A microscale in vitro physiological model of the liver: predictive screens for drug metabolism and enzyme induction.* Curr Drug Metab, 2005. **6**(6): p. 569-91.
172. LeCluyse EL, B.P., Parkinson A, *Strategies for restoration and maintenance of normal hepatic structure and function in long-term cultures of rat hepatocytes.* Adv Drug Deliv Rev, 1996(22): p. 133-186.
173. Harley, B.A., et al., *Fabricating tubular scaffolds with a radial pore size gradient by a spinning technique.* Biomaterials, 2006. **27**(6): p. 866-74.
174. O'Brien, F.J., et al., *Influence of freezing rate on pore structure in freeze-dried collagen-GAG scaffolds.* Biomaterials, 2004. **25**(6): p. 1077-86.
175. O'Brien, F.J., et al., *The effect of pore size on cell adhesion in collagen-GAG scaffolds.* Biomaterials, 2005. **26**(4): p. 433-41.
176. Huh, S.H., et al., *Optimization of 25kDa linear polyethylenimine for efficient gene delivery.* Biologicals, 2006.
177. Moghimi, S.M., et al., *A two-stage poly(ethylenimine)-mediated cytotoxicity: implications for gene transfer/therapy.* Mol Ther, 2005. **11**(6): p. 990-5.
178. Zugates, G., Personal Communication.
179. Banks, G.A., et al., *A model for the analysis of nonviral gene therapy.* Gene Ther, 2003. **10**(20): p. 1766-75.
180. Dinh, A.T., T. Theofanous, and S. Mitragotri, *A model for intracellular trafficking of adenoviral vectors.* Biophys J, 2005. **89**(3): p. 1574-88.
181. Dinh, T., et al., *Understanding Intracellular Transport Processes Pertinent to Synthetic Gene Delivery via Stochastic Simulations and Sensitivity Analyses.* Biophys J, 2006.
182. Ledley, T.S. and F.D. Ledley, *Multicompartment, numerical model of cellular events in the pharmacokinetics of gene therapies.* Hum Gene Ther, 1994. **5**(6): p. 679-91.
183. Akita, H., et al., *Quantitative three-dimensional analysis of the intracellular trafficking of plasmid DNA transfected by a nonviral gene delivery system using confocal laser scanning microscopy.* Mol Ther, 2004. **9**(3): p. 443-51.
184. Tulp, A., et al., *High-resolution density gradient electrophoresis of subcellular organelles and proteins under nondenaturing conditions.* Electrophoresis, 1998. **19**(8-9): p. 1288-93.
185. Lu, H., et al., *A microfabricated device for subcellular organelle sorting.* Anal Chem, 2004. **76**(19): p. 5705-12.
186. Lu, H., M.A. Schmidt, and K.F. Jensen, *A microfluidic electroporation device for cell lysis.* Lab Chip, 2005. **5**(1): p. 23-9.
187. Block, G.D., et al., *Population expansion, clonal growth, and specific differentiation patterns in primary cultures of hepatocytes induced by HGF/SF, EGF and TGF alpha in a chemically defined (HGM) medium.* J Cell Biol, 1996. **132**(6): p. 1133-49.
188. Griffith, L.G. and M.A. Swartz, *Capturing complex 3D tissue physiology in vitro.* Nat Rev Mol Cell Biol, 2006. **7**(3): p. 211-24.
189. Bader, A., et al., *A novel bioreactor design for in vitro reconstruction of in vivo liver characteristics.* Artif Organs, 1995. **19**(4): p. 368-74.

190. Bader, A., et al., *3-D coculture of hepatic sinusoidal cells with primary hepatocytes-design of an organotypical model.* Exp Cell Res, 1996. **226**(1): p. 223-33.
191. Gerlach, J., et al., *Hepatocyte culture between woven capillary networks: a microscopy study.* Artif Organs, 1994. **18**(3): p. 226-30.
192. Gerlach, J.C., et al., *Comparison of hollow fibre membranes for hepatocyte immobilisation in bioreactors.* Int J Artif Organs, 1996. **19**(10): p. 610-6.
193. Ostrovidov, S., et al., *Membrane-based PDMS microbioreactor for perfused 3D primary rat hepatocyte cultures.* Biomed Microdevices, 2004. **6**(4): p. 279-87.
194. Bissell, D.M., et al., *Support of cultured hepatocytes by a laminin-rich gel. Evidence for a functionally significant subendothelial matrix in normal rat liver.* J Clin Invest, 1987. **79**(3): p. 801-12.
195. Bhatia, S.N., et al., *Effect of cell-cell interactions in preservation of cellular phenotype: cocultivation of hepatocytes and nonparenchymal cells.* Faseb J, 1999. **13**(14): p. 1883-900.
196. Bhatia, S.N., M.L. Yarmush, and M. Toner, *Controlling cell interactions by micropatterning in co-cultures: hepatocytes and 3T3 fibroblasts.* J Biomed Mater Res, 1997. **34**(2): p. 189-99.
197. Gebhardt, R., *Co-cultivation of liver epithelial cells with hepatocytes.* Methods Mol Biol, 2002. **188**: p. 337-46.
198. Kern, A., et al., *Drug metabolism in hepatocyte sandwich cultures of rats and humans.* Biochem Pharmacol, 1997. **54**(7): p. 761-72.
199. Zaret, K.S., *Molecular genetics of early liver development.* Annu Rev Physiol, 1996. **58**: p. 231-51.
200. Odom, D.T., et al., *Control of pancreas and liver gene expression by HNF transcription factors.* Science, 2004. **303**(5662): p. 1378-81.
201. Schrem, H., J. Klempnauer, and J. Borlak, *Liver-enriched transcription factors in liver function and development. Part I: the hepatocyte nuclear factor network and liver-specific gene expression.* Pharmacol Rev, 2002. **54**(1): p. 129-58.
202. Suolinna, E.M. and T. Pitkaranta, *Effect of culture age on drug metabolizing enzymes and their induction in primary cultures of rat hepatocytes.* Biochem Pharmacol, 1986. **35**(13): p. 2241-5.
203. Park, S.H., C.A. Wiwi, and D.J. Waxman, *Signalling cross-talk between hepatocyte nuclear factor 4alpha and growth-hormone-activated STAT5b.* Biochem J, 2006. **397**(1): p. 159-68.
204. Wiwi, C.A. and D.J. Waxman, *Role of hepatocyte nuclear factors in growth hormone-regulated, sexually dimorphic expression of liver cytochromes P450.* Growth Factors, 2004. **22**(2): p. 79-88.
205. Wiwi, C.A. and D.J. Waxman, *Role of hepatocyte nuclear factors in transcriptional regulation of male-specific CYP2A2.* J Biol Chem, 2005. **280**(5): p. 3259-68.
206. Duncan, S.A., et al., *Regulation of a transcription factor network required for differentiation and metabolism.* Science, 1998. **281**(5377): p. 692-5.
207. Stoffel, M. and S.A. Duncan, *The maturity-onset diabetes of the young (MODY1) transcription factor HNF4alpha regulates expression of genes required for*

glucose transport and metabolism. Proc Natl Acad Sci U S A, 1997. **94**(24): p. 13209-14.
208. Duncan, S.A., et al., *Expression of transcription factor HNF-4 in the extraembryonic endoderm, gut, and nephrogenic tissue of the developing mouse embryo: HNF-4 is a marker for primary endoderm in the implanting blastocyst.* Proc Natl Acad Sci U S A, 1994. **91**(16): p. 7598-602.
209. Chen, W.S., et al., *Disruption of the HNF-4 gene, expressed in visceral endoderm, leads to cell death in embryonic ectoderm and impaired gastrulation of mouse embryos.* Genes Dev, 1994. **8**(20): p. 2466-77.
210. Roth, C.M. and S. Sundaram, *Engineering synthetic vectors for improved DNA delivery: insights from intracellular pathways.* Annu Rev Biomed Eng, 2004. **6**: p. 397-426.
211. Dong, W., et al., *Cross-linked Polyethylenimine as Potential DNA Vector for Gene Delivery with High Efficiency and Low Cytotoxicity.* Acta Biochim Biophys Sin (Shanghai), 2006. **38**(11): p. 780-7.
212. Bremner, K.H., et al., *Factors influencing the ability of nuclear localization sequence peptides to enhance nonviral gene delivery.* Bioconjug Chem, 2004. **15**(1): p. 152-61.

Appendices: Protocols and Detailed Experimental Methods

Appendix 1 – Isolation and Viability Assessment of Primary Rat Hepatocytes

I Preparation

(Prepare these items at LEAST a day in advance of the perfusion)

Perfusion Kit

Materials

- Tray and Cover
- Scalpel Holder
- 1 pair of Tissue Forceps
- 2 pairs of Small Tooth Curved Forceps (VWR 25601-010)
- Hemostat (Henry Schein 100-2376)
- Small Scissors
- Q-Tips (Puritan)
- Nu Gauze 2x2in, 4 ply (Johnson&Johnson via VWR #7632)
- Ethicon™ Silk – 4 Strands of 4-0 Silk (VWR 25942-249)
- Blue Paper
- 100μm Nytex Filter
- Funnel

Method:

1. Place 100μm Filter on Funnel, tape edges of filter to funnel with autoclave tape, and Wrap in Blue Paper. Seal with autoclave tape.
2. Assemble and Wrap Kit in Blue Paper.
3. AUTOCLAVE DRY Cycle 45 : 15

Ca^{2+} Free Buffer (1L)

Materials	Qty	Notes
Milli-Q Water	1L	
NaCl	8.3g	Sterile Perfusion Stock
KCl	0.5g	Sterile Perfusion Stock
Hepes	2.383g	Sterile Perfusion Stock
NaOH	2 Tabs	

Method:

1. Mix together in a Sterile, Autoclaved Bottle. Use a stir bar.
2. Ensure that the NaOH Tabs have fully dissolved
3. Adjust pH to 7.45 – 7.5 with 1N NaOH or HCl

Notes:

1. Use chemicals on Perfusion Bench
2. Keep these chemicals Sterile! Do not put excess chemicals back into the original container, use a new scooper for each chemical

10X $CaCl_2$ $(H_2O)_2$ Solution

Materials	Qty	Notes
Milli-Q Water		
$CaCl_2$ $(H_2O)_2$	6.36g/L	

DAG

Materials	Qty	Notes
DMEM	500mL (one bottle)	
BSA	1g	
Gentamicin	500uL (one aliquot)	
500mL Sterile filter unit		0.2um pore size, Nalgene

Method:

1. Measure 1g BSA
2. Pour BSA into DMEM bottle and gently swirl until suspended – wait until BSA is completely dissolved
3. Put DMEM + BSA, filter unit, and gentamycin into TC room hood.
4. Vacuum filter
5. Add gentamicin and swirl solution.
6. Aliquot into 50mL centrifuge tubes (one 30mL aliquot for every four 40mL aliquots)

II Perfusion Apparatus Setup

Peristaltic Pump

Materials

- Pump
- Masterflex™ Tubing
  - Small (96410-14)
  - Slightly Larger (96410-16)
- 2 - 500mL Orange Cap Bottles filled with ~350mL 70% Ethanol
- 2 - 500mL Orange Cap Bottles
- Milli-Q Water

Method:

1. Prime the Pump by recirculating the attached 70% Ethanol for ~5min in each bottle at the highest flow rate (86mL/min). Ensure that the bubble trap fills and empties.
2. Remove lines from Ethanol and allow each line to air dry for ~5min or longer. Save and Recap the Ethanol bottles.
3. Run 200-400mL of Milli-Q water through each line using a clean 500mL "Rinse" Bottle and a 500mL "Waste" Bottle. Ensure that the bubble trap fills.
4. Remove lines and allow the lines to air dry until the perfusion time (86mL/min).

Notes:

- The 70% Ethanol should be changed once every 3 weeks. Make a note of when it is changed on the Rat Logbook Sheet.
- You can reuse the "Rinse" and "Waste" bottles. Just rinse and shake them with ~100mL Milli-Q water a few times, and recap them for next time.

Rat and Animal House

Notes:

- Call the DCM office (x3-3050) and request 1-2mL of Pentobarbitol, or leave a message.
- Bring Key Card and the rat room key.
- Update and Initial the Green Rat Inventory Sheet outside the Rat Room
- Note Rat Weight (160-230 g)
- Get Pentobarbitol

Water Bath

Materials

- Milli-Q Water (ddH_2O)
- Celsius Thermometer
- 1 Sterile 500mL Orange Cap Bottle
- 250mL Graduated Cylinder
- 50mL Graduated Cylinder
- 375mL Ca^{2+} Free Solution
- 2 Red Water Bath Weights
- Filter Flask, 0.2μm Nalgene

Methods

1. Set bath Temperature to 43^0 C
2. Sterile Filter 250mL of Ca^{2+}-Free Buffer through a 0.2μM filter and place in bath. Connect the filter solution to the pump and fill up the bubble trap.
3. Prepare Blendzyme 3 Solution. The aliquot of Blendzyme 3 should thaw and be kept on ice until it's ready to be added to its solution.

Notes:

- The 43^O C provides for a 37^OC liquid temperature through the catheter.

Liberase Blendzyme 3 Preparation

Reconstitution:

70mg bottle

1. Add 10mL HPLC quality H_2O
2. On ice, let powder rehydrate for 30min. Mix occasionally by swirling.
3. Aliquot into 1mL centrifuge tubes [715uL each = 5mg]
4. Makes approximately 13-14 aliquots
5. Save extra little bit in a separate tube
6. Label with info: Name, 5mg, date of aliquot, lot#, volume

Materials:

- 28mL 10X $CaCl_2$ $(H_20)_2$ Solution
- 222mL Ca^{2+} Free Buffer
- Filter Flask, 0.2μm (Nalgene)

Materials	Qty	Notes
Ca^{2+} Free Buffer	222mL	
10X $CaCl_2$ $(H_20)_2$	28mL	
Roche Liberase Blendzyme 3	5mg	Cat# 1814184

Method:

1. Combine Ca^{2+} Free Buffer and 10X $CaCl_2$ Solution in a sterile 500mL Orange top bottle.
2. Place in water bath until needed
3. AT THE APPROPRIATE TIME (mentioned later)
   Add Blendzyme 3 to the 250mL of solution
4. Sterile Filter (0.2μm) and place in bath. Attach to the pump.

III Perfusion

Animal Preparation

Materials

- Male Fisher Rat (160-230g)
- 1.25" 20 Gauge Polyethylene Catheter-JELCO, Johnson and Johnson
- 2 1mL Syringes (Becton Dickinson-VWR #309602)
- 1 "Blue" 25G Needle (Becton Dickinson-VWR #305122)
- Sodium Pentobarbitol
- Phosphate Buffered Saline (PBS)
- DecapiCone™
- Procedure Board, Covered with Blue Paper
- Autoclave Tape
- Hair Clippers
- Dust Buster™
- Gauze
- 70% Ethanol
- Betadine

Method:

1. Using a "Blue" 25G Needle anaesthetize rat with Na-Pentobarbitol according to animal weight, diluted with an equal volume of 1x PBS. Inject into the intraperitoneal (IP), just to the left of the midline. Pull back on the plunger and make sure there is a visible bubble to ensure that you are in the body cavity and not in the bladder, intestine, etc.
2. *As soon as the rat shows no reflexes to quick blows of air*, check the drug effect through tail pinches. Do not continue until the rat does not respond to the pinches. Pinching in between the toes is also a good indicator.
3. *Working Quickly*, shave the rat over the entire incision area.
4. Apply Betadine using gauze (Optional).
5. Secure the animal to the procedure board with autoclave tape.
   Fully extend the lower legs and tape them down
   Raise the upper legs and *gently* tape each arm separately.
8. Open the lid of the Surgical Kit *without* touching the inside of the kit or lid.
9. Carefully open the Catheter and 1mL Syringes onto the Surgical Kit without touching the instruments.

Notes:

- Refer back to the Rat Perfusion Logbook to check how much Pentobarbitol to inject given the weight of the rat.
- The most prominent Tail Pinch response is flexing of the abdominal muscles just above the lower legs. It's almost like a shiver.

The Perfusion

Materials:

- Surgical Gloves (Allegiance #2D7254)
- Sterile Gauze (Johnson&Johnson Nu-Gauze™)
  Silk (Ethicon)
  Q-Tips (Puritan)
- 2 Forceps (VWR)
- Tissue Forceps (Henry Schein)
- Scissors (Henry Schein)
- Additional Materials listed above

Method:

1. *From this point move as quickly as possible to maintain adequate blood pressure and to minimize the effects of other unforeseen events.*

2. Don surgical gloves. Keep these sterile to avoid contamination. Only touch the instruments within the Kit and the rat body. Do not touch anything else.

3. Make an "I" incision on the ventral side using the Tissue Forceps and Scissors. The incision should run from the lower abdominal area around the bladder to the Zyphoid process and Rib area. Avoid nicking the liver. As you cut towards the ribs, you may have to gently massage liver through the skin to loosen it from the skin.

4. Gently displace the guts to the right with a fresh Q-Tip, exposing the Inferior Vena Cava (IVC) and Portal Vein (PV).

5. Using fresh, dry Q-Tips further expose the IVC inferior to the liver from the bladder region up to the liver. To do this, apply pressure to the connective tissue in opposite directions until the IVC is completely visible. Be sure not to hinder blood flow while you clear away the excess tissue.

6. Using the forceps, make openings in the connective tissue to the left and right of the IVC just above the branch to the kidney.

7. Pull a silk suture through the opening and tie a loose ligature around the IVC. To do this: grasp the right end of the silk with the left forceps and wrap it twice around the tip of the right forceps. Keeping hold of the right end, grasp the left end of the silk with the right forceps and pull it through the loops.

8. Insert Catheter into the IVC 0.5-1cm away from loose ligature. Remove metal piece and maneuver the catheter past the knot. If there is no blood flowing freely from the catheter, you may have to gently palpate the chest area to draw the blood down, or use a syringe to gently pull blood to the end of the catheter. Tightly tie off the loose ligature around the catheter.

9. Begin perfusing with Ca^{2+} Free Buffer at 25mL/min (15 mL/min to retrieve a greater fraction of NPCs). Immediately cut the Portal Vein (PV) to allow for drainage and prevent over-inflation of the liver. Cut the IVC below the Catheter.

10. Puncture the diaphragm to expose the IVC superior to the liver and tie a ligature around it using the same technique as before.

11. Check to make sure that fluid is freely flowing from the PV. If there is a clot, gently massage the PV until the flow resumes.

12. At this point prepare the Blendzyme 3 Solution. See **Blendzyme Preparation.**

13. Perfuse for 6 to 7 minutes. The liver should clear of blood. Gently roll the liver between two moist cotton swabs to help. The liver should be a light caramel color.

14. After the allotted time for the Calcium free buffer, switch over the Blendzyme solution and perfuse the entire 250mL volume. It should take about 10 minutes at 25mL/min.

15. Throughout the perfusion keep the liver moist by wetting a fresh Q-Tip with run-off buffer and gently dabbing the liver.

16. Remove the liver from the rat and place it in a 50mL Centrifuge Tube filled with 30mL DAG. Avoid cutting or poking other organs to prevent contamination.

V Hepatocyte Isolation

Materials:
- Ice Bucket
- DAG
- Pre-Autoclaved Funnel with 300μm mesh
- Trypan Blue
- Hemostat and tissue forceps

Methods:

1. Prepare an ice bucket with 4- 50mL centrifuge tubes filled with 40ml DAG.
2. Obtain the liver from the perfusionist. Also take with you a flat ice pack, an autoclaved funnel with 100-μm mesh, and a hemostat and tissue forceps with tips wrapped in sterile gauze.
3. In the hood, gently pour the liver with 30ml DAG into a 100mm petri dish. Use the hemostat and forceps to peel back the capsule on each lobe.
4. Use the hemostat to clamp down on the connective tissue of the liver, and gently agitate the liver by knocking the hinge part of the hemostat on the sidewall of the petri dish. Your other hand should hold the petri dish to prevent it from sliding off the ice pack which may become slippery due to condensation. Try to keep most of the liver submerged under liquid and pay attention not to squeeze the liver between the bottom of the dish and the tip of the hemostat. The tip of the hemostat should not touch the bottom of the dish.
5. Break more areas of the capsules if the liver is not breaking up well. Otherwise, when the solution looks like the color of caramel, the shaking should be enough.
6. Prepare a clean 50ml tube and place the funnel into it. Place the remains of the liver on the mesh with the hemostat. Use a pipette to transfer all liquid into the tube through the mesh.
7. Replace the liver in the Petri dish and wash again with 40mL DAG to isolate all the cells you can. Filter this as before into another 50mL tube.
8. Dispose of the mesh and the liver remains. Equilibrate the two tubes by pouring the liquid back and forth between the two tubes. Pour down the walls of the tube to minimize stress to cells.
9. Spin the two cone tubes of cell solution at 50g for 3 minutes at 4°C.
10. Remove supernatant (save it if NPC's are needed). Re-suspend the cell pellets with fresh DAG, 40mL per tube. Carefully pour each tube of DAG into the tubes with the cell pellet. Be careful not to let liquid directly land on top of the pellets. Tilt both tubes so that the liquid is flowing slowly on the tube wall. After both 40ml tubes of DAG are transferred, cap the tube with cells and start re-suspending cells by rocking both tubes gently. Do this until the pellet is completely in suspension.
11. Spin again at 50g for 3 minutes at 4°C.
12. During this spin, prepare the Trypan blue: 700uL DAG, 200ul Trypan blue. Or, if using Vi-Cell Coulter Counter make a 1:10 dilution of the cells suspension by pipetting 900uL of DAG, and 100uL of the final cell solution.
13. Remove supernatant (save it if NPC's are needed). Re-suspend each cell pellet with 20mL of fresh DAG. Make sure that when pipetting in the liquid, the liquid flows

slowly on the wall instead of hitting the pellets directly. Pour one tube of solution into the other to consolidate down to one tube (about 45mL total).

14. Take 100µm from the tube and place it into the Trypan blue tube. Use the hemacytometer to count the cell viability and cell concentration as the first final count. Count all 8 squares.
15. Record on the Hepatocyte count document and save under the date.

VI Troubleshooting

Working Quickly

- Working quickly during the preparation of the rat, and the surgery up to the time of perfusion will help minimize the effects of, for example, the rat dying. It will also help with issues related to blood pressure, and the length of time the liver is exposed to air.
- After the Perfusion has started, quickly cut the Portal Vein to prevent over-inflation of the liver, which can cause cell damage.

Rat Dies

1. Working quickly should minimize the effects of premature rat death. Try to perfuse as soon as possible.
2. Gently palpate the upper abdominal region, near the ribs, to help resuscitate the rat.
3. Be aware that the perfusion with Ca^{2+} Free Buffer may take longer to fully clear out the Red Blood Cells and to become a caramel color.
4. Try to keep the liver moist on the outside by wetting Q-Tips with run-off buffer and gently dabbing the liver.

IVC Catheter Insertion and Placement

- **Insertion**: Keep the catheter parallel to the IVC. Keep the bevel up, and the catheter as horizontal as possible, as to not poke all the way through the vein. Once inserted, **gently** push the catheter further into the vein until the plastic portion of the catheter is just in the vein. Avoid twisting the catheter because you may accidentally create new hole in the IVC. Try to create opposing tension by pulling the IVC downward with a Q-tip. Position the Q-tip on the muscle to the left or right of the IVC and apply gently pressure. This will anchor the IVC a little and make it less apt to stretch as you try to cannulate. Once you remove the metal part, you should feel no resistance at all, and the catheter should readily slip into the vein when you apply even the slightest pressure. Do not push the metal needle of the catheter into the vein more than you need to; once the white plastic is visible inside the vein, remove the needle while inserting the catheter farther up the IVC. Follow the IVC past the loose ligature. Remember this is easier to do if you flex the catheter so you can see the tip through the top of the vein. The vein changes direction as it meet the liver, navigate the catheter accordingly. Note that the degree to which the IVC direction varies from rat to rat.

Portal Vein (PV) Perfusion

1. Expose the Portal Vein.

2. Tie a loose ligature around the Portal Vein, making sure it is located above any branches.

3. Make a small cut approximately 1/2 way through the portal vein. Be careful not to cut through the entire vein.

4. Insert Catheter into portal vein, while using gauze to control blood loss.

5. Remove Metal Portion of catheter and then slide catheter past ligature and tie it off. Connect the pump and start flow of **Ca^{2+} Free Solution** at **8mL/min.**

6. Immediately cut the IVC inferior to the liver to prevent over inflation.

7. Puncture the diaphragm to expose the IVC superior to the liver, then tie a ligature around it.

8. Inflate the liver occasionally by placing a Q-tip on the IVC. Do not over inflate.

9. Perfuse until the liver is cleared of blood.

10. Throughout the perfusion keep the liver moist by wetting a fresh Q-Tip with run-off buffer and gently dabbing he liver. Otherwise, there should be no need to touch the liver.

11. Perfusion with Blendzyme 3 Solution.

Isolation Information

- **Qualitative, Cell Count, and Viability information can be used in conjunction with one another to assess the effectiveness of the perfusion with Blendzyme 3.**
- **Qualitative information about how the liver "breaks up" during the isolation** can clue you into how effective the digestion with Blendzyme 3 was. It is generally good when the liver completely disintegrates, and there is little intact liver. If the liver does not readily disintegrate, the collagenase may not have run long enough to allow for proper separation of the cells.
- **Cell Counts:** High cell counts indicate good separation of the cells. This is usually accompanied by nearly complete disintegration of the liver during isolation. Low cell counts indicate that the perfusion may not have run long enough.
- **Viability:** Low viability may indicate that the cells were exposed to Pentobarbital for too long, the surgery took too long, that the Blendzyme was at a too high/low concentration, etc....

Appendix 2 – Culture Media Formulations for Primary Hepatocyte Culture

HGM (Hepatocyte Growth Medium) Preparation 11/05

Block et al., J. Cell Biol. (1996), 132(6): 1133-1149 (with corrections of typos in paper)

Base Medium:

DMEM, low glucose, pyridoxine HCl, sodium pyruvate, no glutamine, no phenol red; (500ml) — GIBCO 11054-020

Add to Base Medium:

1. **0.015g L-Proline**; 0.03g/l in medium; SIGMA P-4655
2. **0.050g L-Ornithine**; 0.10g/l in medium; SIGMA O-6503
3. **0.1525g Niacinamide**; 0.305g/l in medium; SIGMA N-0636
4. **0.500g D-(+)-Glucose**; 2.25g/l in medium (already has 1g/l); SIGMA G-7021
5. **1.000g D-(+)-Galactose**; 2g/l in medium; SIGMA G-5388
6. **1.000g Bovine Serum Albumin**, Fraction V; 2g/l in medium; SIGMA A-9647
7. **Trace Metals** : Add 5µl from stock solutions:
   Stock concentrations:
   5.44 mg/ml $ZnCl_2$
   7.50mg/ml $ZnSO_47H_2O$
   2.0mg/ml $CuSO_45H_2O$
   2.5mg/ml $MnSO_4$
   (Use 1 Liter of MilliQ water to prepare each stock solution)

Filter the above solution with Nalgene PES .2 um Filter Unit, and then add the frozen aliquots.

Add to Sterile Filtered Medium:

8. **500ul Gentamycin** (sterile)**; SIGMA G-1397
   dispense stock (50mg/mL) into 520ul aliquots, store at –20°C.
9. **2.5 ml L-Glutamine** (sterile); 1mM in medium; GIBCO, 25030-081
   Dispense 200mM stock into 13.0 ml aliquots, store at –20°C.
10. **500µl Insulin-Transferrin-Sodium Selenite** (sterile); ROCHE 1074 547
    5mg/l-5mg/l-5µg/l in medium; ROCHE 1074 547 (50mg); 1213 849 (250mg); dissolve 50mg or 250mg powder in 5ml or 25ml sterile milliQ water, dispense into 520µl aliquots, store at –20°C.
11. **400µl Dexamethasone** (sterile); 0.1µM in medium; SIGMA D-8893
    dissolve 1mg in 1ml EtOH using sterile syringe and needle, after powder is dissolved add 19ml PBS, mix thoroughly, dispense into 420µl aliquots, store at –20°C, expires 3 months from date of reconstitution.

Add to Medium Immediately Prior to First Use:

12. **200µl Epidermal Growth Factor (EGF)** (sterile); BD Biosciences 354001
    20ng/ml in medium; dissolve 100ug powder in 2 ml sterile milliQ water, dispense into 220µl aliquots, store at –20°C, expires 3 months from date of reconstitution.

**Note: In early experiments, Penn-Strep was used as an antibiotic instead of gentamycin. In some cases during giant reactor characterization, this recipe was used without bovine serum albumin for comparison to previous experimental results in the lab.

Appendix 3 – 2-D Adsorbed Collagen and Collagen Gel Sandwich Protocols

2-D Adsorbed Collagen Protocol

As was described in Chapter 2, optimal DGE separation were obtained when primary hepatocytes were cultured on dried adsorbed collagen monolayers that are prepared as follows:

1. Prepare a 30 ug/mL solution of Collagen Type 1 from Rat Tail (BD Biosciences #356236) with sterile 1x PBS and keep on ice. Immediately return the collagen stock to the fridge.
2. Add 3 mL of the solution to each 60 mm treated tissue culture dish.
3. Gently swirl each plate to evenly coat the bottom.
4. Place plates in the incubator at 37°C for 2 hours.
5. After two hours, put plates back in the hood and aspirate the collagen solution. Make sure there is no excess solution on the walls or stuck on the plate top and completely remove all solution from the bottom. Tilt the plate for an additional 3 seconds after the brunt of the solution has been aspirated and run the tip along the circumference of the bottom edge to make sure the plate can completely dry.
6. Let the plates stand in the hood for 2 hours. Place them next to the airflow ducts near the back of the hood. Make sure the UV light doesn't get turned on during this time.
7. Seed 3 mLs of cell suspension to each plate at 800,000 cells per mL, making for a total of 2.4 million cells/plate. Swirl plates and move back and forth to evenly seed.
8. Culture at 37°C and 8.5% CO_2.
9. At 4 hours post seeding, gently aspirate plates and add 3 mLs of fresh HGM. This ensures ~90-95% confluency while removing debris and unattached cells to prevent overcrowding.
10. To ensure maintenance of hepatic phenotype and consistency of data, perform DGE assays within 24 hours of the medium change.

Collagen Gel Sandwich Protocol

Surfaces – Treated plates tend to keep a more uniform gel during culture.

35mm dish or 6-well plate	9.61 cm^2 surface area per well Bottom layer: 600uL collagen gel solution Top layer: 300uL collagen gel solution
12-well plate	3.8 cm^2 surface area per well Bottom layer: 240 uL collagen gel solution Top layer: 120 uL collagen gel solution
24-well plate	2.0 cm^2 surface area per well Bottom layer: 125 uL collagen gel solution Top layer: 62 uL collagen gel solution

Reagents

Collagen Type I, from Rat Tail, Solution
BD Biosciences #356236 More consistent than Vitrogen

10x PBS mix
10x PBS (w/o Ca++ or Mg++)
20 g/L glucose
37 g/L sodium bicarbonate
Sterile filter solution and equilibrate in hood for 30 min
pH to 7.4 using sodium bicarbonate or HCl

Collagen gel solution preparation (%'s are by volume)

80% Collagen solution (3 mg/ml)
10% Sterile diH_2O (autoclaved, sterile-filtered)
10% 10x PBS mix

Store at reagents at 4°C. Prepare on ice to prevent gel formation. Shake 10x PBS mix solution well. Heat in water bath if necessary to fully dissolve. If collagen solution comes at a concentration >3 mg/ml, each time prepare collagen gel solution by using extra sterile diH_2O. For example, if collagen solution comes as 4.8 mg/ml, use 50% collagen solution and 40% sterile diH_2O (and 10% 10x PBS mix). Collagen gel solution can be stored for 4-6 hrs at 4°C.

Add the necessary amount of collagen gel solution to each well. Pipette evenly around the well and move the plate back and forth on the sterile hood floor to evenly distribute. Incubate at 37°C for at least 2 hrs for the bottom layer (until gel solidifies). Before seeding, rinse gel once with PBS. Seed hepatocytes in HGM and incubate at 37°C for 4-6 hours. Using a pipette, carefully aspirate media (and non-attached cells) and add second layer. Incubate without medium for 1-2 hrs (until second layer has solidified) then add media for the duration of the culture. Medium is usually changed daily, and for a 6-well plate, at 1 mL/well. Scale accordingly for the other plate sizes.

Appendix 4 – Detailed Density Gradient Electrophoresis Protocol

Preparation of Cell Samples for DGE

Date: _____	# Petri dishes: _____	Gene Delivery: ☐yes ☐no
Performed by: _____	# cells/dish: _____	Polymer: _____
Perfusion Viability: _____	% confluence: _____	Time Pt: _____
Perfusion Density: _____	DGE Buffer: _____	DNA/plate: _____
Media: _____	Pulse-Chase: ☐yes ☐no	N/P ratio: _____

CHECKLIST

1. **If doing pulse chase,** make **1.5 ml** (per 60 mm dish) of **2 mg/ml** HRP in HGM in a centrifuge tube. Warm in **37°C** water bath along with a centrifuge tube of **5 ml** of HGM in.
2. **If doing a transfection,** make **2 ml** (per 60 mm dish) of **5 ug/ml** total DNA in HGM in a centrifuge tube. Pre-warm 2 mL of media in **37°C** water bath before making the NV complexes.
3. Put rotor in cold room.
4. Turn on ultracentrifuge (upstairs 6th floor Essigmann Lab). Set to 2 C and turn on vacuum, make sure door is closed.
5. Turn on centrifuge in BPEC and set on fast cool (for PNS spin).
6. Check the cells under the microscope at 10x for debris and confluence.
   Comments: _____
7. Gather above materials and the following:
   - ☐ PBS++ and DGE buffer (keep on ice)
   - ☐ Cell scraper
   - ☐ Ice bucket with ice
   - ☐ Syringe and needle
   - ☐ Ice tray for washes and media changes

PULSE-CHASE-PULSE LABELING (OPTIONAL)

* Keep dishes on ice at all times when performing washes and media changes (ice block or wetted ice).

1. Wash the dishes 1x with **3 ml** cold PBS++.
2. Label cells for **4 min** with **1.5 ml** of warm HRP labeled HGM.
3. Recollect HRP medium into centrifuge tube and return to water bath.
4. Wash the dishes on ice 1x with **3 ml** cold PBS++.
5. Chase for **15 min** with **3 ml** of warm unlabeled HGM.
6. Start setting up DGE Device in cold room during your free time.
7. Wash the dishes on ice 1x with **3 ml** cold PBS++.
8. Label cells for **3 min** with **1.5 ml** of warm HRP labeled HGM.
9. Recollect HRP medium into centrifuge tube and return to water bath.

CELL COLLECTION

1. Wash cells 2x with **3 ml** cold PBS++.
2. Wash cells 1x with **3 ml** cold DGE.
3. Scrape cells with rubber policeman in **2 ml** cold DGE buffer. Use a large hard plastic scraper.
4. Collect in pre-chilled centrifuge tube.

5. Re-scrape uncollected cells in **1 ml** cold DGE buffer and collect in same centrifuge tube.
6. Check plate for cells and nuclei. Comments: _____

Lysis

1. Resuspend cells by gently tapping the tube against a hard surface.
2. Incubate on ice for **20 min**, gently re-suspend pellet every **5 min**.
3. Prepare pre-chilled Eppendorf tubes if gene delivery was performed to collect cell fraction aliquots.
4. Lyse with **21G x 2** inch needle with **12 pumps** (8 counts up, 8 counts down) with needle tip at wall.
5. Inspect **10 ul** in microscope on hemacytometer. # Nuclei: _____ # Whole Cell: _____ Comments: _____
6. Save **400 µl** of lysate as "whole cell sample" for PCR.
7. Centrifuge **15 min** at **2500 rpm** to collect nuclei (In the meantime, prepare BSA assay).
8. Remove the supernatant (PNS) with a pipette. PNS volume = _____ ul
9. Save **250 µl** of PNS for PCR.
10. Freeze nuclear pellet for PCR.

Protein Assay

1. Prepare 1.5 ml protein assay reagent (50% A, 48% B, 2% C → 750 µl A, 720 µl B, 30 µl C).
2. Make BSA standards (0, 2, 4, 6, 8, and 10 ug) by using 0-5 ul of 2 mg/ml BSA, prepare in duplicate.
3. Use __ ul of PNS (usually 10 ul).
4. Add filtered water for final volume of 100 µl in each well.
5. Add 100 ul reagent to each well and incubate for 10 min for at least 10 min at 37°C.
6. Once most diluted sample is purplish, read the plate at 562 nm in the plate reader. Make sure the well with 0 µl of BSA is called blank. The PNS protein concentration: ____ ug for __ µl

Trypsin and Protease Inhibitor Treatment

1. Defrost trypsin and protease inhibitors on ice.
2. Warm trypsin in 37°C water bath for 1 min. Warm PNS for 1 minute.
3. Calculate the total protein in PNS. Total protein in PNS = _____ mg.
4. Add ____ ul of 1 ug/ul trypsin and incubate in water bath for ___ minutes (typically 6 min). Use 25 ug per mg of total protein. Trypsin Type: Type 12 A Bovine Pancreas in DGE buffer.
5. Return sample to ice, and add ___ ul of 4 ug/ul trypsin inhibitor (in -80C freezer, keep on ice!).
   Use 4 ug of trypsin inhibitor per for every 1 ug of trypsin (so use same volume).
6. **Final volume** = PNS + trypsin + trypsin inhibitor + PBS buffer = _____ (typically 8100 µl)
7. Add roughly 7 mL of cold PBS to the PNS before adding protease inhibitors.
8. Add protease inhibitors at the following final concentrations
   1 mM PMSF (stock=0.2 M) → **0.005 * final PNS volume =** _____(typically 40.5 µl
   2.5 ug/ml Aprotinin (stock=2.5 mg/ml) → **0.001 * final PNS volume =** _____(typically 8.1 µl
   10 ug/ml Leupeptin (stock=5 mg/ml) → **0.002 * final PNS volume =** _____(typically 16.2 µ

ULTRACENTRIFUGATION

1. Transfer sample to plastic Beckman centrifuge tube (pre-chilled on ice). Top off with PBS at or past fill line.
2. Put stopper and cap on and weigh.
3. Make a balance tube with water within 0.001 g of the sample tube.
4. Place tubes in the Beckman Ti 70.1 rotor and screw on the top firmly.
5. Centrifuge for 1 hour at 100,000 g at 4° = 40,000 rpm.
6. Set up the DGE device in the cold room during the spin time.

NOTES

1. Total protein above 1 mg prevents adequate separation of organelle peaks. Aim to load an endosomal pellet that has around 800 ug of total protein.
2. For best cell collection: press hard on the cell scraper while turning the Petri dish over 720 degrees in a continuous motion so that you accumulate a band of cells on the scraper. Then move the scraper to the center to scrape the cells in the middle in one continuous motion. Then "vibrate"/move quickly from side to side in the DGE buffer to coax the bands of cells off the scraper.

CHECKLIST FOR ALIQUOTS

- ☐ 400 µl Whole Cell
- ☐ 250 µl PNS
- ☐ Nuclear pellet
- ☐ 150 µl endosomal pellet
- ☐ PES
- ☐ Plate of DGE fractions

DENSITY GRADIENT ELECTROPHORESIS DEVICE SETUP

ASSEMBLING THE COLUMN

1. Clear, clean and level the table using the bike pump and level (from the toolbox).
2. Take the DGE column and DGE base out of the soap (no chlorine groups!) solution. Rinse well with de-ionized water and gently dry with KimWipes and compressed air.
3. Cut a square piece of cellophane (7 cm) and soak in de-ionized water along with the O ring.
4. After the membrane is soft, fold it into fourths, and cut into a circle.
5. Place the membrane over the opening of the inner column, wetting the column edge with finger.
6. Using two fingers from each hand spread the O ring over the inner chamber until it fits into the groove. Make sure that excess membrane is evenly sticking out along the membrane.
7. Check for leaks with a little bit of water (dry with a KimWipe so it's easier to see if it's leaking).
8. Grease bottom of the outer column with Vaseline and screw on bottom lid, then place on the stand in the cold room. (***all the rest of the steps are done in the cold room)***
9. Connect wire to the palladium cathode (bottom electrode).
10. Connect the syringe to the T shaped tubing.
11. Clamp the short tube and fill syringe with 10% Ficoll through the medium length tube of the T shaped tubing. Push out the bubbles from the syringe and tubing.
12. Tighten the C-clamp about halfway up the longer outlet tube.
13. Then unplug the short tube and push 10% Ficoll to fill the short tube.
14. Flick the T connector while holding the short tube end to get all of the air from the connector to the top of the short tube.
15. Push the Ficoll to the end of the short tube and connect it to the DGE device's lower chamber at the bottom inlet (don't put the short tube completely onto the entire length of the inlet stem-just enough to be secure).
16. Fill lower reservoir with DGE buffer with the three 50 ml empty syringes on the upper rack.
17. Insert long tubing ends from the pumps into the channels.
18. Slowly fill the inner chamber with about **2-3 ml** of 10% Ficoll using the syringe pump. Adjust the tubing from the syringe pump to make sure there are no bubbles.
19. Then fill separation column with 10% Ficoll to the top using a pipettor.

LAYING THE LOWER GRADIENT (DO JUST BEFORE LOADING THE SAMPLE, WILL TAKE 5-10 MIN)

1. Wipe a little bit of Vaseline around the lip of the top cone and screw on the top cone.
2. Slowly maneuver the gradient mixer so that its tubing connects to the top cone and there are no kinks in the connecting tubing.
3. Secure in place using the Perspex holder and the screw.
4. Slowly infuse 10% Ficoll into the top cone at 3 mL/min and into the tubing of the gradient mixer until it is flush with the floor of the mixing chamber.
5. Fill right leg with **3.5 ml** of **7%** Ficoll and clamp the tube between the legs using the blue clamp when the fluid rushes into the tube (making sure there are no air bubbles). Put any 7% that rushed into the left leg back into the right leg.

6. Slowly fill the left leg with **3 ml** of **10 %** Ficoll. (left leg is one connected to the DGE device)
7. Slowly insert stirrer and plug in, let the solution start stirring, with the power source at **6 V** and then unclamp the blue clamp.
8. Slowly loosen the metal clamp until the solution is dripping into the 10% Ficoll container at an approximate rate of **1 drop per second**. Adjust the clamp at times to maintain a steady flow rate
9. Run the gradient mixer until the entire gradient enters the column and the level of the solution inside the column is about one third of the way down the cone (to leave enough room for sample loading). Then tighten the metal clamp on the outlet tube.
10. Disconnect the stirrer and slowly loosen the Perspex holder to carefully free the gradient mixer. Balance on two of the three legs of the gradient mixer and slowly lift at an angle.
11. Put up warning sign on the door of the cold room – asking people to open/close carefully and to mind the vibration sensitive experiment.
12. Wash the gradient mixer and stirrer with de-ionized water. Dry with KimWipes & compressed air.

APPLYING THE SAMPLE

1. Collect the Post Endosomal Supernatant (PES) in an Eppendorf tube and keep for PCR. Resuspend the pellet **in 650 µl** of cold **6%** Ficoll-70 in DGE Buffer with a **21G x 2** syringe. Break up the pellet a bit more gently than the during the lysis step.
2. Transfer to an Eppendorf tube and spin at full speed in the small table top centrifuge for **15-20 seconds** to determine success of the resuspension. Give a few extra pumps through the syringe if a pellet forms and respin to check again.
3. Take up **500 µl** for DGE run.
4. Using your left hand, slowly squeeze the T tubing between the T and the column so that the level inside the inner column rises to the top of the cone.
5. Using your right hand, slowly pipette **500 µl** of sample using a P1000 onto the top of the cone, while letting go of the tubing slowly. Try to match the rate of addition and downward flow from the release.

LAYING THE UPPER GRADIENT

1. Slowly maneuver the gradient mixer so that its tubing connects to the top cone. Secure in place using the piece of Perspex and the screw.
2. Slowly infuse the sample into the inner column of the gradient mixer using the syringe pump (max speed 2 ml/min) so that the solution inside the top cone enters the tubing of the gradient mixer and ends just below mixing chamber. Leave the sample roughly 3-4 mm below the bottom of the left leg floor or you will get a mushroom in the sample band.
3. Carefully fill right leg with **13 ml** of DGE buffer (0% Ficoll solution) and clamp the tube between the legs using the blue clamp, when the fluid rushes into the tube connecting the two legs.
4. Fill the left leg with **12.5 ml** of **5% Ficoll** --- Add very slowly so you don't disturb the sample band using the **2 ml** pipette to add at least the first **2.5 ml** (stick the pipette to the bottom of the gradient mixer column. Add the remaining 5% Ficoll with a 10 mL pipette release it very slowly right at the upper water level and against the wall.

5. Slowly insert stirrer and plug in, let the solution start stirring, with the power source at **6 V** and then unclamp the blue clamp.
6. Slowly loosen the metal clamp until the solution is dripping into the 10% Ficoll container at an approximate rate of **1 drop per second**.
7. Remember to adjust the clamp at times to maintain a steady flow rate until the entire gradient enters the column and level of the solution has dropped to the top of the inner column.
8. The sample should appear in one flat whitish disc. If you get a mushroom the run is ruined, so perform these steps very carefully.
9. Disconnect the stirrer and slowly loosen the Perspex holder to carefully free the gradient mixer.
10. Wash the gradient mixer and stirrer with de-ionized water. Dry with KimWipes & compressed air.

Filling the Top Chamber and Starting the Run

1. Carefully remove the top cone. Place metal sieve on top of the inner column
2. Turn on the syringe pump at 2 mL/min until the top gradient wets the sieve.
3. Using one or two syringes + tubes, carefully fill the upper chamber with DGE buffer until it reaches the bottom of the horizontal outlet. Squeeze the tubes slightly to slow down the filling rate when the water level approaches the sieve and covers it.
4. Slowly remove the metal sieve without disturbing the contents of the inner chamber
5. Slowly pivot the upper electrode (platinum anode) into the top chamber and secure in place with the Perspex holder.
6. Turn on the pumps to circulate the DGE buffer in the lower chamber. Put 400-500 ml fresh DGE buffer in the recycling beaker.
7. Turn on ammeter to read current. Turn on the power supply. Set to "constant current mode".
   Time= 80 min, **Voltage** = 300V, **Current** = 11mA, unless otherwise specified: _____
8. During the run, wipe top electrode with paper clip to get ride of bubbles **every 10 minutes.**
9. Check that the current is around 10.5-10.7 mA.

Ending the Run and Collecting the Samples

1. Turn off the pumps, power source, and amp-meter.
2. Slowly unscrew the upper electrode and remove from the top chamber. Slowly replace the metal sieve, entering the upper buffer chamber at an angle to prevent large disturbances.
3. Using a syringe and tubing, suck up DGE buffer and dispose in Erlenmeyer waste flask.
4. Loosen brown clamp and allow for about 20 drops to leave the column, so that the level of the solution inside the inner chamber comes below the metal sieve.
5. Remove the metal sieve, then screw on top cone again (with thin tubing already attached).
6. Screw in the long Perspex arm with the same screw as before and thread tubing through the hole on the long arm, adjust tubing height accordingly over the box and collection plate.
7. Infuse at rate of **2 ml/min to fill the cone and tubing, then the flow rate can be switched to 3 mL/min**. Collect **24** fractions from the end of the thin tube in the 96 deep well plate (average volume of fraction = **1.25 ml**).
8. Mix the 2 rows of samples at least 10 times with a multichannel pipette set to 200 uL. Next take 200 uL of the mixed samples out and add to a DNEasy collection plate for storage

before DNA purification. Freeze this plate along with the original deep well collection plate, which will provide material for b-Hex assays and backup samples.

9. Switch input at the power supply, take off top cone, fill upper chamber with buffer and put the short holder back on to secure the upper electrode.
10. Run for the same amount of time in reverse current mode in order to recharge the palladium electrode.
11. Current was reversed for _____ minutes.

96 Well Plate Assays for Fraction Identification

HRP Assay (test for Early and Late endosomes)

1. Transfer 100 ul of the sample.
2. Add 200 µl of the HRP reagent to each well using the multipipettor. Mix well, but NO BUBBLES. Make sure reagent hasn't turned orange and that it is freshly prepared or no more than 3-4 days old if stored in the fridge.
3. Incubate at room temperature until orange color appears (incubation time is approx 60 min).
4. If there are any air bubbles, pop with a syringe needle.
5. Read absorbance at 455 nm.

BCA Assay (test for Total protein)

1. Transfer 40 ul of the sample.
2. Add 60 µl of water
3. Make BCA reagent. Number of wells needed = ( )

   50% A = ( ) * 100 µl = _____
   48% B = ( ) * 96 µl = _____
   2% C = ( ) * 4 µl = _____
4. Add 200 µl of BCA reagent to each well, mix and incubate for 2 hour at 37°C.

If there are any air bubbles, pop with a syringe needle.

5. Read absorbance at 562 nm.

β-Hex Assay (test for Lysosomes)

1. Transfer 60 ul of the sample.
2. Make B-Hex start master mix. Number of wells needed = ( )

   Start = ( ) * 150 µl = _____
   Triton = ( ) * 3 µl = _____
3. Add 153 µl of master mix to each well, mix and incubate for 2 hour at 37°C.
4. Add 90 ul of stop reagent and wait a few minutes.
5. If there are any air bubbles, pop with a syringe needle.
6. Read absorbance at 405 nm.

Solutions for DGE Runs and Assays

A. DGE Buffer

The DGE Buffer is used in both sample preparation and the actual density gradient electrophoresis run itself. To make DGE buffer, combine the following ingredients.

			for 500 mL	for 1 liter	for 2 liters
250 mM	sucrose	(g)	42.78	85.56	171.12
10 mM	acetic acid	(ml)	0.286	0.572	1.144
10 mM	triethanolamine	(ml)	0.6665	1.333	2.666
1 mM	NaEDTA (Titriplex)	(g)	0.186	0.372	0.744

Then add milliQ water until within 5% of the desire final volume.
pH to 7.4 with NaOH and then fill with milliQ water to the final volume.

Typically, three to four 2-liter bottles of DGE buffer are made at a time (total of eight liters). A 2-liter bottle of DGE buffer can typically last for about six to eight DGE runs if you recycle the bottom chamber buffer.

B. 10% Ficoll-70

Typically, one or two liters of 10 % Ficoll-70 are made, using ten or twenty grams of Ficoll-70 dissolved in one or two liters of DGE buffer respectively. The Ficoll-70 powder is very light and floats easily so be careful when measuring and use a cap when putting the solution on the stirrer plate. The Ficoll-70 also takes a long time to dissolve – around one hour. Usually the 10% Ficoll-70 is made in a bottle with a screw cap so that it can be inverted and shaken to help the dissolving process. Once the Ficoll is dissolved, the entire solution should be clear. It may be a good idea to de-gas the solution if using immediately.

C. 5%, 6%, 7% Ficoll-70

The 5%, 6% and 7% Ficoll-70 are typically made by diluting the 10% Ficoll-70 to avoid the complications of dissolving the Ficoll-70 powder. Usually 100 to 200 ml of each concentration is made.

D. PBS ++

Important for cell collection step. Add 1 ml of $MgCl_2$ and 1 ml of $CaCl_2$ to 500 ml of Phosphate Solution Buffer (PBS). Keep refrigerated at 4°C

E. Beta-hexosaminidase Assay Start Reagent (200 ml, 0.2 M NaAC, 4mM PNP)

1. Dissolve 3.28 g NaAc (MW= 82.03g/mol) in 150 ml of MilliQ water.
2. pH 5.4 with HAc.
3. Warm until 50°C then dissolve 274.4 mg of PNP (MW=342.4 mg).
4. Fill up to 200 ml and store in Refrigerator (4°C).

F. Beta-hexosaminidase Assay Stop Reagent

Make 2M glycine, pH10 by:

1. Dissolve 75.07 g glycine (MW = 75.07) in 450 ml of MilliQ water.
2. Then pH to 10 with NaOH.
3. Fill up to 500 ml and store in Refrigerator (4°C).

G. Substrate for Horse Radish Peroxidase Assay

It is preferable to make the reagent a few hours to immediately prior to performing the assay as the reagent is degrades easily. To retard the degradation process, cover the test tube containing the HRP reagent in foil. When the reagent turns yellowish like a straw color, it is no longer suitable for use.

HRP Reagent	15 ml	25 ml	50 ml	Final Conc.	Storage
10 mg/ml o-dianisidine	150 µl	250 µl	500 µl	0.342 mM	in - 80
3% H_2O_2	1.5 µl	2.5 µl	5 µl	0.003% v/v	in fridge
0.5 M NaPi pH 5.0	1.5 ml	2.5 ml	5 ml	50 mM	in fridge
10% Triton	0.45 ml	0.75 ml	1.5 ml	0.3% v/v	on shelf
deionized water	13.05 ml	21.75 ml	43.5 ml	--	--

H. BCA Total Protein Assay Master Mix

The standard proportions for the BCA master mix components are used.

BCA Master Mix	for 1 ml	for 7.5 ml
50% Solution A (µl)	500	3750
48% Solution B (µl)	480	3600
2% Solution C (µl)	20	750

Additional Pointers and Figures for DGE Protocol Steps

1. Cell Scraping and Collection Technique

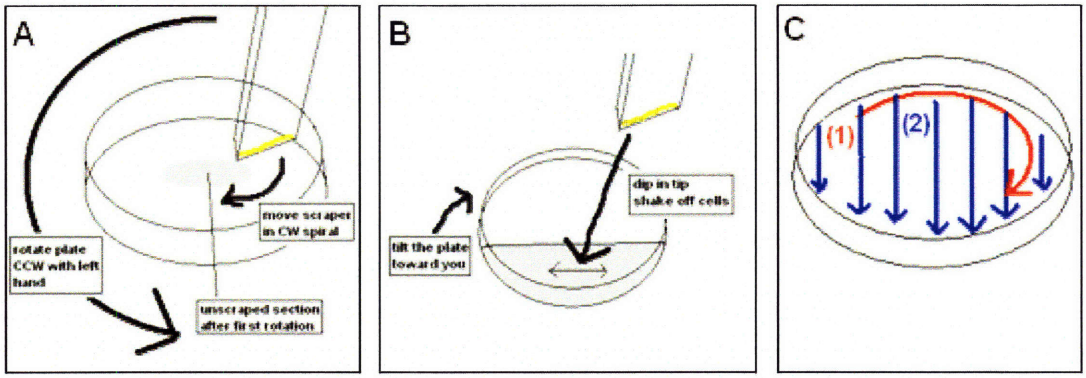

Use the hard plastic white scrapers in the lab. Add 2 mL of DGE buffer and scrape in a circular motion along the outer periphery of the plate by pressing the beveled edge of the scraper down firmly and rotating the plate two times fully with your other hand. Then, tilt the plate so that the DGE buffer pools in the bottom and scrape the small island of cell remaining in the middle down into the buffer. Shake the scraper to remove the large cells clump into the DGE buffer and immediately collect the cells in a prechilled tube on ice. Then add an additional mL of buffer and scrape the entire surface of the plate in a downward motion and collect the extra cells that are pushed into the pool of buffer.

2. Mechanical Lysis Tips

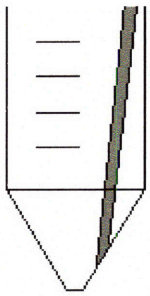

When expelling the cell suspension out of the syringe to lyse the cells, place the beveled edge of the needle flush with the angled wall at the bottom of the 15 mL centrifuge tube and press down fairly hard. Don't put the needle tip too close to the bottom though, the cell suspension will accelerate off the floor and out of the tube, and you can also puncture the tube fairly easily. Keep the syringe one ½ to 2/3 up the side of the angled wall. Remember that for different cell types, different swelling times in the hypotonic buffer and different needle gauges might be required.

Appendix 5 – SDS-Page and Western Blotting Protocols

1. Gel Rig Assembly & Sample Preparation
   a. Assemble gel rig with shorter plates facing inside as according to the Bio-Rad protocol. If running only one plate, be sure to use the buffer dam.
   b. Add running buffer (1X TGS) to inside compartment of the gel rig until the buffer overflows and outside compartment is filled to about one centimeter below the height of the longer plates. This way the temperature along the gels stay stabilized during the electrophoresis.
   c. Turn on the heat block (100C).
   d. Add equal volume of 2x sample buffer to samples and positive control if sample buffer not yet added. Each well can load 50 µl of sample.
   e. Boil samples on heat block for 3 min (Hint: Add plastic caps so tube tops don't pop off).
   f. Meanwhile, carefully remove the combs from the gels and using a plastic pipette, wash the wells with the running buffer.
2. Gel Loading and the Run
   a. Load 5ul of pre-stained Molecular Weight standard.
   b. Load up to 50 µl of each sample, including negative and positive controls.
   c. Run gel at 100V for approximately 1.5 hours @ room temperature until the dye front has reached the bottom of the gel.
3. Western Blotting
   a. Five to ten minutes prior to the SDS-PAGE run ends, make the transfer buffer and soak pre-cut transfer membrane in 100% methanol for a few minutes until the entire membrane is translucent. (Note: always handle membrane with gloves or forceps to prevent contamination).
   b. Then transfer the PVDF membrane into the transfer buffer 1.
   c. Add 2 pieces of thick Whatmans to the transfer buffer container 2.
   d. Place blotting apparatus in transfer buffer with the clear face down.
   e. Add a sponge to the clear face and massage out any air bubbles.
   f. Lay 1 thick pre-soaked Whatman on the blotting apparatus and then lay the PVDF membrane in the center on top of the Whatman, making sure that there are no bubbles between the two.
   g. Disassemble the gel by removing the smaller plastic plate (the gel should remain stuck to the larger plastic plate). Cut off top portion of the gel, where the well lanes and the stacking gel are.
   h. Carefully place the gel on top of the membrane. The lower the percentage of polyacrylamide in the gel, the easier the gel will break.
   i. Smooth out the bubbles carefully with your gloved finger or a flat headed instrument.
   j. Optional: Use a waterproof pen or pencil to mark the position of the standards on the membrane (they don't always transfer).
   k. Place the other thick Whatman on the blotting apparatus. Make sure it is flush with the other Whatman.
   l. Add the second sponge and close the sponge rack.
   m. Place the sponge rack in the transfer chamber (pre-filled with transfer buffer). (Note: The black side of the sponge rack faces the black electrode.

n. Place the transfer apparatus on top of a stir plate in the cold room.
o. Run the transfer 1 hour at 100V at 4°C (Note: 2h at 40V, or overnight at 20V at 4°C also works).

4. Blocking
   a. Cut off the corner of the membrane for orientation and keep the membrane protein side up throughout subsequent steps.
   b. Remove the membrane from the transfer apparatus and rinse in PBS. Note: The gel can be stained in Coomassie or the membrane can be stained with Ponceau S to ensure transfer has occurred.
   c. Place membrane in ~ 30 mL Blocking Solution 1 hour at room temperature on the rocker.
   d. Wash membrane three times in approximately 20 to 30 ml TBS-T 5 minutes each.
5. Optional: Coomassie Stain
   a. For the Coomassie stain (Coomassie dye dissolved in methanol, glacial acetic acid, & water) allow it to incubate for at least 1h-overnight (for low MW proteins).
   b. Destain the gel in the previously mentioned solution without the Coomassie dye. This leeches out the stain to clear the background and leave stained protein bands that can be visualized and photographed.
6. Primary Antibodies
   a. Place membrane heat-sealable bag.
   b. Add the 40 µl primary antibody to 10 ml TBS-T making a 1:250 dilution.
   c. Seal bag and nutate the membrane overnight at 4°C, then empty the contents into a small tray, slightly larger than the blot itself and designated for primary antibody incubation, and incubate for an additional 1 hour at room temperature on the rocker.
7. Secondary Antibodies
   a. Wash membrane three times in approximately 20 to 30 ml TBS-T 5 minutes each.
   b. Place membrane in a second plastic container, designated for secondary antibody incubation.
   c. Add the 12 µl HRP-conjugated secondary to 30 ml of the blocking solution (5% milk powder in TBS-T) making a 1:2500 dilution.
   d. Incubate at room temperature for 1 hour on the rocker.
8. Visualization
   a. Wash membrane three times in approximately 20 to 30 ml TBS-T 15 minutes each. This higher wash time is to compensate for the higher antibody concentrations.
   b. Mix equal volumes of visualizing reagents 1 and 2 together (1 to 5 ml each) in a 15 ml centrifuge tube.
   c. Pour into the container designated for the visualizing reagent and put the membrane face down onto the reagent. Incubate for at least one minute.
   d. Visualize on the Kodak Electronic Developer.

SDS-PAGE and Western Blotting Solutions

5 ml of 2X sample buffer (Store at -80 °C in 1 ml aliquots)

- 0.625 ml 1 M Tris, pH 6.8 (125 mM)
- 1 ml 20% SDS (4%, or 0.2 g)
- 1 ml glycerol (20%)
- 0.1 ml 1% bromphenol blue in 10% EtOH (0.02%)
- Optional: Add 200 mM DTT = 0.1542 g or 10% BME if needed for reducing conditions
- Fill to 5 ml with H_2O (~2.275 ml)

2 L of 1X TGS running buffer (Store at room temperature)

- 5.8 g Tris base (240 mM)
- 28.8 g glycine (1.9 M)
- 2 g SDS
- Volume to 2 L with MilliQ water (don't pH)

2 L of 2x Transfer Buffer without MeOH (Store at room temperature)

- 5.8 g Tris base (12 mM)
- 28.8 g glycine (100 mM)
- 2 ml 20% SDS
- Volume to 1.8 L with MilliQ water (don't pH)

1 L of 1x Transfer Buffer with MeOH (Make fresh, do not store**)**

- 450 ml of 2X Transfer Buffer
- 450 ml of MilliQ water
- 100 ml of MeOH

TBS-Tween (Stable for weeks at room temperature although Tween can oxidize)

- 40 ml 1 M Tris-HCl, pH 7.5 (20 mM)
- 54.8 ml 5 M NaCl (137 mM)
- Volume to 2 L with H_2O, then add:
- 2 ml Tween (0.1%, Fisher Scientific—for TBS just omit this)

Coomassie blue staining solution

- 0.1% w/v Coomassie blue R250
- 40% MeOH
- 10% HAc

Destaining solution

- 30% MeOH
- 10% HAc

Lysis Buffer (Use 100 µl per million cells)

- 1% 0.1M PMSF
- 10% protease inhibitor cocktail
- 89% HNN solution
    - 10 mM Hepes (pH 7.6 in distilled water)
    - 150 mM NaCl
    - 1% NP40

Blocking Solution (Make fresh for each run)

- 5 g Carnation Milk Powder
- 100 ml of TBS-T

Alternate Lysis Buffers:

General BPEC Lab Lysis Buffer and Method

1. To make lysis buffer, make 10mM Hepes pH 7.6 and 150mM NaCl in MilliQ water and autoclave before adding NP40 (1% final concentration).
2. Add the Sigma protease inhibitor cocktail at 1:10 (v/v) and PMSF (0.1M final concentration) just before use. The lysis buffer should be ice cold.
3. 100 µl of lysis buffer is added for every million cells. This would thus include 1 µl of PMSF, 10 µl of the Sigma protease inhibitor cocktail, and 89 µl of the Hepes, NaCl, and NP40 solution.
4. The whole cells and lysis buffer should be mixed with a standard pipette, vortexed, and incubated on ice for 10 minutes before spinning in a centrifuge at 4°C and 10000 rpm for 5 minutes.
5. Transfer the supernatant to a new Eppendorf tube. This whole cell lysate can be stored at -20°C for several months.

DAL Lab's Lysis Buffer Formulation		
Final Concentration.	**Ingredient**	**Amount to add for 10 ml**
Solutions stored at 4 °C		
--	ddH_2O	5.665 ml
50 mM	0.5 M β-glycerophosphate, pH 7.3	1 ml
10 mM	0.1 M NaPP	1 ml
30 mM	0.5 M NaF	0.600 ml
50 mM	1 M Tris, pH 7.5	0.500 ml
1%	20%: Triton X-100	0.500 ml
150 mM	5 M NaCl	0.300 ml

Appendix 6 – Detailed Giant Reactor Assembly, Seeding, Maintenance, and Cell Recovery Protocols

Giant Reactor Assembly Protocol

Materials List:

- 1 top window
- 1 middle body
- 1 bottom piece
- 6 small screws
- 6 large screws
- 2 injection port screws w/ O-rings
- 1 medium-sized silicone O-ring
- 1 large-sized silicone O-ring
- 4 screw end-barbed end connectors w/ silicone O-ring on screw end
- 2 oblong silicone gaskets w/ pin holes
- 2 polycarbonate scaffolds w/ pin holes
- 1 oblong 5 micron Millipore filter w/ pin holes
- 1 Metal retaining ring (oblong shape)
- 6 barbed end-barbed end connectors
- 6 female luer-barbed end connectors
- 2 female luer-sealed end connectors
- 4 male luer-barbed end connectors
- 2 0.093" ID silicone peristaltic tubes
- 1 7.5 cm silastic tube for main flow connection from pump, 1 12 cm tube for x-flow connection, and 1 18 cm outlet tube, 1 2 cm tube to block bottom port
- 1 reservoir w/ 2 inner silastic tubes at 3.5 cm for inlets and 1 inner silastic tube at .5 cm or less for outlet , 2 outer openings sealed with a 3-4 cm tube, 1 outer tube at ~3 cm for air filter, and 2 7.5cm res input tubes
- 1 5 um inline filter, 1 1.2 um inline filter, and 1 0.8/0.2 um inline filter for in-line filters
- 1 0.2 um filter for the reservoir top
- 1 extra reservoir bottom (2 extra per rxr for some experiments)
- 3 150 X 75 Pyrex dishes
- 1 complete peristaltic pump (w/ 2 instech pumps)
- 2 13.5/35 VDC power supply (CAUTION: ALWAYS SET AT 13.5 VDC)
- Autoclaved blue paper (at least 3 squares for RXR assembly in the hood, include some extra sheets for the incubator as well)
- Tools: screwdrivers, tweezers, flat-head tongs, hex wrench
- 30 ug/mL type I rat tail collagen in 1X PBS, prepared fresh and kept on ice
- 1% w/v BSA in 1X PBS, can store at 4 °C after sterile filtering
- 1X PBS
- Pump Grease

Assembly protocol

1. Autoclave the screws, connectors, reservoir with connected tubing, silastic tubing, O-rings, tools (except screwdrivers), gaskets, Millipore filter, retaining ring, 2 Pyrex dishes and blue paper in sterilization packets, with the exception of the reservoir/extra tubings and the Pyrex dishes, which get wrapped in blue paper and sealed with autoclave tape. Make sure that the silicone gaskets don't touch one another in the sterilization pouch before autoclaving.
2. Gently scrub the polycarbonate Giant RXR body parts w/ alconox, rinse with milliQ water, place parts in a previously autoclaved Pyrex dish, and cover the parts with milliQ water.
3. Replace the water with 70% EtOH and let stand at least ten minutes before putting in the hood. Make sure all RXR bodies are completely submerged. CAUTION: POLYCARBONATE SHOULD NOT BE EXPOSED TO EtOH FOR MORE THAN 30 MINS.
4. Place the polycarbonate scaffolds in a Petri dish, cover with alconox water, shake gently, remove alconox, cover with milliQ water to rinse, shake gently, rinse repeatedly.
5. Place the polycarbonate scaffolds in a Petri dish w/ milliQ water, put in the sonicator for 2 mins. Make sure that scaffolds are in their correct pairs if using laser machined scaffolds and write the scaffold numbers on the dish.
6. Remove milliQ water, cover scaffolds with 70% EtOH, sonicate for 2 mins. Leave scaffolds in EtOH. CAUTION: POLYCARBONATE SHOULD NOT BE EXPOSED TO EtOH FOR MORE THAN 30 MINS.
7. Place the RXR body parts in the Pyrex dish and the scaffold pairs in Petri dishes in the sterile hood, along with: the autoclaved the Pyrex dishes, tools (including EtOH sprayed-down screwdrivers), connectors, screws, reservoir, tubing, O-rings, gaskets, Millipore filters, retaining ring, and blue paper. Spray all autoclave packets thoroughly with EtOH before putting them in the hood and keep them away from the blue paper surface that the reservoir is on.
8. Cover surface of working area in sterile cabinet with autoclaved blue paper.
9. Fill one autoclaved Pyrex dish ¾ full with 1X PBS, this will be used to rinse all parts. Fill a 10 cm Petri dish with 1X PBS to rinse the scaffolds separately from other parts.
10. Fill the other smaller autoclaved Pyrex dish ¾ full with 70% EtOH, and use the flat tongs (not the tweezers as the tubes are easily punctured) to place the two peristaltic tubings in the ethanol, swirling the tubes around the dish to get the inner tubing surfaces exposed as well. Make sure all tube ends are submerged in the ethanol.
11. Place the collagen solution (at least 10-15 mL) in a 10 cm Petri dish. Do the same for 1% BSA solution. Be sure to label the plates.
12. Rinse both scaffolds in 1X PBS. Put the top scaffold (lower numbered scaffold of the pair for laser machined scaffolds) into the collagen solution, shaking gently until no air bubbles are seen. The corresponding bottom scaffold can stay in the PBS or be put in another Petri dish with PBS if you are keeping track of many RXRs. For polycarbonate scaffolds, keep in collagen solution for 2 hours, and then dry for 2 hours inside the hood by balancing the scaffold on a 60 mm dish inside a 10 cm dish. For silicon scaffolds only 30 min in the collagen solution is required.
13. Rinse the filter in PBS and then place in the BSA solution for at least 30 minutes.

14. Use the tongs and tweezers to take out the middle body part (sides may be touched by gloved hands, but should be avoided) from EtOH, rinse in 1X PBS, and place on the blue paper top-side up.
15. Using tweezers, rinse the middle-sized silicon O-ring in 1X PBS (this helps the parts interact with each other more smoothly), place the O-ring in its channel on top of middle part. Use tweezers to hold down O-ring while the flathead of tongs are used to smoothly place the O-ring into the channel to avoid tearing the O-ring.
16. Rinse the top window in 1X PBS and place on top of middle body part.
17. Use the 6 small screws to secure the window onto the middle part (PBS rinsed). Tighten the screws (lightly at first) in a crisscross pattern, eventually tightening firmly but without cracking polycarbonate parts. Make sure that the O-ring is compressed uniformly.
18. Screw in the injection port screws slowly and loosely to middle body part, make sure there are no burrs on the screw threads catching as you tighten, as this can permanently damage the threading on the reactor body.
19. Tighten the port screws, stop when you feel a little resistance and the O-rings have been compressed. Otherwise you can break the flow channel inlet and outlet, compression of the O-ring is all that is needed to seal the injection port.
20. Keep middle/top window assembly open chamber face down on the sterile blue paper. Use the hex wrench to lightly-tighten 2 screw end-barbed end connectors to middle body part, ensuring that the O-rings are well compressed.
21. Flip the RXR body around so that the open pocket is facing up. Be very careful not to wave hands or arms over the reactor now.
22. Using tools, rinse 1 silicone gasket in PBS, place the gasket in the middle body part, using the pins/pin holes as a guide. Use the flathead tongs to lay the gasket down flat and make sure that no air bubbles are stuck under the gasket.
23. Place the dried top scaffold in the middle body atop the gasket, using the pin/pin holes as a guide. Make sure the scaffold is flat on the gasket and that the letter or number symbol is facing you at the top pin to ensure alignment with the bottom support scaffold.
24. Place the filter in the middle body atop the scaffold using the pin/pin holes as guide. Flatten with tongs onto the scaffold. Be especially careful not to tear the filter, as this will affect control over the cross-flow.
25. Using tools, rinse the support scaffold in PBS if not already in PBS, place scaffold in middle body atop Millipore filter using pin/pin holes as guide. Make sure the scaffold is flat and that the letter or number is at the top pin and facing you to ensure the best channel alignment.
26. Using tools, rinse the second silicone gasket in PBS and place the gasket in middle body atop the support scaffold using the pin/pin holes as guide. Flatten with tongs onto the scaffold. The pins should only extend about halfway up into the holes on this gasket.
27. Using tools, rinse the metal retaining ring in PBS, place the ring in the middle body atop the gasket with the channel for the large O-ring facing upward.
28. Using tweezers, rinse the large-sized silicon O-ring in 1X PBS, place the O-ring in its channel between the retaining ring and the middle part. Use tweezers to hold down the O-ring while the flathead of tongs is used to smoothly place the O-ring into the channel.

29. Rinse the bottom piece of the RXR in PBS. Place on the middle body part, and use the large screws to secure them together. As with the top window, tighten the screws (lightly at first) in a crisscross pattern, eventually tightening without cracking polycarbonate parts (don't overly tighten). Make sure that the O-ring is compressed uniformly.
30. Use the hex wrench to lightly-tighten the 2 remaining screw end-barbed end connectors to the bottom piece. Flip the RXR top-side up with bottom connectors towards the assembler.
31. Place the 18.5 cm silastic tube onto the top right side connector and the 12 cm cross flow silastic tube on the bottom-right connector. Place the 2 cm silastic tube onto bottom-left connector and a 7.5 cm tube onto the top left side connector.
32. Put dual barbed end connectors into each silastic tube, with the exception of the 2 cm tube at the bottom left port. On this tube attach a female luer barbed, and then screw in a threaded sealed end stopper. Note: It's easiest and safer to avoid contamination to add these connectors onto the tubing before they are wrapped up in blue paper with the reservoir and other tubing and autoclaved.
33. Rinse the peristaltic tubes in PBS and connect the two inlet tubes on the reservoir to the main flow line and cross flow line on the reactor.
34. Lightly grease the peristaltic tubes with pump grease between the plastic knuckles.
35. Put the 0.2 micron filter onto the extra tube on the top of the reservoir. The system is now closed.
36. Add 25 mL of HGM media to the reservoir, unscrewing and screwing the reservoir from the bottom so that the tubes don't get tangled. Be careful that the reservoir stays upright after it's filled so media doesn't get in the filter line
37. Lightly spray a peristaltic pump with ethanol and put it in the hood. Lightly spray and dry two power cords with ethanol and connect to the pump.
38. Turn the main flow pump on to a slow speed and guide the main flow peristaltic tube into the Instech pump. Keep pump going on for a short period to allow all PBS to clear out.
39. Turn on the left Instech pump at 3 mL/min or greater, counterclockwise (calibration should be done before run). Allow top chamber of RXR to fill with HGM, and since the cross flow tube hasn't been loaded onto it's pump yet, the bottom chamber should completely fill as well if the RXR was properly assembled.
40. Turn on the right Instech pump at 1mL/min, clockwise and load the cross flow peristaltic tubing onto the pump. Flip RXR, bottom-side up, put reactor at a 45° angle so that any trapped air in the chamber can flow out towards the reservoir.
41. Let the system prime for ~1 hour.

Seeding protocol

All seeding is done inside the sterile hood. Spheroids should be filtered (50 μm and 300 μm mesh), spun down at 50 g for 3 mins, resuspended in cold fresh medium, and put on ice immediately before beginning this protocol. Two spinner flasks seeded with 30 million hepatocytes each can be filtered together, and resuspended in 20 mL of cold HGM. This provides enough spheroids to seed at least 6-8 giant RXRs. Note: It is much easier and seeding is far more efficient if the system is primed and seeded with HGM that contains BSA.

1. Turn off the main flow pump and turn up the downward flow on the cross flow pump to quickly drain the top chamber halfway. Unscrew top window by removing injection port screws first and then the 6 small screws (this order will insure that the window won't crack). Remove the top window and place it on sterile autoclave paper.
2. Set crossflow rate to 2.5 mL/min downward. Leave main flow at 3 mL/min but keep pump turned off unless there isn't enough media in the chamber.
3. Seed reactor by gently pipetting ~2 mL of spheroid suspension evenly on seeding scaffold. Pipette gently, making sure spheroids are evenly distributed.
4. Gently rock the RXR body at 45 degree angles towards and away from you as the cross flow slowly draws the spheroids into the channels. Media in the chamber can be gently pipetted up from the bottom end of the tilt and slowly repipetted over the channel array at the top of the tilted chamber. This leads to very uniformly seeded cells if you alternate pipetting up and down on each end as you rock the RXR body. Be careful not to suck up too much of the cell suspension each time though to keep the cells in the channels wetted and to prevent air from being drawn into the filter between the scaffolds.
5. Observe channels as well as possible. If all channels are not seeded properly, a smaller volume of spheroid suspension may be added to the required area of the scaffold. Make sure top chamber liquid level is always above scaffold by turning on main flow if it is too low since the downward cross-flow will have removed a good deal of the media at this point. This prevents cells from being exposed from air and getting air trapped in the filter between the scaffolds.
6. Turn off all flow. Replace top window and screw back on in a similar fashion as done during assembly to ensure uniform compression of the medium sized O-ring. Turn main flow on at 3 mL/min, and crossflow at 2.5 mL/min. Gently tilt the reactor with the main flow outlet facing upward so the air easily leaves the top chamber. Wipe down the reactor body with an ethanol soaked Kimwipe. Put reactor in 37°C incubator.
7. Depending on the experimental protocol, you can change medium 1-2 hours after seeding to remove excess cells or simply change the medium when the cross flow is changed the following day. When changing medium, aspirate media out of the reservoir cup and put 30 mL of fresh medium in the reservoir. At 1-2 hours post seeding, two black rubber feet can be screwed into the bottom of the main flow outlet end so that air doesn't collect in the top chamber.

Inserting In-line Filters and Reversing Cross Flow

This protocol should be followed such that cross flow is reversed 24 hrs after seeding. Downward cross flow during the first 24 hrs helps to retain the cells in the channels as they attach to the walls and reorganize. Changing to upward cross flow after this initial period removes debris, as well as unattached and dead cells from the channels. Priming of filters requires an extra reservoir. However, all filters necessary can be primed from the same pump assembly.

1. Soak one peristaltic tube in 70% EtOH for <15 mins.
2. While the tube is soaking, open all in-line filters, screw autoclaved barbed-end/female luer-end connectors onto the broad luer end of each filter and connect the tubes with autoclaved 4 cm segments of silastic tubing. The filters should be in a sequential chain of 5 microns (green), 1.2 microns (red), and .8/.2 microns (blue/green). Connect all of the chains together with autoclaved barbed-end/barbed-end connectors and leave on sterile paper in the hood.
3. Rinse the peristaltic tube in 1X PBS, insert one barbed end-barbed end connector into each end of peristaltic tube and attach one end to a media reservoir and the other end to the filter chain. Connect the outlet end of the filter chain to the reservoir.
4. Put 30 mL of fresh medium into reservoir.
5. Lightly grease the peristaltic tube between the plastic knuckles and load the tube onto a pump head by turning pump on to a low setting. Once loaded, turn the pump to a high flow rate.
6. Hold filters up such that they will be filled from the bottom up so that most air is removed from the filter. After filters have been filled with medium, shake them and tap them gently to shake out any air bubbles that may have been trapped inside them.
7. Once all air bubbles are cleared, allow filters to prime for ~1 hour.
8. Take reactor out of incubator and place in sterile cabinet. Turn off pumps.
9. Remove the reservoir cup and replace with a new autoclaved cup with 30 mL of fresh HGM. This gets rid of a lot of the circulating debris and insures that the filter chain won't get clogged or provide too much resistance to the cross flow pump.
10. Clamp the cross flow silastic tube near it's meeting point with the peristaltic tube.
11. Clamp one set of three filters off from the primed filter chain and remove.
12. Gently remove the peristaltic tube from the cross flow line and attach to the 3 filter chain with the 5 micron filter on the peristaltic tube end. Remove the clamps and turn the cross flow pump to forward flow. Let the pump flow to remove any excess air in the filters from the act of connection. Let media drip from the free .8/.2 filter end of the line onto an ethanol soaked Kimwipe as the line finishes priming.
13. Turn off the pump and set to the desired upward cross flow rate. Gently remove the old silastic crossflow tube from the RXR with that reactor inlet tilted up so that media does not leave the chamber. Connect the filter chain onto the RXR and turn on both upward cross flow at 1 mL/min and main flow at 3 mL min. Note: To be absolutely sure that no short-circuiting is happening between the crossflow input and the main flow outlet. The cross flow input can be switched with the blocked off lower inlet, meaning the crossflow line would be placed onto the lower left chamber

inlet and the blocked 2 cm line would be switched to the lower right chamber inlet. This was normally performed in order to insure more uniform cross flow through the channels.

14. Check that no air bubbles are trapped in the RXR chambers and return to the incubator.

Media and Filter Changing Regiment

After the cross flow change and addition of in-line filters, media should be changed every 48 hours. Media can be aspirated from the reservoir cup after both pumps are turned off, and then 30 mL of fresh media can be added to the same cup.

Filters should be changed every 3 days for long term cultures. A new filter chain should be assembled and primed, and replaced following the above protocol. A filter chain can remain in the cross-flow line for up to 4 days for shorter term cultures before the lines begin to get clogged and seize the pump. This is useful for some transfection experiments for day 3 spheroid seeded reactors that are dosed with gene vectors on day 7 after isolation, since in-line filters typically aren't used during the transfection period to cut down on adsorption of the gene therapy vector in the circulating media. This isn't a problem for the short term transfection period since the vast majority of debris is removed by day 7.

Cell Recovery from the Reactor

Cells can be removed very efficiently from the polycarbonate scaffolds by using Dispase and adhering to the following protocol.

1. Prior to taking down the reactor, thaw frozen aliquots of Dispase and allow them to warm to 37°C. Make sure that you have at least 3 mL of Dispase for each reactor that will be taken down.
2. At the time point of interest, spray down the pump and reactor and place in the hood on autoclaved blue paper.
3. With the pumps still running, remove the peristaltic tubes form the pumps. Turn off the pumps and take out of the hood.
4. Quickly unscrew the top and bottom RXR pieces from the middle RXR body. Gently remove these pieces and then use the flat tongs to slowly push the scaffolds, filter, retaining ring and bottom silicone gasket out of the RXR body and into a 10 cm Petri dish.
5. Pick up the scaffold sandwich and very slowly and gently shear the top, cell containing scaffold away from the filter in a perpendicular direction to the scaffold and filter faces. This prevents loss of cells on the filter, and all of the cells will be retained in the scaffold channels.
6. Place the cell containing scaffold in a 10 cm Petri dish and pipette 3 mL of warm Dispase over the channel array.
7. Place the dish in an incubator for 5 minutes.
8. Take the dish out of the incubator, and in the hood, tilt the plate, lift the scaffold with the flat tongs and gently pipette the Dispase through the channels. The channels should be completely clean in less than a minute.

9. Keeping the Petri dish tilted, gently scrape the cells with a disposable scraper to the bottom of the dish. Collect the cells with a pipette and put into a pre-chilled 15 mL centrifuge tube.
10. Add fresh, chilled media to the plate to collect any cells that remain and add to the same centrifuge tube.
11. Spin down the collected cells at 50xG for 3 minutes.
12. Carefully remove the supernatant with a pipette, and resuspend the cell pellet in the buffer of interest that is optimal for the ensuing assay to be performed, e.g. Trizol for RNA extraction, the appropriate lysis buffer for westerns or gene expression assays, DGE buffer for cell lysis and organelle recovery.

Appendix 7 - RNA Purification Protocol

Standard RNA Isolation Protocol

This protocol utilizes Trizol to lyse cells from any variety of culture systems and stabilize the RNA in the sample for long term storage at -80°C. RNA is then acquired from these thawed samples by a chloroform extraction and the resulting aqueous RNA phase is further purified using a commercial kit such as the Qiagen RNEasy Mini Kit with a modified protocol that is included here.

To initially collect the sample:

1. Aspirate media and wash cells once with PBS.
2. For 6 well tissue culture plates: Add 1mL Trizol to each well; detach cells with cell scraper and transfer sample to RNAse free Eppendorf tube; invert and vortex to mix.
3. For spheroids: Pellet spheroids at 50xG for 3 minutes, aspirate the supernatant and resuspend in 1 mL of Trizol, sample can be transferred to an Eppendorf tube and vortexed to mix.
4. For reactors with polycarbonate scaffolds: Quickly recover the cells from the scaffold via Dispase digestion (See Appendix 5), pellet cells and tissue at 50xG for 3 minutes. Aspirate supernatant and add 1 mL of Trizol. Transfer to an Eppendorf tube and vortex to mix.
5. *In vivo* liver tissue samples: Cut a piece of each of the four lobes of the liver. Put each piece in a separate 15 mL centrifuge tube in 3-5 mL of Trizol. Use a tissue homogenizer at a high speed setting to completely break up the sample, aliquot or keep in the large tube to freeze.
6. Freeze all samples at -80°C for a minimum of 15 min (until completely frozen) to a maximum of 2 months.

Note: From this point it's recommended not to do more than 8 samples at a time to minimize RNA degradation during time of procedure.

7. Thaw sample on ice (or at room temperature as long as you watch it carefully!).
8. Homogenize sample by passing through a 26g needle/syringe (1 ml) 12-15 times.
9. Add 200uL Chloroform to each sample .

10. Invert a few times by hand and then vortex for 5 seconds.
11. Incubate RT for 2-3 mins; sample will start to settle (clear w/ RNA on the top; pink w/ DNA and Protein on the bottom).
12. Centrifuge samples for 15 min @ 12,000 RPM (Cold Room 16-447).
13. (In preparation for later) Warm DEPC Water to 55°C (Bench #3) and label Eppendorf collection tubes.
14. After spin, carefully remove top layer of supernatant (clear; contains the RNA) and place in 1.5mL Eppendorf tube. To do this, set pipette to 200 ul and leave some behind if necessary so that there is no contamination with the pink layer (contains DNA and other cellular components).
    a. Keep track of how much material was removed (should yield about 550-600 ul).
    b. Remaining sample (DNA/Protein) will go into –80C.

From here onward, keep all samples on ice! Follow RNEasy Mini Handbook (Qiagen) from step 4 of protocol *(with a few modifications)*:

15. Add equal volume (or more) of 70% EtOH to sample: mix by tipping and pipetting (do not vortex).
16. Remove up to 700uL solution and place in an RNEasy column with collection tube.
    a. Centrifuge for 15 sec @ ≥ 8000g (10,000 RPM) .
    b. Repeat spin by returning eluent to top of filter (15 seconds).
    c. Discard waste (solution in the bottom of filter unit) after the 2 centrifugation steps.
    d. Add remaining and repeat centrifugation steps 7a-7c .
17. Add 700ul of Buffer RW1 to the RNEasy column. Centrifuge for 15 sec @ ≥ 8000g (10,000 RPM) and discard flow-through and collection tube.
18. Transfer column to a new collection tube and add 500uL of RPE Wash Buffer to filter. Centrifuge for 15 sec @ ≥ 8000g (10,000 RPM) and discard waste.
19. Add another 500uL of RPE Wash Buffer to System and centrifuge for 2 min (15 sec @ ≥ 8000g) to dry membrane.
    a. RECOMMENDED: Place column in new collection tube and centrifuge at full speed for 1 minute to ensure that all ethanol is removed.

20. Add 30uL DEPC treated water (heated to 65°C) to filter; incubate RT for 2-3 minutes.
    a. Centrifuge for 2 minutes in a clean Eppendorf tube to elute.
    b. Repeat with another 30uL DEPC water (if desired, this is requisite if there are one million cells or more).

To measure quantity and purity of RNA:

21. For a traditional spec, remove 2uL water from sample and add to 98uL water in new Eppendorf tube
    a. Also make blank (100ul DEPC water)
22. Return samples (both the Trizol sample and the RNA sample) to the –80C
23. Bring 100uL samples on ice (and blank 100uL DEPC) to spectrophotometer
24. To use Spectrophotometer (Samson lab spec, 56-230):
    a. Nucleic acid (260/280)
    b. Turn Vis on, UV on (wait 1-2 min after machine is ready)
    c. Wipe casings with kimwipes
    d. Insert blank (red dot towards front); click "blank"
    e. Insert samples, click "read sample"; repeat 3x for each sample
    f. Print results, Quit, OK, UV Off
25. To use the NanoDrop in BPEC:
    a. Open ND-100 v3.1.2 on the BPEC PCR computer.
    b. Select "Nucleic Acid" tab.
    c. Clean the sample pedestal with RNAse free water and a Kimwipe.
    d. To initialize, add 2 uL of RNAse free water, put top arm down and click OK.
    e. Select RNA-40 in the sample type window in the upper right corner.
    f. Wipe off the sample pedestal and blank the device with 2 uL of the buffer that the sample is in, which for RNA is usually DEPC water.
    g. Wipe off the sample pedestal and pipette 2 uL of your sample, put the arm down and click on measure.

    Notes: Only read a volume of sample once, you can read another 2 uL and so on if you want replicates. The reading will change on subsequent reads of the same sample. The sample pedestal only needs to wiped clean with a Kimwipe between multiple samples. Keep RNA samples on ice at all times during measurement.

Appendix 8 – cDNA Generation Protocol

This cDNA protocol is based on synthesis from 200 ng of total RNA and will yield 20 uL of cDNA. This is enough to run real-time PCR on 5-6 genes. If you need to measure more genes, or if you want to store some cDNA long term since it degrades less rapidly than the RNA samples, you can double or triple all of the volumes in the protocol and get 40 or 60 uL of cDNA from 400 or 600 ng of RNA, respectively.

1. Add the following to a 0.5 mL Eppendorf tube:

    a. Calculate the volume of the RNA sample to make 200 ng total RNA from nanodrop reading. Make sure to re-read your RNA sample if it's been stored for a while.
    b. Calculate the remaining volume of DEPC water so the total volume (RNA+H_20) is 8 uL.
    c. Add DEPC water, and then RNA and keep all samples on ice.
    d. Add 1 uL of 10x DNAse Buffer to each sample. Mix buffer well with a pipette before adding.
    e. Add 1 uL of DNAse I enzyme (Invitrogen) to each sample. Take DNAse out just before adding (don't need to thaw it) and mix with a pipette before adding.

2. Let the sample sit at room temperature for 15 minutes. Put the remaining RNA back in the -80°C freezer. Turn on the heating block and set to 65°C. Prepare Eppendorfs for dilution in step 5.

3. Add 1 uL of EDTA to each sample (25 mM, Invitrogen) to each sample and return the samples on ice. When EDTA has been added to all samples, centrifuge them at 2000 RPM for ~5 seconds. Incubate samples at 65°C for 10 minutes.

4. Get from the -20°C freezer: Random Hexamer Primers, RT Buffer (Qiagen), RNAse Inhibitor (Ambion). Keep on ice!

5. Make dilutions of 10x RT buffer, Random Hexamers, and RNAse Inhibitor:

    a. RT Buffer: 1:10 dilution of the 10x RT buffer to use in step 5c. Add 9 uL of DEPC water for every 1 uL of 10x RT buffer. Make a little extra so volumes will be correct.
    b. Primer dilution: 1:10 (e.g. 9 uL of DEPC water and 1 uL of Primer working stock. Again, plan to make 1-2 rxns worth extra so volumes will be accurate. Make the dilution fresh every time.
    c. RNAse Inhibitor: 1:4 Dilution with 3 uL of 1x RT buffer from step 5a for every 1 uL of RNAse inhibitor. Make fresh each time, and again make 1-2 rxns additional dilution so volume will be accurate for stock solution.

6. Make the Stock Solution containing for each sample (make one to two extras):

   a. 1 uL DEPC water
   b. 2 uL dNTP (Qiagen)
   c. 2 uL Primer dilution (step 5b)
   d. 1 uL RNAse inhibitor dilution (step 5c)
   e. 2 uL 10x RT buffer (Qiagen)
   f. 1 uL Omniscript Reverse Transcriptase (RT O, Qiagen)

7. Remove samples from heat at the end of 10 minutes from step 3. Centrifuge for ~5 seconds at 2000 RPM. Return samples to ice.

8. Add 9 uL of the Stock Solution from step 6 to each sample to make the total volume 20 uL.

9. Spin down samples for ~5 seconds at 2000 RPM.

10. Incubate samples at 37°C in the water bath. Make sure bottom of tube is in the water but that tube tops aren't submerged.

11. Remove samples from the water bath, centrifuge ~5 seconds at 2000 RPM, and store samples at -80°C.

Note: Catalogue numbers and sources for all currently used reagents are listed in the master lab supplies file.

Appendix 9 – Real-time, Reverse Transcriptase SYBR Green PCR Protocol

This is a general protocol for any primer set of interest to measure mRNA expression using the Chromo4 Real-time PCR set-up and Opticon Monitor 3 software.

1. Make "Master Mix" containing (or 20x):
    a. 25uL SYBR Green (500uL)
    b. 21uL DEPC water (420uL)
    c. 1.5uL forward primer (30uL) (primers boxes, -20°C freezer #5)
    d. 1.5uL reverse primer (30uL) (primers boxes, -20°C freezer #5)
2. Vortex sample and spin down. Vortex master mix and spin down.
3. Get BioRad 96-well plate (white plastic) and place in a black plate tray.
4. Add 49uL master mix (step 1) to each well.
5. Add 1uL cDNA to each sample. Use triplicates. Leave one triplicate for no RT spaces.
6. Cover each well with a sample in it with a clear plastic cap.
7. Return cDNA samples to -80°C freezer.
8. Insert sample into RT-PCR machine. Gently close the top and secure the latch.
9. Open "Opticon Monitor 3" program on the BPEC PCR computer.
10. Open your user profile. Open Master file (top set) and make changes to plate and protocol setup.
11. Change the plate setup so each grid spot where there is a sample has a red circle. Make sure that the proper plate type (MJ White) and dye types (SYBR Green, in this case) are selected – these cannot be changed later.
12. Change the protocol to have the optimal primer annealing temperature and number of cycles. Make sure that the proper reaction volume is typed in (50 uL here) – this cannot be changed later.
13. Save the protocol file, then the plate setup file, then the master file.
14. Click Run: the computer will prompt you for a file name for the data file. The computer automatically saves this file at the end of the run protocol.
15. You can click on 'quantification' during the run to check the status of your sample.

16. When the run is complete, set the threshold magnitude by looking in both the log view and regular view to make sure it is in the early linear range of the amplification. Keep this value consistent between runs for accurate comparison of C_Ts between samples.

Appendix 10 – Vector Specific Gene Delivery Protocols

Deliver 5 ug of plasmid DNA for a 35 mm dish, and 10 ug of DNA for a 60 mm dish.

Keep the concentration at 5 ug/mL in transfection media and add 1 mL for 35 mm and 2 mL for 60 mm to get good coverage and stay consistent between different samples and systems.

For PEI25:

To make NV PEI25 particles at N/P=20:

For every 5 ug of DNA:

1. Add 24 uL of .0005 ug/uL PEI25 solution to 26 uL of sterile water
2. Add this 50 uL of polymer solution to the DNA which has been diluted to .1 ug/ul previously in aliquots.
3. Pipette vigorously and let the tube sit at room temp for 20-25 minutes.
4. Do not prepare more than 800 total volume in one tube (40 ug DNA)
5. By 25 minutes, add 100 uL complex solution for every 900 uL of media.

Add appropriate amount of transfection solution to each plate and incubate at 37C.
Wash 2x in PBS++ at time point of interest.
Scrape up cells, collect with pipette, and spin at 50G, 4C for 4 min.
Aspirate supernatant and freeze pellet at -20C for short-term and -80C for long-term.

Notes:

Make fresh PEI25 at .0005 ug/uL by diluting the stock PEI25 in ethanol (at 100 mg/mL currently) 200 fold in sterile water, making final ethanol concentration less than 0.5%.

For Small X-Linked PEI and Linear PEI22 from the Klibanov Lab:

X-linked PEI at N/P=30 (frozen stock is at 150 mM) for 10 ug of DNA

1. Make a 1:10 dilution of the stock XPEI in water.
2. Add 61.5 uL of the 1:10 polymer dilution to 38.5 uL of water.
3. Add 20 uL of .5 mg/mL plasmid stock to 80 uL of water.
4. Add the 100 uL of polymer to the 100 uL of DNA.
5. Pipette vigorously and let stand at room temp for 10 minutes.
6. Add to 2 mL of pre-warmed medium and add to a washed 60 mm dish. Scale volumes accordingly for other plate types and cell numbers.

Linear PEI22 at N/P=10 (frozen stock is at 150 mM) for 10 ug of DNA

1. Make a 1:10 dilution of the stock LPEI22 in water.

2. Add 20.5 uL of the 1:10 polymer dilution to 79.5 uL of water.
3. Add 20 uL of .5 mg/mL plasmid stock to 80 uL of water.
4. Add the 100 uL of polymer to the 100 uL of DNA.
5. Pipette vigorously and let stand at room temp for 10 minutes.
6. Add to 2 mL of pre-warmed medium and add to a washed 60 mm dish. Scale volumes accordingly for other plate types and cell numbers.

For C32 and Other Langer Lab Poly(β-amino ester)s:

Combine all polymers and DNA at a mass/mass ratio of 100:1.

1. Dilute the 100 mg/mL polymer stocks in DMSO 1:10 in sterile filtered 25 mM sodium acetate buffer.
2. Add 20 uL of plasmid at .5 mg/mL to 80 uL of the sodium acetate buffer.
3. Add 100 uL of the polymer dilution to the 100 uL of DNA (10 ug DNA total).
4. Pipette vigorously and let stand at room temperature for 5 minutes.
5. Add to 2 mL of pre-warmed medium and add to a washed 60 mm dish. Scale volumes accordingly for other plate types and cell numbers.

For Adenovirus:

These amounts are for an MOI of 10 for transduction of 2 million cells in a 60 mm dish. It is not wise to use MOIs greater than 20 for gene delivery experiments in primary hepatocytes.

1. Make a 1:100 dilutions of an Ad5 stock aliquot in 10% glycerol in PBS. Keep the volume small enough in the 1:100 aliquots that one tube will only be thawed once or twice.
2. Thaw a 1:100 aliquot on ice.
3. Add 6 uL of the 1:100 aliquot to 2 mL of pre-warmed medium and add to a washed 60 mm dish. Scale volumes accordingly for other plate types and cell numbers.

Overall Notes:

Adding the polymer to DNA and not the DNA to the polymer is important for good and consistent complex formation.

Do not freeze-thaw DNA plasmid aliquots more than three to four times, keep already thawed aliquots away from the new aliquots in the freezer box.

Appendix 11 – Plasmid and Genomic DNA Purification Protocol

OBJECTIVE:

Purify plasmid DNA in high throughput from total cell or nuclear samples using a Qiagen DNEasy 96 Plate. This is a modified protocol from the standard Qiagen protocol which works well with mechanically lysed samples, nuclear pellets, and samples lysed with 1% NP-40 lysis buffer. Delivered plasmid DNA and endogenous genomic DNA are copurified for the whole cell and nuclear fractions.

METHOD:

1) Thaw frozen samples for 30 min. at room temperature.
2) Add 200uL of room temperature PBS to each nuclear sample, resuspend by repeatedly pipetting.
3) Transfer samples into wells of round-well block. Be sure to note sample layout in the provided plate templates.
4) Add 200uL Buffer ATL + Proteinase K (2mL Proteinase K + 18mL Buffer ATL per plate) to each well. Carefully seal with Qiagen caps and mix by shaking vigorously for 15 sec. Centrifuge at 3000 rpm briefly.
5) Incubate at 70C for 30 min. Tape the clear top down to the blue base so the caps don't pop off.
6) Remove plate from the hybridization oven. Carefully remove the clear top and reseal the caps carefully. Wait 30 seconds to make sure the temperature change of any opened and resealed caps doesn't cause them to pop open.
7) Return top and shake vigorously for 15 sec. Centrifuge at 3000 rpm briefly.
8) Remove caps. Add 410uL Buffer AL/E to each well. Seal with Qiagen caps and mix by shaking vigorously for 15 sec. Centrifuge at 3000 rpm briefly.
9) Place QIAmp 96 plate on a clean S-block. Transfer samples from round-well block to the QIAmp 96 plate. Plate can take up to 900 uL per well.
10) Seal QIAmp 96 plate with AirPore tape. Centrifuge at 6000 rpm for 10 min.
11) Remove tape. Add 500uL Buffer AW1 to each well. Seal QIAmp 96 plate with new AirPore tape. Centrifuge at 6000 rpm for 5 min.
12) Remove tape. Add 500uL Buffer AW2 to each well. Seal with AirPore tape. Centrifuge at 6000 for 5 min.
13) Remove tape. Place DNEasy plate on Qiagen rack of elution tubes. Incubate at 70C for 15 min. to dry the membranes.
14) Add 200uL pre-warmed 70C H_2O to each well. Seal plate with new AirPore tape. Incubate at RT for 2 min. Centrifuge at 6000 rpm for 2 min.
15) Repeat step 14 to obtain a total elution volume of 400 uL.
16) Seal plate with foil adhesive cover. Store at –20C.

Comments: Make sure that the plate centrifuge is well greased at the knuckles so that plates don't get imbalanced. If running one plate at a time, make absolutely sure that the balance plate has the exact same volumes as the sample plate.

Appendix 12 – Quantitative Real-time Taqman PCR Protocol

This protocol allows for sensitive quantification of the gWiz β-Gal plasmid purified from cell samples after gene delivery.

EXPERIMENT:

DNA Quantitation of gWiz β-Gal Plasmid

OBJECTIVE:

Determine plasmid quantity using MJR Chromo 4 System.

Samples: _____

METHOD:

1) Thaw frozen samples for 30 min. at room temperature. Thaw primers and probe and keep on ice.
2) Mix samples well with a multichannel pipette.
3) Prepare Master mix and keep on ice (15uL per well, make for at least 10-15 extra rxns if using electronic multichannel):

	Final Concentration	**Volume (uL) per 25uL**	**Volume (uL) per _____**
2x Master Mix	1x	12.5	
Forward Primer	400nM	0.125	
Reverse Primer	400nM	0.125	
Probe	25nM	0.125	
H_2O	-	2.125	
Add 10 uL sample		10	

4) Prepare standard curve by pipetting 90uL H_2O to wells B1-H1 of first column and A3-C3 in the third column in a new 96-well plate. Pipette 100uL gWiz B-Gal plasmid stock (1E9 copies/uL) into first well using P200 pipette. Perform 10-fold dilutions down column (10uL) using Rainin 10 uL pipette. Scale up these volume as needed if prepping multiple plates.
5) Pipette 15uL master mix per well into MJ White Optical plate using Biocontrol Electronic pipette by setting pipette to 15uL 12x in Stepper Mode. Holding trigger to second stop before aspirating, dispense by pulling trigger to first stop.

6) Pipette 10uL standards or sample into appropriate well. Use PCR layout sheet to note sample locations.
7) Cover and seal plate with caps and sealing tool. Centrifuge at 3000 rpm for 1 min in Qiagen Centrifuge. Perform PCR on MJR Chromo 4 (FAM dye, TAMRA quencher, ROX reference):
    a) Cycle Routine in Protocol File

1. Hold	50C	2 Min
2. Hold	95C	10 Min
3.Cycle	95C	15 Sec 40 times
	60C	1 Min
	Plate Read	
4. Hold	50C 2 Min	

    Make sure rxn volume is 25 uL in upper entry window.
    b) Plate File
        1. Make sure plate type is selected as MJ White
        2. Have every dye designation as sample except for standards wells where FAM should be set to standards or blank with the appropriate copy number added in.
    c) Save Master File to link the Plate and Protocol Files
    d) Click run and save Data File.

8) For data analysis, set cycle threshold level at .025 for these primers to be in the log linear range for nearly all cases. Keep this threshold consistent between plates for the most accurate comparison of copy numbers. Export data by copying output sorted by dye and paste into an Excel sheet.

This protocol allows for quantification of the endogenous rat GAPDH gene purified from cell samples after gene delivery. Comparison to a standard curve generated from the same DNA purification method allows determination of hepatocyte number to normalize samples on a per cell basis.

EXPERIMENT:

DNA Quantitation of Rat Genomic DNA via GAPDH

OBJECTIVE:

Determine cell quantity using MJR Chromo 4 System.

Samples: _____

METHOD:

1) Thaw frozen samples for 30 min. at room temperature.
2) Mix samples well with a multichannel pipette.
3) Prepare Master mix (15uL per well):

	Final Concentration	**Volume (uL) per 25uL**	**Volume (uL) per _____**
2x Master Mix	1x	12.5	
Forward Primer	900nM	1.0	
Reverse Primer	900nM	1.0	
Probe	225nM	0.5	
Add 10 uL sample		10	

4) Pipette 15uL master mix per well into MJ White Optical plate using Biocontrol Electronic pipette by setting pipette to 15uL 6x in Stepper Mode. Holding trigger to second stop before aspirating, dispense by pulling trigger to first stop.
5) Pipette 10uL samples into appropriate well. Use PCR layout sheet to note sample locations.

6) Cover and seal plate with caps with sealing tool. Centrifuge at 3000 rpm for 1 min in Qiagen Centrifuge. Perform PCR on MJR Chromo 4 (FAM dye, TAMRA quencher, ROX reference):
    a) Cycle Routine in Protocol File

1. Hold	50C	2 Min
2. Hold	95C	10 Min
3.Cycle	95C	15 Sec 40 times
	54C	1 Min
	Plate Read	
4. Hold	50C 2 Min	

    Make sure rxn volume is 25 uL in upper entry window.
    b) Plate File
        1. Make sure plate type is selected as MJ White
        2. Have every dye designation as sample.
    c) Save Master File to link the Plate and Protocol Files.
    d) Click run and save Data File.

7) For data analysis, set cycle threshold level at .025 as well for these primers to be in the log linear range for nearly all cases. Keep this threshold consistent between plates for the most accurate comparison of cell numbers. Export data by copying output sorted by dye and paste into an Excel sheet.

Appendix 13 – Gene Expression Assays in 2-D and 3-D Culture Systems

For 2-D Adsorbed Collagen Monolayer Cultures:

1. Prepare fresh 1x reporter lysis buffer at room temp from the 5x stock and water.
2. Take plates out of the incubator and wash 1x with PBS.
3. Add 450 uL of 1x reporter lysis buffer to each plate. Rotate and tilt plates to ensure even coverage.
4. Place plates on the rack in the hybridization oven and turn the tilt speed to maximum to achieve good movement of the lysis buffer. Incubate for 15 minutes at room temp.
5. Scrape each plate with a new hard white scraper. Collect scraped cells in the bottom of the plate with a pipette and put in a pre-chilled 1.5 mL Eppendorf tube on ice.
6. Vortex each sample for 20-30 seconds, then centrifuge the tubes at top speed in a microcentrifuge (at least greater than 12,000 RPM) for 2 minutes.
7. Return the tubes to ice, being very careful not to dislodge the pellet.
8. Transfer 400 uL of the supernatant to a new pre-chilled tube, keeping the pipette tip as far away from the pellet as possible during the transfer.
9. Freeze samples at -80°C. Full β-Gal activity is retained for at least two months.

For 3-D Liver Bioreactor Cultures:

1. Prepare fresh 1x reporter lysis buffer at room temp from the 5x stock and water.
2. Warm up at least 3 mL of Dispase to 37°C per reactor to be taken down.
3. Disassemble reactor and carefully push the scaffold sandwich out of the reactor pocket into a sterile Petri dish in the hood.
4. Carefully shear the top scaffold off of the filter in a direction perpendicular to the scaffold/filter face to ensure that the tissue remains in the channels. Place the top scaffold in a 10 cm Petri dish.
5. Add 3 mL of prewarmed Dispase on top of the channel array and place in the incubator for 5 minutes.
6. After 5 minutes, hold the scaffold up with flat tweezers and gently pipette the cells out of the channel.
7. Collect the cells with a pipette and pellet them at 50xg for 3 minutes at 4°C.
8. Carefully removed the supernatant with a pipette (not the vacuum aspirator) to ensure that the pellet is not dislodged but that as much media as possible is removed.
9. Add 1.5 mL of 1x reporter lysis buffer to the pellet. Resuspended the pellet by pipetting, transfer lysate to a prechilled 1.5 mL Eppendorf tube on ice.
10. Vortex samples for at least 30 seconds to break up any remaining tissue chunks, then centrifuge the tubes at top speed in a microcentrifuge (at least greater than 12,000 RPM) for 2 minutes.
11. Transfer 1400 uL of the supernatant to a new prechilled Eppendorf tube with a pipette keeping the pipette tip as far away from the pellet as possible during the transfer.
12. Freeze samples at -80°C. Full β-Gal activity is retained for at least two months.

Note: If western blots are to be performed on the reactor samples, especially for any membrane surface proteins, an alternative collection and lysis method is to directly pipette 1.5-2 mLs of 1x reporter lysis buffer over the cell array and use a large gauge syringe or pipette to force the cells out of the channels and then proceed with the rest of the protocol. It is more difficult to recover the cells using this technique, but it guarantees that epitope of interest won't get cleaved by the Dispase, and there is little difference in the β-Gal/total between the two methods.

Measuring β-Gal Activity:

1. Thaw the Promega Assay 2x Buffer on ice and the Promega 1 M Sodium Carbonate Stop Buffer at room temp. Ensure that there is no precipitate in the Stop Buffer (if so, place in the water bath and shake until).
2. Thaw lysate supernatants and keep on ice.
3. Prepare a standard curve in duplicate as described for the 96 well assay in the Promega protocol.
4. Place 50 uL of each sample in triplicate into the appropriate sample wells of the plate.
5. Add 50 uL of the Assay 2x buffer with a multiwell pipette, mixing well and using new tips for each row.
6. Put the top on the plate and incubate for 30 min at 37°C in the incubator.
7. Stop the reaction by adding 150 uL of the 1 M Sodium Carbonate to each well. Pop any bubbles that are formed during this step with a syringe tip.
8. Read the absorbance of the samples at 420 nm in the plate reader.

In parallel, prep duplicate 50 uL replicates (triplicate for reactors where there is plenty of supernatant) of the samples with 50 uL of water in another plate and perform the BCA total protein assay as described in Appendix 4 in order to normalize the gene expression levels.

Appendix 14 – Toxicity Assay Protocols

LDH Release Assay:

This assay is a close adaptation of the Promega CytoTox-ONE Homogeneous Membrane Integrity Assay.

1. At the time point of interest, take the plates out of the incubator and let them equilibrate to room temperature. Allow Substrate Mix and Assay Buffer to thaw and equilibrate to room temperature at this time as well.
2. Add 11 mL of Assay Buffer to a vial of Substrate Mix. Mix with the pipette-aid to fully resuspend. Keep the vial closed and protected from light. It is not recommended to reuse reagent past very short term storage contrary to the manufacturer's protocol.
3. Run a no treatment control and a max release control (add 1% NP-40 lysis buffer to untreated cells) along with the samples. Media only blanks should also be used.
4. Remove 50 uL of the media in triplicate from each well and place in the appropriate wells of a new 96 well plate.
5. Add 50 uL of the assay reagent prepared in step 2 to each well with a multichannel pipette, mixing well after adding.
6. Incubate for at least 10 min at room temperature.
7. Add 25 uL of the stop solution.
8. Shake the plate (you can use the plate reader mixing function).
9. Read the fluorescence with Excitation = 560 and Emission = 590 in the plate reader.
10. Use the cells from this plate for the MTT or ATP assay in parallel with this assay.

ATP Assay:

This assay is an adaptation of the Promega CellTiter-Glo® Luminescent Cell Viability Assay.

1. Remove CellTiter-Glo® Luminescent Cell Viability Assay (Promega) buffer and substrate bottles from the -20°C freezer to the 4°C refrigerator the day before intended use. Purchase the buffer-substrate combo in the 10mL increments to avoid reconstituting much more than needed at once.
2. Remove buffer and substrate from the 4°C refrigerator ~1 hour before intended use.
3. Add buffer to substrate ~30 minutes prior to intended use. If the buffer is still not thawed, slightly warmed water may be used to heat up the buffer solution.
4. Shake gently to reconstitute the substrate.
5. Remove tissue culture plate from incubator and allow it to equilibrate to room temperature (~ 15-20 minutes). Already done if coupled with LDH assay.
6. Remove media from the wells. Media can be used for the LDH assay.
7. For a 24-well plate with a nominal seeding density of 50,000 cells/cm^2, add 100 uL of the reconstituted reagent to each well.
8. Shake gently for ~15 seconds.

9. Cover the plate with foil and place on a shaker.
10. Pipette 90 uL of media into a few wells in a white 96-well luminescence plate (no cell control).
11. 30 minutes after adding the reagent to the plate, remove from the shaker.
12. Mix plate gently and pipette 90 uL from each well into a well in the white 96-well luminescence plate.
13. Read luminescence.

Note: Reconstituted substrate should be stored at -20°C if you do not plan on using it soon (~a few days). Otherwise, store it at 4°C. Although the Promega tech bulletin for this assay reports a substantial loss of activity if stored at 4°C, using the amount given in the above protocol will give you a great excess of the luciferin substrate and luciferase enzyme for the luminescence reaction. Therefore, the reconstituted reagent can be stored at 4°C with minimal loss in luminescence production in the collagen gel plates. This keeps day to day readings more consistent in the short term.

MTT Assay:

This assay is adapted from the Promega CellTiter® Non-Radioactive Cell Proliferation Assay for use in 24 well plate cultures.

1. Add 150 uL of the Promega Dye Solution to the media of each sample well.
2. Return the plate to the incubator and allow it to develop for 4 hours.
3. After 4 hours, add 1 mL of Solubilization/Stop Solution to each well.
4. Place the plates in a sealed plastic box with a wet Kimwipe to keep the box humidified. Incubate overnight at 37°C to break up the formazan crystals.
5. The following day, mix the contents of each well with a pipette such that well contents are completely homogeneous.
6. Transfer triplicate volumes (anywhere between 100 and 300 uL as long as you are consistent) of the dissolved lysate to a 96 well plate, and read absorbance at 570 nm in the plate reader.

Appendix 15 – Matlab, Teranode, and Jacobian Models and Code

Matlab Code for Model Extensions

```
%Nathan Tedford
%Code to run the vector specific models
%Nov. 2006

time=[0:120]; %time vector in minutes

%time=[10 20 40 60 120];

IC_Polymer=[5e5 0 0 0 0 0 0 0 0 0 0 0 0 0 0 0];
IC_Ad5=[20 0 0 0 0 0 0 0 0 0 0 0 0 0 0 0];


[t,y]=ode15s(@C32_model,time,IC_Polymer);

plasmid_vesicular_C32 = y(:,2) + y(:,3);
plasmid_cytoplasmic_C32 = y(:,5) + y(:,6) +  y(:,10) + y(:,12);
plasmid_nuclear_C32 = y(:,7) + y(:,8) + y(:,9) + y(:,13) + y(:,14) + y(:,15);
plasmid_total_C32 = plasmid_cytoplasmic_C32 + plasmid_nuclear_C32 +
plasmid_vesicular_C32;


%Experimetal Data

C32Whole = [0 2.22E+04 4.70E+04 9.93E+04 2.34E+05 1.71E+05];
C32LateVes = [0 8.92E+02 1.56E+03 1.29E+03 4.37E+02 7.41E+02];
C32Cyto = [0 5.16E+03 5.18E+03 7.48E+03 7.01E+03 2.34E+03];
C32NucAssoc = [0 1.98E+04 2.24E+04 5.89E+04 1.10E+05 1.23E+05];
C32AllVes = [0 8.97E+02 1.57E+03 1.32E+03 4.45E+02 7.53E+02];

X = [0 10 20 40 60 120];

figure(1);

plot(t,plasmid_cytoplasmic_C32,'k')
hold on
plot(X,C32Cyto,'ko:')
plot(t,plasmid_vesicular_C32,'b')
plot(X,C32AllVes,'bo:')
plot(t,plasmid_nuclear_C32,'g')
plot(X,C32NucAssoc,'go:')
plot(t,plasmid_total_C32,'r')
plot(X,C32Whole,'ro:')
title('Internalization, Trafficking and Nuclear Uptake Kinetics for C32')
```

```
xlabel('Time (min)')
ylabel('Normalized Plasmid Number per Cell')
legend('Cytoplasmic','Vesicular','Nuclear-associated','Total Cellular')


%Now for the Ad5 Specific Model

[t,y]=ode15s(@Ad5_model,time,IC_Ad5);

plasmid_vesicular_Ad5 = y(:,2) + y(:,3);
plasmid_cytoplasmic_Ad5 = y(:,5) + y(:,6) +  y(:,10) + y(:,12);
plasmid_nuclear_Ad5 = y(:,7) + y(:,8) + y(:,9) + y(:,13) + y(:,14) + y(:,15);
plasmid_total_Ad5 = plasmid_cytoplasmic_Ad5 + plasmid_nuclear_Ad5 +
plasmid_vesicular_Ad5;

figure(2);

plot(t,plasmid_cytoplasmic_Ad5,'k')
hold on
plot(t,plasmid_vesicular_Ad5,'b')
plot(t,plasmid_nuclear_Ad5,'g')
plot(t,plasmid_total_Ad5,'r')
title('Internalization, Trafficking and Nuclear Uptake Kinetics for Ad5')
xlabel('Time (min)')
ylabel('Normalized Plasmid Number per Cell')
legend('Cytoplasmic','Vesicular','Nuclear-associated','Total Cellular')

%Now for the X-link Specific Model

[t,y]=ode15s(@Ad5_model,time,IC_Polymer);

plasmid_vesicular_Xlink = y(:,2) + y(:,3);
plasmid_cytoplasmic_Xlink = y(:,5) + y(:,6) +  y(:,10) + y(:,12);
plasmid_nuclear_Xlink = y(:,7) + y(:,8) + y(:,9) + y(:,13) + y(:,14) + y(:,15);
plasmid_total_Xlink = plasmid_cytoplasmic_Xlink + plasmid_nuclear_Xlink +
plasmid_vesicular_Xlink;

figure(3);

plot(t,plasmid_cytoplasmic_Xlink,'k')
hold on
plot(t,plasmid_vesicular_Xlink,'b')
plot(t,plasmid_nuclear_Xlink,'g')
plot(t,plasmid_total_Xlink,'r')
title('Internalization, Trafficking and Nuclear Uptake Kinetics for X-link')
xlabel('Time (min)')
ylabel('Normalized Plasmid Number per Cell')
legend('Cytoplasmic','Vesicular','Nuclear-associated','Total Cellular')
```

```
%The following are the function files that the main script calls.

function dydt=C32_model(t, x)

%All rate constants are in min^-1.
%Inital conditon is: VectPlas_Ext=5e5, everything else is 0;

%These are the rate constant values from the Jacobian fit:
k_bind_uptake=1.99e-2; %fit.
k_traffic=1.07e2; %fit.
k_deg_vesicle=9.53e-1; %fit.
k_escape=9.51e-1; %fit.
k_unpack=2.79e-1; %fit.
k_deg=5e-3;
k_bind_vector=2.99e-1; %fit.
k_bind_plasmid=2e-3;
k_NPC=1e3;
k_in=3e-3;
k_dissociation=1e3; %Written as k_dis in schematic so it would fit in there.
k_protein=1e2;


%Relevant species to put into the ODE function.

VectPlas_Ext=x(1);
VectPlas_Int=x(2);
VectPlas_LateVes=x(3);
X_PLas_Ves=x(4);
VectPlas_Cyt=x(5);
VectPlasBound_Cyt=x(6);
VectPlasBound_NPC=x(7);
VectPlasBound_Nuc=x(8);
VectPlas_Nuc=x(9);
Plas_Cyt=x(10);
Vect_Cyt=x(11);
PlasBound_Cyt=x(12);
PlasBound_NPC=x(13);
PlasBound_Nuc=x(14);
Plas_Nuc=x(15);
X_Plas_Cyt=x(16);
Protein=x(17);
```

```
%Model Equations

dydt(1,:)=-k_bind_uptake*x(1); %VectPlas_Ext
dydt(2,:)=k_bind_uptake*x(1)-k_traffic*x(2); %VectPlas_Int
dydt(3,:)=k_traffic*x(2)-k_deg_vesicle*x(3)-k_escape*x(3); %VectPlas_LateVes
dydt(4,:)=k_deg_vesicle*x(3); %X_Plas_Ves
dydt(5,:)=k_escape*x(3)-k_bind_vector*x(5)-k_unpack*x(5); %VectPLas_Cyt
dydt(6,:)=k_bind_vector*x(5)-k_NPC*x(6); %VectPlasBound_Cyt
dydt(7,:)=k_NPC*x(6)-k_in*x(7); %VectPlasBound_NPC
dydt(8,:)=k_in*x(7)-k_dissociation*x(8); %VectPlasBound_Nuc
dydt(9,:)=k_dissociation*x(8)-k_unpack*x(9); %VectPlas_Nuc
dydt(10,:)=k_unpack*x(5)-k_deg*x(10)-k_bind_plasmid*x(10); %Plas_Cyt
dydt(11,:)=k_unpack*x(5); %VectCyt
dydt(12,:)=k_bind_plasmid*x(10)-k_NPC*x(12); %PlasBound_Cyt
dydt(13,:)=k_NPC*x(12)-k_in*x(13); %PlasBound_NPC
dydt(14,:)=k_in*x(13)-k_dissociation*x(14); %PlasBound_Nuc
dydt(15,:)=k_unpack*x(9)+k_dissociation*x(14); %Plas_Nuc
dydt(16,:)=k_deg*x(10); %X_Plas_Cyt
dydt(17,:)=k_protein*x(15); %Protein


%The Ad5 and Xlink Model Functions have the same variable assignments and model
equations, they just use different parameters, which are listed below for brevity.


function dydt=Ad5_model(t, x)


%All rate constants are in min^-1.
%Inital conditon is: VectPlas_Ext=20, everything else is 0;

%These are the rate constant values from the Jacobian fit:
k_bind_uptake=1.17e-2; %fit.
k_traffic=1.17e1; %fit.
k_deg_vesicle=3.84e-1; %fit.
k_escape=1.15; %fit.
k_unpack=3.48e-1; %fit.
k_deg=5e-3;
k_bind_vector=3.98e-1; %fit.
k_bind_plasmid=2e-3;
k_NPC=1e3;
k_in=3e-3;
k_dissociation=1e3; %Written as k_dis in schematic so it would fit in there.
k_protein=1e2;
```

```
function dydt=Xlink_model(t, x)


%All rate constants are in min^-1.
%Inital conditon is: VectPlas_Ext=20, everything else is 0;

%These are the rate constant values from the Jacobian fit:
k_bind_uptake=5.14e-3; %fit.
k_traffic=9.5e1; %fit.
k_deg_vesicle=9.99e-1; %fit.
k_escape=9.50; %fit.
k_unpack=9.89e-1; %fit.
k_deg=5e-3;
k_bind_vector=9.46e-1; %fit.
k_bind_plasmid=2e-3;
k_NPC=1e3;
k_in=3e-3;
k_dissociation=1e3; %Written as k_dis in schematic so it would fit in there.
k_protein=1e2;
```

Graphical Model Structure Built in Teranode and Imported into Jacobian in SBML

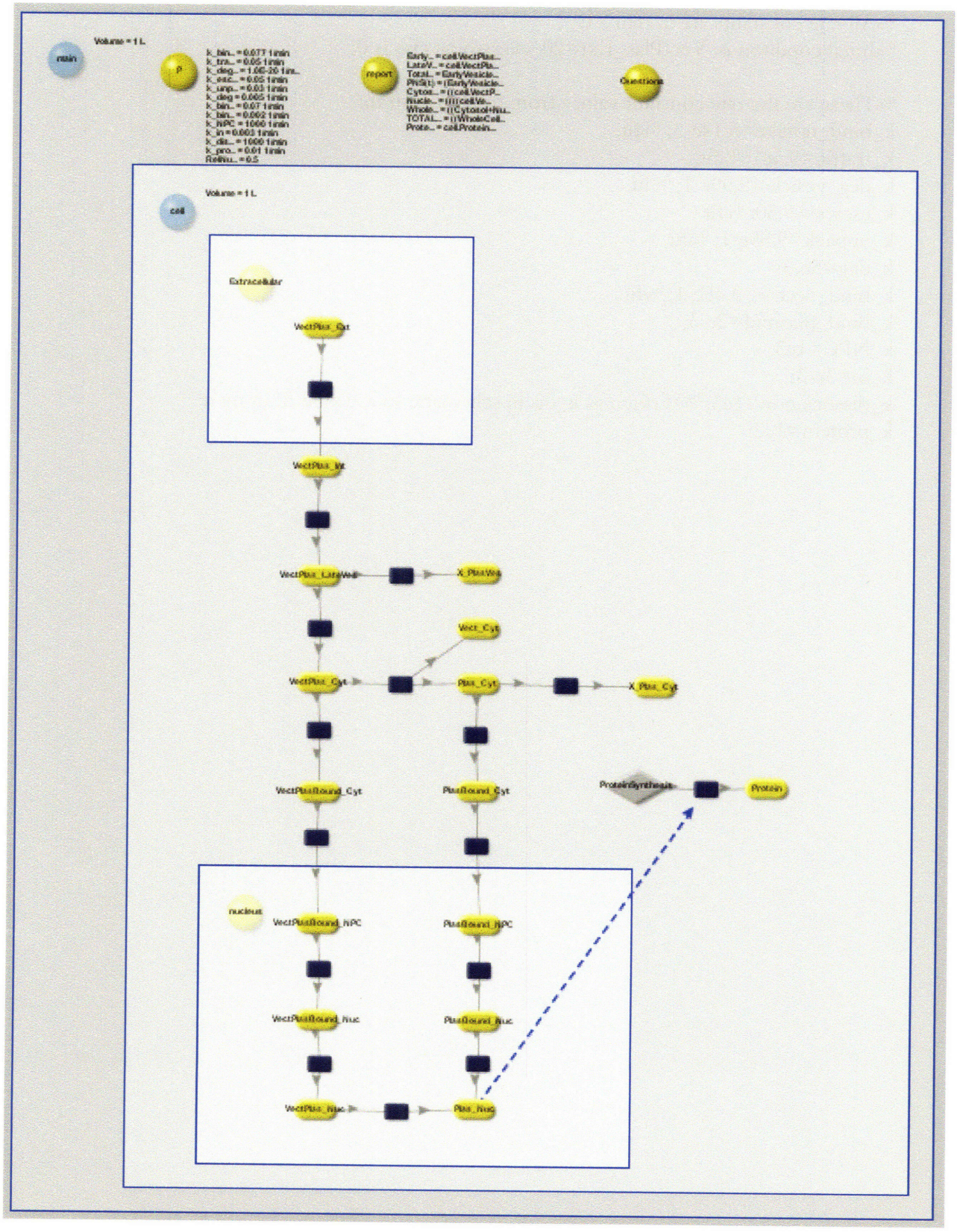

Jacobian Code: Parameter Fitting, Simulations, Sensitivity Analysis and Multi-Start

```
# JACOBIAN input file created from SBML file: "NatesModel_4.xml"#
#########################################################################
##############

DECLARE
TYPE
    JAC_Default_Type = 0.0 : -1.0e20 : 1.0e20    unit = "none"
ENUMERATION
    cell_VARS              IS {PlasBound_Cyt, PlasBound_NPC,
PlasBound_Nuc, Plas_Cyt, Plas_Nuc, Protein, ProteinSynthesis,
Rxn10_Flux, Rxn11_Flux, Rxn12_Flux, Rxn13_Flux, Rxn14_Flux, Rxn15_Flux,
Rxn1_Flux, Rxn2_Flux, Rxn3_Flux, Rxn4_Flux, Rxn5_Flux, Rxn6_Flux,
Rxn7_Flux, Rxn8_Flux, Rxn9_Flux, Rxn_Flux, VectPlasBound_Cyt,
VectPlasBound_NPC, VectPlasBound_Nuc, VectPlas_Cyt, VectPlas_Ext,
VectPlas_Int, VectPlas_LateVes, VectPlas_Nuc, Vect_Cyt, X_PlasVes,
X_Plas_Cyt}
    cell_PARAM             IS {Volume}
    main_VARS              IS {report_Cytosol, report_CytosolX,
report_EarlyVesicles, report_LateVesicles, report_LateVesiclesX,
report_Nuclear, report_PNS, report_PNSX1, report_PNSX2, report_PNSX3,
report_Protein, report_TOTAL, report_TotalVesicles,
report_TotalVesiclesX, report_WholeCell, report_WholeCellX1,
report_WholeCellX2, report_WholeCellX3}
    main_PARAM             IS {P_k_NPC, P_k_bind_plasmid,
P_k_bind_uptake, P_k_bind_vector, P_k_deg, P_k_deg_vesicle,
P_k_dissociation, P_k_escape, P_k_in, P_k_protein, P_k_traffic,
P_k_unpack, PlasBound_Cyt_cell_0, PlasBound_NPC_cell_0,
PlasBound_Nuc_cell_0, Plas_Cyt_cell_0, Plas_Nuc_cell_0, Protein_cell_0,
VectPlasBound_Cyt_cell_0, VectPlasBound_NPC_cell_0,
VectPlasBound_Nuc_cell_0, VectPlas_Cyt_cell_0, VectPlas_Ext_cell_0,
VectPlas_Int_cell_0, VectPlas_LateVes_cell_0, VectPlas_Nuc_cell_0,
Vect_Cyt_cell_0, Volume, X_PlasVes_cell_0, X_Plas_Cyt_cell_0}
    Top_PARAM              IS {Volume}
END


#########################################################################

EXTERNAL PARAM_ASSIGN(STATUS,DEPENDENT,CONSTANT INTEGER,CONSTANT
INTEGER,CHARACTER)
OPTIONS
   LIB_NAME := "ParameterAssign" ;
   LIB_PATH := "C:\Program Files\Jacobian\Lib" ;
   LANGUAGE := "C" ;
   BLACK_BOX := TRUE ;
END
```

```
########################################################################

MODEL cell
PARAMETER
    P AS ARRAY(cell_PARAM) OF REAL DEFAULT 0
    L AS ARRAY(cell_PARAM) OF REAL DEFAULT 0
    U AS ARRAY(cell_PARAM) OF REAL DEFAULT 1e8
    PName AS ARRAY(cell_PARAM) OF STRING DEFAULT ""
    XName AS ARRAY(cell_VARS) OF STRING DEFAULT ""
UNIT
# empty UNIT section
VARIABLE
    X AS ARRAY(cell_VARS) OF JAC_Default_Type
SET
    XName(PlasBound_Cyt)                := "PlasBound_Cyt" ;
    XName(PlasBound_NPC)                := "PlasBound_NPC" ;
    XName(PlasBound_Nuc)                := "PlasBound_Nuc" ;
    XName(Plas_Cyt)                     := "Plas_Cyt" ;
    XName(Plas_Nuc)                     := "Plas_Nuc" ;
    XName(Protein)                      := "Protein" ;
    XName(ProteinSynthesis)             := "ProteinSynthesis" ;
    XName(Rxn10_Flux)                   := "Rxn10_Flux" ;
    XName(Rxn11_Flux)                   := "Rxn11_Flux" ;
    XName(Rxn12_Flux)                   := "Rxn12_Flux" ;
    XName(Rxn13_Flux)                   := "Rxn13_Flux" ;
    XName(Rxn14_Flux)                   := "Rxn14_Flux" ;
    XName(Rxn15_Flux)                   := "Rxn15_Flux" ;
    XName(Rxn1_Flux)                    := "Rxn1_Flux" ;
    XName(Rxn2_Flux)                    := "Rxn2_Flux" ;
    XName(Rxn3_Flux)                    := "Rxn3_Flux" ;
    XName(Rxn4_Flux)                    := "Rxn4_Flux" ;
    XName(Rxn5_Flux)                    := "Rxn5_Flux" ;
    XName(Rxn6_Flux)                    := "Rxn6_Flux" ;
    XName(Rxn7_Flux)                    := "Rxn7_Flux" ;
    XName(Rxn8_Flux)                    := "Rxn8_Flux" ;
    XName(Rxn9_Flux)                    := "Rxn9_Flux" ;
    XName(Rxn_Flux)                     := "Rxn_Flux" ;
    XName(VectPlasBound_Cyt)            := "VectPlasBound_Cyt" ;
    XName(VectPlasBound_NPC)            := "VectPlasBound_NPC" ;
    XName(VectPlasBound_Nuc)            := "VectPlasBound_Nuc" ;
    XName(VectPlas_Cyt)                 := "VectPlas_Cyt" ;
    XName(VectPlas_Ext)                 := "VectPlas_Ext" ;
    XName(VectPlas_Int)                 := "VectPlas_Int" ;
    XName(VectPlas_LateVes)             := "VectPlas_LateVes" ;
    XName(VectPlas_Nuc)                 := "VectPlas_Nuc" ;
    XName(Vect_Cyt)                     := "Vect_Cyt" ;
    XName(X_PlasVes)                    := "X_PlasVes" ;
    XName(X_Plas_Cyt)                   := "X_Plas_Cyt" ;
    # 34 variables
    PName(Volume)                       := "Volume" ;
    P(Volume)                           := 1 ;
    L(Volume)                           := 1 ;
    U(Volume)                           := 1 ;
EQUATION
# empty EQUATION section
END
```

```
MODEL main
PARAMETER
    P AS ARRAY(main_PARAM) OF REAL DEFAULT 0
    L AS ARRAY(main_PARAM) OF REAL DEFAULT 0
    U AS ARRAY(main_PARAM) OF REAL DEFAULT 1e8
    PName AS ARRAY(main_PARAM) OF STRING DEFAULT ""
    XName AS ARRAY(main_VARS) OF STRING DEFAULT ""

UNIT
    cell AS cell
VARIABLE
    X AS ARRAY(main_VARS) OF JAC_Default_Type
SET
    XName(report_Cytosol)                := "report_Cytosol" ;
    XName(report_CytosolX)               := "report_CytosolX" ;
    XName(report_EarlyVesicles)          := "report_EarlyVesicles" ;
    XName(report_LateVesicles)           := "report_LateVesicles" ;
    XName(report_LateVesiclesX)          := "report_LateVesiclesX" ;
    XName(report_Nuclear)                := "report_Nuclear" ;
    XName(report_PNS)                    := "report_PNS" ;
    XName(report_PNSX1)                  := "report_PNSX1" ;
    XName(report_PNSX2)                  := "report_PNSX2" ;
    XName(report_PNSX3)                  := "report_PNSX3" ;
    XName(report_Protein)                := "report_Protein" ;
    XName(report_TOTAL)                  := "report_TOTAL" ;
    XName(report_TotalVesicles)          := "report_TotalVesicles" ;
    XName(report_TotalVesiclesX)         := "report_TotalVesiclesX" ;
    XName(report_WholeCell)              := "report_WholeCell" ;
    XName(report_WholeCellX1)            := "report_WholeCellX1" ;
    XName(report_WholeCellX2)            := "report_WholeCellX2" ;
    XName(report_WholeCellX3)            := "report_WholeCellX3" ;
    # 18 variables

    PName(P_k_NPC)                       := "P_k_NPC" ;
    PName(P_k_bind_plasmid)              := "P_k_bind_plasmid" ;
    PName(P_k_bind_uptake)               := "P_k_bind_uptake" ;
    PName(P_k_bind_vector)               := "P_k_bind_vector" ;
    PName(P_k_deg)                       := "P_k_deg" ;
    PName(P_k_deg_vesicle)               := "P_k_deg_vesicle" ;
    PName(P_k_dissociation)              := "P_k_dissociation" ;
    PName(P_k_escape)                    := "P_k_escape" ;
    PName(P_k_in)                        := "P_k_in" ;
    PName(P_k_protein)                   := "P_k_protein" ;
    PName(P_k_traffic)                   := "P_k_traffic" ;
    PName(P_k_unpack)                    := "P_k_unpack" ;
    PName(PlasBound_Cyt_cell_0)          := "PlasBound_Cyt_cell_0" ;
    PName(PlasBound_NPC_cell_0)          := "PlasBound_NPC_cell_0" ;
    PName(PlasBound_Nuc_cell_0)          := "PlasBound_Nuc_cell_0" ;
    PName(Plas_Cyt_cell_0)               := "Plas_Cyt_cell_0" ;
    PName(Plas_Nuc_cell_0)               := "Plas_Nuc_cell_0" ;
    PName(Protein_cell_0)                := "Protein_cell_0" ;
    PName(VectPlasBound_Cyt_cell_0)      := "VectPlasBound_Cyt_cell_0" ;
    PName(VectPlasBound_NPC_cell_0)      := "VectPlasBound_NPC_cell_0" ;
    PName(VectPlasBound_Nuc_cell_0)      := "VectPlasBound_Nuc_cell_0" ;
    PName(VectPlas_Cyt_cell_0)           := "VectPlas_Cyt_cell_0" ;
    PName(VectPlas_Ext_cell_0)           := "VectPlas_Ext_cell_0" ;
```

```
PName(VectPlas_Int_cell_0)          := "VectPlas_Int_cell_0" ;
PName(VectPlas_LateVes_cell_0)      := "VectPlas_LateVes_cell_0" ;
PName(VectPlas_Nuc_cell_0)          := "VectPlas_Nuc_cell_0" ;
PName(Vect_Cyt_cell_0)              := "Vect_Cyt_cell_0" ;
PName(Volume)                       := "Volume" ;
PName(X_PlasVes_cell_0)             := "X_PlasVes_cell_0" ;
PName(X_Plas_Cyt_cell_0)            := "X_Plas_Cyt_cell_0" ;
# 30 parameters

P(P_k_NPC)                          := 1000 ;
P(P_k_bind_plasmid)                 := 0.002 ;
P(P_k_bind_uptake)                  := 0.077 ;
P(P_k_bind_vector)                  := 0.07 ;
P(P_k_deg)                          := 0.005 ;
P(P_k_deg_vesicle)                  := 1e-2 ;
P(P_k_dissociation)                 := 1000 ;
P(P_k_escape)                       := 0.05 ;
P(P_k_in)                           := 0.003 ;
P(P_k_protein)                      := 0.01 ;
P(P_k_traffic)                      := 0.05 ;
P(P_k_unpack)                       := 0.03 ;
P(Volume)                           := 1 ;

L(P_k_NPC)                          := 1000 ;
L(P_k_bind_plasmid)                 := 0.002 ;
L(P_k_bind_uptake)                  := 0.077 * 1e-2;
L(P_k_bind_vector)                  := 1e-5 ;  # to be fitted
L(P_k_deg)                          := 0.005 ;
L(P_k_deg_vesicle)                  := 1e-4 ;  # to be fitted
L(P_k_dissociation)                 := 1000 ;
L(P_k_escape)                       := 1e-4 ;  # to be fitted
L(P_k_in)                           := 0.003 ;
L(P_k_protein)                      := 0.01 ;
L(P_k_traffic)                      := 1e-4 ;  # to be fitted
L(P_k_unpack)                       := 1e-4 ;  # to be fitted
L(Volume)                           := 1 ;

U(P_k_NPC)                          := 1000 ;
U(P_k_bind_plasmid)                 := 0.002 ;
U(P_k_bind_uptake)                  := 0.077 * 1e2 ;
U(P_k_bind_vector)                  := 1e1 ;  # to be fitted
U(P_k_deg)                          := 0.005 ;
U(P_k_deg_vesicle)                  := 1e0 ;  # to be fitted
U(P_k_dissociation)                 := 1000 ;
U(P_k_escape)                       := 1e2 ;  # to be fitted
U(P_k_in)                           := 0.003 ;
U(P_k_protein)                      := 0.01 ;
U(P_k_traffic)                      := 1e3 ;  # to be fitted
U(P_k_unpack)                       := 1e0 ;  # to be fitted
U(Volume)                           := 1 ;

EQUATION
# empty EQUATION section
END
```

```
# ------------------------------------------------------------------------

MODEL Top
PARAMETER

UNIT
    main AS main
VARIABLE
SET
    # 0 variables

# Zero initial conditions:
    main.P(PlasBound_Cyt_cell_0)        := 0 ;
    main.P(PlasBound_NPC_cell_0)        := 0 ;
    main.P(PlasBound_Nuc_cell_0)        := 0 ;
    main.P(Plas_Cyt_cell_0)             := 0 ;
    main.P(Plas_Nuc_cell_0)             := 0 ;
    main.P(Protein_cell_0)              := 0 ;
    main.P(VectPlasBound_Cyt_cell_0)    := 0 ;
    main.P(VectPlasBound_NPC_cell_0)    := 0 ;
    main.P(VectPlasBound_Nuc_cell_0)    := 0 ;
    main.P(VectPlas_Cyt_cell_0)         := 0 ;
    main.P(VectPlas_Int_cell_0)         := 0 ;
    main.P(VectPlas_LateVes_cell_0)     := 0 ;
    main.P(VectPlas_Nuc_cell_0)         := 0 ;
    main.P(Vect_Cyt_cell_0)             := 0 ;
    main.P(X_PlasVes_cell_0)            := 0 ;
    main.P(X_Plas_Cyt_cell_0)           := 0 ;
# Non-zero initial conditions:
    main.P(VectPlas_Ext_cell_0)         := 500000 ;


# Initial condition LOWER bounds .....................
# Zero initial conditions:
    main.L(PlasBound_Cyt_cell_0)        := 0 ;
    main.L(PlasBound_NPC_cell_0)        := 0 ;
    main.L(PlasBound_Nuc_cell_0)        := 0 ;
    main.L(Plas_Cyt_cell_0)             := 0 ;
    main.L(Plas_Nuc_cell_0)             := 0 ;
    main.L(Protein_cell_0)              := 0 ;
    main.L(VectPlasBound_Cyt_cell_0)    := 0 ;
    main.L(VectPlasBound_NPC_cell_0)    := 0 ;
    main.L(VectPlasBound_Nuc_cell_0)    := 0 ;
    main.L(VectPlas_Cyt_cell_0)         := 0 ;
    main.L(VectPlas_Int_cell_0)         := 0 ;
    main.L(VectPlas_LateVes_cell_0)     := 0 ;
    main.L(VectPlas_Nuc_cell_0)         := 0 ;
    main.L(Vect_Cyt_cell_0)             := 0 ;
    main.L(X_PlasVes_cell_0)            := 0 ;
    main.L(X_Plas_Cyt_cell_0)           := 0 ;
# Non-zero initial conditions:
    main.L(VectPlas_Ext_cell_0)         := 20;


# Initial condition UPPER bounds .....................
# Zero initial conditions:
    main.U(PlasBound_Cyt_cell_0)        := 0 ;
```

```
    main.U(PlasBound_NPC_cell_0)          := 0 ;
    main.U(PlasBound_Nuc_cell_0)          := 0 ;
    main.U(Plas_Cyt_cell_0)               := 0 ;
    main.U(Plas_Nuc_cell_0)               := 0 ;
    main.U(Protein_cell_0)                := 0 ;
    main.U(VectPlasBound_Cyt_cell_0)      := 0 ;
    main.U(VectPlasBound_NPC_cell_0)      := 0 ;
    main.U(VectPlasBound_Nuc_cell_0)      := 0 ;
    main.U(VectPlas_Cyt_cell_0)           := 0 ;
    main.U(VectPlas_Int_cell_0)           := 0 ;
    main.U(VectPlas_LateVes_cell_0)       := 0 ;
    main.U(VectPlas_Nuc_cell_0)           := 0 ;
    main.U(Vect_Cyt_cell_0)               := 0 ;
    main.U(X_PlasVes_cell_0)              := 0 ;
    main.U(X_Plas_Cyt_cell_0)             := 0 ;
# Non-zero initial conditions:
    main.U(VectPlas_Ext_cell_0)           := 20;

INTERMEDIATE
    Rxn3_Kf                               := main.P(P_k_escape) ;
    Rxn2_Kf                               := main.P(P_k_deg_vesicle) ;
    Rxn4_Kf                               := main.P(P_k_bind_vector) ;
    Rxn_Kf                                := main.P(P_k_bind_uptake) ;
    Rxn8_Kf                               := main.P(P_k_dissociation) ;
    Rxn10_Kf                              := main.P(P_k_dissociation) ;
    Rxn1_Kf                               := main.P(P_k_traffic) ;
    Rxn5_Kf                               := main.P(P_k_unpack) ;
    Rxn12_Kf                              := main.P(P_k_bind_plasmid) ;
    Rxn11_Kf                              := main.P(P_k_deg) ;
    Rxn15_Kf                              :=
main.P(P_k_protein)*main.cell.X(Plas_Nuc) ;
    Rxn9_Kf                               := main.P(P_k_unpack) ;
    Rxn13_Kf                              := main.P(P_k_NPC) ;
    Rxn7_Kf                               := main.P(P_k_in) ;
    Rxn14_Kf                              := main.P(P_k_in) ;
    Rxn6_Kf                               := main.P(P_k_NPC) ;

EQUATION
# Flux Equations:
    main.cell.X(Rxn2_Flux)                =
Rxn2_Kf*main.cell.X(VectPlas_LateVes)*main.cell.P(Volume) ;
    main.cell.X(Rxn4_Flux)                =
Rxn4_Kf*main.cell.X(VectPlas_Cyt)*main.cell.P(Volume) ;
    main.cell.X(Rxn3_Flux)                =
Rxn3_Kf*main.cell.X(VectPlas_LateVes)*main.cell.P(Volume) ;
    main.cell.X(Rxn1_Flux)                =
Rxn1_Kf*main.cell.X(VectPlas_Int)*main.cell.P(Volume) ;
    main.cell.X(Rxn8_Flux)                =
Rxn8_Kf*main.cell.X(VectPlasBound_Nuc)*main.cell.P(Volume) ;
    main.cell.X(Rxn11_Flux)               =
Rxn11_Kf*main.cell.X(Plas_Cyt)*main.cell.P(Volume) ;
    main.cell.X(Rxn10_Flux)               =
Rxn10_Kf*main.cell.X(PlasBound_Nuc)*main.cell.P(Volume) ;
    main.cell.X(Rxn12_Flux)               =
Rxn12_Kf*main.cell.X(Plas_Cyt)*main.cell.P(Volume) ;
    main.cell.X(Rxn_Flux)                 =
Rxn_Kf*main.cell.X(VectPlas_Ext)*main.cell.P(Volume) ;
```

```
    main.cell.X(Rxn5_Flux)              =
Rxn5_Kf*main.cell.X(VectPlas_Cyt)*main.cell.P(Volume) ;
    main.cell.X(Rxn15_Flux)             = Rxn15_Kf*main.cell.P(Volume)
;
    main.cell.X(Rxn14_Flux)             =
Rxn14_Kf*main.cell.X(PlasBound_NPC)*main.cell.P(Volume) ;
    main.cell.X(Rxn7_Flux)              =
Rxn7_Kf*main.cell.X(VectPlasBound_NPC)*main.cell.P(Volume) ;
    main.cell.X(Rxn9_Flux)              =
Rxn9_Kf*main.cell.X(VectPlas_Nuc)*main.cell.P(Volume) ;
    main.cell.X(Rxn6_Flux)              =
Rxn6_Kf*main.cell.X(VectPlasBound_Cyt)*main.cell.P(Volume) ;
    main.cell.X(Rxn13_Flux)             =
Rxn13_Kf*main.cell.X(PlasBound_Cyt)*main.cell.P(Volume) ;
# Algebraic Equations:
    main.X(report_EarlyVesicles)        = main.cell.X(VectPlas_Int) ;
    main.X(report_CytosolX)             =
main.cell.X(VectPlas_Cyt)+main.cell.X(Plas_Cyt)+main.cell.X(VectPlasBou
nd_Cyt)+main.cell.X(PlasBound_Cyt)+main.cell.X(X_Plas_Cyt) ;
    main.X(report_Nuclear)              =
main.cell.X(VectPlasBound_NPC)+main.cell.X(VectPlasBound_Nuc)+main.cell
.X(VectPlas_Nuc)+main.cell.X(PlasBound_NPC)+main.cell.X(PlasBound_Nuc)+
main.cell.X(Plas_Nuc) ;
    main.X(report_Protein)              = main.cell.X(Protein) ;
    main.X(report_LateVesiclesX)        =
main.cell.X(VectPlas_LateVes)+main.cell.X(X_PlasVes) ;
    main.X(report_WholeCellX3)          =
main.X(report_CytosolX)+main.X(report_Nuclear)+main.X(report_EarlyVesic
les)+main.X(report_LateVesiclesX) ;
    main.X(report_TotalVesiclesX)       =
main.X(report_EarlyVesicles)+main.X(report_LateVesiclesX) ;
    main.X(report_Cytosol)              =
main.cell.X(VectPlas_Cyt)+main.cell.X(Plas_Cyt)+main.cell.X(VectPlasBou
nd_Cyt)+main.cell.X(PlasBound_Cyt) ;
    main.X(report_LateVesicles)         = main.cell.X(VectPlas_LateVes)
;
    main.X(report_PNSX3)                =
main.X(report_EarlyVesicles)+main.X(report_LateVesiclesX)+main.X(report
_CytosolX) ;
    main.X(report_WholeCellX2)          =
main.X(report_Cytosol)+main.X(report_Nuclear)+main.X(report_EarlyVesicl
es)+main.X(report_LateVesiclesX) ;
    main.X(report_TOTAL)                = main.X(report_WholeCellX3) ;
    main.X(report_PNS)                  =
main.X(report_EarlyVesicles)+main.X(report_LateVesicles)+main.X(report_
Cytosol) ;
    main.X(report_PNSX2)                =
main.X(report_EarlyVesicles)+main.X(report_LateVesiclesX)+main.X(report
_Cytosol) ;
    main.X(report_PNSX1)                =
main.X(report_EarlyVesicles)+main.X(report_LateVesicles)+main.X(report_
CytosolX) ;
    main.X(report_WholeCell)            =
main.X(report_Cytosol)+main.X(report_Nuclear)+main.X(report_EarlyVesicl
es)+main.X(report_LateVesicles) ;
```

```
    main.X(report_WholeCellX1)          =
main.X(report_CytosolX)+main.X(report_Nuclear)+main.X(report_EarlyVesic
les)+main.X(report_LateVesicles) ;
    main.X(report_TotalVesicles)        =
main.X(report_EarlyVesicles)+main.X(report_LateVesicles) ;
    main.cell.X(ProteinSynthesis)       = 1 ;
# ODEs:
    main.cell.$X(VectPlas_Int)*main.cell.P(Volume)                  =  +
(main.cell.X(Rxn_Flux)) - (main.cell.X(Rxn1_Flux));
    main.cell.$X(VectPlas_LateVes)*main.cell.P(Volume)              =  +
(main.cell.X(Rxn1_Flux)) - (main.cell.X(Rxn2_Flux)) -
(main.cell.X(Rxn3_Flux));
    main.cell.$X(X_PlasVes)*main.cell.P(Volume)                     =  +
(main.cell.X(Rxn2_Flux));
    main.cell.$X(VectPlas_Cyt)*main.cell.P(Volume)                  =  +
(main.cell.X(Rxn3_Flux)) - (main.cell.X(Rxn4_Flux)) -
(main.cell.X(Rxn5_Flux));
    main.cell.$X(VectPlasBound_Cyt)*main.cell.P(Volume)             =  +
(main.cell.X(Rxn4_Flux)) - (main.cell.X(Rxn6_Flux));
    main.cell.$X(Plas_Cyt)*main.cell.P(Volume)                      =  +
(main.cell.X(Rxn5_Flux)) - (main.cell.X(Rxn11_Flux)) -
(main.cell.X(Rxn12_Flux));
    main.cell.$X(Vect_Cyt)*main.cell.P(Volume)                      =  +
(main.cell.X(Rxn5_Flux));
    main.cell.$X(PlasBound_Cyt)*main.cell.P(Volume)                 =  +
(main.cell.X(Rxn12_Flux)) - (main.cell.X(Rxn13_Flux));
    main.cell.$X(X_Plas_Cyt)*main.cell.P(Volume)                    =  +
(main.cell.X(Rxn11_Flux));
    main.cell.$X(Protein)*main.cell.P(Volume)                       =  +
(main.cell.X(Rxn15_Flux));
    main.cell.$X(VectPlasBound_NPC)*main.cell.P(Volume)             =  -
(main.cell.X(Rxn7_Flux)) + (main.cell.X(Rxn6_Flux));
    main.cell.$X(VectPlasBound_Nuc)*main.cell.P(Volume)             =  +
(main.cell.X(Rxn7_Flux)) - (main.cell.X(Rxn8_Flux));
    main.cell.$X(VectPlas_Nuc)*main.cell.P(Volume)                  =  +
(main.cell.X(Rxn8_Flux)) - (main.cell.X(Rxn9_Flux));
    main.cell.$X(PlasBound_NPC)*main.cell.P(Volume)                 =  -
(main.cell.X(Rxn14_Flux)) + (main.cell.X(Rxn13_Flux));
    main.cell.$X(PlasBound_Nuc)*main.cell.P(Volume)                 =  -
(main.cell.X(Rxn10_Flux)) + (main.cell.X(Rxn14_Flux));
    main.cell.$X(Plas_Nuc)*main.cell.P(Volume)                      =  +
(main.cell.X(Rxn9_Flux)) + (main.cell.X(Rxn10_Flux));
    main.cell.$X(VectPlas_Ext)*main.cell.P(Volume)                  =  -
(main.cell.X(Rxn_Flux));
    # 52 equations (variables)
END

##########################################################################
```

```
SIMULATION Sim
OPTIONS
    INIT_RELATIVE_TOLERANCE     := 1.0e-12 ; # Tolerances may need to be
adjusted ... as high as 1e-8, 1e-8, 1e-4, 1e-8
    INIT_ABSOLUTE_TOLERANCE     := 1.0e-12 ;
    DYNAMIC_RELATIVE_TOLERANCE  := 1.0e-7  ;
    DYNAMIC_ABSOLUTE_TOLERANCE  := 1.0e-12 ;
    DYNAMIC_REPORTING_INTERVAL  := 1       ;
    NORMALIZED_SENS             := TRUE    ;
    COMPUTE_METRICS             := TRUE    ; # compute integrals and
such
    CSVOUTPUT                   := TRUE    ; # write output files in csv
format
    DYNAMIC_PRINT_LEVEL         := 0 ; # suppress screen output
    DYNAMIC_MAXIMUM_STEPS       := 50000 ; # limit max steps
PARAMETER
    SimulationTime AS REAL DEFAULT 120

UNIT
   Top AS Top
REPORT
    Top.main.X(report_Cytosol)
    Top.main.X(report_CytosolX)
    Top.main.X(report_EarlyVesicles)
    Top.main.X(report_LateVesicles)
    Top.main.X(report_LateVesiclesX)
    Top.main.X(report_Nuclear)
    Top.main.X(report_PNS)
    Top.main.X(report_PNSX1)
    Top.main.X(report_PNSX2)
    Top.main.X(report_PNSX3)
    Top.main.X(report_Protein)
    Top.main.X(report_TOTAL)
    Top.main.X(report_TotalVesicles)
    Top.main.X(report_TotalVesiclesX)
    Top.main.X(report_WholeCell)
    Top.main.X(report_WholeCellX1)
    Top.main.X(report_WholeCellX2)
    Top.main.X(report_WholeCellX3)
SENSITIVITY
## initial conditions (only non-zero initial conditions are listed):
(uncomment desired lines to activate)
#    Top.main.P(VectPlas_Ext_cell_0)
## parameters: (uncomment desired lines to activate)
#    Top.main.P(P_k_NPC)
#    Top.main.P(P_k_bind_plasmid)
#    Top.main.P(P_k_bind_uptake)
#    Top.main.P(P_k_bind_vector)
#    Top.main.P(P_k_deg)
#    Top.main.P(P_k_deg_vesicle)
#    Top.main.P(P_k_dissociation)
#    Top.main.P(P_k_escape)
#    Top.main.P(P_k_in)
#    Top.main.P(P_k_protein)
#    Top.main.P(P_k_traffic)
#    Top.main.P(P_k_unpack)
SET
```

```
EQUATION
# empty equation section
INPUT
# empty input section

PRESET
# empty preset section
SELECTOR
# empty selector section
INITIAL
    Top.main.cell.X(PlasBound_Cyt)          =
Top.main.P(PlasBound_Cyt_cell_0) ;
    Top.main.cell.X(PlasBound_NPC)          =
Top.main.P(PlasBound_NPC_cell_0) ;
    Top.main.cell.X(PlasBound_Nuc)          =
Top.main.P(PlasBound_Nuc_cell_0) ;
    Top.main.cell.X(Plas_Cyt)               =
Top.main.P(Plas_Cyt_cell_0) ;
    Top.main.cell.X(Plas_Nuc)               =
Top.main.P(Plas_Nuc_cell_0) ;
    Top.main.cell.X(Protein)                =
Top.main.P(Protein_cell_0) ;
    Top.main.cell.X(VectPlasBound_Cyt)      =
Top.main.P(VectPlasBound_Cyt_cell_0) ;
    Top.main.cell.X(VectPlasBound_NPC)      =
Top.main.P(VectPlasBound_NPC_cell_0) ;
    Top.main.cell.X(VectPlasBound_Nuc)      =
Top.main.P(VectPlasBound_Nuc_cell_0) ;
    Top.main.cell.X(VectPlas_Cyt)           =
Top.main.P(VectPlas_Cyt_cell_0) ;
    Top.main.cell.X(VectPlas_Ext)           = 20;
#Top.main.P(VectPlas_Ext_cell_0) ;
    Top.main.cell.X(VectPlas_Int)           =
Top.main.P(VectPlas_Int_cell_0) ;
    Top.main.cell.X(VectPlas_LateVes)       =
Top.main.P(VectPlas_LateVes_cell_0) ;
    Top.main.cell.X(VectPlas_Nuc)           =
Top.main.P(VectPlas_Nuc_cell_0) ;
    Top.main.cell.X(Vect_Cyt)               =
Top.main.P(Vect_Cyt_cell_0) ;
    Top.main.cell.X(X_PlasVes)              =
Top.main.P(X_PlasVes_cell_0) ;
    Top.main.cell.X(X_Plas_Cyt)             =
Top.main.P(X_Plas_Cyt_cell_0) ;
SCHEDULE
    CONTINUE FOR SimulationTime
END

##########################################################################
###############
##########################################################################
###############
##########################################################################
###############

SIMULATION Sim_Sensitivity
```

```
OPTIONS
    INIT_RELATIVE_TOLERANCE     := 1.0e-12 ; # Tolerances may need to be
adjusted ... as high as 1e-8, 1e-8, 1e-4, 1e-8
    INIT_ABSOLUTE_TOLERANCE     := 1.0e-12 ;
    DYNAMIC_RELATIVE_TOLERANCE  := 1.0e-7  ;
    DYNAMIC_ABSOLUTE_TOLERANCE  := 1.0e-12 ;
    DYNAMIC_REPORTING_INTERVAL  := 1      ;
    NORMALIZED_SENS             := TRUE    ;
    COMPUTE_METRICS             := TRUE    ; # compute integrals and
such
    CSVOUTPUT                   := TRUE    ; # write output files in csv
format
    DYNAMIC_PRINT_LEVEL         := 0 ; # suppress screen output
    DYNAMIC_MAXIMUM_STEPS       := 50000 ; # limit max steps
PARAMETER
    SimulationTime AS REAL DEFAULT 120

UNIT
   Top AS Top
REPORT
    Top.main.X(report_Cytosol)
    Top.main.X(report_CytosolX)
    Top.main.X(report_EarlyVesicles)
    Top.main.X(report_LateVesicles)
    Top.main.X(report_LateVesiclesX)
    Top.main.X(report_Nuclear)
    Top.main.X(report_PNS)
    Top.main.X(report_PNSX1)
    Top.main.X(report_PNSX2)
    Top.main.X(report_PNSX3)
    Top.main.X(report_Protein)
    Top.main.X(report_TOTAL)
    Top.main.X(report_TotalVesicles)
    Top.main.X(report_TotalVesiclesX)
    Top.main.X(report_WholeCell)
    Top.main.X(report_WholeCellX1)
    Top.main.X(report_WholeCellX2)
    Top.main.X(report_WholeCellX3)
SENSITIVITY
## initial conditions (only non-zero initial conditions are listed):
(uncomment desired lines to activate)
   Top.main.P(VectPlas_Ext_cell_0)
## parameters: (uncomment desired lines to activate)
   Top.main.P(P_k_NPC)
   Top.main.P(P_k_bind_plasmid)
   Top.main.P(P_k_bind_uptake)
   Top.main.P(P_k_bind_vector)
   Top.main.P(P_k_deg)
   Top.main.P(P_k_deg_vesicle)
   Top.main.P(P_k_dissociation)
   Top.main.P(P_k_escape)
   Top.main.P(P_k_in)
   Top.main.P(P_k_protein)
   Top.main.P(P_k_traffic)
   Top.main.P(P_k_unpack)
SET
```

```
EQUATION
# empty equation section
INPUT
# empty input section

PRESET
# empty preset section
SELECTOR
# empty selector section
INITIAL
    Top.main.cell.X(PlasBound_Cyt)          =
Top.main.P(PlasBound_Cyt_cell_0) ;
    Top.main.cell.X(PlasBound_NPC)          =
Top.main.P(PlasBound_NPC_cell_0) ;
    Top.main.cell.X(PlasBound_Nuc)          =
Top.main.P(PlasBound_Nuc_cell_0) ;
    Top.main.cell.X(Plas_Cyt)               =
Top.main.P(Plas_Cyt_cell_0) ;
    Top.main.cell.X(Plas_Nuc)               =
Top.main.P(Plas_Nuc_cell_0) ;
    Top.main.cell.X(Protein)                =
Top.main.P(Protein_cell_0) ;
    Top.main.cell.X(VectPlasBound_Cyt)      =
Top.main.P(VectPlasBound_Cyt_cell_0) ;
    Top.main.cell.X(VectPlasBound_NPC)      =
Top.main.P(VectPlasBound_NPC_cell_0) ;
    Top.main.cell.X(VectPlasBound_Nuc)      =
Top.main.P(VectPlasBound_Nuc_cell_0) ;
    Top.main.cell.X(VectPlas_Cyt)           =
Top.main.P(VectPlas_Cyt_cell_0) ;
    Top.main.cell.X(VectPlas_Ext)           = 20;
#Top.main.P(VectPlas_Ext_cell_0) ;
    Top.main.cell.X(VectPlas_Int)           =
Top.main.P(VectPlas_Int_cell_0) ;
    Top.main.cell.X(VectPlas_LateVes)       =
Top.main.P(VectPlas_LateVes_cell_0) ;
    Top.main.cell.X(VectPlas_Nuc)           =
Top.main.P(VectPlas_Nuc_cell_0) ;
    Top.main.cell.X(Vect_Cyt)               =
Top.main.P(Vect_Cyt_cell_0) ;
    Top.main.cell.X(X_PlasVes)              =
Top.main.P(X_PlasVes_cell_0) ;
    Top.main.cell.X(X_Plas_Cyt)             =
Top.main.P(X_Plas_Cyt_cell_0) ;
SCHEDULE
    CONTINUE FOR SimulationTime
END

##########################################################################
##############
##########################################################################
##############

ESTIMATION Est_Ad5
OPTIONS
    INIT_RELATIVE_TOLERANCE     := 1.0e-8 ;
    INIT_ABSOLUTE_TOLERANCE     := 1.0e-8 ;
```

```
    DYNAMIC_RELATIVE_TOLERANCE := 1.0e-6  ;
    DYNAMIC_ABSOLUTE_TOLERANCE := 1.0e-8 ;
    INIT_PRINT_LEVEL := 0 ;
    DYNAMIC_PRINT_LEVEL := 0 ;
    ESTIMATION_PRINT_LEVEL := 0 ;
    ESTIMATION_TOLERANCE := 1e-6 ;
    DYNAMIC_MAXIMUM_STEPS := 50000 ;
PARAMETER
    path AS STRING DEFAULT ""
    SimulationTime AS REAL DEFAULT 120
UNIT
    Top AS Top
VARIABLE

UNCERTAIN
## Parameter := [value] : [lower bound] : [upper bound] ; # (uncomment
desired lines to activate)
## Initial Conditions:
#    Top.main.P(VectPlas_Ext_cell_0)                :=
Top.main.P(VectPlas_Ext_cell_0) : Top.main.L(VectPlas_Ext_cell_0)
: Top.main.U(VectPlas_Ext_cell_0)                ;
# Parameters:
#     Top.main.P(P_RelNucVol)                      :=
Top.main.P(P_RelNucVol)     : Top.main.L(P_RelNucVol)
: Top.main.U(P_RelNucVol);
#    Top.main.P(P_k_NPC)                           :=
Top.main.P(P_k_NPC) : Top.main.L(P_k_NPC)                              :
Top.main.U(P_k_NPC)                          ;
#    Top.main.P(P_k_bind_plasmid)                  :=
Top.main.P(P_k_bind_plasmid) : Top.main.L(P_k_bind_plasmid)
: Top.main.U(P_k_bind_plasmid)                   ;
   Top.main.P(P_k_bind_uptake)                    :=
Top.main.P(P_k_bind_uptake) : Top.main.L(P_k_bind_uptake)
: Top.main.U(P_k_bind_uptake)                    ;
   Top.main.P(P_k_bind_vector)                    :=
Top.main.P(P_k_bind_vector) : Top.main.L(P_k_bind_vector)
: Top.main.U(P_k_bind_vector)                    ;
#    Top.main.P(P_k_deg)                           :=
Top.main.P(P_k_deg) : Top.main.L(P_k_deg)                              :
Top.main.U(P_k_deg)                          ;
   Top.main.P(P_k_deg_vesicle)                    :=
Top.main.P(P_k_deg_vesicle) : Top.main.L(P_k_deg_vesicle)
: Top.main.U(P_k_deg_vesicle)                    ;
#    Top.main.P(P_k_dissociation)                  :=
Top.main.P(P_k_dissociation) : Top.main.L(P_k_dissociation)
: Top.main.U(P_k_dissociation)                   ;
   Top.main.P(P_k_escape)                         :=
Top.main.P(P_k_escape) : Top.main.L(P_k_escape)
: Top.main.U(P_k_escape)                         ;
#    Top.main.P(P_k_in)                            :=
Top.main.P(P_k_in) : Top.main.L(P_k_in)                                :
Top.main.U(P_k_in)                           ;
#    Top.main.P(P_k_protein)                       :=
Top.main.P(P_k_protein) : Top.main.L(P_k_protein)
: Top.main.U(P_k_protein)                        ;
```

```
   Top.main.P(P_k_traffic)                          :=
Top.main.P(P_k_traffic) : Top.main.L(P_k_traffic)
: Top.main.U(P_k_traffic)                          ;
   Top.main.P(P_k_unpack)                           :=
Top.main.P(P_k_unpack) : Top.main.L(P_k_unpack)
: Top.main.U(P_k_unpack)                           ;

SET
    path := "C:\Documents and Settings\Nate Tedford\Desktop\Model\"; #
directory containing the data files
    SimulationTime := 120;

INTERMEDIATE

EQUATION

OBJECTIVE WEIGHTED_LEAST_SQUARES
EXPERIMENT Expt_1
    DATA
        Top.main.X(report_Cytosol) :=
IMPORT_DATA(path+"Ad5_Cytosol_2.csv", 6) ;
#          Top.main.X(report_LateVesiclesX) :=
IMPORT_DATA(path+"Ad5_LateVesicles.csv", 6) ;
        Top.main.X(report_Nuclear) :=
IMPORT_DATA(path+"Ad5_Nuclear.csv", 6) ;
        Top.main.X(report_TotalVesicles) :=
IMPORT_DATA(path+"Ad5_TotalVesicles.csv", 5) ;
        Top.main.X(report_WholeCell) :=
IMPORT_DATA(path+"Ad5_WholeCell.csv", 6) ;
    INPUT

    PRESET
        # variable_name := default_value : lower_bound : upper_bound ;
    SELECTOR
        # selector_name := selector_value ;
    INITIAL
        Top.main.cell.X(PlasBound_Cyt)           =
Top.main.P(PlasBound_Cyt_cell_0) ;
        Top.main.cell.X(PlasBound_NPC)           =
Top.main.P(PlasBound_NPC_cell_0) ;
        Top.main.cell.X(PlasBound_Nuc)           =
Top.main.P(PlasBound_Nuc_cell_0) ;
        Top.main.cell.X(Plas_Cyt)                =
Top.main.P(Plas_Cyt_cell_0) ;
        Top.main.cell.X(Plas_Nuc)                =
Top.main.P(Plas_Nuc_cell_0) ;
        Top.main.cell.X(Protein)                 =
Top.main.P(Protein_cell_0) ;
        Top.main.cell.X(VectPlasBound_Cyt)       =
Top.main.P(VectPlasBound_Cyt_cell_0) ;
        Top.main.cell.X(VectPlasBound_NPC)       =
Top.main.P(VectPlasBound_NPC_cell_0) ;
        Top.main.cell.X(VectPlasBound_Nuc)       =
Top.main.P(VectPlasBound_Nuc_cell_0) ;
        Top.main.cell.X(VectPlas_Cyt)            =
Top.main.P(VectPlas_Cyt_cell_0) ;
```

```
        Top.main.cell.X(VectPlas_Ext)            = 20 ;
#Top.main.P(VectPlas_Ext_cell_0) ;
        Top.main.cell.X(VectPlas_Int)            =
Top.main.P(VectPlas_Int_cell_0) ;
        Top.main.cell.X(VectPlas_LateVes)        =
Top.main.P(VectPlas_LateVes_cell_0) ;
        Top.main.cell.X(VectPlas_Nuc)            =
Top.main.P(VectPlas_Nuc_cell_0) ;
        Top.main.cell.X(Vect_Cyt)                =
Top.main.P(Vect_Cyt_cell_0) ;
        Top.main.cell.X(X_PlasVes)               =
Top.main.P(X_PlasVes_cell_0) ;
        Top.main.cell.X(X_Plas_Cyt)              =
Top.main.P(X_Plas_Cyt_cell_0) ;
    SCHEDULE
        SEQUENCE
            CONTINUE FOR SimulationTime
        END
END # ESTIMATION Est_Ad5

##########################################################################
#################
##########################################################################
##############

ESTIMATION Est_C32
OPTIONS
    INIT_RELATIVE_TOLERANCE     := 1.0e-6 ;
    INIT_ABSOLUTE_TOLERANCE     := 1.0e-6 ;
    DYNAMIC_RELATIVE_TOLERANCE := 1.0e-6  ;
    DYNAMIC_ABSOLUTE_TOLERANCE := 1.0e-6 ;
    INIT_PRINT_LEVEL := 0 ;
    DYNAMIC_PRINT_LEVEL := 0 ;
    ESTIMATION_PRINT_LEVEL := 0 ;
    ESTIMATION_TOLERANCE := 1e-6 ;
    DYNAMIC_MAXIMUM_STEPS := 50000 ;
PARAMETER
    path AS STRING DEFAULT ""
    SimulationTime AS REAL DEFAULT 120
UNIT
    Top AS Top
VARIABLE

UNCERTAIN
## Parameter := [value] : [lower bound] : [upper bound] ; # (uncomment
desired lines to activate)
## Initial Conditions:
#    Top.main.P(VectPlas_Ext_cell_0)                :=
Top.main.P(VectPlas_Ext_cell_0) : Top.main.L(VectPlas_Ext_cell_0)
: Top.main.U(VectPlas_Ext_cell_0)                ;
# Parameters:
#    Top.main.P(P_RelNucVol)                        :=
Top.main.P(P_RelNucVol)     : Top.main.L(P_RelNucVol)
: Top.main.U(P_RelNucVol);
#    Top.main.P(P_k_NPC)                            :=
Top.main.P(P_k_NPC) : Top.main.L(P_k_NPC)                                :
Top.main.U(P_k_NPC)                          ;
```

```
#    Top.main.P(P_k_bind_plasmid)                    :=
Top.main.P(P_k_bind_plasmid) : Top.main.L(P_k_bind_plasmid)
: Top.main.U(P_k_bind_plasmid)                      ;
   Top.main.P(P_k_bind_uptake)                      :=
Top.main.P(P_k_bind_uptake) : Top.main.L(P_k_bind_uptake)
: Top.main.U(P_k_bind_uptake)                       ;
   Top.main.P(P_k_bind_vector)                      :=
Top.main.P(P_k_bind_vector) : Top.main.L(P_k_bind_vector)
: Top.main.U(P_k_bind_vector)                       ;
#    Top.main.P(P_k_deg)                            :=
Top.main.P(P_k_deg) : Top.main.L(P_k_deg)                                  :
Top.main.U(P_k_deg)                              ;
   Top.main.P(P_k_deg_vesicle)                      :=
Top.main.P(P_k_deg_vesicle) : Top.main.L(P_k_deg_vesicle)
: Top.main.U(P_k_deg_vesicle)                       ;
#    Top.main.P(P_k_dissociation)                   :=
Top.main.P(P_k_dissociation) : Top.main.L(P_k_dissociation)
: Top.main.U(P_k_dissociation)                      ;
   Top.main.P(P_k_escape)                           :=
Top.main.P(P_k_escape) : Top.main.L(P_k_escape)
: Top.main.U(P_k_escape)                            ;
#    Top.main.P(P_k_in)                             :=
Top.main.P(P_k_in) : Top.main.L(P_k_in)                                    :
Top.main.U(P_k_in)                               ;
#    Top.main.P(P_k_protein)                        :=
Top.main.P(P_k_protein) : Top.main.L(P_k_protein)
: Top.main.U(P_k_protein)                           ;
   Top.main.P(P_k_traffic)                          :=
Top.main.P(P_k_traffic) : Top.main.L(P_k_traffic)
: Top.main.U(P_k_traffic)                           ;
   Top.main.P(P_k_unpack)                           :=
Top.main.P(P_k_unpack) : Top.main.L(P_k_unpack)
: Top.main.U(P_k_unpack)                            ;

SET
    path := "C:\Documents and Settings\Nate Tedford\Desktop\Model\" ; #
directory containing the data files
    SimulationTime := 120;

INTERMEDIATE

EQUATION
#    output = data_scalefactor*[variable_name] ;
OBJECTIVE WEIGHTED_LEAST_SQUARES
EXPERIMENT Expt_1
    DATA
        Top.main.X(report_Cytosol) :=
IMPORT_DATA(path+"C32_Cytosol_2.csv", 6) ;
#         Top.main.X(report_LateVesiclesX) :=
IMPORT_DATA(path+"C32_LateVesicles.csv", 6) ;
        Top.main.X(report_Nuclear) :=
IMPORT_DATA(path+"C32_Nuclear.csv", 6) ;
        Top.main.X(report_TotalVesicles) :=
IMPORT_DATA(path+"C32_TotalVesicles.csv", 5) ;
        Top.main.X(report_WholeCell) :=
IMPORT_DATA(path+"C32_WholeCell.csv", 6) ;
    INPUT
```

```
    PRESET
        # variable_name := default_value : lower_bound : upper_bound ;
    SELECTOR
        # selector_name := selector_value ;
    INITIAL
        Top.main.cell.X(PlasBound_Cyt)          =
Top.main.P(PlasBound_Cyt_cell_0) ;
        Top.main.cell.X(PlasBound_NPC)          =
Top.main.P(PlasBound_NPC_cell_0) ;
        Top.main.cell.X(PlasBound_Nuc)          =
Top.main.P(PlasBound_Nuc_cell_0) ;
        Top.main.cell.X(Plas_Cyt)               =
Top.main.P(Plas_Cyt_cell_0) ;
        Top.main.cell.X(Plas_Nuc)               =
Top.main.P(Plas_Nuc_cell_0) ;
        Top.main.cell.X(Protein)                =
Top.main.P(Protein_cell_0) ;
        Top.main.cell.X(VectPlasBound_Cyt)      =
Top.main.P(VectPlasBound_Cyt_cell_0) ;
        Top.main.cell.X(VectPlasBound_NPC)      =
Top.main.P(VectPlasBound_NPC_cell_0) ;
        Top.main.cell.X(VectPlasBound_Nuc)      =
Top.main.P(VectPlasBound_Nuc_cell_0) ;
        Top.main.cell.X(VectPlas_Cyt)           =
Top.main.P(VectPlas_Cyt_cell_0) ;
        Top.main.cell.X(VectPlas_Ext)           = 5e5;
#Top.main.P(VectPlas_Ext_cell_0) ;
        Top.main.cell.X(VectPlas_Int)           =
Top.main.P(VectPlas_Int_cell_0) ;
        Top.main.cell.X(VectPlas_LateVes)       =
Top.main.P(VectPlas_LateVes_cell_0) ;
        Top.main.cell.X(VectPlas_Nuc)           =
Top.main.P(VectPlas_Nuc_cell_0) ;
        Top.main.cell.X(Vect_Cyt)               =
Top.main.P(Vect_Cyt_cell_0) ;
        Top.main.cell.X(X_PlasVes)              =
Top.main.P(X_PlasVes_cell_0) ;
        Top.main.cell.X(X_Plas_Cyt)             =
Top.main.P(X_Plas_Cyt_cell_0) ;
    SCHEDULE
        SEQUENCE
            CONTINUE FOR SimulationTime
        END
END # ESTIMATION Est_C32

##############################################################################
```

```
ESTIMATION Est_XPEI
OPTIONS
    INIT_RELATIVE_TOLERANCE     := 1.0e-6 ;
    INIT_ABSOLUTE_TOLERANCE     := 1.0e-6 ;
    DYNAMIC_RELATIVE_TOLERANCE := 1.0e-6  ;
    DYNAMIC_ABSOLUTE_TOLERANCE := 1.0e-6 ;
    INIT_PRINT_LEVEL := 0 ;
    DYNAMIC_PRINT_LEVEL := 0 ;
    ESTIMATION_PRINT_LEVEL := 0 ;
    ESTIMATION_TOLERANCE := 1e-6 ;
    DYNAMIC_MAXIMUM_STEPS := 50000 ;
PARAMETER
    path AS STRING DEFAULT ""
    SimulationTime AS REAL DEFAULT 120
UNIT
    Top AS Top
VARIABLE

UNCERTAIN
## Parameter := [value] : [lower bound] : [upper bound] ; # (uncomment
desired lines to activate)
## Initial Conditions:
#    Top.main.P(VectPlas_Ext_cell_0)                :=
Top.main.P(VectPlas_Ext_cell_0) : Top.main.L(VectPlas_Ext_cell_0)
: Top.main.U(VectPlas_Ext_cell_0)                ;
# Parameters:
#    Top.main.P(P_RelNucVol)                        :=
Top.main.P(P_RelNucVol)      : Top.main.L(P_RelNucVol)
: Top.main.U(P_RelNucVol);
#    Top.main.P(P_k_NPC)                            :=
Top.main.P(P_k_NPC) : Top.main.L(P_k_NPC)                                :
Top.main.U(P_k_NPC)                           ;
#    Top.main.P(P_k_bind_plasmid)                   :=
Top.main.P(P_k_bind_plasmid) : Top.main.L(P_k_bind_plasmid)
: Top.main.U(P_k_bind_plasmid)                ;
   Top.main.P(P_k_bind_uptake)                      :=
Top.main.P(P_k_bind_uptake) : Top.main.L(P_k_bind_uptake)
: Top.main.U(P_k_bind_uptake)                 ;
   Top.main.P(P_k_bind_vector)                      :=
Top.main.P(P_k_bind_vector) : Top.main.L(P_k_bind_vector)
: Top.main.U(P_k_bind_vector)                 ;
#    Top.main.P(P_k_deg)                            :=
Top.main.P(P_k_deg) : Top.main.L(P_k_deg)                                :
Top.main.U(P_k_deg)                           ;
   Top.main.P(P_k_deg_vesicle)                      :=
Top.main.P(P_k_deg_vesicle) : Top.main.L(P_k_deg_vesicle)
: Top.main.U(P_k_deg_vesicle)                 ;
#    Top.main.P(P_k_dissociation)                   :=
Top.main.P(P_k_dissociation) : Top.main.L(P_k_dissociation)
: Top.main.U(P_k_dissociation)                ;
   Top.main.P(P_k_escape)                           :=
Top.main.P(P_k_escape) : Top.main.L(P_k_escape)
: Top.main.U(P_k_escape)                      ;
#    Top.main.P(P_k_in)                             :=
Top.main.P(P_k_in) : Top.main.L(P_k_in)                                  :
Top.main.U(P_k_in)                            ;
```

```
#    Top.main.P(P_k_protein)                          :=
Top.main.P(P_k_protein) : Top.main.L(P_k_protein)
: Top.main.U(P_k_protein)                            ;
   Top.main.P(P_k_traffic)                           :=
Top.main.P(P_k_traffic) : Top.main.L(P_k_traffic)
: Top.main.U(P_k_traffic)                            ;
   Top.main.P(P_k_unpack)                            :=
Top.main.P(P_k_unpack) : Top.main.L(P_k_unpack)
: Top.main.U(P_k_unpack)                             ;

SET
    path := "C:\Documents and Settings\Nate Tedford\Desktop\Model\" ; #
directory containing the data files
    SimulationTime := 120;

INTERMEDIATE

EQUATION
#    output = data_scalefactor*[variable_name] ;
OBJECTIVE WEIGHTED_LEAST_SQUARES
EXPERIMENT Expt_1
    DATA
        Top.main.X(report_Cytosol) :=
IMPORT_DATA(path+"XPEI_Cytosol_2.csv", 6) ;
#         Top.main.X(report_LateVesiclesX) :=
IMPORT_DATA(path+"XPEI_LateVesicles.csv", 6) ;
        Top.main.X(report_Nuclear) :=
IMPORT_DATA(path+"XPEI_Nuclear.csv", 6) ;
        Top.main.X(report_TotalVesicles) :=
IMPORT_DATA(path+"XPEI_TotalVesicles.csv", 5) ;
        Top.main.X(report_WholeCell) :=
IMPORT_DATA(path+"XPEI_WholeCell.csv", 6) ;
    INPUT

    PRESET
        # variable_name := default_value : lower_bound : upper_bound ;
    SELECTOR
        # selector_name := selector_value ;
    INITIAL
        Top.main.cell.X(PlasBound_Cyt)           =
Top.main.P(PlasBound_Cyt_cell_0) ;
        Top.main.cell.X(PlasBound_NPC)           =
Top.main.P(PlasBound_NPC_cell_0) ;
        Top.main.cell.X(PlasBound_Nuc)           =
Top.main.P(PlasBound_Nuc_cell_0) ;
        Top.main.cell.X(Plas_Cyt)                =
Top.main.P(Plas_Cyt_cell_0) ;
        Top.main.cell.X(Plas_Nuc)                =
Top.main.P(Plas_Nuc_cell_0) ;
        Top.main.cell.X(Protein)                 =
Top.main.P(Protein_cell_0) ;
        Top.main.cell.X(VectPlasBound_Cyt)       =
Top.main.P(VectPlasBound_Cyt_cell_0) ;
        Top.main.cell.X(VectPlasBound_NPC)       =
Top.main.P(VectPlasBound_NPC_cell_0) ;
        Top.main.cell.X(VectPlasBound_Nuc)       =
Top.main.P(VectPlasBound_Nuc_cell_0) ;
```

```
        Top.main.cell.X(VectPlas_Cyt)            =
Top.main.P(VectPlas_Cyt_cell_0) ;
        Top.main.cell.X(VectPlas_Ext)            = 5e5 ;
#Top.main.P(VectPlas_Ext_cell_0) ;
        Top.main.cell.X(VectPlas_Int)            =
Top.main.P(VectPlas_Int_cell_0) ;
        Top.main.cell.X(VectPlas_LateVes)        =
Top.main.P(VectPlas_LateVes_cell_0) ;
        Top.main.cell.X(VectPlas_Nuc)            =
Top.main.P(VectPlas_Nuc_cell_0) ;
        Top.main.cell.X(Vect_Cyt)                =
Top.main.P(Vect_Cyt_cell_0) ;
        Top.main.cell.X(X_PlasVes)               =
Top.main.P(X_PlasVes_cell_0) ;
        Top.main.cell.X(X_Plas_Cyt)              =
Top.main.P(X_Plas_Cyt_cell_0) ;
    SCHEDULE
        SEQUENCE
            CONTINUE FOR SimulationTime
        END
END # ESTIMATION Est_XPEI

#############################################################################
```

```
SCRIPT MultiStartEstimation
#
# Starting points are equally spaced on a log scaled between lower and
upper bounds.

PARAMETER
    i, j, k, m, n, p, q, steps, count, nParameters AS INTEGER DEFAULT 0
    EstName, OutputFileName, filepath, OutputFileID AS STRING DEFAULT
""
    ObjectiveResult AS REAL DEFAULT 0
    k_traffic_0, k_deg_vesicle_0, k_escape_0, k_unpack_0,
k_bind_vector_0 AS ARRAY(steps) OF REAL DEFAULT 0

SET
   EstName := "Est_C32"; # name of Estimation routine you want to run
   nParameters := 30;
   filepath := "C:\Documents and Settings\hendrb\Desktop\NatesModel";
   OutputFileName := "061129_MultiStartFit_C32.csv"; # File with
parameter results
   OutputFileID := "fid";
   steps := 4; # this must equal the number of elements in the
parameter vectors!!


RUN
    INSTANTIATE EstName

    FDIR filepath
    FOPEN (ID=OutputFileID,FILE=OutputFileName, ftype="out")
    FWRITE (ID=OutputFileID, FMT="%s")
"PARAMETER_SET,STATUS,OBJECTIVE,," END
    q := 1;
    WHILE (q < nParameters) DO
        FWRITE (ID=OutputFileID, FMT="%s, ") Top.main.PName(q) END
        q := q+1;
    END
    FWRITE (ID=OutputFileID, FMT="%s\n") Top.main.PName(q) END


    count := 0;
    i := 1;
    WHILE (i <= steps) DO
        k_traffic_0(i) :=
10^(log10(Top.main.L(P_k_traffic))+(log10(Top.main.U(P_k_traffic))-
log10(Top.main.L(P_k_traffic)))/(steps-1)*(i-1));

        j := 1;
        WHILE (j <= steps) DO
            k_deg_vesicle_0(j) :=
10^(log10(Top.main.L(P_k_deg_vesicle))+(log10(Top.main.U(P_k_deg_vesicl
e))-log10(Top.main.L(P_k_deg_vesicle)))/(steps-1)*(j-1));

            k := 1;
            WHILE (k <= steps) DO
                k_escape_0(k) :=
10^(log10(Top.main.L(P_k_escape))+(log10(Top.main.U(P_k_escape))-
log10(Top.main.L(P_k_escape)))/(steps-1)*(k-1));
```

```
                m := 1;
                WHILE (m <= steps) DO
                    k_unpack_0(m) :=
10^(log10(Top.main.L(P_k_unpack))+(log10(Top.main.U(P_k_unpack))-
log10(Top.main.L(P_k_unpack)))/(steps-1)*(m-1));

                    n := 1;
                    WHILE (n <= steps) DO
                        k_bind_vector_0(n) :=
10^(log10(Top.main.L(P_k_bind_vector))+(log10(Top.main.U(P_k_bind_vecto
r))-log10(Top.main.L(P_k_bind_vector)))/(steps-1)*(n-1));

                        p := 1; # additional loop structure if you want
to add another parameter
                        WHILE (p <= 1) DO


#                           WRITE "k_traffic = ", k_traffic_0(i), ";
k_deg_vesicle = ", k_deg_vesicle_0(j), "; k_escape = ", k_escape_0(k),
"; k_unpack = ", k_unpack_0(m), "; k_bind_vector = ",
k_bind_vector_0(n) END
#                           WRITE "k_traffic = ", i, "; k_deg_vesicle =
", j, "; k_escape = ", k, "; k_unpack = ", m, "; k_bind_vector = ", n
END

                            count := count+1;
                            WRITE "Iteration: ", count END
                            Top.main.P(P_k_traffic) := k_traffic_0(i);
                            Top.main.P(P_k_deg_vesicle) :=
k_deg_vesicle_0(j);
                            Top.main.P(P_k_escape) := k_escape_0(k);
                            Top.main.P(P_k_unpack) := k_unpack_0(m);
                            Top.main.P(P_k_bind_vector) :=
k_bind_vector_0(n);
                            SOLVE EstName
                            IF (STATUS <> "SUCCESS") THEN
                                WRITE "Estimation failed. Skipping
iteration ..." END
                                FWRITE (ID=OutputFileID,
FMT="%s,%s,%g\n") Str(count), STATUS, -1 END
                                n := n+1;
                                CONTINUE
                            END
                            ObjectiveResult := GetObjective(STATUS,
EstName) ;
                            WRITE "Objective = ", ObjectiveResult END

                            # Write optimal parameters to file:
                            FWRITE (ID=OutputFileID, FMT="%s,%s,%g,,")
Str(count), STATUS, ObjectiveResult END
                            q := 1;
                            WHILE (q < nParameters) DO
                                FWRITE (ID=OutputFileID, FMT="%g, ")
Top.main.P(q) END
                                q := q+1;
                            END
```

```
                                FWRITE (ID=OutputFileID, FMT="%g\n")
Top.main.P(q) END
                                FCLOSE (ID=OutputFileID) # close and open
file to save results as it calculates
                                FOPEN (ID=OutputFileID,FILE=OutputFileName,
ftype="append")

                                    p := p+1;
                                END # WHILE p
                                n := n+1;
                            END # WHILE n
                            m := m+1;
                        END # WHILE m
                        k := k+1;
                    END # WHILE k
                    j := j+1;
                END # WHILE j
                i := i+1;
            END # WHILE i

            FCLOSE(ID=OutputFileID)
            WRITE "SCRIPT MultiStartEstimation Complete!" END
        END # SCRIPT MultiStartEstimation

        ##########################################################################
```

```
SCRIPT SensitivityOutput
#
# This just runs the sensitivity analysis with the default parameters
in 'Sim_Sensitivity"
# and outputs the integral to the screen.

PARAMETER
    j, k, nParameters, nVariables AS INTEGER DEFAULT 0
    timepoint AS REAL DEFAULT 0
    ModelName, SimName AS STRING DEFAULT ""
    value AS ARRAY(nVariables) OF REAL DEFAULT 0
    integral AS ARRAY(nVariables, nParameters) OF REAL DEFAULT 0

SET
    ModelName := "Sim_Sensitivity" ;
    nParameters := 30;
    nVariables := 18;
    timepoint := 30;

RUN

    INSTANTIATE ModelName

    SOLVE ModelName
    IF (STATUS <> "SUCCESS") THEN WRITE "Solve failed." END END
    SimName := "temp";
    MOVE ModelName TO SimName # this gets rid of all the info that is
solved for, but not reported.
    k := 1;
    WHILE (k <= nVariables) DO
        j := 1;
        WHILE (j <= nParameters) DO
            integral(k,j) :=
GetIntegralAbs(STATUS,SimName,Top.main.X(k)/Top.main.P(j)) ; # I am
using this function to figure out if an output exists ...
            IF (STATUS <> "SUCCESS") THEN
                j := j+1;
                CONTINUE
            END

            # Putting GetFirstValue after the GetIntegrals (and
contingent on its success makes sure
            #that we only track the reported variables and not all of
them. This is a dirty trick.
            IF (j = 1) THEN
                value(k) := GetFirstValue(STATUS, SimName,
Top.main.X(k), TIME, timepoint);
            END

            j := j+1;
       END # while j
       k := k+1;
    END # while k

    # WRITE results to screen:
    WRITE "Integrals of Sensitivity:" END
    k := 1;
```

```
    WHILE (k <= nVariables) DO
        j := 1;
        WHILE (j <= nParameters) DO
            IF integral(k,j) <> -1 THEN
                WRITE "Integral of ", Top.main.XName(k), "/",
Top.main.PName(j), " = ", integral(k,j), ":" END
            END
            j := j+1;
        END # while j

        k := k+1;
    END # while k
    WRITE "" END

    WRITE "Value at t = ", timepoint, ":" END
    k := 1;
    WHILE (k <= nVariables) DO
        IF value(k) <> -1 THEN
            WRITE Top.main.XName(k), " = ", value(k) END
        END

        k := k+1;
    END # while k
    WRITE "" END

END # SCRIPT Sensitivity Output
```